

N 7 3 - 1 3 7 8 0

NATIONAL AERONAUTICS AND SPACE ADMINISTRATION

Technical Report 32-1571

Trajectory Correction Propulsion for TOPS

Hartwell R. Long

Roy A. Bjorklund

**CASE FILE
COPY**

**JET PROPULSION LABORATORY
CALIFORNIA INSTITUTE OF TECHNOLOGY
PASADENA, CALIFORNIA**

November 15, 1972

NATIONAL AERONAUTICS AND SPACE ADMINISTRATION

Technical Report 32-1571

Trajectory Correction Propulsion for TOPS

Hartwell R. Long

Roy A. Bjorklund

**JET PROPULSION LABORATORY
CALIFORNIA INSTITUTE OF TECHNOLOGY
PASADENA, CALIFORNIA**

November 15, 1972

Prepared Under Contract No. NAS 7-100
National Aeronautics and Space Administration

Preface

The work described in this report was sponsored by the NASA/OSS Launch Vehicle and Propulsion Programs Office and the NASA/OAST Space Propulsion and Power Division and was performed by the Propulsion Division of the Jet Propulsion Laboratory.

Acknowledgment

Of the many people who contributed to the success of the program reported herein, the authors would like to particularly acknowledge the assistance and contributions of L. E. Baughman, D. L. Bond, R. Hagler, G. R. Heidenreich, O. F. Keller, J. H. Kelley, R. W. Riebling, and L. R. Toth.

Contents

I. Introduction	1
A. TOPS AST Project	1
B. TOPS Spacecraft	2
C. Propulsion Program Objectives	3
II. TCPS System Configuration Selection	3
A. Basic System Selection	4
B. Configuration Selection	7
C. Thrust Vector Control Considerations	9
D. Baseline TOPS TCPS	9
III. Component Evaluation	9
A. Rocket Engine	11
1. Thrust limitation	11
2. Test program objectives	11
3. Engine hardware	12
4. Test facility, procedures, and conditions	15
5. Test firing results with hydrazine propellant	19
6. Test firing results with hydrazine/hydrazine nitrate	23
7. Discussion of results	25
8. Rocket exhaust plume considerations	29
B. Solenoid Valves	30
1. Valve survey	31
2. Valve evaluation program	33
3. Test results	34
4. Leakage limit specification	34
5. Magnetic field suppression	35
C. Pyrovalves	35
1. Aluminum valve development program	36
2. Titanium valve development program	41
D. Propellant Acquisition	42
E. Unevaluated Components	43
1. Transducers	43
2. Filter	44
3. Service valve	44

Contents (contd)

4. Propellant tank	44
F. Hydrazine/Material Interaction	44
1. Material compatibility test program	44
2. Posttest evaluation	46
3. Method of rating materials	46
4. Provisional material selection	49
G. Hydrazine/Radiation Interaction	49
1. Test program	49
2. Test results	50
IV. System Evaluation	51
A. Demonstration System Test Criteria	51
B. Demonstration System Design	52
1. Rocket engine	55
2. Engine gimbal assembly	55
3. Gimbal actuator	57
4. Hydrazine tank	58
5. Orifice plate assembly	58
6. Pyrovalve manifold	59
7. Pyrovalve squibs	60
8. Fuel-line filter	60
9. Bellows accumulator	60
10. Latching solenoid valves	60
11. Normally closed solenoid valves	60
12. Manual service valves	61
13. Assembled demonstration system	61
C. Test Program	61
1. Test facilities	61
2. Test description	64
3. Test system instrumentation	66
D. Test Results	67
1. Steady-state performance	67
2. Transient response and roughness	72
3. Temperature response	76

Contents (contd)

4. Exhaust gas analysis	80
5. Pyrotechnic valve shock loading	81
6. Thrust vector control	91
7. Performance prediction parameters	93
8. Posttest inspection	99
E. Discussion of Demonstration Test Results	100
1. Configuration verification	100
2. Steady-state performance	101
3. Transient performance	101
4. Thermal response	101
5. Shock response	101
6. Thrust vector control characteristics	102
7. Modeling and control parameter characteristics	102
V. Definition of Flight TCPS	102
A. System Characteristics	103
B. System Sizing	103
C. Spacecraft Interfaces	104
1. Attitude propulsion subsystem (APS)	104
2. Pyrotechnic subsystem (PYRO)	104
3. Attitude-control subsystem (A/C)	104
4. Measurement processor subsystem (MPS)	105
5. Structure subsystem (STRU)	105
6. Temperature control subsystem (T/C)	106
D. Preliminary Propulsion Module Design	106
E. TCPS Operation and Control	107
1. Maneuver sequence	108
2. Engine cutoff control	108
3. Fault detection and correction	109
VI. Summary and Recommendations	110
References	111
Appendix. Summary of Demonstration System Test Instrumentation and Digital Data	115

Contents (contd)

Tables

1. Mission requirements for trajectory correction propulsion	3
2. Typical maneuver schedules	4
3. Results of monopropellant vs bipropellant study	7
4. Description of thrust chambers	12
5. Summary of test conditions and results for firings with hydrazine	21
6. Summary of test conditions and results for firings with hydrazine/hydrazine nitrate	22
7. Characteristics and performance of QCM system containing six independent sensors	30
8. Results of solenoid valve industry survey	31
9. Propellant control valve performance and design criteria	32
10. Propellant shutoff valve performance and design criteria (Ref. 25)	32
11. Experimental data from valve magnetic field tests	36
12. Pyrovalve performance and design criteria	38
13. Pyrovalve test requirements	39
14. Peak response points for vibration tests	39
15. Physical characteristics of prototype pyrovalves	40
16. Amplitude magnification ratios at pyrovalve manifold vibration response frequencies	41
17. Propellant acquisition concept selection	42
18. Assays of hydrazine and hydrazine/hydrazine nitrate used in TOPS material compatibility test program	47
19. Material compatibility specimens in storage test in hydrazine	48
20. Material compatibility specimens in storage test in hydrazine/hydrazine nitrate	48
21. Compatibility ratings for TOPS materials in contact with hydrazine	49
22. Flow through capillary before and after irradiation	50
23. TOPS—TCPS test duty cycle	51
24. Demonstration system design requirements	52
25. Component parts for demonstration propulsion test module	57
26. Hydrazine assay—demonstration testings	64

Contents (contd)

Tables (contd)

27. Summary of mass change versus integrated propellant flow rate	71
28. Rocket engine transient start, stop, and roughness characteristics	73
29. Rocket engine performance transient characteristics	76
30. Minimum-to-maximum temperature ranges for engine components and support structures	76
31. Exhaust gas sample assay	80
32. Summary of acceleration response to pyrovalve actuation shock	90
33. Summary of strain response to pyrovalve actuation shock	93
34. Summary of results from thrust vector control program for test No. 5	94
35. Spectrographic analysis of particulate residue from propellant line filters	101
36. Estimate of nominal system characteristics	103
37. Mass estimate for TOPS TCPS	104
38. Monopropellant hydrazine propulsion system mass fraction	104
39. Power supplied by PYRO to TCPS	104
40. TCPS telemetry during maneuvers	105
41. Power required for TCPS measurements	105
42. Typical maneuver sequence of events	108
A-1. Summary of test system measured parameters	115
A-2. Summary of test system calculated parameters	116
A-3. Summary of steady-state test data at time 0 s	117
A-4. Summary of steady-state test data at time 10 s	118
A-5. Summary of steady-state test data at time 20 s	119
A-6. Summary of steady-state test data at time 40 s	120
A-7. Summary of steady-state test data at time 90 s	122
A-8. Summary of steady-state test data at time 150 s	123

Figures

1. Thermoelectric Outer Planet Spacecraft (TOPS)	2
2. Trajectory correction maneuver plan for JSP mission	5
3. Propulsion system configurations used in selection tradeoff study (a) monopropellant, (b) bipropellant	6

Contents (contd)

Figures (contd)

4. Propulsion system cost effectiveness vs ΔV and reliability	7
5. TCPS configuration candidates	8
6. TOPS-TCPS baseline system schematic diagram	10
7. Bolt-up 102-N- (23 lbf-) thrust hydrazine engine (configuration Nos. 1 and 2, Table 4)	14
8. Transtage monopropellant hydrazine rocket engine assembly (configuration Nos. 3 and 4, Table 4) (from Ref. 4)	15
9. R-24C experimental monopropellant engine (configuration No. 5, Table 4)	16
10. Bolt-up Mariner Mars 1969 222-N- (50-lbf) thrust trajectory correction engine (configuration Nos. 6A through 6D, Table 4)	17
11. Welded flight version of Mariner Mars 1969 222-N- (50 lbf-) thrust trajectory correction engine (configuration No. 7, Table 4)	18
12. Exploded view of thermal bed with catalytic pilot starter (configuration No. 9, Table 4)	18
13. Evidence of washout phenomenon: variation of c^* with time	23
14. Combustion roughness in chamber (configuration No. 2, Table 4) with hydrazine/hydrazine nitrate	24
15. Upper bed chamber temperature measured downstream from injector face	24
16. Micrographs of hydrazine catalysts; (a) Shell-405, and (b) Esso-500 (25- to 30-mesh, unfired, 50 \times)	26
17. Catalysts after three open-air flame tests; (a) Esso-500, (b) Shell-405	26
18. Carleton bistable (latching) solenoid valve	33
19. Hydraulics Research normally closed solenoid valve	33
20. Marquardt bistable (latching) solenoid valve	33
21. Marquardt normally closed solenoid valve	34
22. Pyrovalve manifold schematic diagram	37
23. Pyrovalve manifold assembly for prototype demonstration test system	37
24. Cross section of aluminum NO and NC pyrovalves after actuation	40
25. Pyrovalve manifold vibration test configuration and axis designation	40
26. Cross section of titanium NO and NC pyrovalves after actuation	42

Contents (contd)

Figures (contd)

27. Candidate design for TCPS propellant acquisition device	43
28. Typical specimen/capsule used in hydrazine material compatibility tests	45
29. Radiation-caused decomposition of hydrazine in titanium vessels	50
30. TOPS-TCPS demonstration test system schematic diagram	53
31. Component arrangement on the tank side of the support plate	54
32. Component arrangement of the engine side of the support plate	56
33. Engine and gimbal support mount assembly	58
34. Gimbal actuator with instrumented flexural engine attachment	58
35. Orifice plate flowmeter assembly	59
36. Final assembly of engine, gimbal actuators, and pyrovalve manifold	59
37. Bellows accumulator cross-section drawing	60
38. Compact latching and NC solenoid valve assembly	60
39. Final assembly of demonstration system	60
40. DV test stand complex at JPL's Edwards Test Station	62
41. Metric frame installed in six-component thrust stand	63
42. Schematic drawing of the six-component thrust stand load lines	63
43. Location of force application and measurement points on the metric frame	64
44. Demonstration system installed in thrust stand in test cell	64
45. Block diagrams of instrumentation systems used for demonstration tests	65
46. Steady-state tank pressure versus time	67
47. Steady-state propellant flow rate versus time	68
48. Steady-state chamber pressure versus time	68
49. Steady-state thrust versus time	69
50. Steady-state specific impulse versus time	69
51. Steady-state characteristic velocity versus time	70
52. Steady-state total impulse versus time	70
53. Typical hard-start transient (test No. 2)	74
54. Typical hard-stop transient (test No. 2)	74
55. Typical smooth-start transient (test No. 6)	75
56. Typical smooth-stop transient (test No. 6)	75

Contents (contd)

Figures (contd)

57. Engine components and structures thermocouple locations	77
58. Steady-state engine temperatures (T_B and T_{C2}) versus time	78
59. Engine injector temperature versus time	79
60. Injector maximum posttest temperature versus test duration	79
61. Accelerometer and strain gauge locations	82
62. Acceleration responses to pyrovalve actuation shock: (a) support structure, (b) manifold, (c) base mounting plate	83
63(a). Peak shock response versus frequency for accelerometer A1, test Nos. 1 to 8	84
63(b). Peak shock response versus frequency for accelerometer A3, test Nos. 1 to 8	85
63(c). Peak shock response versus frequency for accelerometer A5, test Nos. 1 to 8	86
64(a). Energy density spectrum for acceleration response of pyrovalve support structure	87
64(b). Energy density spectrum for acceleration response of pyrovalve manifold	88
64(c). Energy density spectrum for acceleration response of base mounting plate	89
65(a). Pyrovalve support structure strain response to actuation shock	92
65(b). Pyrovalve manifold strain to actuation shock	92
65(c). Base mounting plate strain response to actuation shock	92
66(a). Energy density spectrum for strain response of pyrovalve support structure	95
66(b). Energy density spectrum for strain response of pyrovalve manifold	96
66(c). Energy density spectrum for strain response of base mounting plate	97
67. Test No. 5 thrust vector control program command signal versus time	97
68. Steady-state fluid resistance factor versus time	99
69. Mass flow rate constant versus time	100
70. Chamber pressure constant versus time	100
71. TOPS propulsion bay and neighboring assemblies	106
72. Preliminary TOPS propulsion module design emphasizing TCPS components	107

Abstract

A blowdown-pressurized hydrazine propulsion system was selected to provide trajectory correction impulse for outer planet flyby spacecraft as the result of cost/mass/reliability tradeoff analyses. Present hydrazine component and system technology and component designs were evaluated for application to the Thermoelectric Outer Planet Spacecraft (TOPS); while general hydrazine *technology* was adequate, component *design* changes were deemed necessary for TOPS-type missions. A prototype hydrazine propulsion system was fabricated and fired nine times for a total of 1600 s to demonstrate the operation and performance of the TOPS propulsion configuration. A flight-weight trajectory correction propulsion subsystem (TCPS) was designed for the TOPS based on actual and estimated advanced components.

Trajectory Correction Propulsion for TOPS

I. Introduction

The spacecraft propulsion requirements of early exploration missions to the nearby planets Mars and Venus were one or two rocket firings spaced over six months. The task of propulsion for these flyby missions was to correct the trajectory for the planetary quarantine launch bias, launch vehicle errors, and trajectory and ephemeris prediction errors. The flyby spacecraft is now being replaced in the exploration of the near planets with orbiter and lander spacecraft.

The same evolutionary pattern of progressive spacecraft capability and complexity will be followed in the exploration of the outer planets just starting. The giant planet Jupiter will be surveyed first by flyby spacecraft and then the Jovian gravitational field will be used to boost flyby spacecraft onto trajectories to other outer planets. Multiple-planet gravity assist missions vary from two-planet missions comparable to the Mariner Venus-Mercury mission in 1973 to the four-planet mission, which has been named The Grand Tour.

The change of emphasis from single- to multiple-planet missions, especially missions to the outer planets, requires an order of magnitude change in many important aspects of propulsion capability. Now at least five or six separate rocket firings are required over a five- to ten-year period

with the capability for many more. The flight environment is more hostile, especially with the substitution of radioisotope power sources for solar panels. The selection of the best propulsion system configuration for multiple-planet flyby missions and the evaluation of the adequacy of the present state of the art as reflected in the selected system are described in this report.

A. TOPS AST Project

While a particular type of propulsion system can be selected and evaluated for the entire class of outer planet flyby missions, a complete study is best made through participation in an interdisciplinary team study of a specific, typical mission. The Thermoelectric Outer Planet Spacecraft (TOPS) mission was the focus for the study summarized in this report.

The TOPS Project was an Advanced Systems Technology (AST) project of the Jet Propulsion Laboratory. These research and development projects lay the groundwork for prospective flight projects by demonstrating the advanced technology and basic spacecraft design concepts required to perform a specific set of missions—in this case, the set of missions generally labeled Grand Tours. The design and hardware experience from the TOPS effort provides a basis for realistic estimates of performance, cost, reliability, and scheduling that is vital in selecting and

defining the specific outer planets flyby mission set for a formal NASA flight project.

B. TOPS Spacecraft

The flight-project type of organizational structure and practices used by the TOPS Project guaranteed that each spacecraft subsystem could both execute its function in the flight environment and properly interface with the rest of the spacecraft. The proving ground was the TOPS configuration. The configuration shown in Fig. 1 was the product of a long line of evolution resulting from increased understanding of the implications of performance requirements, subsystem interfaces, and the flight environment. In general, analyses and tests made for one phase of the development were not repeated unless the new conditions fell outside the range of validity of the original work. Thus, the early work described in this report was for the four-planet missions while later work was for the less restricted three-planet missions.

The general form of the TOPS subsystems was described in the September 1970 issue of *Astronautics and Aeronautics* (Ref. 1) devoted almost entirely to the TOPS. The final form of the TOPS was described at the TOPS Industry Briefing given at JPL over the period September 21 to October 1, 1971 (Ref. 2), and documented in the TOPS Functional Requirements documents released at that time (Ref. 3). Looking at Fig. 1, we see the most obvious differences from past planetary spacecraft are the large high-gain antenna for very long-range communication, the radioisotope thermoelectric generators (RTG's) for solar-independent power, and the long booms necessary to isolate the magnetometers from the slightly magnetic spacecraft bus. Although the STAR (self-test and -repair) computer probably symbolizes the less obvious, but more important, spacecraft changes made to attain 10-yr reliability, each subsystem, including propulsion, has been greatly influenced by the long-life reliability requirement.

The spacecraft propulsion unit is called the trajectory correction propulsion subsystem (TCPS).¹ It is physically located on the spacecraft roll axis pointing diametrically opposite from the high-gain antenna (Fig. 1). The TCPS is enclosed in a fabric-covered bay that provides thermal control and some micrometeoroid protection.

The major interface of the TCPS is with the attitude propulsion subsystem (APS) composed of an array of very

small hydrazine engines used to unload the momentum wheels that provide three-axis attitude stabilization. The TCPS and APS are integrated to form the propulsion module. The TCPS and the TCPS designer's view of the propulsion module are discussed in this report, and APS

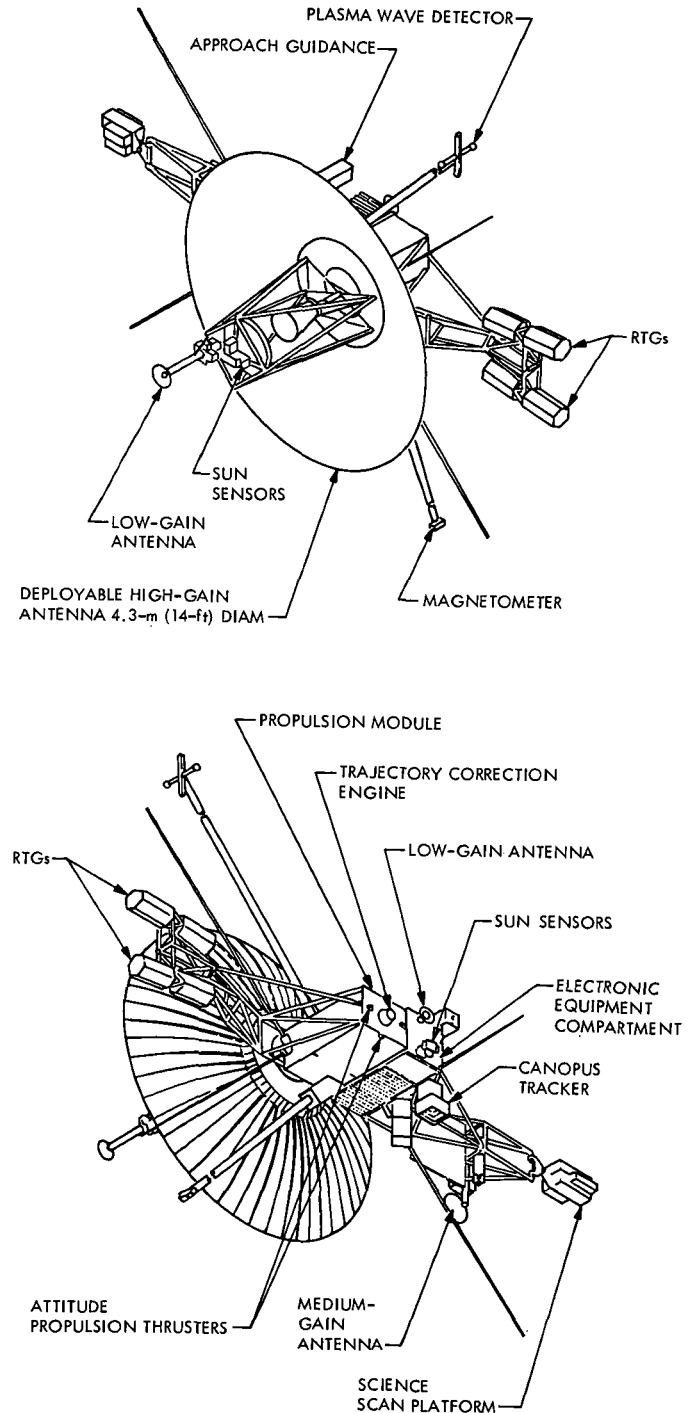


Fig. 1. Thermoelectric Outer Planet Spacecraft (TOPS)

¹The propulsion "system" is a spacecraft "subsystem," so system and subsystem are essentially synonymous in this report. The use of one term or the other depends on the context of the given section.

topics are presented in a separate report (Ref. 4). The APS report is recommended as a companion volume to this report because some of the results reported in detail there are relevant to the TCPS also.

C. Propulsion Program Objectives

The objectives of the supporting research and technology program for the trajectory correction propulsion capability required by TOPS-type missions were:

- (1) Determine the most cost-effective trajectory correction propulsion system for outer planet flyby missions.
- (2) Establish the optimum (mass/reliability) system configuration.
- (3) Assess the applicability of present system and component technology and hardware for the selected system.
- (4) Determine any new technology required for a TOPS-type propulsion system.
- (5) Develop any major components that cannot currently meet TOPS mission requirements.
- (6) Fabricate and test a prototype demonstration propulsion system for TOPS.
- (7) Evaluate the required interfaces with other spacecraft systems.
- (8) Develop a detailed propulsion system design for TOPS.

All of these objectives were fulfilled, although some, such as Nos. 3 and 5, were necessarily limited by the available resources.

II. TCPS System Configuration Selection

Mission requirements are the primary input for the system configuration selection process. Because TOPS mission requirements changed over the span of the project in response to new information, early analyses and decisions were always subject to review. The major change was the switch from a four-planet mission to a pair of three-planet missions. Fortunately, of these changes, only the changes in ΔV affected the propulsion subsystem through changes in propellant tank size (and further changes in tank size could be expected before a flight design is finalized).

The final TOPS mission requirements on propulsion listed in Table 1 summarize the TCPS Functional Require-

Table 1. Mission requirements for trajectory correction propulsion

A. Specific requirements		
No.	Item	Nominal value
1	Maximum ΔV (mean + 3σ)	205 m/s (673 ft/s)
2	Minimum single maneuver ΔV	1 m/s (3.28 ft/s)
3	Minimum number of maneuvers	9
4	Time from launch to last maneuver	9-10 yr
5	Rocket engine thrust	< 445 N (100 lbf)
6	Minimum service life (fueled)	10^5 h
B. General requirements		
7	Operational environment: <ol style="list-style-type: none"> (a) Space vacuum (b) Radiation (RTG's, Jovian belts) (c) Particles (asteroid belt) 	
8	Spacecraft design limits <ol style="list-style-type: none"> (a) Magnetic (b) Electromagnetic interference (c) Man-rated when fully pressurized 	

ments document (Ref. 5). The rationale behind each of the requirements follows:

- (1) The ΔV required for a flight to Jupiter, Uranus, and Neptune to be launched in 1979 (JUN79) is 205 m/s (673 ft/s). This capability compensates for planetary quarantine bias and flight trajectory and planetary ephemeris prediction errors. The two Jupiter-Saturn-Pluto (JSP76 and JSP77) missions require less capability, 167 m/s (548 ft/s). The only affect on the propulsion system caused by changes in this key requirement is a change in propellant tank size. The value of spacecraft nonpropulsive mass used for propellant mass calculations is 715.3 kg (1577 lbm).
- (2) Although the candidate propulsion systems can easily deliver less than 1 m/s (3.28 ft/s), there is no current need for that capability.
- (3) At least nine maneuvers are required for the three-planet missions. They are the one initial postlaunch correction, and two preencounter and one post-encounter maneuvers required at each planet except the last where the postencounter maneuver is unnecessary. The planned maneuver schedules for JSP77 and JUN79 are given in Table 2, and the JSP77 schedule is illustrated in Fig. 2. Eight maneuvers are planned for JSP77 and nine for JUN79, which sets the requirement. Capability to execute considerably more maneuvers is highly desirable.
- (4) The encounter with Pluto on a JSP mission occurs about nine years after launch and the encounter

Table 2. Typical maneuver schedules

Planet	JSP77 maneuvers		JUN79 maneuvers	
	Event	Elapsed time, days (yr)	Event	Elapsed time, days (yr)
Earth	Launch 1	Sep. 4, 1977 10	Launch 1	Nov. 4, 1979 10
	2	522	2	553
Jupiter	3	537	3	568
	Encounter 4	542 (1.5) 562	Encounter 4	573 (1.6) 593
	5	1131		
Saturn	6	1146		
	Encounter 7	1151 (3.2) 1171		
			5	2252
Uranus			6	2267
			Encounter 7	2272 (6.2) 2292
			8	3560
Neptune			9	3575
			Encounter	3580 (9.8)
			8	3270
Pluto	9 ^a			
	Encounter	3290 (9.0)		

^aNot currently planned.

with Neptune on a JUN mission occurs about ten years after launch. Actual flight times may be more or less than these nominal values. Notice also that as long as six years elapses between maneuvers on the JSP77 mission (Table 2).

- (5) Rocket engine thrust must be less than 445 N (100 lbf) to avoid applying unacceptable forces to spacecraft appendages during maneuvers. This requirement arises for outer planet missions because unheated booms can reach temperatures on the order of 60 K (-350°F), where even small shock loads might cause a brittle fracture. Low thrust also simplifies dynamic control of the spacecraft with its flexible booms and deployed masses.
- (6) The minimum service life of 10⁵ h (11.4 yr) is the sum of the 10-yr flight time, launch preparation and hold time, and some margin to cover possible increases in flight time to the last planet.
- (7) The outer planets spacecraft will explore a new environment, one where the influence of the sun becomes insignificant. The spacecraft must be resistant to nuclear radiation from the on-board RTCs and planetary radiation belts, and to micrometeor-

oids especially prevalent in the asteroid belt between Mars and Jupiter.

- (8) The desired thresholds for the magnetometer and the charged particle and other experiments result in magnetic and electromagnetic radiation field restrictions that can significantly impact system design. The system must also be designed so that it is safe for personnel to work around when fueled, pressurized, and armed.

The TOPS mission requirements are typical of outer planets flyby missions using launch vehicles as large as the Titan III. The likely range of each quantitative requirement should be considered in selecting the best system mechanization. Hopefully no major dividing points appear in any of the key variable ranges.

A. Basic System Selection

A cost effectiveness analysis based on mass, reliability, and cost was used to select the type of propulsion system that best satisfies outer planet flyby mission requirements. This analysis was completed early in the TOPS program when the baseline mission was the four-planet Grand Tour, JSUN77. At that time the ΔV requirement was 320 m/s (1050 ft/s) and the total spacecraft mass was 453.6 kg (1000 lbm) (the launch mass was fixed and the payload was a variable). All other requirements were identical with those listed in Table 1.

Two propulsion systems were analyzed: a monopropellant hydrazine system operating at a specific impulse of 2305 N-s/kg (235 lbf-s/lbm), and a bipropellant nitrogen tetroxide/monomethyl hydrazine system operating at a specific impulse of 2893 N-s/kg (295 lbf-s/lbm). Schematics of the competing systems are shown in Fig. 3. Both systems use blowdown pressurization where the original tank pressurization gas forces the propellant to the engine without the use of a high-pressure gas supply. Tank pressure and thrust decrease as propellant is expended, as opposed to their remaining constant in a pressure regulated system. Both the blowdown and pressure regulated systems were studied in the selection analysis. Also both systems rely on pyrotechnic-actuated (pyro) valves² for propellant isolation between maneuvers. Solenoid-actuated valves³ were considered for this application, but such valves did not appear capable of meeting mission leakage requirements at the time of the study.

²Pyrotechnic-actuated valves, often also called explosive valves, or squib valves, are referred to as pyrovalves throughout this report.

³Solenoid-actuated valves are referred to as solenoid valves throughout this report.

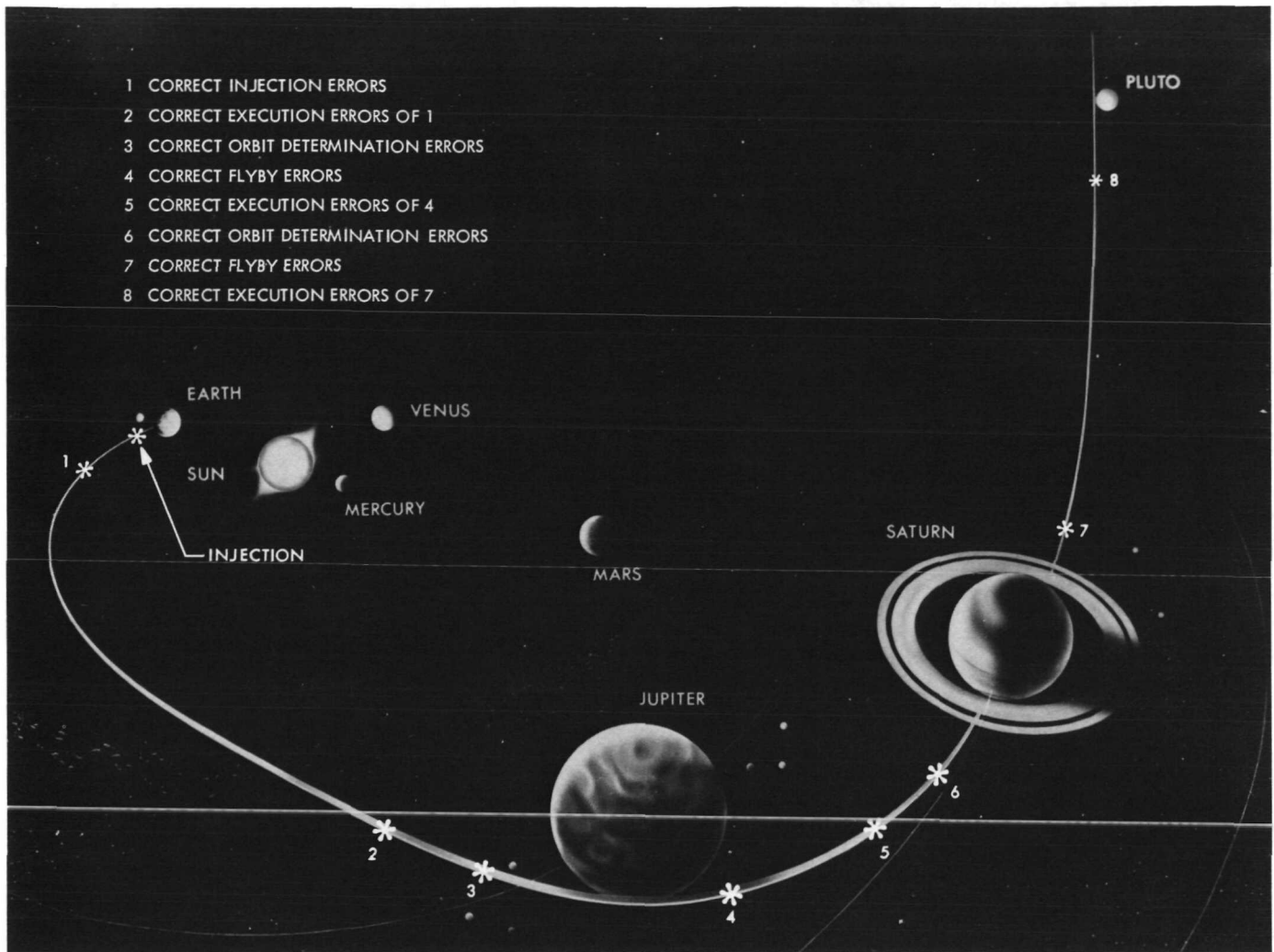


Fig. 2. Trajectory correction maneuver plan for JSP Mission

Propulsion system selection was based primarily on a quantitative comparison of mass, reliability, and cost. Reliability was the most difficult of these quantities: long-term data is not available and there is no agreement on the type of model that should be used to extrapolate short-term data. Under these circumstances, one-year reliability values were used for relative comparisons of the systems. Since the competing systems do not contain the same number of a particular component or the same components, system reliability is sensitive to ratios of the reliabilities of different components. Therefore a range of one-year reliability values was used in the study. The absolute values of system reliability were given no significance for the reasons just discussed—only the difference between systems was used.

The requirements of outer planets missions represent significant increases over those of previous planetary

missions. Some technological verification and component development will be required for these missions. The cost computations of the system selection study included both development and flight system costs.

The results of the propulsion system selection study are summarized in Table 3. The quantitative results are normalized to the monopropellant system and the qualitative factors are stated relative to that same system. Reliability, cost, and the qualitative factors favor the monopropellant, while mass favors the bipropellant. Cost is the major difference. The relative results are essentially the same if *both* systems are pressure regulated. Therefore the blow-down monopropellant hydrazine system was selected for outer planet flyby missions.

The sensitivity of the monopropellant selection to changes in required ΔV , and implicitly to changes in

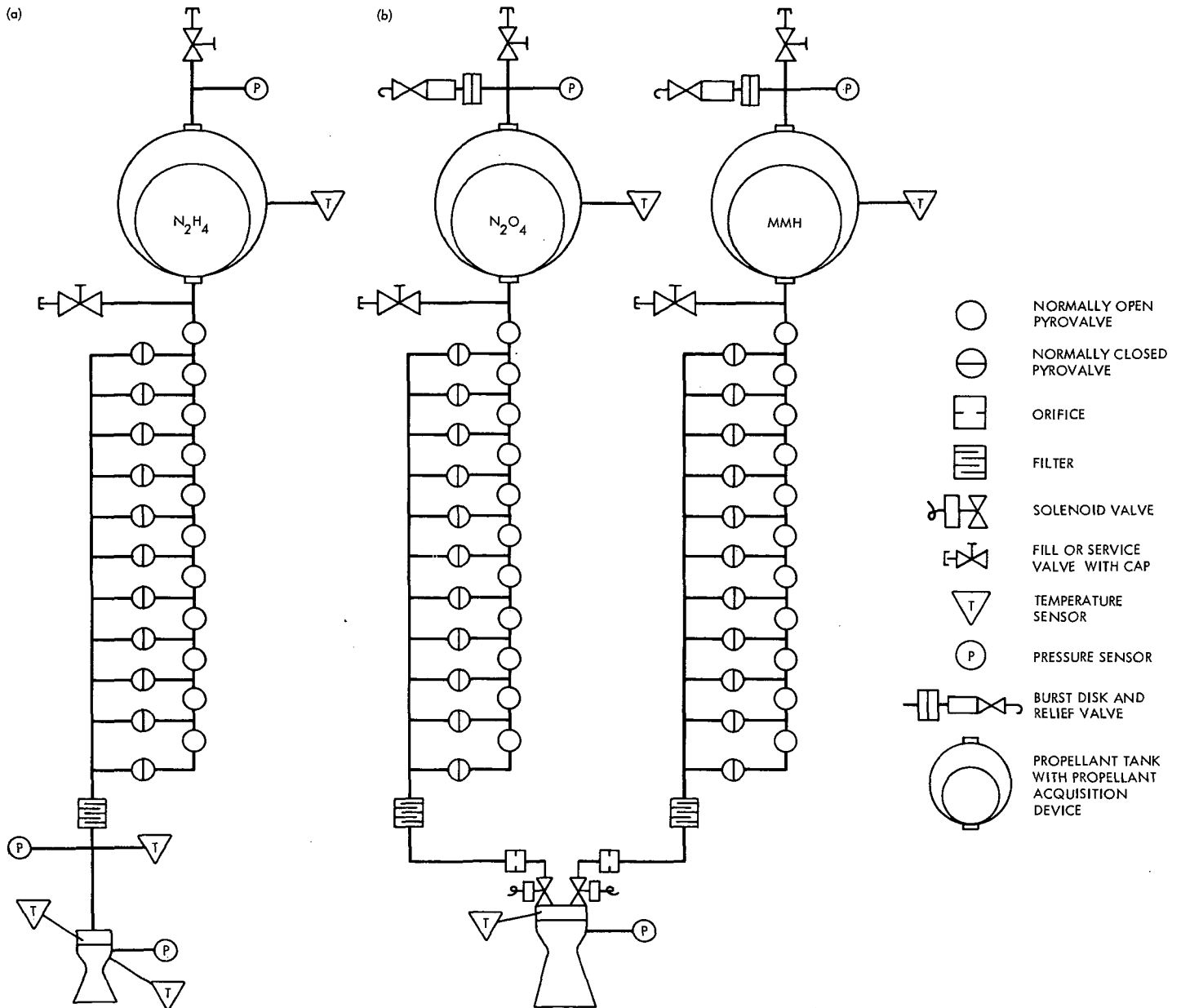


Fig. 3. Propulsion system configurations used in selection tradeoff study: (a) monopropellant; (b) bipropellant

Table 3. Results of monopropellant vs bipropellant study

A. Quantitative factors		
No.	Parameter	Advantage for
1	Mass: $(M_M - M_B)/M_M = +6.5\%$	Bipropellant system
2	Reliability: $(R_M - R_B)/R_M = +1.6\%$	Monopropellant system
3	Cost: $(C_M - C_B)/C_M = -62.5\%$	Monopropellant system
B. Qualitative factors		
In contrast with the monopropellant system, the bipropellant system has:		
4	Less long-term space experience	
5	Greater leakage potential	
6	Hotter, chemically more complex rocket exhaust	
7	Need for more electrical power	
8	No capability to incorporate a hot-gas attitude propulsion system (without adding a separate hydrazine tank)	

spacecraft mass, was determined from a cost-effectiveness analysis. The results of this analysis are shown in Fig. 4. A band of possible results is plotted rather than a single line to illustrate different possible levels of reliability. The high bound represents high component reliabilities and a high-reliability return for a small increase in system mass; the low bound represents low reliabilities and low-reliability return for a mass increase. An expected trend line is also shown.

The monopropellant system is clearly most cost effective for ΔV s less than 300 m/s (984 ft/s) where a monopropellant system advantage was found for the entire range of reliabilities. The trend line indicates the decision cross-over point is more like 700 m/s (2297 ft/s) for the 453.6-kg (1000-lbm) spacecraft studied. However, the final TOPS nonpropulsive mass increased to 715.3 kg (1577 lbm) while the ΔV decreased to 205 m/s (673 ft/s). The trend line adjusted for the increase in spacecraft mass indicates a monopropellant system advantage for ΔV s less than 335 m/s (1100 ft/s), so the original selection remains valid.

B. Configuration Selection

A second study was undertaken to determine the best configuration for the blowdown monopropellant hydrazine system. This study was also made when the four-planet Grand Tour was the baseline mission. The configuration used in the cost-effectiveness system selection study

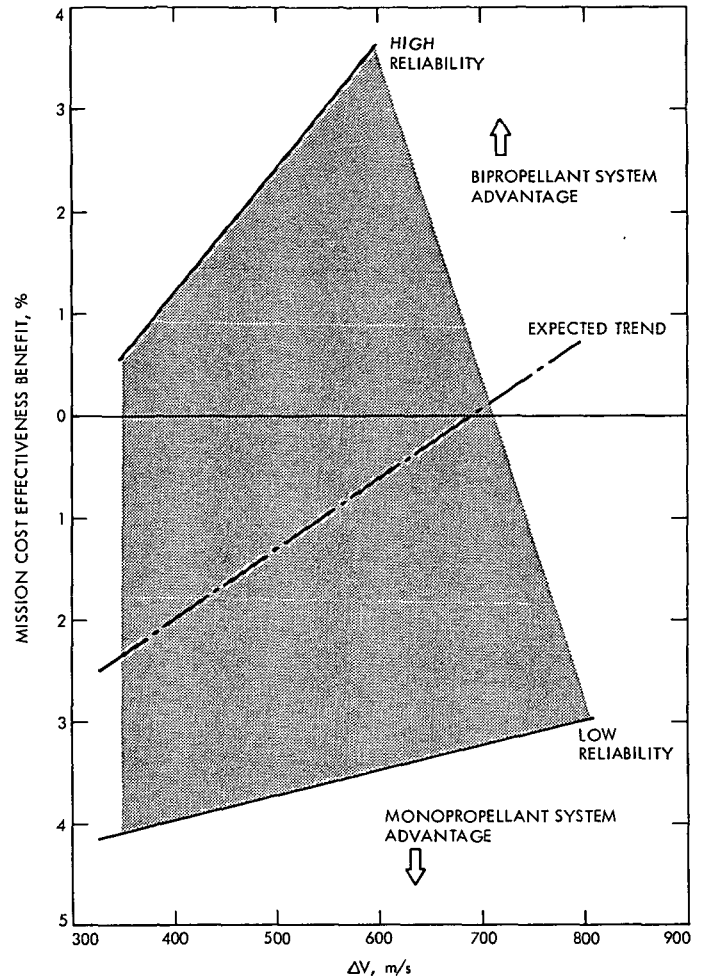


Fig. 4. Propulsion system cost effectiveness vs ΔV and reliability

(Fig. 3a) was not necessarily the best configuration. Many other configurations were examined, and ultimately reduced to the four additional candidates shown with the original configuration in Fig. 5. Other configurations featuring parallel-redundant tanks or engines were deleted because their small potential reliability improvement did not appear worth their increased complexity, mass, and cost.

Configuration (a) in Fig. 5 is identical to the configuration studied earlier: a pair of pyrovalves is provided for each of the nine required maneuvers and two pairs are provided for backup. Using solenoid valves instead of pyrovalves, configuration (e) makes the system more versatile by permitting an unlimited number of maneuvers. However, it was not obvious that solenoid valves could meet 10-yr leakage requirements. Configurations (b), (c), and (d) represent suitable compromises where pyrovalves

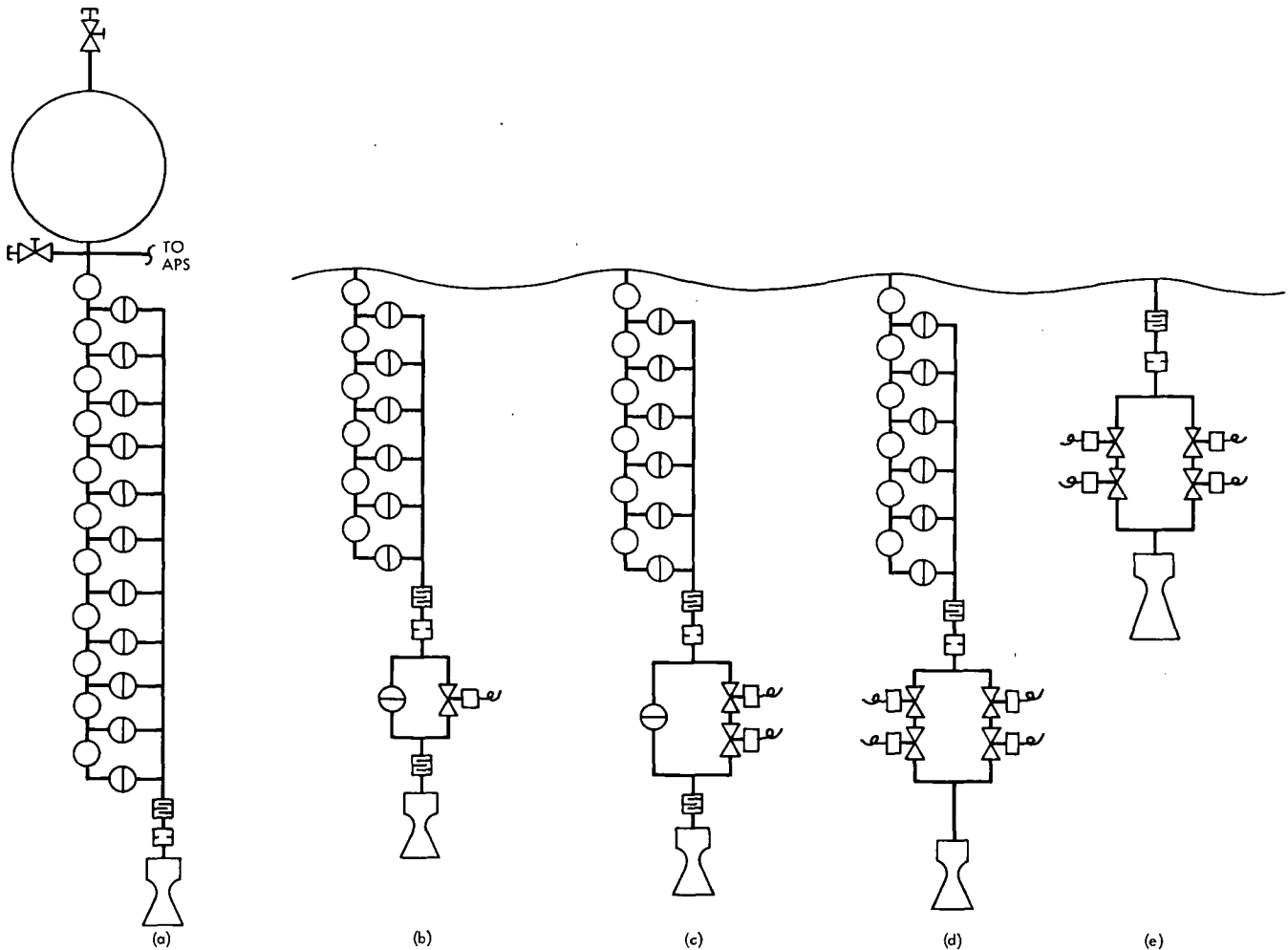


Fig. 5. TCPS configuration candidates

are used for cruise propellant isolation, and solenoid valves are used for engine control and encounter period propellant isolation.

A mass estimate was made for each of the system configurations. The spread in mass from the lightest to the heaviest was an insignificant 3.8%.

Configuration reliability was computed with three independent sets of component reliabilities. As discussed earlier, the absolute reliability values are unimportant—it is the relative ranking of system reliabilities computed from a single set of component reliabilities that is important. The greatest spread in the five system reliabilities calculated from a single set of component reliabilities was 2.0%, again insignificant. An attempt to compute system reliability as a function of elapsed time from launch and treating the different system states in detail was unsuccessful.

ful. Basic data or models of the reliability implications of system operation and aging were not available.

The results of the mass and reliability studies do not differ sufficiently to support the choice of one configuration over the others. A brief failure modes and effects analysis (FMEA) also was unable to differentiate between the candidate configurations. Two secondary considerations thus became important. First, there was concern that solenoid valves could not meet the 10-yr leakage requirement. Second, an objective of the propulsion program was to evaluate all types of components that might be used in propulsion systems for outer planets flyby missions.

For these reasons, configuration (d) in Fig. 5 was selected as the TOPS baseline TCPS. This selection does not commit future flight projects. Such projects can draw on results from the TOPS-TCPS program to fashion the best configuration for their specific requirements.

C. Thrust Vector Control Considerations

The thrust vector control (TVC) function is shared between the propulsion and attitude control systems. The exact location or nature of the interface between these systems depends on the type of TVC mechanization selected. A gimbal actuator system was selected at the outset of the TOPS program when it appeared that a bipropellant propulsion system would best meet the ΔV requirements of the four-planet Grand Tour. The competing system, jet vanes, could not operate in the high-temperature bipropellant engine exhaust.

The final selection of the blowdown monopropellant hydrazine system reported in Section II-A brought new TVC alternatives into consideration. The viable alternatives were identified in a brief study, but a detailed intersystem tradeoff study could not be scheduled. The four most promising TVC alternatives are based on:

- (1) Gimbal actuators.
- (2) Jet vanes.
- (3) Small auxiliary hydrazine pulse engines.
- (4) Replacing the single main engine with four engines that can be separately pulsed off—the four engines produce the same total thrust as the single engine.

The attitude propulsion subsystem does not appear on this list because the APS and TVC thrust requirements differ by about an order of magnitude.

Each of the TVC alternatives has a different impact on the propulsion and attitude control system designs. The optimum choice may not be optimum for one or both of the interfacing systems. Since the necessary resources were unavailable for such an intersystem study, gimbal actuators were retained for TOPS TVC.

D. Baseline TOPS TCPS

The final TOPS-TCPS configuration schematic for a three-planet mission is given in Fig. 6. This schematic is Fig. 5d with transducers added and one set of pyrovalves subtracted for a three- instead of a four-planet mission. The principal operational features of this monopropellant hydrazine system are best explained in terms of valving and pressurization.

The two valve functions are hydrazine isolation and flow control. The pyrovalves provide the multiyear cruise isolation while the solenoid valves, particularly the reserve unit, which will probably be a latching solenoid valve,

provide encounter isolation between the first preplanet maneuver and the last postplanet maneuver. The solenoid valve nearest the engine controls hydrazine flow to the engine. This configuration has up to two levels of redundancy for both the isolation and control functions.

When the appropriate valves are opened, hydrazine is forced from the tank to the engine by the original charge of nitrogen gas. There is no additional supply of gas to maintain constant tank pressure throughout the mission, as is done in pressure-regulated systems. Engine thrust decreases as tank pressure decreases with the outflow of hydrazine. The small decrease in performance seen at lower thrust is insignificant compared to the mass saving and reliability increase gained by using blowdown pressurization. The location of the hydrazine and nitrogen in the tank is controlled by a surface-tension-type propellant acquisition device. This device maintains a liquid prime from the tank to the controlling TCPS valve at all times so that no nitrogen other than that dissolved in the hydrazine is fed to the engine. Bubble-free operation is particularly important to the APS, which also draws hydrazine from the TCPS tank. Compared to the amount of hydrazine consumed in a single APS engine pulse, a nitrogen bubble would be quite significant (the TCPS/APS interface is treated in more detail in Subsection V-C-1).

The system requirements, configuration, and basic operational characteristics defined in this section are the criteria against which current component technology and designs must be evaluated.

III. Component Evaluation

The requirements of TOPS-type missions are more severe than those of past planetary flyby missions. Not only are the radiation and micrometeoroid fields more hazardous, but the spacecraft must operate far longer in them. Further, the magnetic and electrical fields generated in normal subsystem operation must be curbed to maximize science return. Thus it is not obvious that current component technology, and especially designs, are adequate for outer planets missions.

Component evaluation proceeded in two steps. First, surveys were made for each of the major propulsion components shown in Fig. 6 to locate the best available designs. Sample components of each type were tested. Those components passing the tests are considered adequate for flight, although ideas for improvement may have arisen in the course of the program.

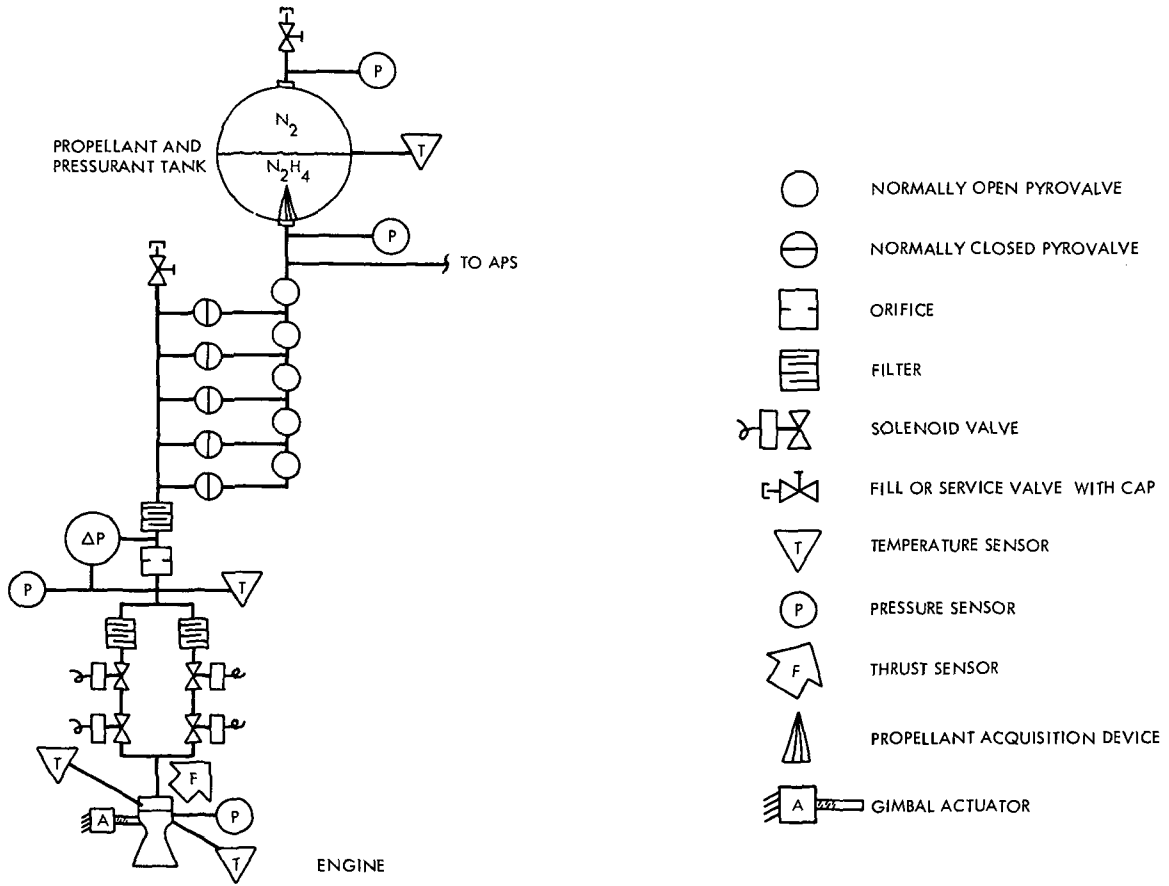


Fig. 6. TOPS-TCPS baseline system schematic diagram

Second, where test components were judged inadequate, the focus shifted to evaluation of the supporting technology. A judgement was made whether design improvements would produce an adequate component for flight use, and in some cases the improvements were tested. The development of new component designs was limited to relatively straightforward changes to the simpler components.

The evaluation of each major component is described in one of the following subsections.

A. Rocket Engine

A monopropellant hydrazine rocket engine system was found most cost effective for TOPS-type missions. Engines of this type have been used on lunar and planetary spacecraft since the beginning of the space program. The evaluation program focused on the increased number of starts and the longer cumulative firing time required. The possibility of using a mixture of 76% hydrazine (N_2H_4) and 24% hydrazine nitrate ($N_2H_5NO_3$) for increased performance and better thermal properties was also investigated.

1. Thrust limitation. The dynamic behavior of the TOPS spacecraft during rocket engine firing was analyzed early in the TOPS program. The primary concern was the structural integrity of the magnetometer booms at 60 K ($-350^\circ F$) under loads induced by engine start and stop transients. The question of whether the autopilot used on Mariner spacecraft could control the TOPS spacecraft, with its deployed RTGs and science instruments and the long magnetometer booms, during engine operation with adequate margin was also of concern.

The result of this simulation analysis was to put a limit on spacecraft acceleration of about 1 m/s^2 (0.1 g), which limited engine thrust to a maximum of 445 N (100 lbf). This limit presented no hardship since most developed monopropellant hydrazine engines were designed for lower thrust applications.

2. Test program objectives. Although there had been extensive development experience with catalytic hydrazine engines over the past several years, the applications had been either those that demanded one or two short duration (5- to 100-s) steady-state firings (Refs. 6, 7, and 8) or those that operated in a pulsed mode (Ref. 9). There was a lack of necessary empirical information about the combined effects of long duration (800 s or longer) steady-state firings, and multiple starts with both propellant and hardware at low temperatures (277 to 289 K (40 to $60^\circ F$)),

on monopropellant engines using the spontaneous Shell-405⁴ catalyst.

The characteristics and availability of off-the-shelf spontaneous catalytic monopropellant engines in the 89- to 267-N (20- to 60-lbf) thrust range were explored by means of an industry survey. Analysis of the responses to this survey showed that the design life of all available engines was less than that of the TOPS requirement, and that several of these engines had been designed primarily for pulse-mode, rather than steady-state operation. Thus, it was imperative to determine the capabilities of state-of-the-art catalytic hydrazine engines in this category to meet the requirements of the TCPS duty cycle.

Life tests were conducted on several immediately available experimental engine configurations, and on two flight-type engines purchased from industrial sources. The objectives of these test firings with hydrazine were (1) to demonstrate at least 9 starts and 1600-s cumulative firing duration without significant engine performance degradation, and (2) to expose any engine or catalyst problems that might be associated with the TOPS-TCPS duty cycle.

To achieve better overall system performance, a binary blend of 75% anhydrous hydrazine, 24% hydrazine nitrate by mass (with 1% water impurity) was initially considered as the baseline for the advanced technology program because this blend offers a 6% increase in specific impulse and a 9% increase in density compared to hydrazine. In addition, the blend has about a 17 K ($30^\circ F$) lower freezing point (257 K, $4^\circ F$) than hydrazine (274 K, $34^\circ F$). The lower freezing point is a definite advantage in missions to the far reaches of the solar system, where thermal control becomes increasingly difficult. However, both types of engines would use the same tankage, and the state of development for both is far more advanced with hydrazine than with any hydrazine blend. Second, while the Shell-405 catalyst will spontaneously initiate the nitrate blend decomposition reaction at ambient temperatures, serious doubt existed as to whether it could operate for a long time with up to 10 ambient temperature restarts because of its known surface area deterioration as a result of a solid phase transition at the higher steady state decomposition temperatures of the nitrate.

Thus, a secondary objective was to evaluate the capability of the Shell-405 catalyst to repeatedly start the nitrate blended fuel and to maintain its integrity in the high operating temperature. Preliminary investigations of

⁴A product of Shell Development Company, Houston, Texas.

noncatalytic configurations that might perform satisfactorily with this propellant were also carried out. Modifications of existing flight-type monopropellant hydrazine engines were used in these experiments.

3. Engine hardware. The various thrust-chamber configurations employed are summarized in Table 4. In most cases, the fuel decomposition zones in the engines consisted of a shallow upstream (or upper) bed of relatively fine catalytic particles to ensure smooth, rapid ignition, and a deeper downstream (or lower) bed of relatively coarse catalytic particles to sustain the monopropellant decomposition. The characteristic lengths (L^*) shown in Table 4 are in each case the quotient of the empty chamber volume (on a catalyst-free basis) and the nozzle throat area. The design value of the catalytic-bed loading (superficial mass velocity) is also given for each engine.

One "workhorse" engine used for long-duration firings with hydrazine was a bolt-up 102-N (23-lbf) thrust engine available from a previous program (Ref. 10). It is listed as configuration Nos. 1 and 2 in Table 4 and is illustrated in Fig. 7. This engine had been originally designed for fast response in pulse-mode operation. Both versions (Nos. 1 and 2) were identical except for the catalytic-particle size in the lower bed. The upper bed was retained by a 3.17-mm- (0.125-in.-) thick plate welded to a central spud on the injector body. This prevented void formation in the upper bed. Three high-response, 0.125-mm- (0.005-in.-) diam chromel-alumel thermocouples were installed in the upper bed.

Another engine used for extensive life testing was a 111-N (25-lbf) thrust engine (configuration No. 3 of Table 4) obtained on loan from the Air Force (Titan Tran-

Table 4. Description of thrust chambers

Chamber configuration		Catalyst configuration		Injector configuration	Characteristic length L^* , m (in.)	Design value of bed loading G , kg/m ² -s (lbm/in. ² -s)
No.	Identification	Upper bed	Lower bed			
1	102 N (23 lbf), Boltup ^a	Shell 405, 25-30 mesh	Shell 405, 8-12 mesh	Showerhead, 0.64-mm (0.025-in.) diam orifices, circular pattern	0.37 (14.5)	49.2 (0.070)
2	102 N (23 lbf), Boltup ^a	↓	Shell 405, 14-18 mesh	Showerhead, 0.64-mm (0.025-in.) diam orifices, circular pattern	0.37 (14.5)	49.2 (0.070)
3	Transtage ^b 111 N (25 lbf), S/N 0110, with Moog valve		Shell 405, 3.2- × 3.2-mm (1/8- × 1/8-in.) pellets	Rigimesh	1.40 (55.0)	34.5 (0.049)
4	Transtage ^b 111 N (25 lbf), S/N 0110 (refurbished), with Moog valve		Shell 405, 25-30 mesh	Shell 405, 3.2- × 3.2-mm (1/8- × 1/8-in.) pellets	Rigimesh	1.40 (55.0)
5	Model R-24C ^c 111 N (25 lbf), P/N X27400, S/N 0001, with R-4D valve	Single bed of Shell 405, 25-30 mesh		Nine penetrant orifices	0.71 (27.8)	22.6 (0.032)
6A	Mariner 1969 222 N (50 lbf), Boltup	Shell 405, 25-30 mesh	Shell 405, 3.2- × 3.2-mm (1/8- × 1/8-in.) pellets	Showerhead orifices	1.63 (64.0)	32.4 (0.046)
6B	Mariner 1969 222 N (50 lbf), Boltup	Shell 405, 25-30 mesh	Shell 405, 3.2- × 3.2-mm (1/8- × 1/8-in.) pellets	Showerhead orifices	1.02 (40.0)	32.4 (0.046)

^aProduct of Rocket Research Corp., Redmond, Wash. Delivered to JPL under Contract No. NAS 7-583.

^bProduct of Rocket Research Corp., Redmond, Wash. Pulse-mode engine used for attitude control on Transtage of the Titan launch vehicle.

^cProduct of the Marquardt Co., Van Nuys, Calif. Modified version of pulse-mode engine made for Sandia Corp. for a classified military application.

Table 4 (contd)

Chamber configuration		Catalyst configuration		Injector configuration	Characteristic length L^* , m (in.)	Design value of bed loading G , kg/m ² -s (lbm/in. ² -s)	
No.	Identification	Upper bed	Lower bed				
6C	Mariner 1969 222 N (50 lbf), Boltup	Shell 405, 25-30 mesh	HA-3, ^d 3.2- × 3.2-mm (1/8- × 1/8-in.) pellets	Showerhead orifices ↓	1.02 (40.0)	32.4 (0.046)	
6D	Mariner 1969 222 N (50 lbf), Boltup	Shell 405, 25-30 mesh	HA-3, ^d 3.2- × 3.2-mm (1/8- × 1/8-in.) pellets		0.74 (29.0)		
6E	Mariner 1969 222 N (50 lbf), Boltup	Shell 405, 14-18 mesh	H-7, ^e 4.75-mm- (3/16-in.-) diam spheres		0.74 (29.0)	32.4 (0.046)	
7	Mariner 1969 flight spare 222 N (50 lbf), S/N 008	Shell 405, 20-30 mesh	75% Shell 405 and 25% HA-3, 3.2- × 3.2-mm (1/8- × 1/8-in.) pellets	Showerhead orifices	1.63 (64.0)	24.7 (0.035)	
8	Thermal with catalytic pilot	Esso 500, ^f 14-18 mesh	6.3-mm- (1/4-in.-) diam high carbon steel balls	Single orifice, 0.56-mm- (0.021-in.-) diam	0.05 ^g (2.1)	— —	
9	Thermal with catalytic pilot	Esso 500, ^f 14-18 mesh	Empty	Single orifice, 0.56-mm-(0.021-in.-) diam	0.21 (8.3)	— —	

^dJPL catalyst, manufactured by Harshaw Chemical Co., Cleveland, Ohio. Cylinders of porous alumina saturated with equimolar solution of iron, nickel, and cobalt nitrates.

^eSame as footnote d, except for geometry.

^fProduct of Esso Research Labs, Linden, New Jersey.

^g L^* of the pilot catalytic bed alone; L^* of thermal bed was 13.5 m (532 in.).

stage) hydrazine retrofit program. It had already accumulated 380 s of pulse-mode operation in a flight qualification program, so it could not be considered a new engine. However, since the design life was 1000 s, and since it was a highly developed flightweight and flight-qualified engine, it was felt that valuable information on its life potential could be obtained in spite of its prior test history. This engine is represented in Fig. 8, along with its important dimensions. After extensive testing (discussed in Subsection III-A-7), it was returned to the manufacturer for refurbishment, which consisted principally of replacing the used catalyst with fresh, and the injector with a new one. The refurbished engine is identified as configuration No. 4 in Table 4.

Engine configuration No. 5 was a modified version of a pulse-mode engine proposed to Sandia Corporation by the Marquardt Company for a military application. The test

history on this engine prior to its delivery to JPL was limited to several hundred seconds firing time on a single prototype engine and two 20-s calibration firings on the delivered engine. It is shown with its key dimensions in Fig. 9. This engine was different from the others evaluated in several respects. It had a single, rather shallow spring-loaded bed of uniformly sized catalytic particles, and used nine penetrant injectors (which injected hydrazine nearly radially within the bed) in contrast to the showerhead injectors employed in the other configurations. Engine No. 5 was furnished with very small (1.59-mm (0.0625-in.)) outside diam tubing pressure taps.

Configurations Nos. 6 and 7 were used in test-firings with the hydrazine/hydrazine-nitrate monopropellant blend. No. 7 was a welded flight version of the Mariner 1969 trajectory correction engine, while No. 6 in its several variations was a bolt-up, take-apart version of the same

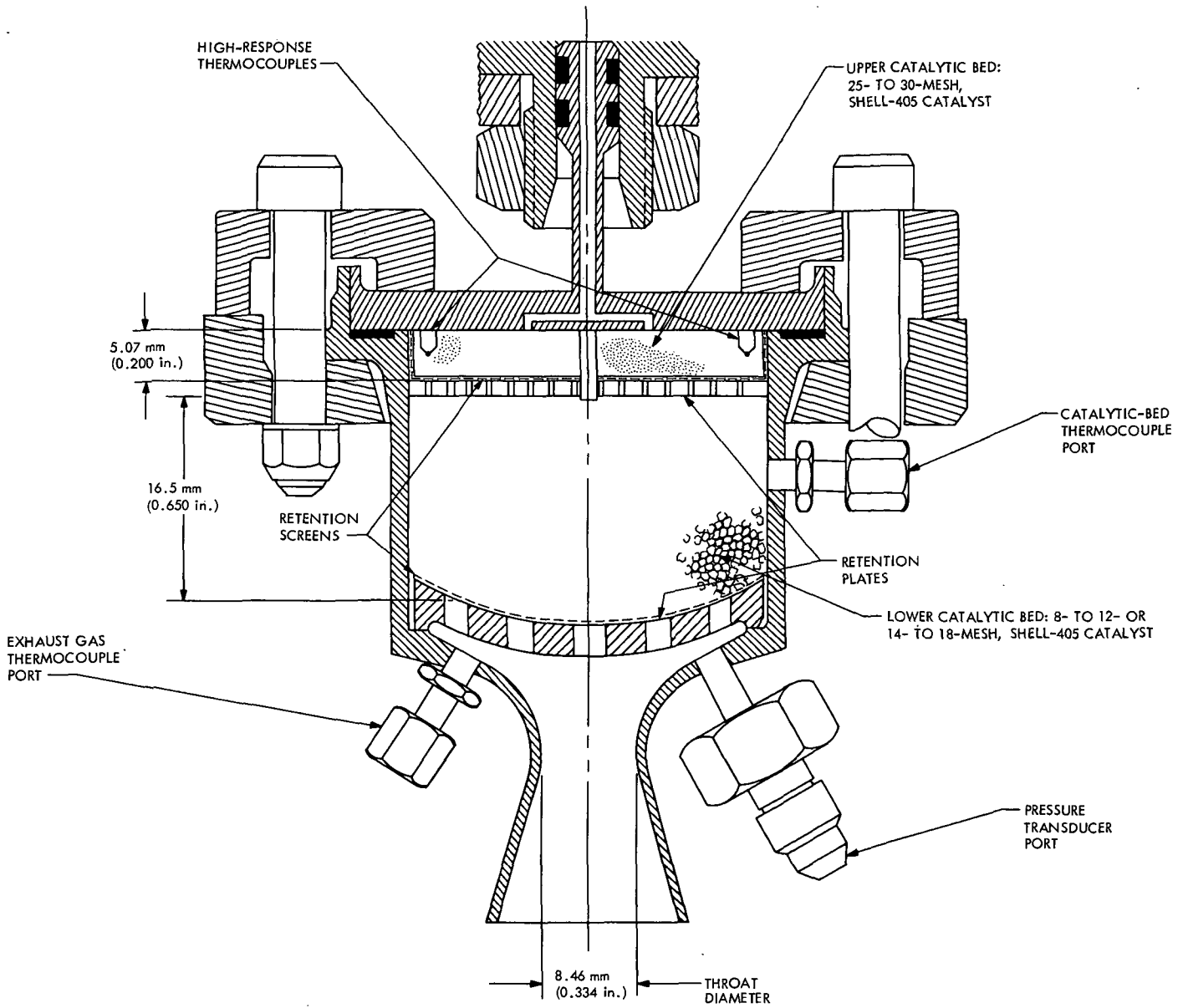


Fig. 7. Bolt-up 102-N- (23-lbf-) thrust hydrazine engine (configuration Nos. 1 and 2, Table 4)

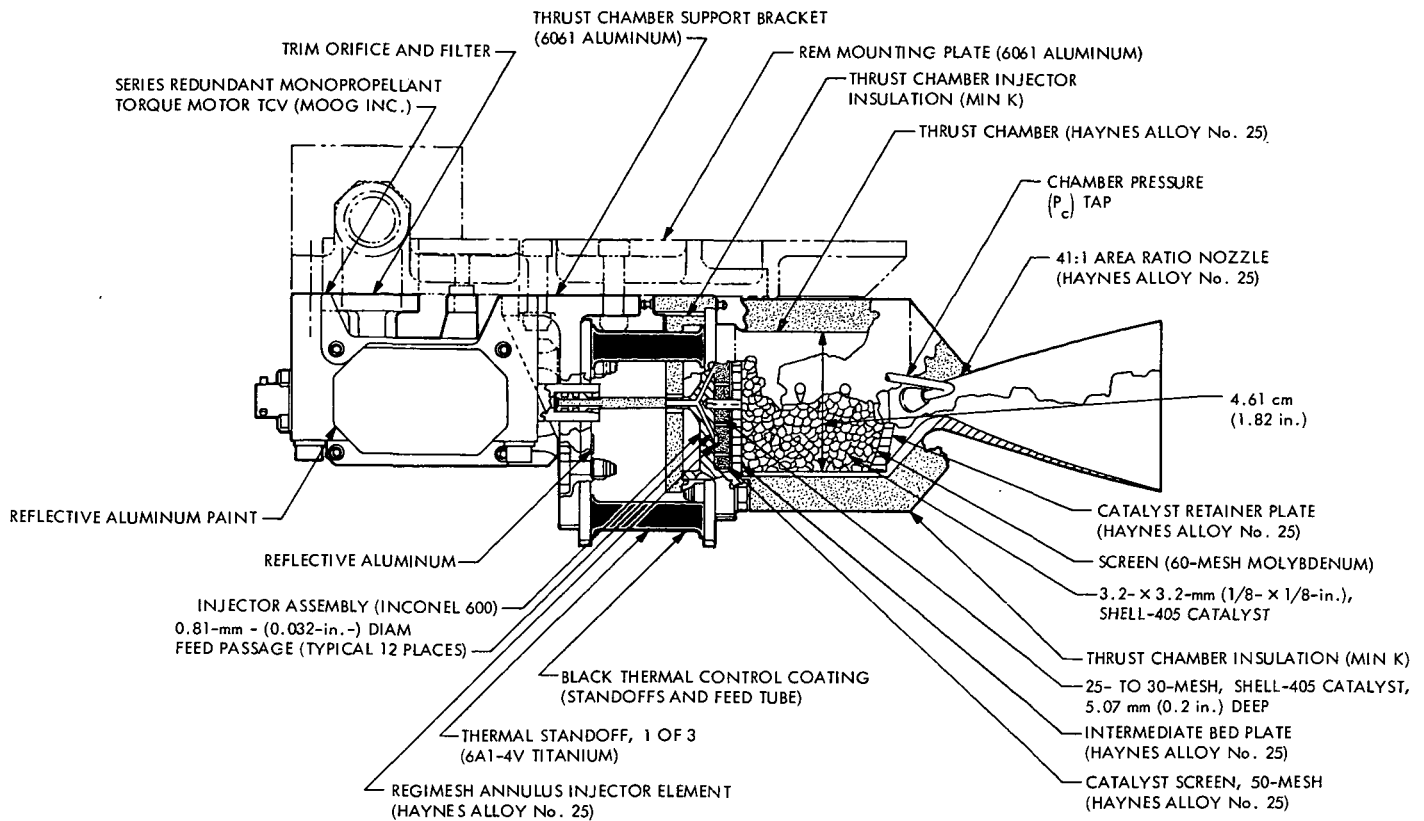


Fig. 8. Transtage monopropellant hydrazine rocket engine assembly (configuration Nos. 3 and 4, Table 4) (from Ref. 17)

engine, which permitted systematic evaluation of various catalytic combinations and catalytic-bed lengths (by means of variable-length spacers) with the nitrate blend. Three thermocouples were located in the lower bed. Configurations No. 6 and 7, and their key dimensions, are depicted in Figs. 10 and 11.

Preliminary evaluation of a new catalyst (Esso 500) was done using a modified chamber (configuration Nos. 8 and 9) from the Ranger program (Ref. 6). This concept uses a thermal decomposition chamber started by a pilot catalytic bed. In configuration No. 8, the lower bed was filled with steel balls, while in configuration No. 9 it was empty. Figure 12 shows an exploded view of configuration No. 9.

The basic philosophy of the concept follows. The pilot-bed fuel flow, from 10 to 25% of the full-rated value, would be catalytically decomposed in the normal manner. This flow would heat the inside of the chamber as well as some heat sink material. After 0.5 to 4.0 s of pilot flow, the main flow would be cut in, simultaneous with, or slightly leading, the pilot-bed flow cutoff. The pilot-bed catalyst temperature would then be reduced below the high flame temperature of the nitrated fuel. Since the reduction of

catalyst surface area in a rocket chamber is time and temperature dependent, reducing the time the catalyst sees the maximum temperature should increase its life and restart capability. To date, however, only the catalytic pilot-bed part of this chamber concept has been studied.

4. Test facility, procedures, and conditions. All firing tests were conducted at the JPL Pasadena facility. The cleanliness of the flow system and provisions of the operating procedures were reviewed before testing to reduce the possibility of the facility or propellant contaminating the valves or engines during the life tests. No extensive contamination was found, but several procedures were modified to further reduce any potential problems. The analysis of the hydrazine used in the life tests was: hydrazine 99.03%, ammonia 0.42%, aniline 0.25%, and water 0.30% by weight.

The engines were mounted to fire vertically downward against ambient back pressure at the nozzle exit, because of the unavailability of a vacuum chamber at the test site. Exhaust gas flow in the altitude expansion nozzles would thus have been separated, and posttest contact of the catalyst with ambient air might have resulted in its high-temperature oxidation and rapid degradation.

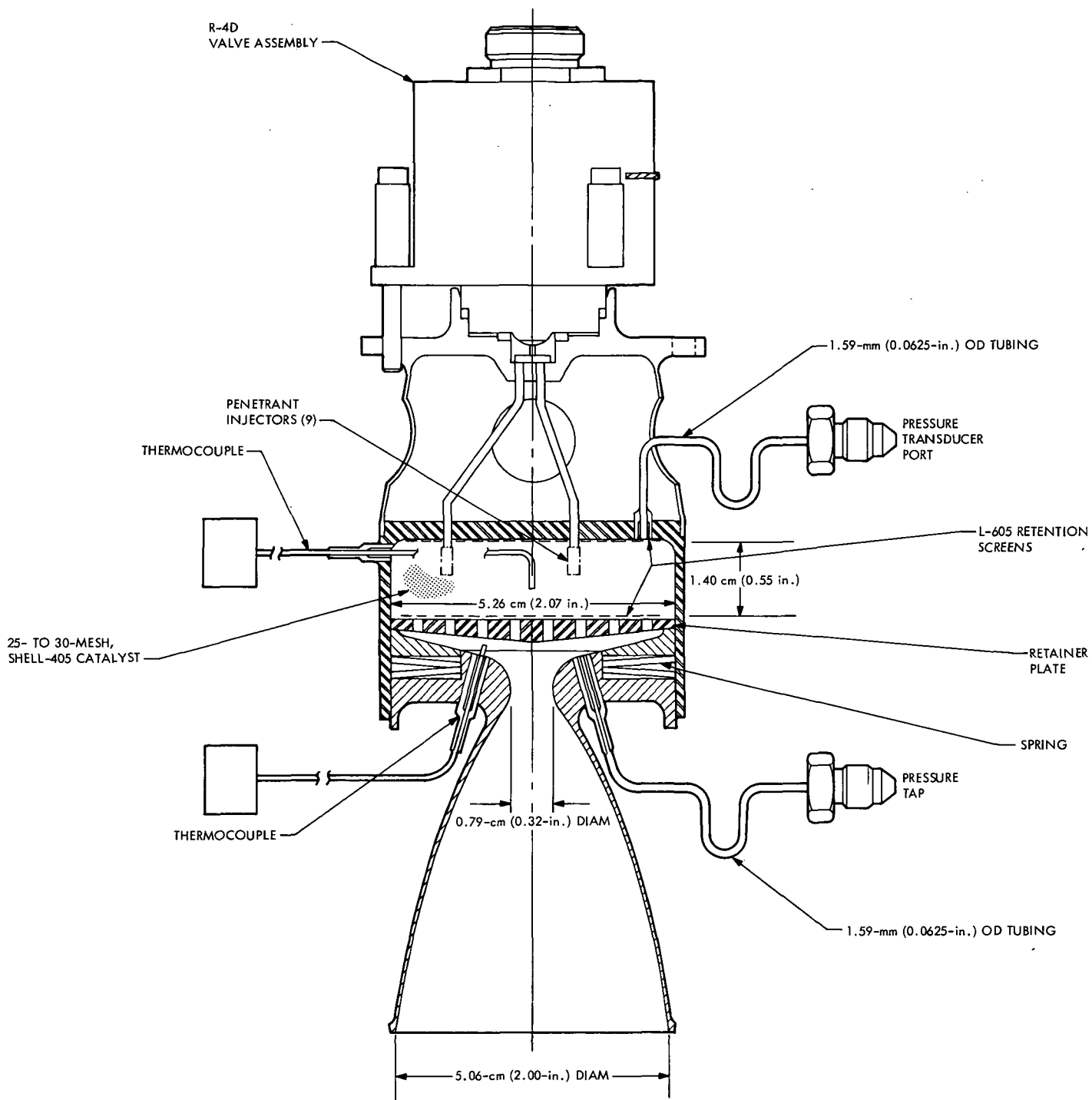


Fig. 9. R-24C experimental monopropellant engine (configuration No. 5, Table 4)

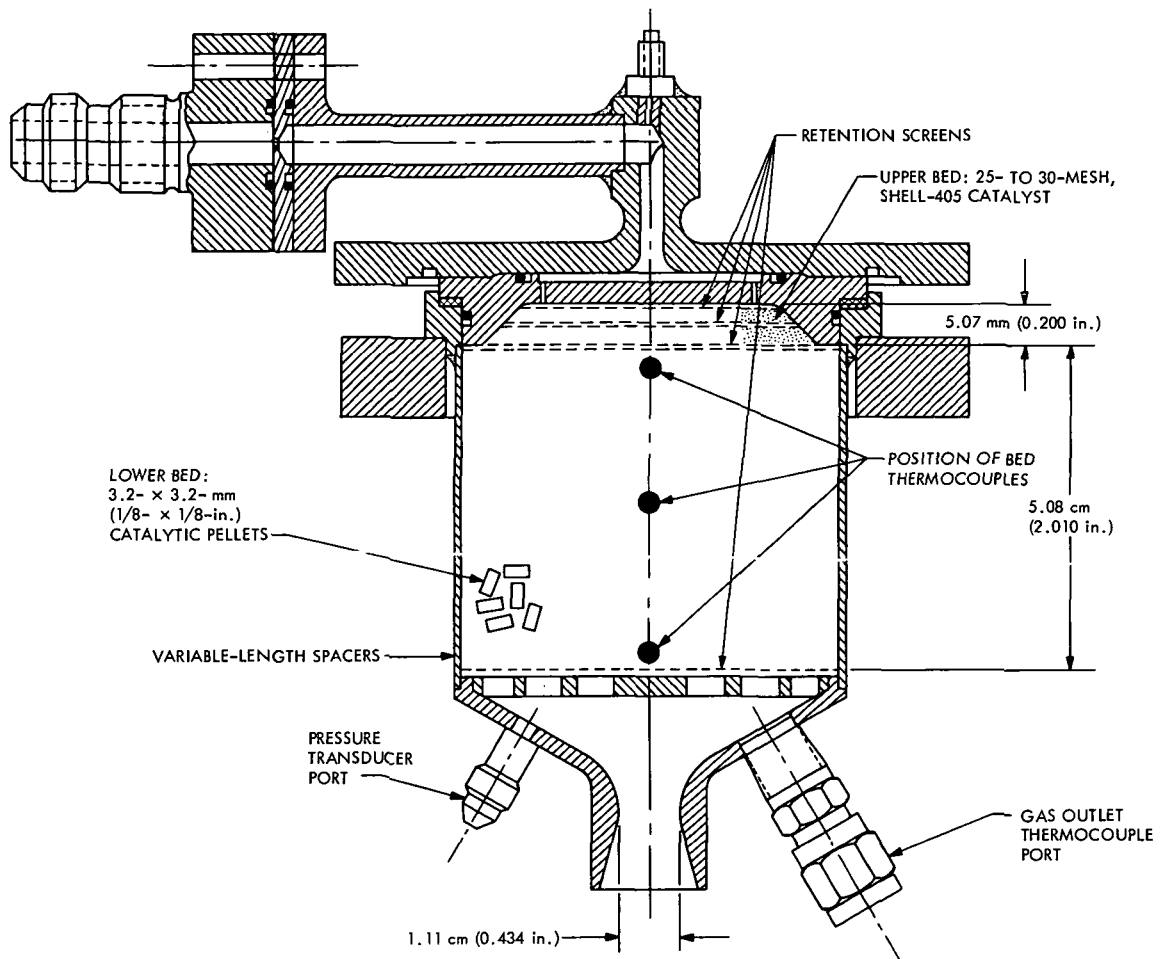


Fig. 10. Bolt-up Mariner Mars 1969 222-N (50-lbf) thrust trajectory correction engine (configuration Nos. 6A through 6D, Table 4)

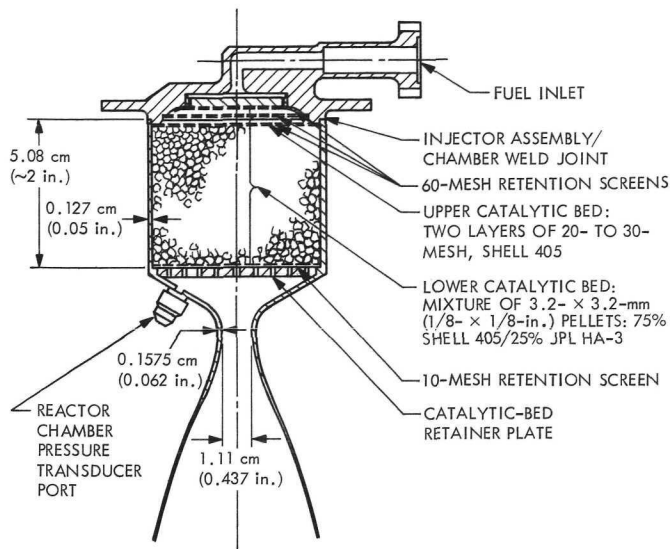


Fig. 11. Welded flight version of Mariner Mars 1969 222-N (50-lbf) thrust trajectory correction engine (configuration No. 7, Table 4)

Flow separation was deemed acceptable for those engines with high area-ratio expansion nozzles (configuration Nos. 3, 4, 5, and 6 of Table 4). For all *experimental* engines (configuration Nos. 1, 2, and 6) an automatic nitrogen purge, actuated upon engine shutdown, purged any propellant remaining in the fuel lines out through the engine, and blanketed the catalytic bed with an inert atmosphere until it had cooled sufficiently that a high-temperature oxidation reaction with ambient air could no longer occur.

For the purchased *flight* engine configurations Nos. 4 and 5 of Table 4, the gaseous nitrogen (GN_2) purge was eliminated to preclude catalyst (and therefore engine-life) degradation as a result of the thermal shock of cold purge gas contacting a hot bed. These engines were protected from ambient air by applying a vacuum of about 0.94 N/m^2 (7×10^{-3} torr) to the nozzle exit by means of a blowoff cap that was physically replaced on the nozzle within 30 s after engine shutdown. This partially simu-

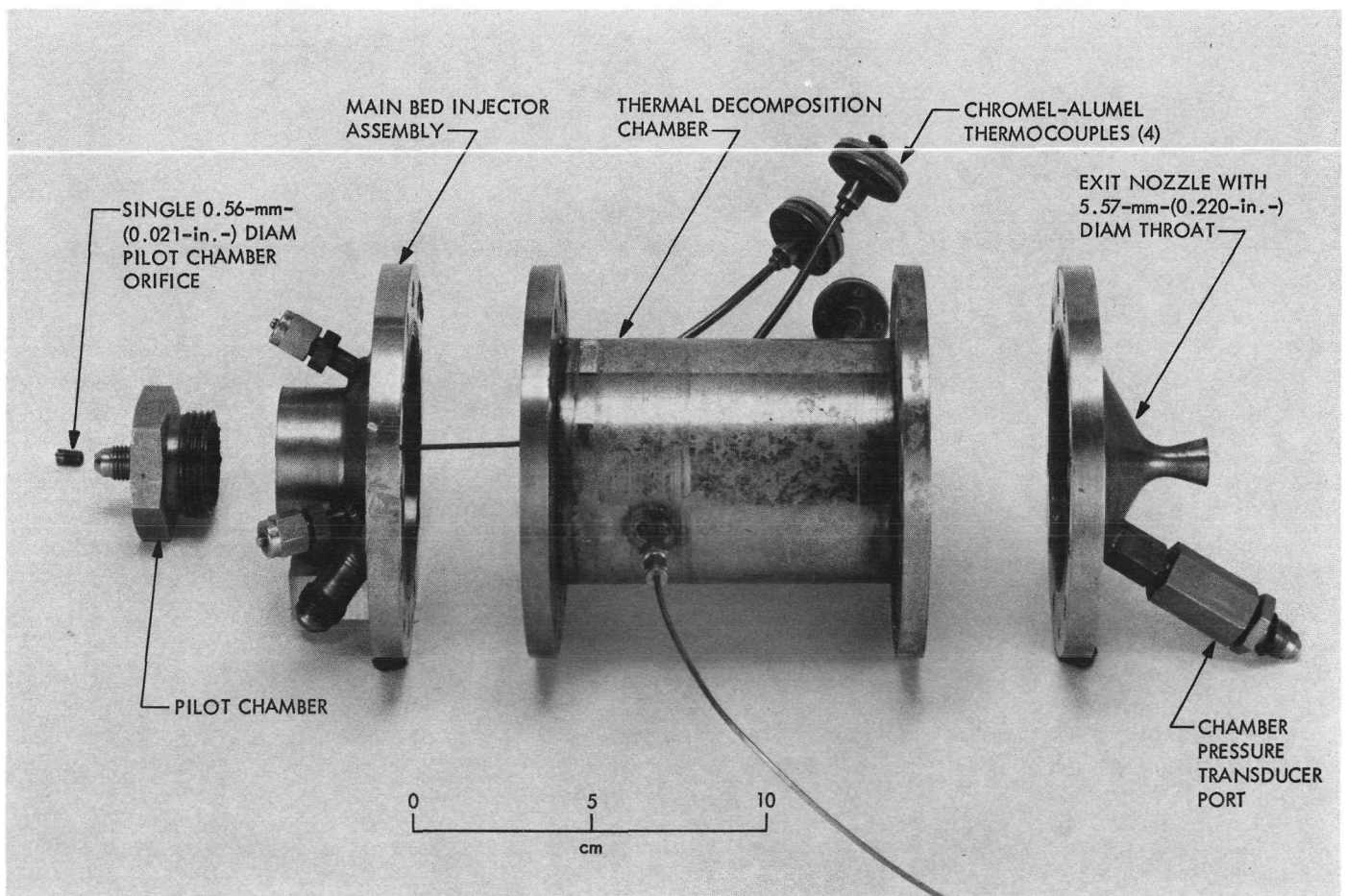


Fig. 12. Exploded view of thermal bed with catalytic pilot starter (configuration No. 9, Table 4)

lated space startup and postfiring bed cooldown conditions, which was important because both ignition delay and catalyst life are believed to depend to some extent on catalyst history and conditioning.

Propellant inlet temperatures were controlled between 277 K (40°F) and 311 K (100°F) depending on the experimental conditions desired. Engine hardware was at ambient temperature before firing, except for configuration Nos. 4 and 5, where it was maintained at about 277 K (40°F) by a chilled brine solution circulated through a rubber jacket surrounding the thrust chambers. Prior to each test, the fuel line between the fire valve and a facility safety valve was evacuated by means of a water aspirator. Then the line to the fire valve was filled under gravity feed. This minimized startup delays due to system hydraulic lags.

To simulate postlaunch TCPS engine firing conditions, engine configuration Nos. 4 and 5 were subjected to environmental vibration and acoustic noise tests prior to hot firing. The test conditions were obtained from the pre-release version of the TOPS Environmental Requirements document (Ref. 11). Facility acceleration limiter trips precluded the desired vibration level from being obtained in the transverse axes for both engines due to resonant responses. Limiter trips were also encountered with engine No. 5 in the sinusoidal vibration tests, but these were suspected to be the result of high-frequency resonant oscillation of the R-4D valve (the Moog valve was not installed on engine No. 4 because the catalytic bed was the component under investigation, and to facilitate fixturing). However, both engines were subjected to 147 m/s² (15 g) rms. in the longitudinal axis (thrust direction). No catalytic particles or fines were observed with engine No. 4 after the tests. Two grains of catalyst were found in the nozzle exit of engine No. 5 after the first vibration period. No further catalyst was shaken out during the remaining exposures. In general, both engines completed the environmental tests in good condition.

Test conditions and results are summarized in Table 5 for those firings made with hydrazine, and in Table 6 for those made with hydrazine/hydrazine nitrate.

All propellant flow rate measurements were made with turbine-type flow meters. Chamber pressure was measured with strain-gage-type transducers at static-pressure taps located in the entrance region of the converging portion of the nozzle, at contraction area ratios of approximately 10.

Because of these large area ratios, the measured pressures were taken as stagnation values. Injector manifold pressure was measured only for engine configuration Nos. 4 and 5, where ignition overpressure on startup was of primary interest. Ignition delay is defined as the time from the electrical signal to the fire valve to the time when chamber pressure reached 2% of its final steady-state value. The throat areas used in calculating values of c^* were not corrected for thermal changes during the firings, except for Tests 29 through 46. Pressure drops across the catalyst beds are not reported in Tables 5 and 6 because, with the exception of engine configuration No. 5, the engines tested did not have pressure ports at the upstream end of their beds. Engine No. 5 had a drop of 551 kN/m² (80 lbf/in.²) at a propellant mass flow of 0.034 kg/sec (0.075 lbfm/s).

As will be discussed subsequently, significant changes in flow rate and chamber pressure occurred during Tests 1 through 21 because of a phenomenon known as "wash-out." For these tests, therefore, the columns in Table 5 headed, "Flow rate," "Bed loading," and "Chamber pressure" show dual values, except for Test No. 17 where washout did not occur, and No. 21 where bed loading did not change significantly. The first number in each case is the value at about 10 s after ignition, and the second number is the value measured just prior to engine shutdown. Because of the relatively high chamber pressure roughness encountered in Tests 22 through 28, which increased with firing duration, flow rate and chamber pressure for these tests were measured only 10 s after ignition. For the remaining tests in Table 5, the values of these three parameters were recorded just prior to shutdown.

Because of an instrumentation recording system failure on the day on which Tests 38, 40, 41, and 43 were conducted, digital data were not recorded on tape for these tests. Consequently, the flow rates reported for Tests 38, 40, 41, and 43 in Table 5 were estimated from their corresponding tank pressures and the relationship between flow rate and tank pressure known from the other tests with configuration No. 5. Bed loadings were derived from the estimated flow rates in the usual manner. Values of characteristic velocity just prior to shutdown for these four tests were derived from the known chamber pressure and throat area, and the estimated flow rates.

5. Test firing results with hydrazine propellant. One series of tests (1 through 10 in Table 5) was conducted to demonstrate the capability of a state-of-the-art thrust

chamber (configuration No. 1 of Table 4) to meet the TOPS-TCPS engine total life requirements and 10 ambient (283 to 294 K (50 to 70°F)) temperature starts with hydrazine. For Tests 1 through 5, the fuel tank pressure was progressively decreased from one firing to the next, both to simulate TOPS blowdown mode operation, and to evaluate engine behavior at off-design conditions. In a like manner, the fuel inlet temperature was decreased in small steps from Test 1 through Test 5 to simulate progressively cooler propellant temperatures as an outer planets spacecraft proceeded further away from the sun.

As can be seen from Table 5, the characteristic velocity c^* deteriorated between the start and the end of almost every test. By Test 5, the performance was considerably worse than in Test 1 and the engine was exhibiting definite evidence of what has been termed "the washout phenomenon." This is a change in engine operation from conditions of essentially constant c^* to those characterized by a decrease in chamber pressure and an increase in fuel flow rate, and therefore a decrease in c^* and specific impulse. The c^* profile of this firing is shown in Fig. 13. For the next test, No. 6, the fuel temperature was lowered another 4 K (8°F), from 290 K (63°F) to 286 K (55°F). At startup, the c^* value was only 732 m/s (2400 ft/s) compared with an expected value of 1295 to 1310 m/s (4250 to 4300 ft/s). In an attempt to verify the reports of some workers who had found that a short shutdown, followed by an immediate restart, could rejuvenate the bed, a 1-s shutdown with no purge, followed by an immediate restart was attempted. The c^* jumped from 498 to 1310 m/s (1600 to 4300 ft/s), where it remained for some 40 s before it started falling. Another 1-s shutdown was made with similar results. Test 6 of Table 5 therefore consists of three separate starts in rapid succession. The c^* profile of this test is also shown in Fig. 13.

Test 7 was made with the inlet propellant warmed to 305 K (90°F) to determine the effects of higher propellant temperature on engine washout. With the warmer inlet temperature, the c^* decreased slowly to 945 m/s (3100 ft/s) in more than 400 s. A 1-s shutdown and restart, as in Test 6, was attempted. The chamber pressure recovered as before and, at shutdown some 100 s later, the c^* was 1305 m/s (4270 ft/s). Tests 8 through 10 were made with cold propellant but lower tank pressure to attempt to reduce the catalytic-bed loading (G). However, c^* was lower than expected on startup, which resulted in a higher bed loading than desired. Washout occurred within 50 s in the last two tests. Upper bed catalyst weight loss after 10 tests totaling 1630 s was 7%. Thus, although this series be-

gan as an engine evaluation for a simulated TOPS-TCPS duty cycle, it evolved into a cursory investigation of washout because of the unexpected appearance of that phenomenon.

Another series of tests was run (Tests 11 through 21, Table 5) to ascertain whether the washout encountered in Tests 1 through 10 was the result of a combination of bed length and catalyst specific area that was inadequate to sustain steady-state engine operation. The lower bed catalyst was changed to 14 to 18 mesh (configuration No. 2) giving 67% more specific surface area compared with that of the 8 to 12 mesh of configuration No. 1. The initial propellant inlet temperature was held at about 289 K (60°F), and L^* remained the same as before. Eleven starts and a total of 2017 s were accumulated, exceeding the longest presently envisioned TOPS mission burn time by 20%. c^* performance was high, and did not deteriorate during any run. Maximum chamber pressure roughness was 166 kN/m² (24 lbf/in.²) peak-to-peak, or $\pm 6\%$ of mean chamber pressure. Less than 1% by weight of the catalyst was lost.

Still another series of tests was conducted with a lightweight 111-N (25-lbf) thrust engine (configuration No. 3) obtained from the Transtage hydrazine retrofit program. The main objective was to determine the life capability of this engine in steady-state operation, instead of its original pulse-mode duty cycle. The lower catalytic bed in this engine is 5.15 cm (2.03 in.) long, compared to the 1.65-cm (0.65-in.) length of the engine in Tests 1 through 21. The test summary is shown in Table 5 under Tests 22 through 28. A total of seven tests and 1270-s burn time were accumulated. The duty cycle was a series of steady-state firings ranging from 16 to 753 s. Ignition delay, after the first two tests, increased to over 100 ms. By the sixth and seventh runs (Tests 27 and 28 in Table 5) random maximum chamber pressure roughness had increased to over ± 172 kN/m² (± 25 lbf/in.²). Because of the 160-ms ignition delay in run 28 and the high chamber pressure roughness level, the series was terminated. Mean steady-state performance was surprisingly good, with only a 1.3% decrease in c^* from the end of the first test (Test 22) to the end of the last (Test 28). This was over a tank blowdown ratio of about 2:1. Ignition delays longer than 100 ms resulted in transient overpressurization of the chamber. Maximum transient chamber pressures ranged between 1380 and 1720 kN/m² (200 and 250 psia), except for Test 25, where the pressures went off scale and the best estimate is that a pressure spike of over 4800 kN/m² (700 psia) occurred.

Table 5. Summary of test conditions and results for firings with hydrazine

Test No.	Chamber configuration No.	Duration, s	Initial tank pressure, kN/m ² gauge (psig)	Initial fuel temperature, K (°F)	Initial bed temperature, K (°F)	Flow rate w , kg/s (lbm/s)	Bed loading G_s kg/m ² -s (lbm/in. ² -s)	Maximum injector manifold pressure on startup, kN/m ² (psia)	Ignition delay, ms	Chamber pressure, kN/m ² (psia)	Maximum chamber pressure roughness, \pm kN/m ² (\pm psi)	c^* at + 10 s, m/s (ft/s)	c^* just prior to shutdown, m/s (ft/s)	Remarks
1	1	152	2241 (325)	301 (83)	286 (55)	0.049 → 0.058 (0.108 → 0.127)	49.9 → 59.1 (0.071 → 0.084)		70	1124 → 1110 (163 → 161)	14 (2)	1301 (4270)	1125 (3690)	
2	1	45	2172 (315)	299 (79)	298 (77)	0.049 → 0.051 (0.108 → 0.113)	49.9 → 52.0 (0.071 → 0.074)		80	1034 → 1041 (150 → 151)	14 (2)	1198 (3930)	1152 (3780)	
3	1	95	2137 (310)	295 (71)	298 (77)	0.048 → 0.053 (0.106 → 0.117)	49.2 → 54.1 (0.070 → 0.077)		75	1055 → 1014 (153 → 147)	14 (2)	1242 (4075)	1082 (3550)	
4	1	73	2103 (305)	294 (69)	295 (72)	0.049 → 0.052 (0.109 → 0.115)	50.6 → 53.4 (0.072 → 0.076)		70	1034 → 1027 (150 → 149)	14 (2)	1183 (3880)	1116 (3660)	
5	1	307	2068 (300)	290 (63)	300 (81)	0.051 → 0.059 (0.112 → 0.131)	52.0 → 60.5 (0.074 → 0.086)		70	986 → 579 (143 → 84)	14 (2)	1097 (3600)	552 (1812)	
6	1	345	2068 (300)	286 (55)	291 (65)	0.052 → 0.087 (0.115 → 0.192)	53.4 → 89.3 (0.076 → 0.127)		180	717 → 738 (104 → 107)	14 (2)	777 (2550)	481 (1578)	
7	1	518	2068 (300)	306 (92)	292 (66)	0.042 → 0.031 (0.093 → 0.070)	43.6 → 33.0 (0.062 → 0.047)		140	931 → 717 (135 → 104)	14 (2)	1295 (4250)	1301 (4270)	
8	1	130	1655 (240)	287 (57)	289 (60)	0.032 → 0.037 (0.070 → 0.082)	33.0 → 38.0 (0.047 → 0.054)		85	641 → 421 (93 → 61)	14 (2)	1143 (3750)	640 (2100)	
9	1	50	1655 (240)	287 (57)	300 (80)	0.042 → 0.044 (0.092 → 0.097)	42.9 → 45.0 (0.061 → 0.064)		170	586 → 496 (85 → 72)	14 (2)	792 (2600)	640 (2100)	
10	1	50	1448 (210)	287 (57)	328 (130)	0.039 → 0.037 (0.086 → 0.081)	39.4 → 37.3 (0.056 → 0.053)		110	538 → 421 (78 → 61)	14 (2)	785 (2575)	646 (2120)	7% upper bed catalyst lost 4% lower bed catalyst lost
11	2	105	2068 (300)	286 (55)	287 (57)	0.035 → 0.034 (0.077 → 0.075)	35.9 → 34.4 (0.051 → 0.049)		70	765 → 752 (111 → 109)	83 (12)	1240 (4068)	1279 (4195)	
12	2	103	2068 (300)	287 (57)	288 (59)	0.039 → 0.036 (0.087 → 0.079)	40.1 → 36.7 (0.057 → 0.052)		—	883 → 786 (128 → 114)	14 (2)	1273 (4175)	1272 (4173)	
13	2	132	2068 (300)	287 (58)	295 (72)	0.042 → 0.039 (0.092 → 0.086)	42.9 → 39.4 (0.061 → 0.056)		130	945 → 883 (137 → 128)	14 (2)	1281 (4204)	1284 (4211)	
14	2	160	2068 (300)	288 (59)	295 (71)	0.043 → 0.040 (0.094 → 0.088)	43.6 → 40.1 (0.062 → 0.057)		130	965 → 903 (140 → 131)	14 (2)	1283 (4208)	1284 (4214)	
15	2	198	2000 (290)	288 (59)	296 (74)	0.041 → 0.038 (0.091 → 0.084)	42.2 → 38.7 (0.060 → 0.055)		130	931 → 862 (135 → 125)	14 (2)	1273 (4178)	1282 (4207)	
16	2	421	1965 (285)	289 (60)	296 (74)	0.040 → 0.035 (0.089 → 0.078)	40.8 → 36.6 (0.058 → 0.052)		130	903 → 793 (131 → 115)	14 (2)	1269 (4164)	1275 (4184)	
17	2	111	1965 (285)	289 (60)	302 (85)	0.035 (0.078)	36.6 (0.052)		70	793 (115)	14 (2)	1276 (4188)	1275 (4183)	
18	2	330	1793 (260)	289 (60)	297 (76)	0.035 → 0.031 (0.078 → 0.069)	36.6 → 31.6 (0.052 → 0.045)		90	793 → 696 (115 → 101)	41 (6)	1270 (4167)	1266 (4153)	
19	2	107	1793 (260)	283 (50)	285 (53)	0.031 → 0.030 (0.069 → 0.066)	31.6 → 30.2 (0.045 → 0.043)		80	683 → 655 (99 → 95)	41 (6)	1239 (4066)	1245 (4084)	
20	2	225	1793 (260)	284 (51)	294 (70)	0.034 → 0.030 (0.074 → 0.066)	33.7 → 30.2 (0.048 → 0.043)		80	738 → 662 (107 → 96)	41 (6)	1238 (4063)	1254 (4115)	
21	2	125	1793 (260)	284 (52)	295 (72)	0.034 → 0.033 (0.074 → 0.073)	33.7 (0.048)		190	731 → 724 (106 → 105)	48 (7)	1237 (4057)	1240 (4069)	Large pressure spike on ignition, >3447 kN/m ² (>500 psi)
22	3	16	2758 (400)	285 (54)	288 (59)	0.054 (0.118)	39.4 (0.056)		64	1145 (166)	21 (3)	1292 (4238)	1303 (4274)	
23	3	100	2758 (400)	289 (60)	325 (125)	0.053 (0.117)	38.7 (0.055)		60	1103 (160)	83 (12)	1263 (4145)	1294 (4246)	
24	3	25	2606 (378)	289 (60)	294 (70)	0.051 (0.112)	37.3 (0.053)		128	1062 (154)	41 (6)	1268 (4161)	1287 (4223)	
25	3	50	2551 (370)	287 (57)	294 (70)	0.046 (0.102)	33.7 (0.048)		136	965 (140)	69 (10)	1266 (4152)	1275 (4182)	
26	3	57	2517 (365)	290 (63)	303 (86)	0.044 (0.096)	32.3 (0.046)		142	917 (133)	28 (4)	1272 (4173)	1293 (4243)	
27	3	753	2482 (360)	292 (66)	300 (81)	0.033 (0.072)	33.9 (0.034)		130	690 (100)	159 (23)	1270 (4167)	1301 (4268)	
28	3	270	1793 (260)	291 (64)	299 (79)	0.032 (0.071)	23.2 (0.033)		160	669 (97)	200 (29)	1264 (4146)	1286 (4218)	
29	4	100	2482 (360)	288 (59)	277 (39)	0.052 (0.114)	30.9 (0.044)	4875 (707)	63	1110 (161)	26 (4)	1288 (4227)	1299 (4261)	
30	4	22	2448 (355)	286 (55)	276 (38)	0.049 (0.108)	29.5 (0.042)	4875 (707)	64	1096 (159)	14 (2)	1339 (4394)	1354 (4443)	
31	4	54	2344 (340)	286 (55)	277 (40)	0.048 (0.105)	28.1 (0.040)	4813 (698)	73	1062 (154)	14 (2)	1334 (4376)	1359 (4460)	
32	4	58	2275 (330)	281 (47)	275 (36)	0.049 (0.107)	28.8 (0.041)	7378 (1070)	76	1020 (148)	34 (5)	1275 (4183)	1282 (4207)	
33	4	817	2172 (315)	283 (50)	277 (39)	0.038 (0.083)	22.5 (0.032)	5861 (850)	62	800 (116)	48 (7)	1290 (4232)	1294 (4246)	Complete TOPS duty cycle
34	4	275	1600 (232)	284 (52)	280 (44)	0.035 (0.078)	21.1 (0.030)	3985 (578)	64	779 (113)	41 (6)	1338 (4391)	1352 (4435)	
35	4	186	1427 (207)	284 (52)	276 (38)	0.032 (0.071)	19.0 (0.027)	3448 (500)	64	717 (104)	34 (5)	1343 (4405)	1359 (4460)	
36	4	17	1344 (195)	288 (59)	275 (35)	0.028 (0.061)	16.2 (0.023)	2068 (300)	41	607 (88)	41 (6)	989 (3244)	1297 (4256)	
37	4	281	1310 (190)	286 (55)	277 (39)	0.030 (0.067)	18.3 (0.026)	3758 (545)	73	683 (99)	62 (9)	1331 (4368)	1371 (4497)	
38	5	102	2193 (318)	281 (46)	277 (39)	0.056 (0.123)	25.3 (0.036)	3530 (512)	40	1193 (173)	21 (3)	—	1131 (3710)	
39	5	22	2103 (305)	281 (46)	277 (40)	0.050 (0.110)	22.5 (0.032)	2703 (392)	34	1158 (168)	14 (2)	1280 (4200)	1256 (4120)	
40	5	49	2041 (296)	283 (50)	277 (39)	0.049 (0.108)	21.8 (0.031)	5171 (750)	56	1145 (166)	14 (2)	—	1234 (4050)	
41	5	55	1965 (285)	283 (50)	280 (44)	0.048 (0.105)	21.8 (0.031)	3461 (502)	49	1103 (160)	14 (2)	—	1225 (4020)	
42	5	814	1937 (281)	283 (50)	—	0.043 (0.095)	19.7 (0.028)	2565 (372)	36	820 (119)	21 (3)	1262 (4140)	1250 (4100)	Complete TOPS duty cycle
43	5	271	1393 (202)	282 (48)	283 (50)	0.034 (0.074)	15.5 (0.022)	1875 (272)	34	779 (113)	26 (4)	—	1227 (4025)	
44	5	185	1344 (195)	286 (56)	278 (41)	0.034 (0.075)	15.5 (0.022)	2744 (398)	55	814 (118)	14 (2)	1306 (4285)	1248 (4093)	
45	5	18	1310 (190)	285 (53)	—	0.033 (0.072)	14.8 (0.021)	1496 (217)	35	793 (115)	14 (2)	1273 (4178)	1249 (4097)	
46	5	227	1276 (185)	287 (57)	—	0.031 (0.069)	14.1 (0.020)	2358 (342)	48	758 (110)	21 (3)	1261 (4137)	1259 (4132)	

Table 6. Summary of test conditions and results for firings with hydrazine/hydrazine nitrate

Test No.	Chamber configuration No.	Duration, s	Initial tank pressure, kN/m ² gauge (psig)	Initial fuel temperature, K (°F)	Initial bed temperature, K (°F)	Ignition delay, ms	Maximum chamber pressure roughness, ± kN/m ² (± psi)	c* at + 10 s, m/s (ft/s)	c* just prior to shutdown, m/s (ft/s)	Remarks
47	6A	60	1572 (228)	302 (84)	302 (84)	160 ^a	82.7 (12)	— —	1283 (4210)	
48	6A	60	1751 (254)	302 (84)	318 (112)	215 ^a	75.8 (11)	— —	1318 (4325)	
49	6A	30	1517 (220)	303 (86)	320 (117)	215 ^a	55.2 (8)	— —	— —	
50	6A	30	1379 (200)	302 (85)	319 (115)	280 ^a	48.3 (7)	— —	— —	
51	6A	60	1379 (200)	302 (85)	318 (112)	220 ^a	55.2 (8)	— —	1311 (4300)	
52	6B	200	1655 (240)	305 (89)	301 (82)	110		— —		
53	6B	40	1655 (240)	305 (90)	309 (97)	140		— —		
54	6C	200	1407 (204)	304 (88)	302 (85)	115	41.4 (6)	— —		
55	6C	4	1420 (206)	309 (96)	311 (100)	120		— —		
56	6D	75	1379 (200)	302 (84)	302 (84)	120	20.7 (3)	— —		
57	6D	120	1517 (220)	302 (85)	322 (120)	126	62.1 (9)	— —		Pressure spike on start > 2068 kN/m ² (> 300 psi)
58	6D	2 ^b	1517 (220)	304 (88)	301 (82)	240	—	— —	—	Very slow pressure rise; ≈ 2 s
59	6E	100	1407 (204)	—	296 (73)	110	31.0 (4.5)	— —	1315 (4315)	
60	6E	105	1434 (208)	—	347 (165)	195	20.7 (3)	— —		Startup pressure spike > 2758 kN/m ² (> 400 psi)
61	6E	100		—	296 (73)	≈300	17.2 (2.5)	— —		
62	2	13	2068 (300)	292 (66)	292 (67)	52	20.7 (3)	— —	Footnote c	
63	2	17	2068 (300)	291 (64)	292 (67)	58	13.8 (2)	1280 (4200)	≈ 1280 (≈ 4200)	
64	2	17	2000 (290)	287 (58)	289 (61)	134	13.8 (2)	1332 (4370)	≈ 1332 (≈ 4370)	
65	2	7	1862 (270)	289 (61)	300 (80)	135	55.2 (8)	— —	Footnote c	
66	2	12	2000 (290)	285 (53)	287 (57)	90	6.9 (1)	1315 (4315)	1317 (4320)	
67	2	19	1979 (287)	286 (55)	298 (77)	104	124.1 (18)	1320 (4330)	1332 (4370)	
68	7	11	1551 (225)	291 (65)	291 (65)	145 (20) ^d	13.8 (2)	— —	1317 (4320)	
69	7	12	1551 (225)	293 (68)	294 (70)	170 (45) ^d	13.8 (2)	— —	1311 (4300)	
70	7	13	1551 (225)	292 (67)	297 (76)	162 (50) ^d	13.8 (2)	— —	1314 (4310)	
71	7	14	1551 (225)	293 (68)	297 (76)	165 (55) ^d	20.7 (3)	— —	1301 (4270)	
72	7	16	1551 (225)	293 (68)	295 (72)	168 (55) ^d	55.2 (8)	— —	1350 (4430)	
73	7	17	1551 (225)	293 (68)	295 (72)	210 (105) ^d		— —	1353 (4440)	Large pressure overshoot off scale
74	7	12	1551 (225)	293 (68)	293 (68)	187 (70) ^d			1347 (4420)	Footnote c
75	8	5	620 (90)	302 (84)	302 (84)					
76	8	6	483 (70)	301 (82)	298 (77)					
77	8	17	483 (70)	309 (97)	304 (88)					
78	8	9	414 (60)	312 (103)	329 (132)					
79	8	10	414 (60)	298 (77)	296 (73)					
80	8	2.5	414 (60)	307 (94)	307 (93)					
81	8	13	414 (60)	307 (94)	310 (99)					
82	9	3	862 (125)	298 (77)	298 (77)					
83	9	3	965 (140)	300 (81)	301 (82)					Footnote c

^aTime from fire valve electrical signal to 90% of average chamber pressure, instead of 2% of average chamber pressure.

^bTest terminated when chamber pressure failed to increase significantly after 2 s; upper, small-mesh catalyst lost when retention screen broke, probably as a result of nitriding.

^cSteady-state values not reached.

^dFirst number is the ignition delay from fire valve to 2% average chamber pressure; second number is time from 2% injector pressure to 2% chamber pressure.

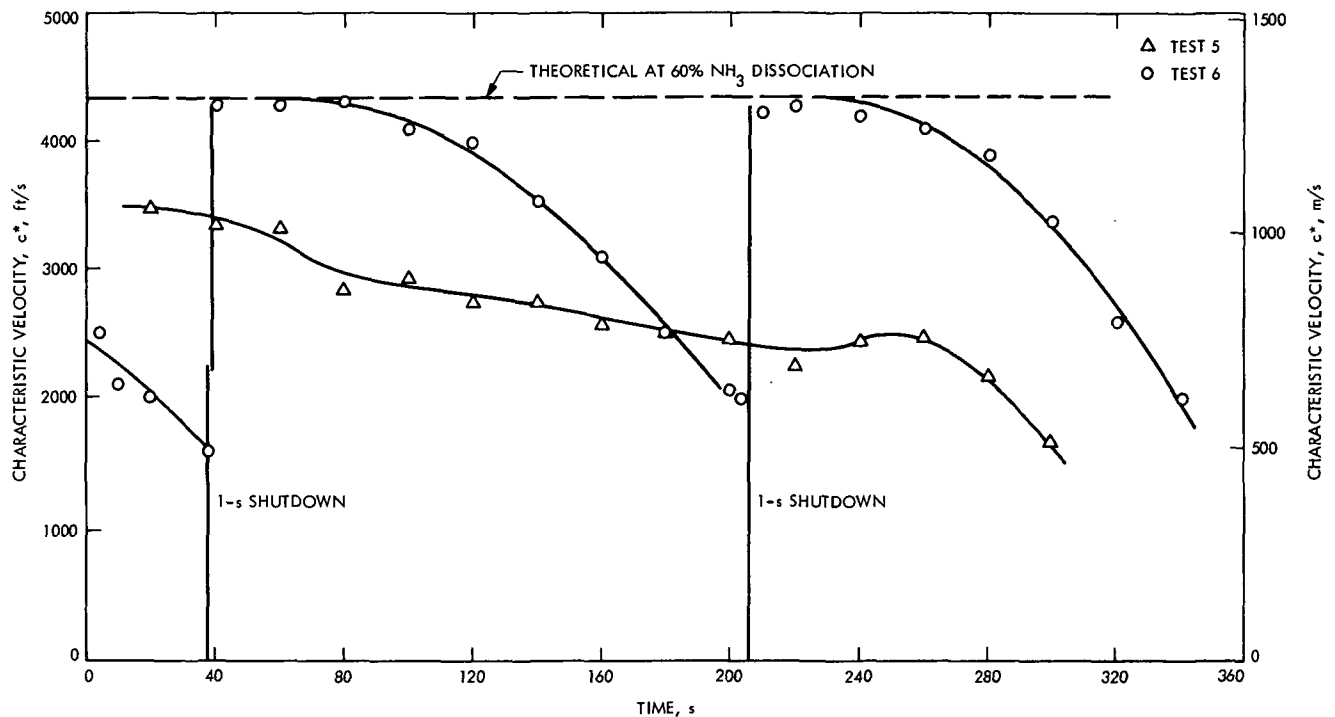


Fig. 13. Evidence of washout phenomenon: variation of c^* with time

Two final test series evaluated the two purchased flight-type thrusters in simulated TOPS-TCPS duty cycles. Engine configuration No. 4 (the refurbished version of No. 3) was evaluated in Tests 29 through 37, and engine configuration No. 5 in Tests 38 through 46. In both cases, propellant feed pressures were progressively reduced from one firing to the next to simulate a blowdown mode of operation. A total of 1810 s was accumulated on engine No. 4 in the nine tests. A total of 1741 s was accumulated on engine No. 5 in the same number of tests. (An additional 120 s was accumulated on this engine in 2 other tests not reported in Table 5 due to a valve anomaly.)

For engine No. 4, c^* was corrected for throat area increase due to thermal growth, (Ref. 12) and the thrust coefficient (C_F) was 1.72 to 1.71 throughout the blowdown range.⁵ For engine No. 5, the c^* was not corrected for throat area growth, nor for heat loss from the uninsulated chamber. The C_F varied from 1.76 to 1.74.⁶

Both engines (Nos. 4 and 5) performed well throughout their respective test series, and both appeared capable of

performing any of the TCPS functions for outer planet flyby missions.

6. Test firing results with hydrazine/hydrazine nitrate.

A series of tests was run to determine how many cold (<319 K (115°F)) starts and how long a total firing time could be accumulated on a single bed (Tests 47 through 51, Table 6). Various catalytic-bed lengths and configurations (Nos. 6A through 6E) were tried, as noted in Table 6. Five cold starts and a total of 240 s of firing time were obtained with an all Shell-405 catalytic bed in the 222-N (50-lbf) thrust Mariner configuration using the nitrate blend (configuration No. 6E, Table 4). Examination of the chamber showed the upper bed retention screen to be still in place; however analysis of the Shell-405 catalyst from the upper bed revealed that appreciable amounts of iron, nickel, and cobalt from the H-7 catalyst in the lower bed had been deposited on it (see Footnotes d and e of Table 4).

The results of these Shell-405 bed tests (Tests 47 through 51, Table 6) were encouraging. The maximum number of starts and total firing duration seemed to be at least 5 and 240 s, respectively. Therefore, another series of tests, using the small 102-N (23-lbf) thrust boltup engine (configuration No. 2), was attempted. This engine has a 3.177-mm-(0.125-in.-) thick upper bed retention plate welded to a

⁵Private communication from Rocket Research Corp. to G. Nail (JPL), Nov. 20, 1970.

⁶Private communication from Marquardt Co. to G. Heidenreich (JPL), Dec. 18, 1970.

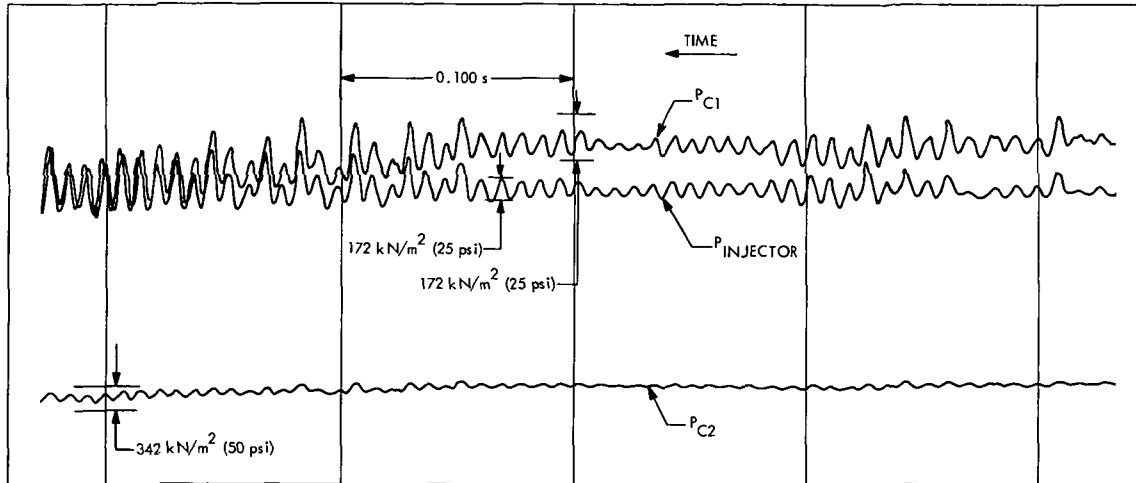


Fig. 14. Combustion roughness in chamber configuration No. 2 (Table 4) with hydrazine/hydrazine nitrate

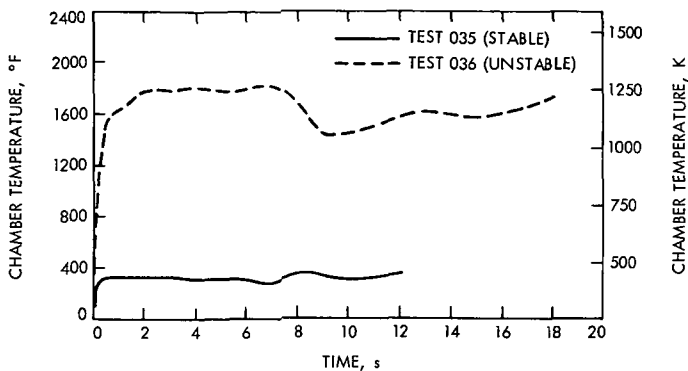


Fig. 15. Upper bed chamber temperature measured downstream from injector face

central spud on the injector. This design was intended to prevent voids, which can accelerate catalyst mechanical breakup and attrition, from forming in the upper bed.

Three sets of two tests each were run with Configuration No. 2. These are Tests 62 through 67 in Table 6. Test 65 was terminated when a loud resonating sound from the engine was heard. Examination showed that the upper bed retention plate weld to the injector had broken. Also, the screen covering the orifices was broken, catalyst was under the screen, and nitrate salts were clogging a few of the orifices. The injector was cleaned, new catalyst was installed, and the plate was rewelded. In the first test with the refurbished hardware (Test 66), the chamber pressure remained constant to within ± 7 kN/m² (± 1 lbf/in.²) of the nominal value (920 kN/m² (133 psia)). However, during the next test, Test 67, the chamber pressure became unstable. A resonating audible sound was heard. Figure 14 shows the chamber pressure trace for this

test. These tests were the first firings ever made with the nitrate blend on the small engine. No previous test with hydrazine had shown evidence of such chamber instability with this engine.

Figure 15 is a plot of the upper bed catalyst temperature, 1.27 mm (0.050 in.) downstream from the injector face, vs time, for Tests 66 and 67. The data on this figure indicates that the flame front was closer to the injector face during the unstable firing, which was the second one (Test 67). This is contrary to what is often seen; that is, a reduction of catalyst activity after some time, and consequent movement of the flame front down the chamber, is more common.

Since the instability problem with configuration No. 2 had prevented the determination of the start/life limits of the Shell-405 catalyst with the nitrate blend, another series was run with a welded 222-N (50-lbf) prototype Mariner 1969 engine, configuration No. 7 of Table 4. The engine was modified by installing a 3.17-mm- (0.125-in.-) thick Haynes-25 plate for upper bed retention, since the double screen in the original design had proven inadequate for multiple restart operation. These are Tests 68 through 74 in Table 6. There are two numbers for ignition delay times in Table 6. The first is the time from the fire-valve electrical signal to 2% chamber pressure. The second, in parentheses, is the time from 2% injector pressure rise to 2% chamber pressure. Thus, while the second number shows that most of the delay is really due to hydraulic time lag it also shows more clearly the increase of fuel/catalyst delay with the number of starts.

The chemical reaction delay increased by a factor of five from the first start (20 ms) to the sixth start (105 ms). On

the sixth start there was a very large pressure spike, estimated to be 3450 kN/m² (500 psia), which drove the charts off the scale.

Seven firings (totaling 95 s) were made. During the seventh test (Test 74), the pressure drop across the catalyst was only about 15 kN/m² (2 lbf/in.²) strongly suggesting the loss of the upper bed. The engine was therefore cut open and examined. The upper bed was found to be gone. A small amount of fine mesh catalyst was found interspersed with the lower bed pellets; the rest evidently passed out through the nozzle.

Tests 75 through 83 (Table 6) were made with two experimental thermal bed chamber configurations (configuration Nos. 8 and 9 in Table 4). This concept comprises a thermal decomposition chamber started by a pilot catalytic bed.

A new catalyst, Esso-500, was used in the pilot chamber of the thermal bed. This catalyst was originally developed under Air Force sponsorship (Ref. 13). It proved to be considerably different from the Shell-405. Figure 16 compares scanning electron micrographs of unfired 25- to 30-mesh Shell-405 and Esso-500 catalyst grains magnified 50 times. The Esso catalyst shows a general absence of large pores compared to the Shell, and has sharp angular features. The Esso particles resemble polyhedra, as opposed to the spheroidal shapes of the Shell catalyst particles. The thin, sharp edges would appear to be very susceptible to breakage, with resulting loss of catalyst as fines. Open-air flame tests did show this to be exactly what happened. Figure 17a shows the Esso catalyst after three open-air flame tests with hydrazine. A small amount, 0.150 g, of the catalyst was placed on a flat glass dish, open to the atmosphere, and 2 cm³ of fuel was injected onto the catalyst. The Esso catalyst, as seen in Fig. 17a, was severely pulverized. In contrast, Fig. 17b shows the excellent condition of the Shell-405 catalyst after the same tests. From visual observation, the Esso did not react as quickly with hydrazine as did the Shell. The second and third tests with the Esso resulted in longer and longer delays before any reaction was noticed. Similar tests were performed using the hydrazine/hydrazine nitrate blend. With this propellant, the Esso catalyst ignited with a flame more quickly than the Shell. Seven starts were made. By the seventh start with the Shell catalyst, the reaction was slow in starting. Breakup of the Esso was not as severe as with the hydrazine, confirming the visual observation that the reaction occurred on the surface. This would prevent the fuel from penetrating into the pores where, upon decomposition, it could blow the catalyst apart, especially at the thin edges.

The initial tests of Configuration No. 8 were run with only the pilot bed operating. This was to evaluate the characteristics of the Esso catalyst. The first test, Test 75 of Table 6, was made with 14- to 18-mesh Esso catalyst in the as-received condition, and produced no evidence of ignition. For the next run, the pilot-bed catalyst was replaced by some more Esso catalyst that had been previously tumbled for three hours. A 23% increase in catalytic-bed weight was realized in this second loading as a result of better packing of the tumbled particles. In addition, the catalytic-bed loading, G , was reduced for the second run by reducing the tank pressure. Tests 76 through 81 demonstrated the activity of the Esso catalyst under cold restart conditions. Visual examination after Test 78 and again after Test 81, revealed the pilot-bed catalyst to be sintered together, although it was not packed into any substantially smaller volume. By Test 81, the fused catalyst caused the pressure drop across the bed to increase such that with the low tank pressure, the flow rate was reduced to almost zero.

In Tests 82 and 83 with engine configuration No. 9, ignition did not occur, so only initial conditions are reported in Table 6.

7. Discussion of results.

a. Washout and ignition delay with hydrazine. The first series of tests on the 102-N (23-lbf) thrust engine using hydrazine (Tests 1 through 10 of Table 5) exhibited evidence of the washout phenomenon. In these tests, a large mesh size (8 to 12) catalyst was used instead of the normal 14- to 18-mesh, to reduce the pressure drop across the catalyst, since bed life was known to be a function of pressure drop as well as of bed loading. However, the larger catalytic particles used have a lower specific surface area, which would require, a priori, a bed length greater than that employed. The bed was marginal to begin with, even for 14- to 18-mesh catalyst, when compared to the catalytic-bed length predicted by the frequently used equation of Ref. 14, and could not be lengthened. In addition, the water content of the hydrazine (1.9%) was high. High water content has been shown by some researchers to precipitate washout.

Tests 6 and 7 show the great impact of propellant inlet temperature. An increase of inlet temperature from 286 K (55°F) to 305 K (92°F) delayed the onset of washout and reduced the magnitude of the degradation. Also noteworthy was the fact that the catalytic bed was probably not becoming less active due to catalyst loss or breakup since only 7% of the upper bed and 4% of the lower bed was lost during 1766 s of testing, and the maximum chamber

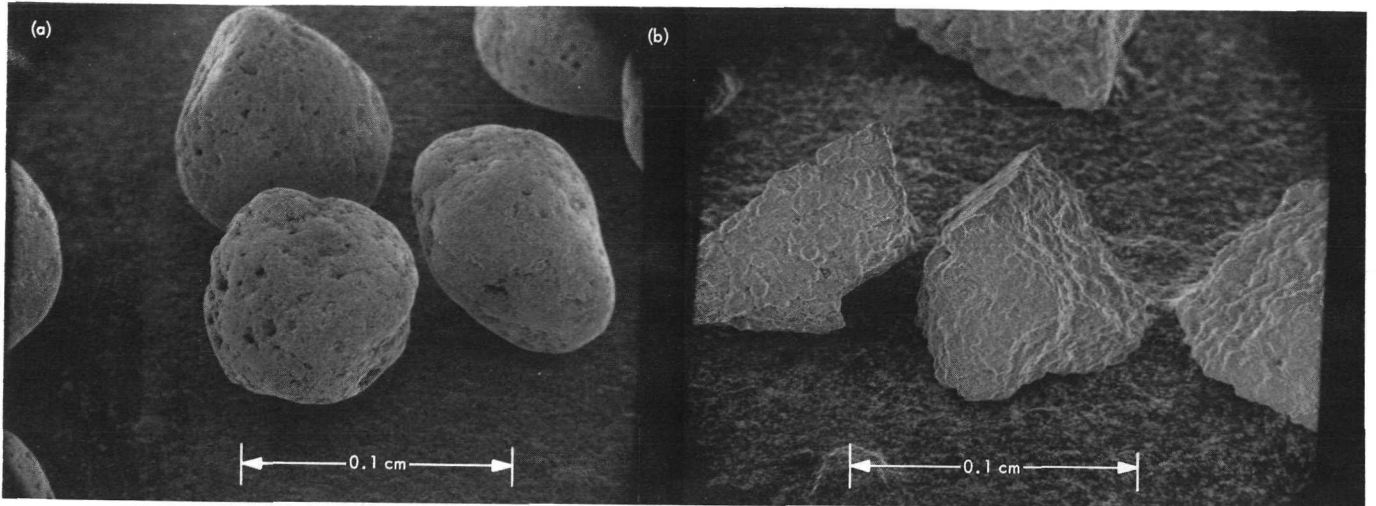


Fig. 16. Micrographs of hydrazine catalysts; (a) Shell 405, (b) Esso 500 (25- to 30-mesh, unfired, 50X)

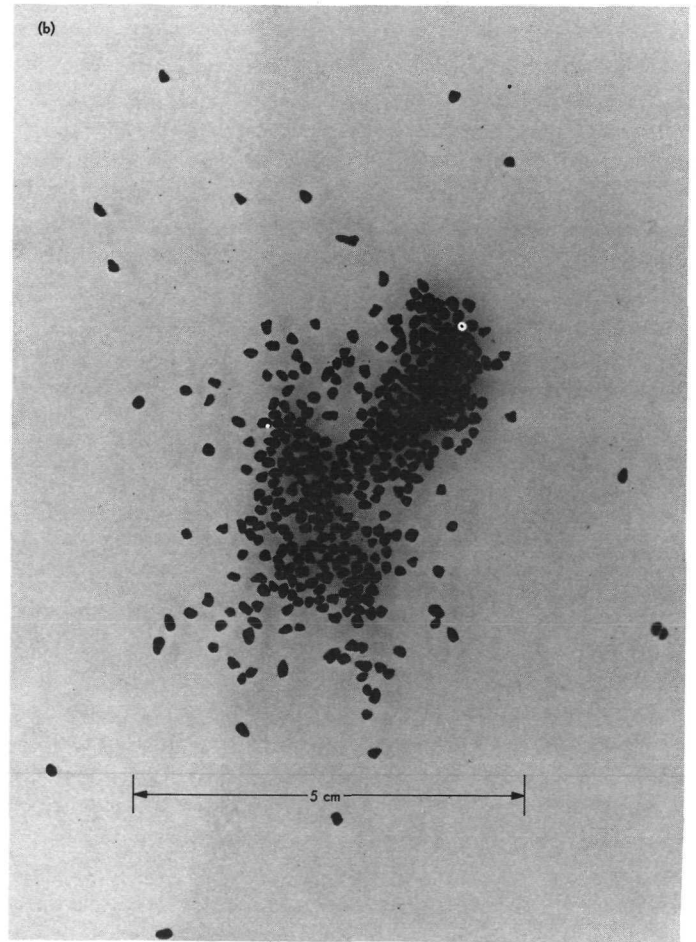
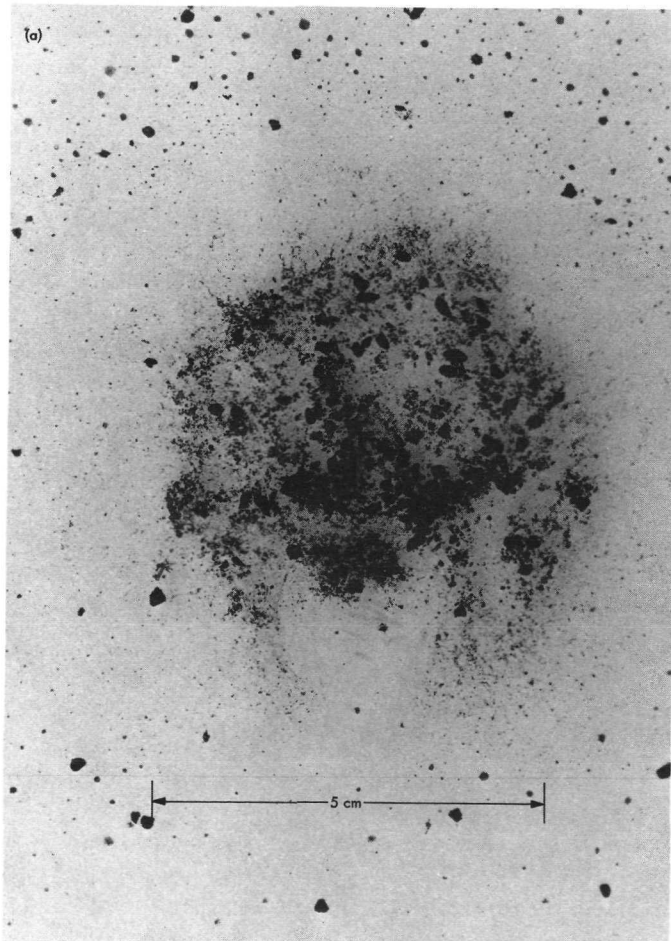


Fig. 17. Catalysts after three open-air flame tests; (a) Esso-500, (b) Shell-405

pressure roughness was very low, about 27 kN/m² (4 lbf/in.²) peak-to-peak. Other explanations for this washout, such as temporary inactivation of catalytically active sites, must be sought.

The second series of tests depressed several of the variables known to influence or suspected of influencing the onset of washout. Low (0.7%) water content hydrazine was used, and larger specific surface area catalytic particles were installed in the lower bed. The summary (Table 5) shows that under these conditions there was no decrease in performance during firings as long as 421 s, even though relatively cool (~ 285 K (55°F)) hydrazine was used. It may be inferred from the results of these tests that the time to onset of washout with cold hydrazine can be appreciably lengthened through manipulation of such factors as catalyst surface area and propellant water content, and that attainment of the TCPS 1600-s life requirement (Table 4) may be possible with engines of the type of configuration No. 2. However, the data are insufficient to enable one to say with any confidence that washout would not have occurred at some time in excess of 421 s, even under conditions of relatively low propellant water content and relatively high catalyst specific surface area. Washout is a phenomenon that is only poorly understood at present, and the reader is cautioned against assuming that the simplistic engineering "fix" employed successfully in the present circumstances is a panacea by means of which future instances of washout can always be mitigated. Confident prediction and control of this phenomenon can result only from a thorough understanding of its causes on a fundamental level.

The results of the testing with configuration No. 3 (Tests 22 through 28, Table 6) offer further verification of the contention that a state-of-the-art hydrazine engine is suitable for application to the envisioned outer planet missions. Performance, for example, remained virtually constant. However, the increase in ignition delay with the number of starts, and the excessive chamber pressure roughness observed in some instances are causes for some concern.

One important factor that may affect ignition delay (which has not yet been completely investigated) is propellant temperature. The induction time (time from liquid entrance into the chamber until noticeable pressure rise due to gaseous decomposition products) has been found to be predictable using the liquid residence time as determined from an analysis of liquid penetration into the pores (Ref. 15). This induction period is a strong inverse function of the liquid hydrazine inlet temperature. For

instance, with the catalytic bed at 294 K (70°F), a decrease in inlet propellant temperature from 295 K (71°F) to 278 K (40°F) increases the induction time from 15 to 27 ms. Pressure overshoots and ignition delays increase with increased induction time, but the magnitude of the overshoot is not as yet a predictable quantity.

Another first-order temperature effect is the catalytic-bed temperature. In one instance (Ref. 16), lowering the bed temperature from 293 K (67°F) to 262 K (12°F) resulted in an ignition delay increase from about 20 to 280 ms. Greer (Ref. 16) found that with the hydrazine temperature between 279 K (42°F) and 293 K (67°F), and the catalytic-bed temperature lowered below 273 K (32°F), a large pressure spike occurred on the first pulse, with no subsequent pressure traces (vacuum conditions). The fuel was judged to have frozen in the injector, blocking further flow on subsequent pulses, and also on the catalyst. Deliberately warming the bed to 278 K (40°F) generated gas as the melted fuel reacted with the catalyst. Thus the temperature of both the fuel and catalytic bed must be taken into consideration. The injector manifold and lines should be kept above 275 K (35°F) to prevent freezing of the incoming fuel.

Several aspects of the experimental procedure may also have influenced ignition delay and chamber pressure roughness. For example, the tests were not conducted in a vacuum because of high cost and scheduling conflicts with a flight program. Also, to prevent high-temperature post-test oxidation of the catalyst by ambient air, a low-pressure GN₂ purge on shutdown was normal operating procedure. There are definite possibilities of catalyst thermal shock and nitriding of metal surfaces. In addition, the catalyst might have been contaminated by absorption of ammonia, or impurities in the GN₂ or air between tests. The exact effects of these test conditions are not yet known with certainty, but their possible influence must be kept in mind.

Both flight engines (configuration Nos. 4 and 5, Table 4) performed well throughout the entire test series (Tests 29 through 46, Table 5) and, on this basis, both appeared adequate to perform any of the presently envisioned TCPS functions for outer planet flyby missions. No attempt was made to compare these engines in terms of characteristic velocity performance, chiefly because vacuum specific impulse, which was to be measured during subsequent testing of one engine, is a more meaningful descriptor, and also because of the uncertainties in the calculated values of c^* for some of the firings made with configuration No. 5. It was expected, however, that the generally

lower characteristic velocities of engine No. 5 would be at least partially compensated for by the higher thrust coefficient (1.74 to 1.76) of engine No. 5 relative to that of engine No. 4 (1.71 to 1.72), so that roughly equivalent vacuum specific impulses would be anticipated.

The engines were, however, characterized and compared with respect to ignition delay, chamber overpressure on startup, and chamber pressure roughness. In each of these three critical areas, engine No. 5 showed a slight but definite advantage over engine No. 4.

The ignition delay, defined earlier in Subsection III-A-4, varied between 34 and 56 ms for engine No. 5, with the average for the nine tests being 43 ms. The ignition delay for engine No. 4 varied between 41 and 76 ms with the average at 64 ms. As can be seen from Table 5, engine No. 5 started more quickly on every test. It must be mentioned again that these times may not be truly representative of vacuum start times. A series of vacuum tests conducted by Rocket Research Corporation (Ref. 17) on an engine virtually identical to No. 4 had cold start ignition delays from 25 to 45 ms, with the average being 33 ms. The ignition delay for engine No. 5, during vacuum acceptance tests conducted at The Marquardt Company's facility under ambient temperature conditions, was about 24 ms.

The ignition delay is important in catalytic engines since it is often a good indicator of the magnitude of the overpressure spike, which, if severe enough, can break up the catalyst. The injector design of engine No. 5 is such that it greatly minimizes the startup overpressure. In fact, due partly perhaps to the small size of the pressure transducer lines, no chamber overpressure was observed. However, a direct comparison between the engines can be made by observing the inlet manifold pressure. The overpressure in the manifold correlates quite well with ignition delay, and again, it is seen that engine No. 5 had lower overpressures than engine No. 4.

A third important parameter is chamber pressure roughness, which is a good indication of bed condition and useful remaining life. Engine Nos. 4 and 5 both ran smoothly throughout their test series. From Table 5, it can be observed that engine No. 5 apparently is smoother than No. 4. Again, the smaller diameter [1.59-mm- (0.0625-in.-) OD] transducer transmission lines may cloud the true magnitude of roughness for No. 5. The roughness of engine No. 5 reached a peak value of $\pm 3.7\%$ of steady-state chamber pressure during run 43, and was at $\pm 2.3\%$ at the end of Test 46. Engine No. 4 was $\pm 3.5\%$ rough dur-

ing the first test, but then the roughness dropped to $\pm 2\%$ by run 31. During the latter tests, the roughness was ± 5 to $\pm 6\%$. However, during the last test, the roughness rose to $\pm 9\%$. The last test also had a high ignition delay and overpressure (for the low feed pressure). Whether these were indications that the bed was approaching the end of its life could be checked only by further testing. The roughness experienced in these tests was slightly higher than that reported in Ref. 17.

Although the roughness cited in Ref. 17 was still ± 3 to $\pm 4\%$ at the end of nine tests, further testing on the bed without cold starts resulted in greater roughness. It should be noted also that the tests described in Ref. 17 had not been preceded by vibration and acoustic tests.

b. Firings with the blend of 76% hydrazine and 24% hydrazine nitrate. The tests made with the nitrate blend (Table 6) indicated that the Shell-405 spontaneous catalyst is not satisfactory for the maximum performing blend of hydrazine/hydrazine-nitrate. If system considerations necessitated a lower freezing point propellant, one viable solution might be a ternary blend of hydrazine, hydrazine-nitrate, and water. Such blends have been investigated previously, both analytically and experimentally (Refs. 18 and 19).

Another lower freezing point blend might result from recent work on hydrazine azide (Ref. 20). The lack of oxygen in this propellant blend may give it better material compatibility characteristics, although it should be mentioned that the stability of the azide must be fully determined. For the maximum system performance, it would seem that some such high performing blend might also be used with thermal decomposition chambers if these are considered for future work.

From the initial tests (Nos. 75 to 83, Table 6) with the Esso catalyst, several observations and recommendations can be made regarding its utility. The open-area loading of the pilot bed at the injector face should be minimized, perhaps through the use of additional injection orifices. Operation with relatively high-bed loading (mass flow/pilot-bed cross-sectional area) indicated flooding at conditions where the Shell-405 catalyst does not normally flood. Parametric studies need to be performed, similar to the extensive characterization of the Shell catalyst (Ref. 14). Brunauer, Emmett, and Teller (BET) analysis indicated a 37% decrease in surface area after six ambient starts and a total run time of 95 s in the nitrate blend's environment. Although the remaining area is sufficiently high for ambient temperature ignition, longer duration testing must be done to determine whether this catalyst retains its

surface area at the nitrate blend decomposition temperature of about 1478 K (2200°F). One configuration that could be tried is a mixture of Esso and Shell catalyst.

8. Rocket Exhaust Plume Considerations. The plume from a monopropellant hydrazine engine, composed of nitrogen, hydrogen, and ammonia at a maximum stagnation temperature of about 1250 K (1800°F), is one of the most benign encountered in rocketry. Still, the possibility of plume impingement problems exists. Impingement effects can be divided into two classes: gross heating, corrosion, and erosion of surfaces located in the plume core flow, and subtle chemical corrosion of sensitive surfaces located in the plume boundary flow region.

The answer to core-flow impingement is a clear firing area, although this restriction can be a difficult spacecraft design limitation. A conical zone free of spacecraft appendages was provided in the TOPS design. This cone was centered in the engine and its apex half-angle was conservatively set at 75°. The results of impingement tests reported in Ref. 21 indicate that, from the standpoint of surface protection, no configuration limitations are necessary for a monopropellant hydrazine plume. However, plume impingement also results in unwanted forces and torques that complicate thrust vector control. Thus, a smaller apex half-angle, say 45°, could probably be safely used if necessary.

The second class of impingement results from the small amount of nozzle boundary layer gas that flows forward of the engine and over the spacecraft itself. Although there is no way to avoid this impingement flow, it is generally of no concern because of the very small gas flux involved. However, workers at Goddard Space Flight Center⁷ have found that small amounts of ammonia alter the performance of the detector elements of some advanced science instruments. Such detectors are based on special coatings just a few molecules thick, which are therefore especially sensitive to chemical attack.

This problem cannot be handled analytically because neither the detector damage threshold nor the gas flow pattern are known. The problem is also experimentally difficult because high vacuums must be maintained in the face of inflow from the nozzle, and then the results are not general because of the strong configuration dependence of plume flows. The first difficulty can be satisfactorily overcome using very low thrust rocket engines in a vacuum

chamber using the molecular pump principle, and then scaling the results to larger engines. The second difficulty is not so easily handled, although scaling between similar configurations may be possible once enough experiential data are available.

A test program based on the APS 0.45-N (0.1-lbf) thrust engines, the TOPS configuration, and the JPL MOLSINK vacuum facility was proposed but could not be funded. Although specific TOPS Project concerns cannot be answered without such a test program, a better understanding of the general problem will come from an on-going JPL research and development investigation into the basics of plume backscatter. In this program, experimental data will be used to develop and test analytical models and scaling laws. References 22 and 23 describe the most recent work.

The second, more direct, approach to defining the magnitude and significance of plume backscatter was also proposed to the TOPS Project: fly an engineering experiment on the spacecraft to measure the actual forward TCPS plume mass flux in situ (in space). Spacecraft contamination due to outgassing from other spacecraft hardware would also be detected. This experiment would aid in identifying and quantifying spacecraft contributions to its local space environment. Such data would also be a valuable diagnostic tool for isolating the causes of anomalous spacecraft instrument operation and readings.

The proposed experiment was based on a network of six independent quartz crystal microbalance (QCM) sensors mounted on the propulsion and science bays of the TOPS spacecraft. The key element of each QCM sensor is a piezoelectric crystal whose resonant frequency is a linear function of mass deposition on its surface. It can detect and quantify mass fluxes that deposit less than a molecular monolayer on the crystal. QCM systems have been flown on several Earth-orbital missions; a current state-of-the-art system is scheduled to be flown on Skylab I,⁸ primarily as a contamination monitor in the Apollo telescope canister.

The Skylab I system was the basis for the estimates of size, mass, power, and sensitivity given in Table 7 for the TOPS experiment. The experiment hardware is very light and uses little power. The Skylab I design can be lightened by changing from stainless steel to titanium and eliminating the electrical connector in favor of direct integration of wiring into a control cable.

⁷ Private communication between L. E. Baughman (JPL) and J. H. Trainor (GSFC), May 14, 1970.

⁸ Private communication between the author and R. Chuan of Celesco Industries, Jan. 18, 1972.

Table 7. Characteristics and performance of QCM system containing six independent sensors^a

Parameter	Nominal value
Mechanical	
Sensor diameter	3 cm
Sensor length	8 cm
System weight	
Skylab I design	0.72 kg
Minimum mass design	~0.45 kg
Electrical	
Input voltage (unregulated)	28 ± 4 Vdc
System current consumption	< 180 mA
Difference frequency output	14 V peak-to-peak
Analog voltage	0 to 5 V
Operating	
Dynamic range	0.1 kHz to 12 kHz
Sensitivity	10^8 Hz/gm
Mass change resolution	$\leq 10^{-9}$ gm

^aBased on Skylab I QCM system (Footnote 8).

In situ measurements with QCMs or other sensors are the only way to obtain unambiguous data on plume backscatter, especially for engines of the TCPS class and larger. Unfortunately, the TOPS experiment proposal was completed and submitted to the TOPS Design Team too late in the program to be formally evaluated for possible inclusion on the TOPS baseline spacecraft.

B. Solenoid Valves

Four valves are utilized to control the propellant flow to the TCPS rocket engine. The valves are installed in two parallel flow paths. In each path, a normally closed valve is used for engine firing control and a bistable (latching) valve is used for propellant isolation and redundant shut-off. When an engine firing is required, the appropriate latching valve is opened to provide pressurized propellant to the inlet of the normally closed valve in that flow path. Engine firing is initiated when electrical power is supplied to the normally closed valve and terminated when the power is removed. During periods when engine firing is not required, the latching valve can be closed to provide a redundant seal to prevent propellant from leaking into the engine.

General design criteria for the TCPS solenoid valves are:

- (1) Materials of construction must be compatible with hydrazine and those in the flow path should have a minimum catalytic effect on hydrazine decomposi-

tion. Titanium and aluminum are the most desirable materials for minimum catalysis. Stainless steel (CRES) is conditionally satisfactory for corrosion resistance and tests are being conducted to establish hydrazine decomposition rates with various CRES materials (Subsection III-F). The final mission profile and propulsion system configuration will determine if the hydrazine decomposition from CRES components can be tolerated.

- (2) Materials of construction must also provide satisfactory performance during and after exposure to the radiation environments imposed by the RTGs and those encountered in outer space and during planetary flybys.
- (3) A soft seat design using an elastomeric seal would be desirable to minimize the probability of internal leakage, but sensitivity to radiation renders this design questionable for 10-yr missions. A hard all-metal seat for the normally closed valves would be desirable from a durability standpoint, but sensitivity to particulate contamination makes this design concept less reliable. A compromise with a soft seat in the latching valve and a hard seat in the normally closed valve may represent an optimum configuration. Satisfactory seats using TFE Teflon for the seal material are available, but these seals are difficult to fabricate and are especially sensitive to radiation. Allowable tolerances in TFE seat dimensions are so small that verification of seat reliability by inspec-

tion is difficult. Use of recently developed elastomers that are more resilient than TFE Teflon may be the solution to the seat-seal fabrication and radiation sensitivity problems. Materials that are currently being evaluated are AF-E-102 [HYSTL-filled ethylene propylene terpolymer (EPT)] and a copolymer of TFE Teflon and perfluorovinyl methyl ether ("new" Teflon). Both of these compounds can be molded and are compatible with hydrazine.

- (4) The valve interior must be easily cleanable after assembly. Cavities that could entrap propellant and flushing fluid should be minimized. Particle generation by abrasion due to relative motion between surfaces in the propellant flow path must be avoided.
- (5) Generated magnetic fields must be kept to the lowest level commensurate with required valve performance. Required permanent fields must remain constant or be predictable throughout valve operational life. The amount of magnetic materials must be minimized.
- (6) The electrical power required for valve operation must be minimized.
- (7) Envelope size for all valves must be minimized.
- (8) All external leak paths and coil cavities must be sealed by welding.
- (9) A position (open or closed) indicator must be incorporated on all latching valves.

Using these criteria to establish valve requirements, an industry survey was conducted to determine the availability of suitable solenoid valves for the TOPS TCPS.

1. Valve survey. A JPL Source Information Request was sent to 40 valve manufacturers, and 11 submitted technical data for solenoid valve designs that were available and could provide performance capability commensurate with JPL requirements. Some manufacturers submitted more than one design, although in most cases these designs were all variations of a single basic approach.

The technical data were evaluated and the valves categorized as shown in Table 8. None of the submitted valve designs were judged suitable for TCPS flight use without significant modification and requalification (Category III). About half of the submissions had very little promise of meeting TCPS requirements, even with modifications (Category IV), because they were untested concepts, or too complex, or too large. Six of the valves might meet

Table 8. Results of solenoid valve industry survey

Category	Description	Manufacturer responses
I	Suitable for TCPS initial feasibility demonstrations as submitted. The design may or may not have potential for upgrading to flight hardware.	5
II	Potential for upgrading to flight hardware, but the valve was not readily available for initial feasibility demonstrations.	1
III	Suitable for flight hardware with or without minor redesign and reverification.	0
IV	Unsuitable for TCPS.	5

TCPS requirements with significant modifications (Categories I and II). The primary discrepancies were:

- (1) Designs included sliding surfaces in the presence of propellant, body cavities that made cleaning difficult, polymeric O-ring sealing of external leak paths, nonhermetically sealed solenoid coil cavities, and soft seats that could deform with time, altering flow characteristics.
- (2) Fabrication techniques included press fits and mechanical joints.
- (3) Materials in contact with propellant included Permendur or the softer magnetic steels and stainless steel in general, and some parts were electroless nickel plated. The compatibility of these materials with hydrazine is questionable at best.
- (4) Interfaces included a variety of large fittings, large dribble volumes, and large connectors and housings for internal electronics.
- (5) Excessive power required for valve actuation.

A recommendation for a design study to optimize the TCPS valve configuration was made. Areas cited for specific emphasis were materials and processing, fabrication techniques, and envelope, power, and seat design. Resource limitations restricted TOPS valve studies to the seat design problem, which is crucial to limiting valve leakage. The APS valve seat problem was studied because it is more difficult than, and directly applicable to, the TCPS design. This work is reported in Ref. 4. Also the results of the APS solenoid valve industry survey reported in Ref. 4 are complimentary to the TCPS results just discussed.

Table 9. Propellant control valve performance and design criteria (Ref. 24)

Characteristics	Requirement
Operation	Normally closed
Pressure	
Operating	2,760 kN/m ² (400 lbf/in. ² gauge), max
Proof	5,520 kN/m ² (800 lbf/in. ² gauge), min
Burst	11,040 kN/m ² (1600 lbf/in. ² gauge), min
Leakage	
External, He ^a	10 ⁻⁷ STP cm ³ /s from 0 to 2,760 kN/m ² (400 lbf/in. ² gauge), max
Internal, GN ₂	2.8 × 10 ⁻⁴ STP cm ³ /s from 0 to 2,760 kN/m ² (400 lbf/in. ² gauge), max
Flow rate, hydrazine	0.07 kg/s (0.15 lbm/s)
Differential pressure	69 kN/m ² (10 lbf/in. ²)
Temperature, operating	277.4 K (40°F) to 344.4 K (160°F)
Voltage	
Operating	20 to 32 Vdc
Pull-in	15 Vdc with 2,760 kN/m ² (400 lbf/in. ² gauge) and 344.4 K (160°F), max
Drop-out	5 Vdc at ambient pressure and 277.4 K (40°F), min
Power	10 W at 30 Vdc and 294.1 K (70°F), max
Response	
Opening with 20 Vdc	15 ms with 2,760 kN/m ² (400 lbf/in. ² gauge) and 344.4 K (160°F), max
Closing from 30 Vdc	10 ms with rated flow at 277.4 K (40°F), max
Life	10 ⁵ actuation cycles, min
Port, inlet and outlet	0.64 cm (0.25 in.) diam by 05.1 cm (2 in.) length of 0.038 cm (0.015 in.) wall tube
Electric connector	To be determined
Mounting	To be determined
Material	
Construction	6Al-4V Ti for flow passages
Seat (hard)	Tungsten carbide
Seat (soft)	AF-E-102 (EPT)
Weight	0.36 kg (0.8 lbm), max
Dielectric strength	100 μA at 600 Vac rms (60 cycle), max
Insulation resistance	100 MΩ at 500 Vdc, min
Envelope	To be determined
Flow media	Hydrazine, isopropyl alcohol, water, helium, and nitrogen.

^aLeakage shall be measured with a mass-spectrometer-type leakage detector and the recorded value shall be the largest rate indicated during a test period of at least 30 min.

Table 10. Propellant shutoff valve performance and design criteria (Ref. 25)

Characteristic	Requirement
Operation	Bistable (latching)
Pressure	
Operating	2,760 kN/m ² (400 lbf/in. ² gauge), max
Proof	5,520 kN/m ² (800 lbf/in. ² gauge), min
Burst	11,040 kN/m ² (1600 lbf/in. ² gauge), min
Leakage	
External, He ^a	10 ⁻⁷ STP cm ³ /s from 0 to 2,760 kN/m ² (400 lbf/in. ² gauge), max
Internal, GN ₂	2.8 × 10 ⁻⁴ STP cm ³ /s from 0 to 2,760 kN/m ² (400 lbf/in. ² gauge), max
Flow rate, hydrazine	0.07 kg/s (0.15 lbm/s)
Differential pressure	69 kN/m ² (10 lbf/in. ²)
Temperature, operating	277.4 K (40°F) to 322.2 K (120°F)
Voltage	
Operating	20 to 32 Vdc
Opening	15 Vdc with 2,760 kN/m ² (400 lbf/in. ² gauge) and 322.2 K (120°F), max
Closing	15 Vdc at ambient pressure and 322.2 K (120°F) min
Power	10 W at 30 Vdc and 294.1 K (70°F), max
Response	
Opening with 20 Vdc	15 ms with 2,760 kN/m ² (400 lbf/in. ² gauge) and 322.2 K (120°F), max
Closing with 20 Vdc	15 ms with rated flow at 322.2 K (120°F), max
Life	5000 actuation cycles, min
Port, inlet and outlet	0.64 cm (0.25 in.) diam by 5.1 cm (2 in.) length of 0.038 cm (0.015 in.) wall tube
Electric connector	To be determined
Mounting	To be determined
Material	
Construction	6Al-4V Ti for flow passages
Seat (soft)	AF-E-102 (EPT)
Weight	0.36 kg (0.8 lbm), max
Dielectric strength	100 μA at 600 Vac rms (60 cycle), max
Insulation resistance	100 MΩ at 500 Vdc, min
Envelope	To be determined
Flow media	Hydrazine, isopropyl alcohol, water, helium, and nitrogen

^aLeakage shall be measured with a mass-spectrometer-type leakage detector and the recorded value shall be the largest rate indicated during a test period of at least 30 min.

As TCPS requirements became specific, detailed requirements for TOPS normally closed and latching valves were generated and released in JPL Specifications CS 506221 and CS 506226 (Refs. 24 and 25). The performance and design criteria shown in Tables 9 and 10 were extracted from the JPL specifications to illustrate the current status of normally closed and latching valve requirements.

2. Valve evaluation program. Valves in the TCPS size range for hydrazine control are readily available and performance capabilities have been well documented during qualification testing and flight usage on previous aerospace programs. Several existing valves could be used for the TCPS after appropriate changes in mechanical and electrical interfaces and electrical characteristics if stainless steel is proven acceptable for long-duration missions. Since requisite funding for flight-type hardware was not available, an alternate plan to evaluate as many of the existing valve designs (of Categories I and II of Table 8) as practical during prototype demonstration system testing was adopted.

The demonstration system used two redundant hydrazine flow paths for engine firing. Each path contained a bistable (latching) and a normally closed solenoid valve. The valves in the first path were the Carleton bistable (mechanical latch), soft seat valve, Part No. 2217-07-2-1; and the Hydraulic Research normally closed, hard seat valve, Part No. 48000360. The valves in the second path were the Marquardt bistable (magnetic latch), soft seat valve, Part No. T-8700; and the Marquardt normally closed, soft seat valve Part No. 228511. These valves, pic-

tured in Figs. 18 through 21 respectively, all passed a GN_2 bubble-leak acceptance test indicating a leakage rate of less than 2.8×10^{-4} STP cm^3/s . The simulated mission requirements for the TCPS module were successfully attained during tests at the JPL Edwards Test Station (ETS). Detailed results are presented in Section IV.

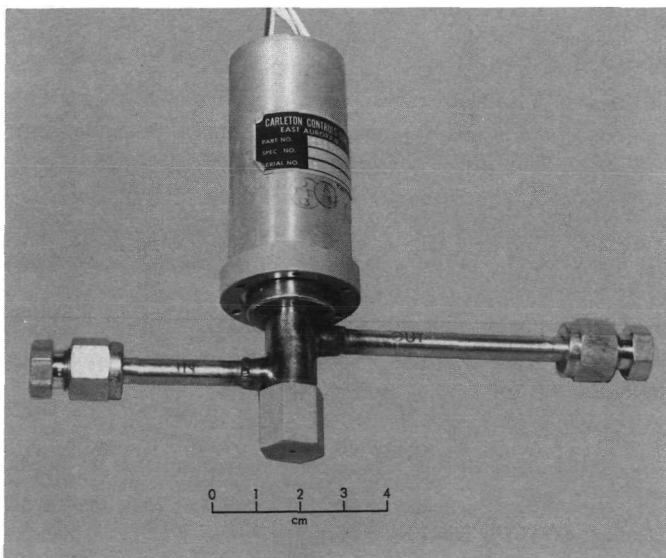


Fig. 18. Carleton bistable (latching) solenoid valve

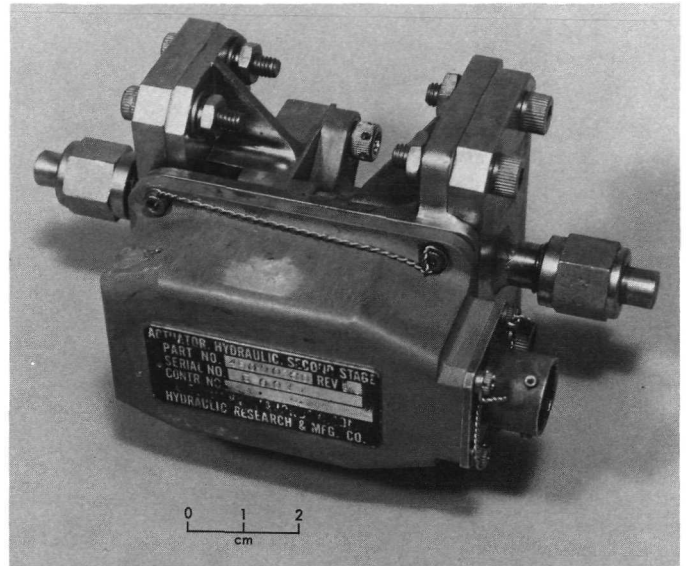


Fig. 19. Hydraulic Research normally closed solenoid valve

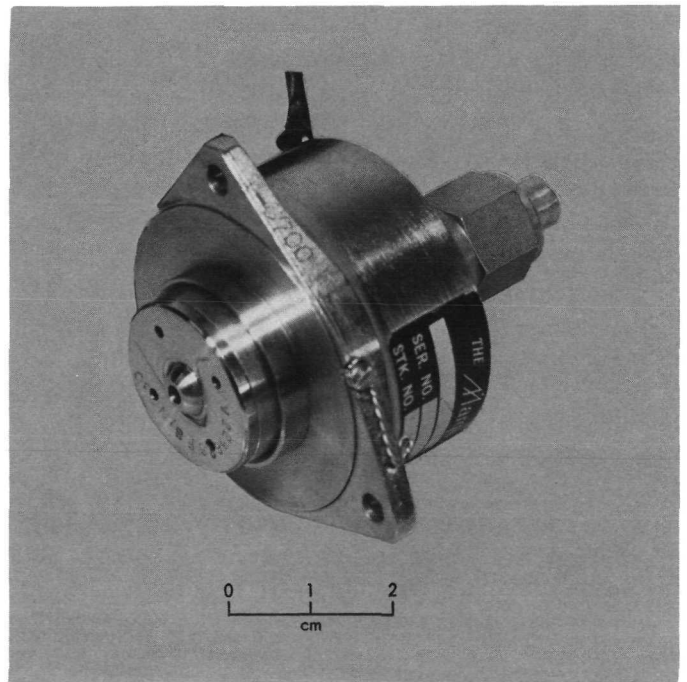


Fig. 20. Marquardt bistable (latching) solenoid valve

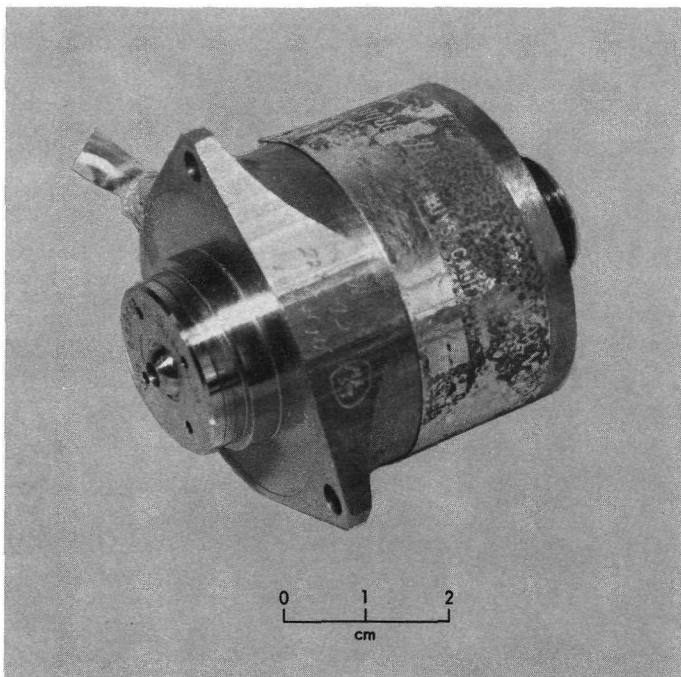


Fig. 21. Marquardt normally closed solenoid valve

The quantity of available performance data for the TCPS size valves minimized the requirement for test verification of valve capability. The small number of actuations required of TCPS valves and the long-term nature of TOPS environmental requirements rendered short-term test verification of design adequacy almost meaningless. Even if flight hardware were available now, the proposed launch dates would preclude real-time verification of the major unknown, which involves valve capability for satisfactory performance during missions as long as ten years. Some limited valve testing was conducted under over-stress conditions to provide the basis for future efforts and to determine an approximate magnitude for the long-term operation problem.

To test valve endurance, valves were cycled many times in a closed-loop recirculation system during relatively short (one- to nine-month) time periods of exposure to hydrazine. Many more cycles than anticipated during the TOPS mission were programmed and accumulated during these tests. Also, hydrazine exposure testing was initiated at ETS. Valves are occasionally cycled to verify performance during continuing exposure to hydrazine. A small hydrazine sample drawn from the tank/valve system during each valve actuation is analyzed for decomposition and corrosion products. These tests will be continued as long as possible with approximately three years as the target duration.

3. Test results. The majority of the TOPS valve testing was performed on valves in the smaller (APS) size range to minimize the amount of hydrazine required for a flow-test setup. This test program was justified on the basis that:

- (1) An adequate amount of short-term performance data for the TCPS size valves that were selected for initial feasibility demonstrations were available from previous aerospace programs.
- (2) Testing of the smaller valves was more economical and, since most problems are common to both TCPS and APS size valves, solutions to any problem would be equally apt. Any redesign or rework for solution to problems is generally more difficult to achieve in the smaller sizes.

During endurance tests, one TCPS valve, Carleton Part No. 2217-07-2-1, was cycled 3,100 times during a seven-month exposure period. The primary purpose of this test was to evaluate the performance of the over-center Belleville spring, which is used for the mechanical latching mechanism. Performance of the valve was satisfactory but the response traces after 2,700 cycles indicated that the opening time had increased from 9 to 10 ms. The cause for the increase was not determined. The valve was removed from the endurance test setup and installed in the APS thruster test stand as a facility shutoff valve. Usage in this setup will provide long-term exposure to hydrazine with only occasional actuations. Performance will be monitored for additional evidence of degradation in opening response.

Three valves in storage test at ETS are continually exposed to the local ambient conditions encountered in an uncontrolled desert environment. Temperatures during winter nights are below the freezing point for hydrazine and, during summer days, may approach 339 K (150°F). Temperatures continuously cycle between daytime highs and nighttime lows to provide rather severe test conditions. Only one of the three valves, Marquardt Part No. 228510, is in the TCPS size range, and performance of this valve has been satisfactory during the 18 months that the valve has been in test. The test is programmed to continue until the associated tank test is completed or the valve fails. Cumulative exposure under these severe test conditions should be approximately three years.

4. Leakage limit specification. The solenoid valve leakage limit requirement is the end product of a long line of analysis and assumption. The starting point is the spacecraft specification of an upper limit for unpredictable and unmodelable spacecraft accelerations. This limit is derived

largely from past flight experience. The maximum acceleration is the vector sum of accelerations from unscheduled events like leakage and from the unpredictable part of scheduled events like rocket engine firings. The preliminary TOPS mission steady state value is 10^{-12} km/s².

The spacecraft limit is then statistically apportioned among the subsystems containing fluids; the TCPS and APS get the lion's share, although other sources like the fluid-filled tape recorder and the RTC's get a share also. Finally, each spacecraft subsystem must apportion its limit among the appropriate components giving due consideration to the possibility of vectorial cancellation of forces. In the case of the all-welded TCPS, the solenoid valves are expected to be the prime sources of any leakage.

The component limit applies throughout the mission, so the valve leakage requirement must be an end-of-mission requirement. Thus, there is a need for accelerated test techniques to demonstrate compliance with the 10-yr requirement, or the acceptance test leakage requirement must be conservative enough to make the end-of-mission value realizable.

The detailed analytical process just outlined requires more detailed spacecraft information than the TOPS program generated. Thus, firm leakage requirements were not developed for TCPS components, particularly the solenoid valves. A provisional solenoid valve leakage requirement of 2.8×10^{-4} STP cm³/s of GN₂ was established as an upper bound for valves sealing liquids; this requirement is realizable with present technology, although not necessarily with current designs. Actual outer planets flight projects will have to establish their own leakage requirement when their design has matured to the point where the necessary spacecraft design details are available.

5. Magnetic field suppression. The TOPS requirements for control of spacecraft magnetic fields are one to two orders of magnitude more restrictive than those for any previous JPL program. The TOPS magnetic field sensor requires the stability of the magnetic field at its location [about 9.4 m (31 ft) from the closest bus-mounted assembly] to be 0.01 nT (0.01 gamma) or less, which essentially limits the spacecraft magnetic field (at the sensor) to 0.01 nT. The component or subsystem requirement is even lower than 0.01 nT. The limited TOPS activities in this area were directed toward minimizing and stabilizing the magnetic fields of each subassembly and component.

The electrical actuators for the TOPS propellant control valves rank among the offenders in that, by design, rela-

tively powerful magnetic fields are required to actuate the valve mechanisms when engine operation is required. Magnetic materials and circuit efficiencies can be optimized to minimize external fields, but shielding and compensation techniques will probably be required to limit the influence on the magnetometer.

Resources were not available to explore the magnetic field problem in depth during the TOPS program, but the cursory examination that was accomplished indicated that this area requires a significant amount of investigation to ensure that effective control can be obtained. Table 11 lists the magnetic fields of several existing valve designs that were mapped by the JPL Electromagnetic Compatibility Group. Attempting to relate this data is not too meaningful because of the wide variance in valve operating conditions. In no case was the magnetic field of the energized solenoid low enough to meet the design goal of 20 nT at 0.15 m (6 in.) from the center of the component. The unenergized field strength of some valves without permanent magnets approached the design goal. Since the valves operate only intermittently, scheduling of science observations during quiescent periods may suffice to solve the magnetic field problem provided that the stability of the unenergized field is not affected by strong planetary fields or time (age).

The limited data that are available indicate that the most promising approach involves limiting the strength of the generated fields by good design rather than trying to shield or compensate for unnecessarily large field strengths. Specific tasks for future effort are:

- (1) Evaluation of material properties, shapes, and processing.
- (2) Analytical modeling of magnetic circuits.
- (3) Magnetic circuit design and evaluation.
- (4) Magnetically "clean" valve design and evaluation.
- (5) Shielding and compensation techniques.

Further effort with shielding and compensation is programmed when the final valve configurations are available. The final designs will minimize generated magnetic fields by limiting power inputs, utilizing optimum magnetic materials, and maximizing magnetic circuit efficiency.

C. Pyrovalves

The TOPS TCPS uses five normally closed (NC) and five normally open (NO) pyrovalves to initiate propellant

Table 11. Experimental data from valve magnetic field tests

Vendor and part No.	Maximum field strength at 0.15 m (6 in.), nT		Valve type	Test conditions	Comment	
	Energized	Deenergized				
Moog, Model 52X140	110,000	—	External torque motor	28 V	Shielding reduced field by a factor of five. Performance degraded	
Marquardt, 225930	186,000	—	Dual coil in-line solenoid	0.5 A	Coil 1	
	216,000	—		2.0 A	Coil 2	
	338,000	890		2.5 A	Both coils	
Moog, Model 53-106	95,000	91,000	External torque motor	28 V 0.5 A	—	
Marquardt, 228511	55,300	2,760	Dual coil in-line solenoid	26 V	Lunar Orbiter	
	60,500	2,920		30 V	Apollo R4D (Fuel)	
Marquardt, T 8700	26,700	378	Magnetic latching	30 V	Opening	
	12,700	810		30 V	Closing	
Marquardt, 228684, SN 027	67,800	1,950	Dual coil in-line solenoid	30 V	Apollo R4D (Oxidizer)	
Marquardt, 228684, SN 045	77,000	1,860	Dual coil in-line solenoid	30 V	Apollo R4D (Oxidizer)	
Carleton, 2217001-2-1	60,500	730	Mechanical latching	28 V	Opening	Intelsat 4
	60,300	324			Closing	

flow from, and to isolate residual propellant and pressurant within, the propellant supply tank. These valves perform redundant functions for the solenoid valves that are used for operating the trajectory correction engine. The propellant feed line is opened when engine operation is required for velocity corrections and closed when the maneuver period is completed.

The pyrovalves are installed in a ladder arrangement, providing four trajectory correction maneuvers with one of each type valve available as a spare (Fig. 22). This arrangement permits the next valve of each type in sequence to perform the opening or closing of the feed tube should the preceding valve fail to perform the commanded function. Figure 23 shows the physical arrangement of the ten valves that were used for the TCPS demonstration system tested at ETS. Details of the system tests are presented in Section IV.

1. Aluminum valve development program. A JPL Source Information Request was submitted to 13 manufacturers to determine the existence and developmental status of zero-blowby-type pyrovalves. Seven manufacturers responded to the request, but only one submission was fully responsive to the requirements in the SIR. The full specifications for the NC and NO valves follow.

The general pyrovalve requirements are:

- (1) Materials and processing shall be compatible with hydrazine. Use of magnetic materials shall be minimized.
- (2) External leakage shall be less than 10^{-6} STP cm^3/s of He when pressurized at 5,500 kN/m² (800 psig). Welding is the preferred process for fabricating the valve bodies.
- (3) Valve actuation shall not introduce metal fragments into the propellant passage.
- (4) All products of combustion shall be contained in the cavity between the explosive actuator (squib) and the ram. A metal barrier between the products of combustion and the propellant is desirable.
- (5) Explosive actuators must be removable.
- (6) Envelope, weight, and pressure drop at rated flow should all be minimized within the constraints of the valve designs.
- (7) Pressures:
 - Operating—0 to 2,750 kN/m² (0 to 400 psig)
 - Proof—5,500 kN/m² (800 psig) (min)
 - Burst—11,000 kN/m² (1600 psig) (min).

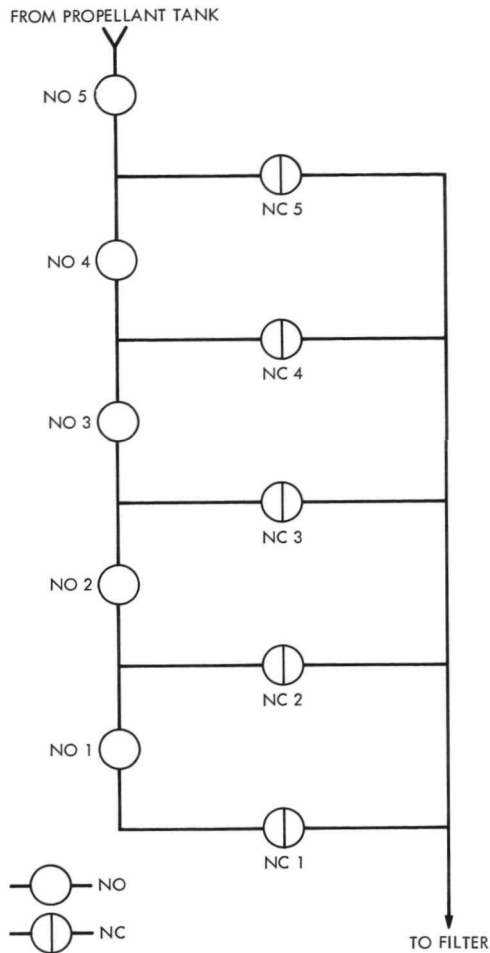


Fig. 22. Pyrovalve manifold schematic diagram

- (8) Temperature: 255 to 311 K (0 to 100°F).
- (9) Flowrate: 0.113 kg/s (0.25 lbm/s) hydrazine (max).
- (10) One NC and one NO valve may be manifolded or fabricated from a single housing. Fittings (MS-33656-4) shall be provided for installing valves in test setups and systems. Mounting provisions are optional.

The normally-closed valve requirements are:

- (1) Prior to actuation, inlet and outlet ports shall be sealed with parent-metal membranes that will withstand the specified proof pressure without leakage into the ram cavity.
- (2) Subsequent to actuation, the valve shall provide a straight-through flow path with a minimum pressure drop at rated flow, and withstand proof pressure without retraction of the ram or leakage into the squib cavity.

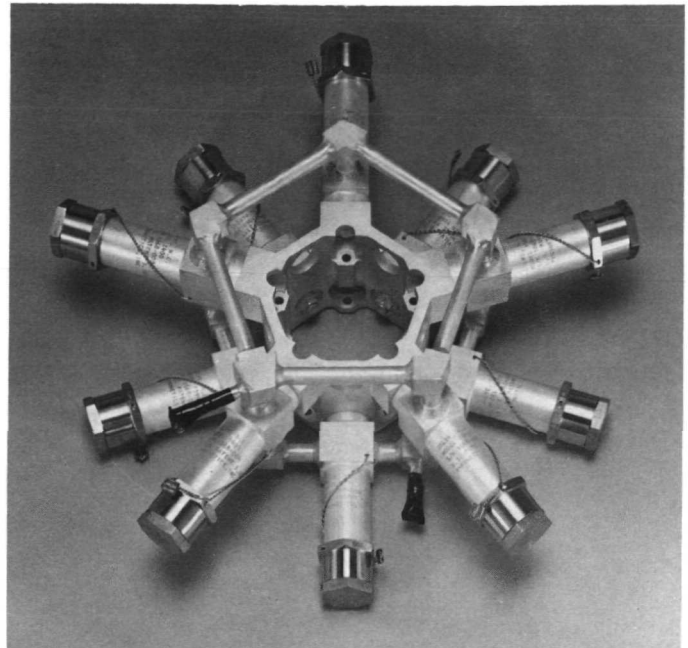


Fig. 23. Pyrovalve manifold assembly for prototype demonstration test system

- (3) Opening of the valve shall be accomplished by shearing rather than cutting the parent-metal membranes.
- (4) A plug shall be provided to properly position the ram and prevent foreign materials from entering the squib installation port when the squib is not installed.

The normally-open valve requirements are:

- (1) Prior to actuation, the valve shall provide a straight-through flow path with a minimum pressure drop at rated flow, and withstand proof pressure without retraction of the ram or leakage into the squib cavity.
- (2) Actuation shall not cause large pressure transients in the propellant supply lines.
- (3) After closing, the valves shall withstand proof pressure without leakage through the valve or into the cavity between the squib and the ram.
- (4) A plug shall be provided to properly position the ram and prevent foreign materials from entering the squib installation port when the squib is not installed.

The JPL Standard Squib as defined by Refs. 26 and 27 is the preferred squib for use in all valves. In the event

that a proposed valve design requires or is presently qualified with a different squib, that squib shall be described as completely as possible, including a graph of output pressure vs time and a qualification history.

Six each NO and NC pyrovalves were fabricated, tested, and delivered to JPL by Pyronetics, Inc. These valves met the performance requirements shown in Table 12 and the environmental requirements of Ref. 11 as verified by the acceptance and lot-sample test requirements shown in

Tables 13 and 14. Results of this effort are presented in Refs. 28 and 29. Both valve designs provided capability that met or exceeded design requirements. Basic valve characteristics are listed in Table 15.

The unique feature of these valves is the sealing system that keeps squib gas from entering the propellant flow passage. A separate actuator assembly forces the ram to translate and operate the valve as shown in Fig. 24. A metal bellows welded to the actuator housing and the

Table 12. Pyrovalve performance and design criteria

Valve	Characteristic	Dimension	Requirement
Both	Pressure		
	Operating	kN/m ² (psig)	0 to 3,450 (0 to 500)
	Proof	kN/m ² (psig)	6,890 (1000) (min)
	Burst	kN/m ² (psig)	13,800 (2000) (min)
Both	Leakage, external (He) ^a	STP cm ³ /s	10 ⁻⁶ (max) from 0 to 6,890 kN/m ² (0 to 1000 psig) before and after actuation
1399 (NO)	Leakage, internal (He) ^a	STP cm ³ /s	10 ⁻⁶ (max) from 0 to 3,450 kN/m ² (0 to 500 psig) (after actuation)
1400 (NC)	Leakage, internal (He) ^a	STP cm ³ /s	10 ⁻⁶ (max) from 0 to 3,450 kN/m ² (0 to 500 psig) (before actuation)
1399	Flowrate, hydrazine	kg/s (lb/s)	0.068 (0.15) (before actuation)
1400	Flowrate, hydrazine	kg/s (lb/s)	0.068 (0.15) (after actuation)
Both	Pressure drop at 0.068 kg/s (0.15 lb/s), hydrazine	kN/m ² (psid)	34.4 (5) (max)
Both	Temperature, operating	K (°F)	277 to 345 (+40 to +160)
Both	Line size, nominal ID	cm (in.)	0.437 (0.172) diam
Both	Ports		
	Nominal OD	cm (in.)	1.07 (0.420) diam
	Nominal length	cm (in.)	5.08 (2.0) from C _L of valve
Both	Mounting brackets	—	None (tube mounted)
Both	Flow media	—	Hydrazine, isopropyl alcohol, water, helium, and GN ₂
Both	Metals	—	6061-T6 aluminum bodies and nipples; CRES acceptable for balance
Both	Elastomers	—	EPR (Parker E515-8 or equivalent)
Both	Fabrication	—	Welding for nipple-to-body joints
Both	Weld rod	—	4043 aluminum
Both	Products of combustion	—	Contained within a metal barrier between the squib cavity and the valve body cavity
Both	Metal fragments	TBD	A minimum amount shall be introduced into the propellant passage during actuation
Both	Squib (JPL furnished)	—	JPL Standard Part No. 10028049; Spec ES504522
Both	Plug	—	Close squib boss when the squib is not installed
Both	Cleanliness	—	Level D2 of JPL Spec FS504574

^aLeakage shall be measured with a mass spectrometer type leakage detector and the recorded value shall be the largest rate indicated during a test period of at least 30 min.

Table 13. Pyrovalve test requirements

Test	Acceptance		Evaluation	
	NO	NC	NO	NC
Before assembly				
Proof pressure	X	X	X	X
Body and nipples at 6,890 kN/m ² (1000 psig)				
Bellows at 3,450 kN/m ² (500 psig) of He ^a				
Leakage	X	X	X	X
Body and nipples at 6,890 kN/m ² (1000 psig) of He ^a				
Bellows after proof with He ^a				
After Assembly				
Examination of product	X	X	X	X
Cleanliness	X	X	X	X
Actuation with H ₂ O			X	X
Ram stroke			—	X
Proof pressure at 6,890 kN/m ² (1000 psig)			X	X
Internal leakage at 6,890 kN/m ² (1000 psig) (He) ^a			X	—
Pressure drop at rated flow (H ₂ O)			—	X
After Disassembly				
Leakage at 6,890 kN/m ² (1000 psig) (He) ^a			X	X
Body, nipples, and ram				
Bellows				
Burst pressure [to rupture or 68,900 kN/m ² (10,000 psig)] (H ₂ O)			X	X

^aSee footnote a in Table 12.

Table 14. Peak response points for vibration tests

Frequency, Hz	Input level, m/s ² (g)	Response level, m/s ² (g)	Valve		Response, axis
			NO	NC	
X-axis					
800	10 (1)	981 (100)	X		X
		29 (3)	X		Y
		414 (45)	X		Z
		1177 (120)		X	X
		29 (3)		X	Y
		392 (40)		X	Z
794	98 (10)	4805 (490)		X	X
		88 (9)		X	Y
		1530 (156)		X	Z
877	98 (10)	5689 (580)	X		X
		118 (12)	X		Y
		981 (100)	X		Z
Y-axis					
491	10 (1)	20 (2)	X		X
		902 (92)	X		Y
		98 (10)	X		Z
		10 (1)		X	X
		628 (64)		X	Y
		39 (4)		X	Z
491	98 (10)	3236 (330)		X	Y
		137 (14)		X	Z
530	98 (10)	3187 (325)	X		Y
		147 (15)	X		Z
806	98 (10)	59 (6)		X	X
820	98 (10)	137 (14)	X		X
Z-axis					
830	10 (1)	29 (3)	X		X
		20 (2)	X		Z
		34 (3.5)		X	X
		20 (2)		X	Z
853	98 (10)	373 (38)	X		X
		167 (17)	X		Z
800	98 (10)	392 (40)		X	X
		196 (20)		X	Z
530	98 (10)	304 (31)	X		Y
500	98 (10)	343 (35)		X	Y

Table 15. Physical characteristics of prototype pyrovalves

Parameter	Aluminum valves	Titanium valves
Pyrotechnic (squib)		
Designation (JPL Part No.)	10028049	10000029
Size; cm diam, threads/cm (in. diam, threads/in.)	2.22, 5.5 (0.875, 14)	1.59, 7.1 (0.625, 18)
Valve dimensions, cm (in.)		
Inlet and outlet port ID	0.45 (0.178)	0.45 (0.178)
Valve body OD (largest)	3.0 (1.2)	2.2 (0.875)
Overall length	12. (4.8)	12. (4.6)
Distance across tube ends	7.6 (3.0)	8.1 (3.2)
Valve mass, kg (lbm)		
Body	0.12 (0.27)	0.075 (0.17)
Actuator	0.13 (0.30)	0.090 (0.20)
Pyrotechnic	0.07 (0.15)	0.028 (0.06)
Total	0.32 (0.72)	0.193 (0.43)

piston prevents any of the squib combustion products from entering the flow passage; redundant seals prevent direct impingement of the hot gases on the thin metal bellows. A thin boattail section on the piston expands to provide a metal-to-metal seal when pressurized by the squib gases. Any gas that leaks past the metal-to-metal seal is retained by the ethylene propylene rubber (EPR) O-ring. Should any gas leak past the EPR O-ring, the bellows will prevent blowby into the propellant flow passage.

Five each NO and NC valves were manifolded into the assembly shown in Fig. 23. This assembly was heat-treated to return all of the 6061 aluminum welds to the T6 condition prior to final cleaning and installation of the rams and actuator units. The manifolded assembly was exposed to 9.8 m/s^2 (1-g) sinusoidal sweeps to map natural frequencies and determine amplitude ratios for resonant peaks. The input axes and the response accelerometers are shown in Fig. 25. The resonant frequencies and output responses are shown in Table 16. The large responses indicate that the manifolded assembly will require additional stabilization to minimize compliance before exposure to higher vibration levels. Supports at the squib end of the valves will probably be sufficient to stabilize the assembly. Alternate valve mounting methods with the mounts nearer the center of gravity would also be beneficial.

The remaining valves, one each NO and NC, were delivered as spares and ultimately tested as components to determine capability to withstand the TOPS vibration and shock environments (Ref. 11). All tests were satisfactory.

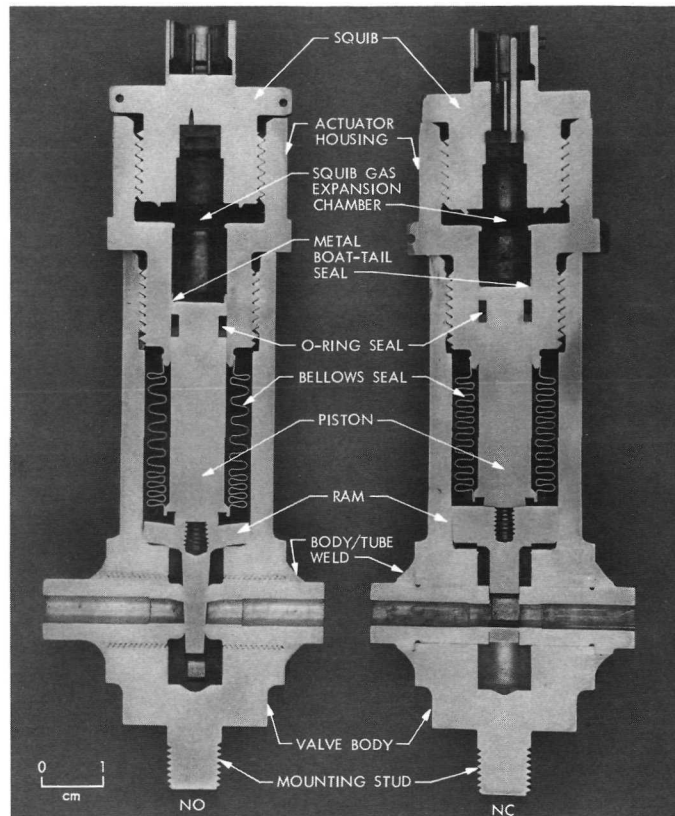


Fig. 24. Cross section of aluminum NO and NC pyrovalves after actuation

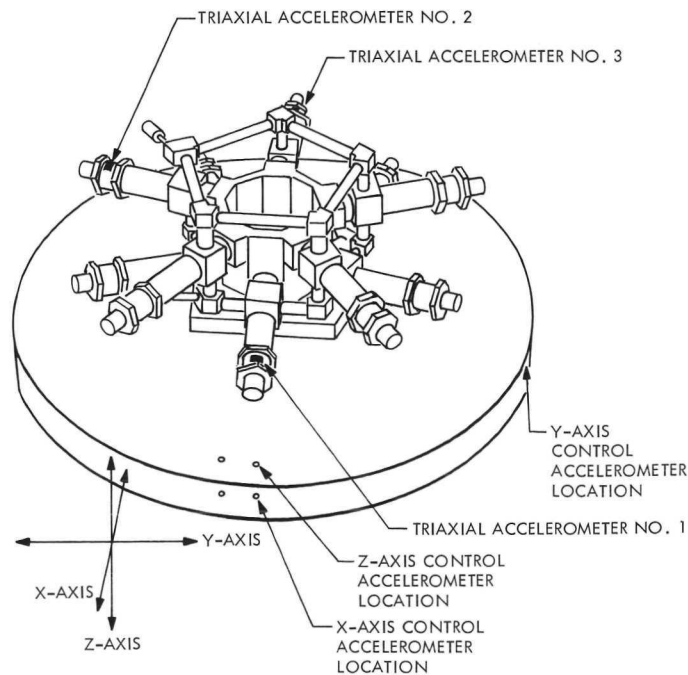


Fig. 25. Pyrovalve manifold vibration test configuration and axis designation

Table 16. Amplitude magnification ratios at pyrovalve manifold vibration response frequencies

Accelerometer location and axis	Response frequencies, Hz														
	Input to X-axis									Input to Y-axis			Input to Z-axis		
	250	280	310	350	375	700	1300	270	370	600	650	1250	1275	350	700
Amplitude magnification ratios															
1 X-axis	—	13	—	—	—	15	23	10	—	—	15	26	20	42	—
1 Y-axis	10	23	—	—	26	34	27	—	40	—	200	—	—	—	—
1 Z-axis	26	70	30	22	24	23	—	40	—	—	30	—	—	168	20
2 X-axis	28	—	13	—	30	—	—	33	38	—	15	27	—	19	—
2 Y-axis	13	—	10	—	30	30	68	36	—	—	36	80	—	12	10
2 Z-axis	—	13	—	—	—	35	23	42	22	—	—	36	—	90	36
3 X-axis	—	13	—	—	—	45	63	17	12	—	—	55	—	30	—
3 Y-axis	36	38	20	—	42	—	—	100	104	—	—	—	—	19	—
3 Z-axis	—	—	—	—	15	20	30	68	50	58	70	74	—	68	34

Results of the development program indicate that the valves, as designed, would provide satisfactory flight hardware for an aluminum, propellant-feed system. Two design changes should be made to optimize valve envelope and decrease the high-amplitude responses during exposure to mechanical environments:

- (1) The squib, JPL Part No. 10028049, should be replaced with another squib having identical output pressure but enveloped with a 1.27-cm-diam, 7.9-threads/cm (0.5-in.-diam, 20-threads/cm) shell instead of the 1.59-cm-diam, 5.5-threads/cm (0.875-in.-diam, 14-threads/in.) shell. The change would allow the size of the actuator to be reduced.
- (2) Mounting provisions should be redesigned to locate mounts nearer the center of gravity or provide supports at the squib end of the valves.

2. Titanium valve development program. Following the demonstration of the aluminum zero-blowby pyrovalve, the 6061-T6 aluminum in that valve was replaced with titanium without changing the demonstrated performance capability of the valve design. Changing the ram material from CRES to titanium completed the conversion to titanium of all valve parts that contact the hydrazine. The same CRES actuator assembly design was used since hydrazine does not contact any actuator assembly surfaces. Five each NO and NC valves, similar to the original aluminum valves except that the bodies, nipples, and rams were of 6Al-4V titanium, were fabricated by Pyronetics, Inc. An identical acceptance and evaluation test program was specified to provide data for direct comparison with that from the aluminum valves.

The valve envelope was reduced commensurate with titanium's high strength-to-weight ratio. At the same time, the actuator assembly was also reduced in size by using a JPL Part No. 10000029 (Hi-Shear PC-27) squib that has the same output pressure as the JPL Part No. 10028049 but uses a 1.59-cm-diam, 7.1-threads/cm (0.625-in.-diam, 18-threads/in.) shell. The PC-27 squib was used by JPL for the Mariner Mars missions in 1964 and 1969 and the Mariner Venus mission in 1967. The actuator envelope could have been further reduced by using a squib with a 1.27-cm-diam, 7.9-threads/cm (0.5-in.-diam, 20-threads/in.) shell, but JPL did not have a qualified squib with that configuration.

The NO and NC valves, shown in Fig. 26, use a common actuator assembly and are identical in external appearance. Appropriate internal dimensions, rams, and nipples provide the difference in NO or NC designs as indicated in the figure. Basic valve characteristics are listed in Table 15. The relative mass and size advantages of titanium over aluminum are obvious.

Engineering prototype valves were tested with 75% output pressure (Hi-Shear PC-46) squibs. Valve performance was satisfactory but posttest examination showed that the loads on the tip of the actuator piston had distorted the areas where the bellows was welded and had cracked the bellows. The redundant EPR seals on the piston had retained the squib gases in this case. The actuator assembly was redesigned to stop the piston in the housing so that the tip would not be overstressed by contact with the actuated ram.

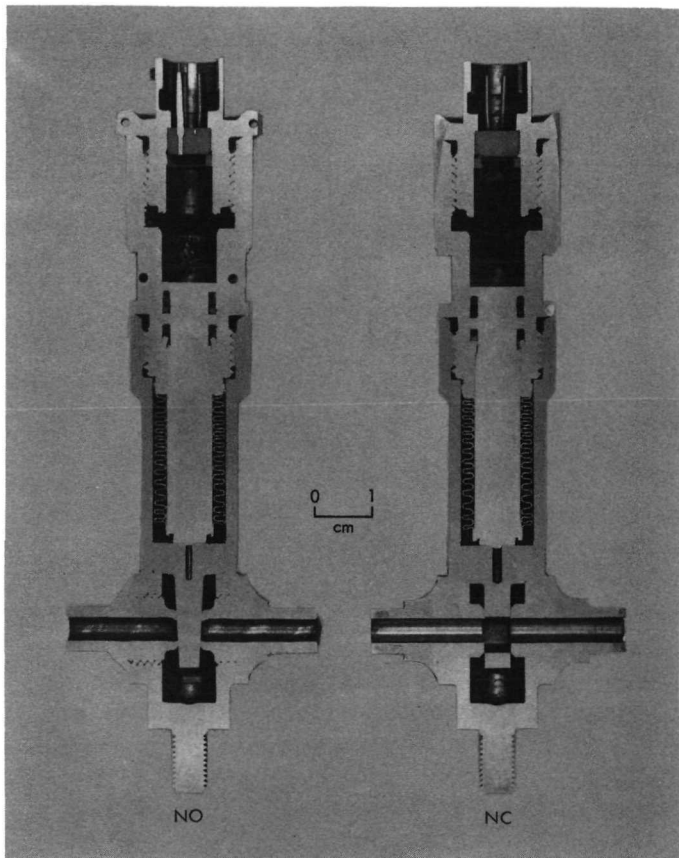


Fig. 26. Cross section of titanium NO and NC pyrovalves after actuation

Two additional valves of each type incorporating the redesigned actuator assemblies and PC-27 (100% output pressure) squibs were tested. Valve performance was satisfactory (Refs. 30 and 31) and two each NO and NC valves were accepted by JPL for evaluation testing similar to that conducted with the aluminum valves (Refs. 30 and 31). Three areas have been identified for further effort with the titanium pyrovalves:

- (1) Manifolding and mounting methods for groups of NO and NC valves in the ladder configuration to withstand spacecraft vibration requirements with minimum mass structure need further investigation.
- (2) The actuator assembly should be made from titanium so that the joint between the actuator and the valve body can be reduced in size and sealed by welding. This redesign would completely eliminate any possibility for leakage and would shorten the overall length of the valve assembly. A titanium bellows is required to effect this redesign. Bellows manufacturers have been contacted and JPL is con-

sidering development of an appropriate convoluted titanium bellows.

- (3) A 1.27-cm- (0.5-in.-) diam dual-bridgewire squib with the pressure output of the larger PC-27 would be ideal for the titanium valve. With such a squib, the valve actuator assembly and chamber could be redesigned to the smaller diameter of the lower part of the chamber (Fig. 26).

D. Propellant Acquisition

A general study of competing types of propellant acquisition devices suitable for TOPS-type missions was completed under the first phase of a JPL-managed contract. A preliminary design of the most promising candidate for the recommended type of device was completed under the second phase of the same contract. These studies are documented in Refs. 32 and 33 respectively.

The nine propellant acquisition concepts identified in the study are shown in Table 17. For reasons described in detail in Ref. 32, only three concepts are applicable to small monopropellant hydrazine systems. Each concept was given a numerical rating in each of six categories that were summed with weighting factors to give the single figure of merit shown in the table. The categories and their respective weighting factors were:

Reliability	25%
Mass	20%
Testability	20%
System compatibility	20%
Availability	10%
Design versatility	5%

Table 17. Propellant acquisition concept selection

Candidate concept	Figure of Merit
Capillary/bellows	NA ^a
Convoluted spherical diaphragms	0.44
Dielectrophoresis	NA
Metal bellows	NA
Polymeric bladders	NA
Polymeric diaphragms	NA
Ring-reinforced diaphragms	NA
Settling rockets	0.38
Surface tension	0.90

^aJudged not applicable for TOPS-type mission

A metallic surface-tension-type of acquisition device is the clear choice for a 10-yr mission. Such devices are lighter, more reliable, and more compatible with hydrazine and the spacecraft nuclear radiation environment. However, these devices are difficult to test before launch. The property of whether or not a design can feed bubble-free propellant against 9.8 m/s^2 (1 g) divides surface-tension devices into two classes: one based on screen traps and the other on a pillar with channels. Thus a study of a design of each type is reported in Ref. 33.

The design that cannot be tested at 9.8 m/s^2 (1 g) is shown in Fig. 27. The central tapered pillar centers the fuel over the tank outlet. The channels located on the tank walls are designed to return fuel displaced by any disturbance from the outlet area back to that area. The tank outlet is thus the only equilibrium location for the propellant in the tank. The pillar is sized for the TCPS application where the initial hydrazine tank ullage is 50%. Were the initial ullage smaller, a higher pillar would be required.

This particular design meets all of the evaluation criteria discussed earlier except testability. Although not testable at 9.8 m/s^2 (1-g), its operation can be adequately verified through model testing and actual flight experience once the design is flown. Reference 33 recommends this design for all applications where the 9.8 m/s^2 (1-g) test requirement is not absolutely necessary.

The surface-tension-class of acquisition devices was selected for the TOPS baseline TCPS configuration. A specific design was not chosen because this area of technology is still in too early a stage of development and flight experience

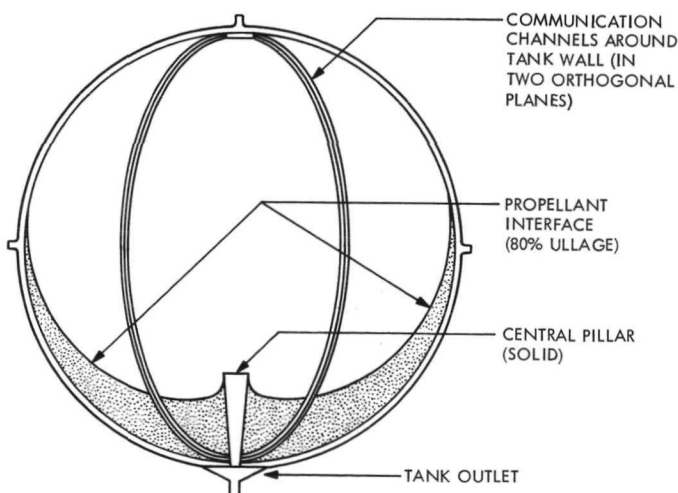


Fig. 27. Candidate design for TCPS propellant acquisition device

for a reasonable consensus on an optimum design to have appeared. Such a selection is left to the actual flight projects to make when they must with the then available information.

Some surface-tension-device designs have flown in parallel with other acquisition devices, such as polymeric bladders, and some designs are now coming into service as the primary propellant acquisition method. The TOPS program followed the Viking Orbiter propulsion contract work on a pillar and channel device in particular. This design is similar to Fig. 27; it differs in having a taller pillar with flexible baffles attached to it as a result of the requirement to positively center the ullage bubble for ullages of 10 to near 100%.

E. Unevaluated Components

For various reasons to be discussed, some minor components were not evaluated for the TOPS application.

1. Transducers. The need to evaluate several aspects of current transducer technology and designs was identified early in the TOPS program. However, the investigations of the major components was of higher priority. Work completed in this field for other JPL programs did supply some useful general information.

Two general questions about transducers were raised: the first concerned building standard transducers of new materials, and the second involved estimating the utility/cost ratio of the less often used, more difficult measurements. In the first case, transducers built primarily of titanium promise improved compatibility with hydrazine for a lower mass than previously flown hardware. For maximum accuracy and reliability, the pressure transducers should be of the strain gage type. Flightweight strain gage transducers made of stainless steel have been extensively evaluated for the Mariner-Venus-Mercury (1973) and Viking (1975) Projects. Experimental, nonflightweight strain gage transducers made of titanium are available. The results of this work indicate that flightweight titanium strain gage pressure and differential pressure transducers can be readily achieved for a minor cost increase relative to current stainless steel models.

A flightweight titanium strain gage pressure transducer with its associated electronics should weigh about 0.17 kg (0.38 lb) and be smaller than 2.5-cm (1-in.) diam by 8.9 cm (3.5 in.) long. Similarly, the differential pressure transducer parameters are 0.2 kg (0.44 lb) and 3.8-cm (1.5-in.) diam by 8.9 cm (3.5 in.) in length.

The materials question also arises with immersion thermocouples. To avoid mechanical seals in favor of welded joints, the thermocouple sheath must be made of the same material as the hydrazine line, which in the case of TOPS is titanium. Neither the fabrication of titanium immersion thermocouples or the welding process appear particularly difficult, but this could not be verified in the TOPS program.

The rocket engine immersion thermocouple falls in the second case, that of infrequently used, difficult measurements. This thermocouple must be sheathed in an L-605 or L-605-compatible material like Inconel, welded in place, and survive the flow and thermal cycling forces encountered in the catalyst bed. The reliability of current hardware is questionable in light of the failure of the catalyst bed thermocouple late in the system demonstration test series (Subsection IV-D-3). This thermocouple application was not evaluated in detail in the TOPS program.

The direct measurement of thrust has not been made on U.S. planetary spacecraft. This measurement is useful for inflight performance evaluation and might be used for engine cutoff control (Subsection V-E-2). Although several means of making this measurement exist, a strain gage mounted on the engine support structure appears simplest. However, this constrains the design of the engine support. Thrust measurement was considered for the demonstration system, but the engine support was judged too massive to give meaningful strain gage data, so the test of this concept was deleted.

2. Filter. The primary TCPS filter specifications are:

- (1) Titanium material as part of the all-titanium feed system.
- (2) Filtration rating of 10 to 25 μm (microns) absolute.
- (3) Stacked disc design for easy cleaning and minimum particle generation.

The absolute filtration rating must be fine enough to preclude particulate damage to polymeric valve seats. A definitive analysis for the maximum particle size for which no seat damage occurs has not been formulated, so a range of filtration is shown.

APS filter requirements are identical to the TCPS requirements except for the filtration rating, which was set at 1 μm (micron) for evaluation purposes. Because the APS requirements are more severe, they were used in the development of a TOPS filter. A 1- μm (micron) absolute filter

composed of stainless steel discs in a titanium housing was developed. Titanium discs were investigated and proved feasible, although an all-titanium filter was not fabricated for TOPS. This work, described in Ref. 4, applies to the TCPS application with a change in disc etch depth, and thereby filtration rating, and filter surface area.

3. Service valve. The TCPS requires titanium service or fill valves. Since such valves have been used successfully on several spacecraft, such as Intelsat IV, they were not included in the TOPS component or system test program.

4. Propellant tank. Titanium hydrazine tanks have been flown on all Mariner spacecraft, so evaluation testing was not required.

F. Hydrazine/Material Interaction

Material-compatibility data for liquid propellants, such as hydrazine and hydrazine/hydrazine nitrate, with spacecraft materials of construction are inadequate for the design of spacecraft propulsion systems for long-duration missions. Materials that are incompatible with propellants can result in propellant decomposition, affecting adversely the performance of the liquid propulsion system and generating gases that can affect adversely the fluid dynamics of metering orifices and capillary tubes. Corrosion and the formation of salt deposits or other corrosion products can plug filters and orifices, allow seal leakage, affect valve operation, weaken structural members, and affect overall propulsion feed-system performance.

The design of spacecraft propulsion feed systems that require 10-year containment of liquid propellants has been compromised because of the lack of reliable propellant/material compatibility information. Although numerous material-compatibility experiments have been conducted over the years, the results of these tests are inadequate or sufficiently misleading to limit trade-off flexibility in the selection of acceptable materials, or combinations of materials, for construction of high-performance propulsion systems. No fully satisfactory substitute for real-time material compatibility testing has been found; therefore, a test program based upon long-term exposure of materials to propellants was initiated to determine any noncompatible tendencies.

1. Material compatibility test program. The overall objective of the material-compatibility effort was to demonstrate acceptably inert materials of construction for the TOPS hydrazine monopropellant propulsion systems, which involved 10-year storage of hydrazine. More specifically, the overall aim was to determine material selections

for the liquid propulsion components and feed-system elements, from tests lasting from 1970 and 1971 until about 1974 when component designs for missions of the late Seventies are finalized.

Typical specimens of TOPS candidate materials, were tested in as-received (or Mil-Spec) hydrazine, purified hydrazine, and hydrazine/hydrazine nitrate. Test capsules containing the specimens and propellants were placed in long-term storage testing at the Compatibility Test Facility located at ETS. This test program incorporates some basic improvements over earlier programs, such as improved techniques for the measurement of test-capsule pressures. The stainless steel Bourdon-tube gage, utilized in an earlier program, as reported in Ref. 34, has been replaced by an externally mounted transducer to prevent a chemical reaction from taking place between the Bourdon-gage material and the propellant. A hermetic seal at the top of the capsule prevents any external elements other than the ambient temperature in the test area, which is maintained at 316 K (110°F), from affecting possible chemical reactions. Readout of specimen/capsule pressures is accomplished remotely.

All of the specimen/capsules have been prepared, using semiproduction techniques to reduce cost, to achieve uniformity among specimens and capsules, and to provide a sufficient number of specimen/capsules for multiple identical experiments replication. Figure 28 is a photograph of a typical specimen/capsule used on the TOPS material compatibility program. The major items pictured include: (1) the TOPS propellant, in this case as-received or purified hydrazine or hydrazine/hydrazine nitrate; (2) the slug-type metallic specimen, made of certified materials only, all steps in the preparation being documented for complete traceability; (3) the externally mounted transducer that senses internal capsule pressure and transmits the information to a remote control room; and (4) the hermetic seal at the top of the capsule to isolate chemical reactions within the capsule from external influences. The specimen/capsules were prepared in a clean room with a Federal Standard 209A, Class 100 Certification.

One of the program goals was to maintain a high degree of control over all phases of specimen preparation including dimension and configuration control. The classification of specimens according to configuration is as follows: slug or coupon, bimetal-contact, bimetal-separated, stressed, welded, brazed, coated, plated, and screens. Each specimen was fabricated to specified dimensions and tolerances; for example, the slug-type specimen is rectangular, 76.2 mm (3.00 in.) long, 12.7 mm (0.50 in.) wide, and

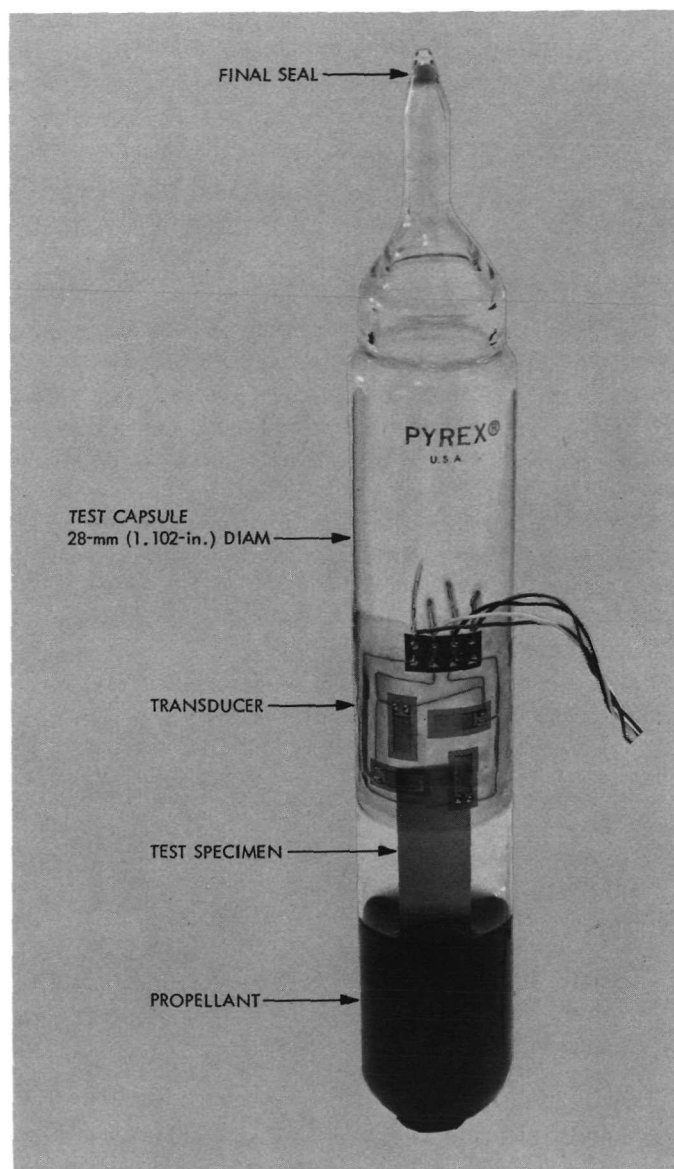


Fig. 28. Typical specimen/capsule used in hydrazine/material compatibility tests

0.76 mm (0.030 in.) thick. Bimetal-contact specimens are similar to the slug-type with the exception that one of the two specimens has an offset bend to facilitate contact at the specimen ends. A glass C-type clip is used to maintain contact between the ends of the bimetal-contact specimens. The bimetal-separated specimens are also similar to the slug-type specimen, or coupon. In this case, a glass separator is used to prevent any contact between the two specimens. A specially designed stressing fixture is used to maintain slug-type specimens at $\frac{2}{3}$ of yield stress while undergoing immersion testing. Welded specimens are similar to the slug-type configuration with the weld bead

running in a longitudinal direction. Similarly, the brazed specimens are of the slug-type configuration with the brazed joint oriented in a longitudinal direction. Coated and plated specimens are obtained by coating or plating slug-type specimens. Screens, for use in surface-tension studies, are cut in the shape of the slug-type specimen. For a more detailed description of both specimens and capsules prepared under contract, see Ref. 35.

Compatibility tests for three different monopropellants were started under the TOPS program. First, more tests of as-received hydrazine with materials likely to be used on TOPS-type missions were added to those put into test under the earlier research and advanced development program that pioneered the test techniques and procedures. Second, tests of JPL-purified hydrazine were started, again emphasizing TOPS materials. Note that both as-received and purified hydrazine meet the military specification for hydrazine. Third, exploratory tests were begun with a JPL-produced blend of hydrazine and hydrazine nitrate (76:24 by mass) with general classes of materials since no data were found in the literature for this monopropellant.

Table 18 gives the detailed assays of propellant used in this test program. The number and type of each specimen put into test for each of the three propellants are given in Tables 19 and 20. Pertinent details on each group of specimen/capsules are:

- (1) As-received hydrazine: the fifty specimen/capsules were placed in test in FY 1971 bringing the total number of capsules in test for this propellant at JPL to 231.
- (2) Purified hydrazine: twenty-four specimen/capsules were placed in test during FY 1972. Under this work, studies were directed toward investigating the effect of reduced ammonia and water content on the long-term-storage characteristics of purified hydrazine. Concentrations of ammonia, aniline, and water occurring in as-received hydrazine have been reduced to trace amounts using a distillation process.
- (3) Hydrazine/hydrazine nitrate: seventy-two specimen/capsules were placed in test in FY 1971. This blend is thought to be compatible with fewer materials than hydrazine, although the nitric acid element may be stabilizing in some cases.

2. Post-test evaluation. Post-test evaluation accomplished to date has included scanning-electron micro-

scopy, electron microprobe analysis, corrosion, hardness, and surface analysis, as well as microscopic study of latitudinal and longitudinal sections in the liquid-phase and gaseous-phase portions of the specimens. Fifty as-received hydrazine, and 36 hydrazine/hydrazine nitrate specimen/capsules have been removed from test to date, primarily because of overpressurization, and are currently being stored under refrigeration awaiting posttest evaluation. Because of the relatively high cost of posttest evaluation, and the relatively large number of specimen/capsules available, a high degree of selectivity is being exercised in choosing specimens for extensive analysis. Some of the less-interesting specimens will therefore be evaluated on a minimal basis. Some specimens might be stored under refrigeration only and considered as "insurance" specimens. These specimens can be subsequently evaluated depending on the specific needs of future flight projects.

Four test specimens of 6Al-4V titanium in as-received hydrazine, removed from the fuel test-bay at JPL Edwards Test Station, have been evaluated extensively by the Stanford Research Institute (Ref. 36) to determine the reason for the occurrence of hydrogen embrittlement. The conclusion reached was that decomposition of the hydrazine and corrosion of the titanium resulted from a reaction between the hydrazine and Freon-TF used as a cleaning agent. Thus isopropyl alcohol is the recommended cleaning and rinsing agent for all 6Al-4V titanium that will be in contact with hydrazine; the use of Freon, or Freon-type materials, should be prohibited as cleaning or rinsing agents for all 6Al-4V titanium that will be in contact with liquid or gaseous hydrazine. Isopropyl alcohol is better than Freon for removing inorganic material and does not interact with the hydrazine or the titanium. This information has been included in NASA Pre-Alert No. E4-70-03A (Ref. 37).

Although none of the hydrazine/hydrazine nitrate specimen/capsule analyses have been completed, it is obvious that this blend is not compatible with stainless steel. All but two of the capsules containing stainless steel were removed from the test facility shortly after being installed because of overpressurization. The pressure in the two remaining specimen/capsules has risen, but it is still less than the 345-kN/m² (50-lbf/in.²) limit set for capsule removal. All aluminum and titanium specimen/capsules, except those also containing stainless steel, are still in test.

3. Method of rating materials. A materials rating system has been developed to derive engineering and design guidelines or rules from test data reported in the literature

Table 18. Assays of hydrazine and hydrazine/hydrazine nitrate used in TOPS material compatibility test program

Constituent or property	MIL-P-26536B ^a specification limits	Assay ^b of hydrazine as received (drum H-3155)	Assay of JPL-purified hydrazine	Assay of JPL-produced hydrazine/hydrazine nitrate
Hydrazine assay, % by weight	97.5 min	98.2	99.9 ^c	75.2
Other major constituent, % by weight	NA ^d	NA	NA	24.0 (N ₂ H ₅ NO ₃)
Water plus soluble impurities, % by weight	2.5 max	0.45	H ₂ O < 0.02	0.4
Density at 298 K (77°F), g/cm ³	1.004 ± 0.002	—	—	—
Particulate, mg/cm ³	0.01 max	—	—	—
Ammonia plus amines, % by weight	Not required	1.18 (NH ₃) 0.20 (C ₆ H ₅ NH ₂)	0.08 (NH ₃) < 5 ppm (C ₆ H ₅ NH ₂)	0.1 (NH ₃) 0.3 (C ₆ H ₅ NH ₂)
Dissolved metals, % by weight	Not required			
Iron		0.01	Not determined because levels assumed below detection threshold ↓ Not determined because levels assumed below detection threshold	Not determined ↓ Not determined
Aluminum		None detected		
Nickel		↓		
Manganese		None detected		
Cobalt		None detected		
Chromium		0.003		
Copper		0.003		
Zinc		None detected		
Silicon		0.008		
Magnesium		0.002		
Sodium		0.075		
Calcium		0.009		
Barium		0.005		
Boron		0.005		
Dissolved anions, % by weight	Not required			
Chloride		None detected	None detected	Not determined
Sulfate		None detected	None detected	↓
Nitrate		None detected	None detected	↓
Nonvolatile residue, mg/cm ³	Not required	Not determined	Not determined	Not determined

^aVersion of hydrazine specification in force at start of program.

^bFrom Ref. 36.

^cAssay by titration with acid indicated 100% hydrazine; assay by titration with chloramine T, 99.9% hydrazine.

^dNot applicable.

Table 19. Material compatibility specimens in storage test in hydrazine

Primary material	Specimen type	As-received hydrazine specimen/capsules in test	JPL-purified hydrazine specimen/capsules in test
6Al-4V titanium	Slug	4	4
6Al-4V titanium	Bimetal contact (with 6061-T6 aluminum)	3	
6061-T6 aluminum	Slug	4	4
304L stainless steel	Slug	4	4
304L stainless steel	Bimetal contact (with 6061-T6 aluminum)	3	
17-7 PH stainless steel	Slug	3	
430 stainless steel	Slug	3	
430 stainless steel	Chrome plated	3	
446 stainless steel	Slug	3	
446 stainless steel	Chrome plated	3	
Tungsten carbide	Slug	3	
AM 350	Slug	3	
AM 355	Slug	3	
LRV-448 (Teflon)	Slug	3	
EPT-10	Slug	3	
Standard control		2	2
Hydrazine control			10
Total		50	24

Table 20. Material compatibility specimens in storage test in hydrazine/hydrazine nitrate

Primary material	Specimen type	Number in test
6Al-4V titanium	Slug	1
	Bimetal contact (with 347 stainless steel)	1
	Bimetal contact (with 6061-T6 aluminum)	1
	Stressed slug	4
	Welded and stressed	3
6061-T6 aluminum	Welded	4
	Bimetal contact (with 347 stainless steel)	1
	Bimetal contact (with 6Al-4V Titanium)	3
347 stainless steel	Stressed slug	1
	Welded	2
	Bimetal contact (with 6061-T6 aluminum)	1
303 stainless steel	Bimetal contact (with 6Al-4V Titanium)	1
	Stressed slug	2
	Slug	2
304 stainless steel	Bimetal contact (with 347 stainless steel)	2
	Bimetal contact (with 6061-T6 aluminum)	1
	Bimetal contact (with 6Al-4V Titanium)	2
	Stressed slug	2
	Slug	3
316 stainless steel	Bimetal contact (with 347 stainless steel)	2
	Bimetal contact (with 6061-T6 aluminum)	2
	Bimetal contact (with 6Al-4V Titanium)	2
	Stressed slug	1
	Stressed slug	1
Screens (CRES)	Welded and stressed	1
	Welded	2
	Filter	5
Screens 304 stainless steel	Surface tension	15
Standard control		4
Total		72

or from JPL and other current test programs. The specific goals of the compatibility rating system are to:

- (1) Provide a basis for selecting structural or component material candidates based on the application and operating environment. Few materials are generally always bad.
- (2) Rate or rank the candidate acceptable materials in terms of the best data currently available.

Specific materials for a given application are determined to be either acceptable "A" or not acceptable "N" in terms of compatibility with the environmental fluids over the time and dynamics of the mission. However, since an "A" rating is in fact a prediction based on available data, a qualifying code is required to define the basis and validity of the prediction. The approach used is to add a rating qualifier or modifier to each where required. The symbols used are "I" for Incomplete and "R" for Restricted; thus materials are rated as follows: "A", "A-I", or "A-R" or "N". The "I" and "R" in each case would be

explained with background information. The definitions of "I" and "R" are as follows:

"I"—Incomplete compatibility data (a data void) with respect to conditions or time.

"R"—Restricted compatibility indicated by corrosive degradation or propellant contamination at conditions that may influence the mission, component, or operating specifications.

Table 21 is a compilation of the candidate TOPS materials, listed by basic groups, along with their material compatibility ratings and qualifiers. The qualifier "R" for 304L, 316L, and 347 types of corrosion-resistant steel, for example, indicates a temperature limitation as well as incomplete data. The qualifier "I," which indicates incomplete data, in some cases refers to the existence of short-term data only, making extrapolation difficult. In other cases, the "I" refers to gaps in the available data. These material ratings will be updated as new knowledge becomes available from the JPL test program, from a continuing industry-wide survey, and from other sources. In conclusion, it should be noted that no material is rated completely acceptable, without qualification, for the TOPS Project at this time, since past compatibility tests rarely lasted even two years, let alone ten years. And there are no generally accepted extrapolation rules to bridge the gap at this time.

4. Provisional material selection. That hydrazine is a corrosive chemical given to catalytic decomposition is both the foundation of its use as a high-energy monopropellant and the source of the problem of controlling the decomposition. Decomposition in tanks, valves, and lines was not a significant problem on planetary missions lasting

a year or less, so materials were selected for ease of fabrication and cost rather than compatibility, and stainless steel was the most common choice. However, stainless steel appears to be marginally compatible with hydrazine, and its use on 10-year missions is doubtful.

Aluminum appeared to be the best choice at the outset of the TOPS program. Titanium was questionable because several JPL titanium specimen/capsules were withdrawn from test after capsule overpressurization indicated a significant decomposition reaction. Hence, aluminum pyrovalves were developed and an aluminum tank was carried in the component mass list. Aluminum is not without disadvantages, such as high mass, welding difficulties, and susceptibility to water damage; so titanium was carried as the backup material until the cause of the capsule overpressurization could be definitely established.

Titanium was provisionally selected as the primary TOPS propulsion system material when the capsule problem was traced to a preventable Freon reaction. Aluminum is the backup material. Titanium's major disadvantage is cost, which is insignificant for small systems. It is light, compatible with most chemicals, and appropriate fabrication technology has been developed in the aerospace industry. The TOPS propulsion module design discussed in Subsection V-D is based on an all-titanium feed system except for necessary electrical and magnetic elements. The flow path from the tank to the engine control valve is welded titanium. The engine that sees hydrazine for just 1600 s is the only nontitanium element.

G. Hydrazine/Radiation Interaction

A related part of the compatibility program involved the investigation of nuclear radiation effects on hydrazine including any interaction that might occur with typical propulsion subsystem components and materials. This was the result of the planned use of radioisotope thermoelectric generators (RTGs) aboard the spacecraft for the generation of electrical power.

1. Test program. The purpose of these tests was to investigate radiation effects on hydrazine and hydrazine/hydrazine nitrate. Metallic capsules were used to contain a maximum of 10 cm³ of propellant, or various fractions of this amount. Propellant-container materials included 6061-T6 aluminum alloy, 1100 aluminum, type 347 corrosion-resistant steel, and 6Al-4V titanium. Control specimens outside the radiation field were used to account for any autodecomposition effects of the propellant and any gas pressure generation resulting from a reaction between the propellant and the capsule wall material.

Table 21. Compatibility ratings for TOPS materials in contact with hydrazine

Material	Rating	Qualifier
Aluminum		
6061-T6	A	I
1100	A	I
Corrosion-resistant steel		
304L, 316L, 347	A	R
430, 446	A	I
17-7 PH	A	I
Titanium, 6Al-4V	A	I
Other		
Chrome plate	A	I
TFE Teflon	A	I

The mission time-integrated level of gamma-type radiation was specified as 0.01 Mrad-Si (Table XXII of Ref. 11). This corresponds to a minimum separation distance of five feet between the RTGs and any engineering subsystem or assembly. Throughout these experiments, a cobalt-60 gamma-type radiation source has been used. The justification for this choice of radiation source, according to Ref. 38, follows:

Cobalt-60 gamma radiation was used throughout the experiments since radiation-induced decomposition is, in general, independent of the nature of the radiation and is a function only of the amount of energy deposited in the fuel materials. Also, in an on-board situation, the major radiation to which a fuel would be exposed may well be bremsstrahlung from the RTG, which is electromagnetic radiation of the same nature as gamma rays. The deleterious reactions occurring in the fuel systems generally result from free radicals, atoms, and excited molecules produced by the radiation. The reactions initiated by such chemically active species, however, are independent of the mode of formation of the initiating species. That is, the reaction of a free radical, for instance, in the fuel does not generally depend on the way in which the free radical was formed. Thus, the results generated in the research reported here should be generally applicable, regardless of the nature of RTG in an actual flight situation.

2. Test results. Figure 29 is a sample of radiation-effects data obtained using liquid hydrazine in titanium vessels. The gas formed is shown as a function of total dose for both high- and low-dose rates. The total anticipated TOPS dose, 0.01 Mrad-Si, is very small compared with the experimental dosages used. It should be noted that Fig. 29 indicates that more gas is generated at the lower, rather than at the higher, dose rate. The radiation exposure temperature for these tests was 295 K (71.6°F).

In addition to the metallic capsules described above, individual components, typical of the TOPS propellant feed system, were also tested in a radiation field with hydrazine and hydrazine/hydrazine nitrate. Three capillary-tube assemblies were constructed of 61-cm (24-in.) long capillary tubes, of 0.25-mm (0.0095-in.) ID, and wound in a 1.27-cm (0.50-in.) diam helix. The capillary-tube assemblies, made of Type-304 hardened stainless steel, were irradiated while containing hydrazine and hydrazine/hydrazine nitrate. Flow testing of the capillary-tube assemblies, before and after irradiation, indicated no appreciable change in pressure drop. Propellant flow rates were determined before and after a 119-h exposure to a radiation dose of 60 Mrad. The results tabulated in Table 22 show no significant plugging after exposure to either propellant.

Table 22. Flow through capillary before and after irradiation

Propellant	Flow rate, cm ³ /s	
	Before	After
Hydrazine at 552 kN/m ² gauge (80 lbf/in. ² gauge)	0.083 ± 0.001	0.080 ± 0.001
Hydrazine/hydrazine nitrate at 586 kN/m ² gauge (85 lbf/in. ² gauge)	0.059 ± 0.001	0.061 ± 0.001

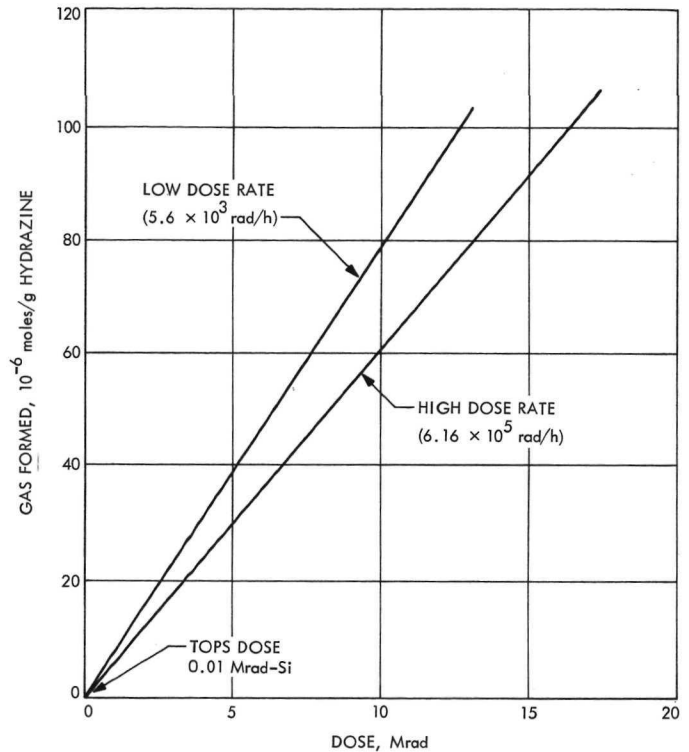


Fig. 29. Radiation-caused decomposition of hydrazine in titanium vessels

ciable change in pressure drop. Propellant flow rates were determined before and after a 119-h exposure to a radiation dose of 60 Mrad. The results tabulated in Table 22 show no significant plugging after exposure to either propellant.

A stainless steel labyrinth-type filter assembly was also irradiated while containing hydrazine and hydrazine/hydrazine nitrate. No evidence of filter plugging was noted as a result of irradiation. There was no measurable resistance of flow of either propellant through the filters for the quantities (~50 cm³/s) used. After exposure of the filter in hydrazine to 60 Mrad of radiation, there was no change in flow characteristics. For further information regarding these data, see Refs. 38 and 39.

Propellant gas generation is the most significant radiation-effects problem uncovered by the work accomplished to date. Gas generation increases with increased chemical compound or mixture complexity. For example, more gas formation occurred with hydrazine/hydrazine nitrate than with hydrazine. For this reason, it is believed that purified hydrazine (Subsection III-F-1) would tend to be more stable, when irradiated, for example, than as-received hydrazine.

Since the synergistic effects of radiation dose rate and total dosage were not completely investigated during this program, it is recommended that a flight-type tank, containing purified hydrazine, be subjected to long-term combined environmental testing, including radiation, using the anticipated mission dose rate and total dosage.

IV. System Evaluation

The primary objective of the TCPS prototype demonstration system test program was to demonstrate the reliable performance and multiple restart capability necessary to successfully complete the TOPS-TCPS mission duty cycle. Although the final TOPS mission was a three-planet mission, the original four-planet schedule shown in Table 23 was used for engine testing throughout the TOPS program to make all test series directly comparable. Fortunately, the final TOPS requirements (Table 1) are essentially identical to the nine firings and 1600-s cumulative firing time used for all testing. The ten pyrovalve events shown in Table 23 provide the propellant isolation during spacecraft cruise periods between the planet encounters for the JSUN77 mission. When the nine maneuvers are reordered, as shown in Table 2 for a three-planet mission, only eight pyrovalve events are required.

The secondary objectives of the test program were to evaluate the propulsion system operational characteristics for use in future flight system design and specifications. Included in these are:

- (1) Steady state engine performance variations with increasing cumulative engine firing time and number of restarts.
- (2) Transient engine performance during start and shut-down as a function of increasing cumulative firing time and decreasing chamber pressure levels.
- (3) Thermal characteristics of the engine and support structures during and after engine firing.
- (4) Shock loading imparted to the engine and support structures by pyrovalve actuations.

Table 23. TOPS-TCPS test duty cycle

Pyro event No.	Pyro valve No.	Engine firing No.	Trajectory correction description	Firing duration, s	Cumulative firing duration, s
1	NC 1				
		1	Post-Earth	99	99
2	NO 1				
3	NC 2				
		2	Pre-Jupiter	22	121
		3	Post-Jupiter	47	168
4	NO 2				
5	NC 3				
		4	Pre-Saturn	56	224
		5	Post-Saturn	749	973
6	NO 3				
7	NC 4				
		6	Pre-Uranus	269	1242
		7	Post-Uranus	185	1427
8	NO 4				
9	NC 5				
		8	Pre-Neptune	15	1442
		9	Post-Neptune	158	1600
10	NO 5				

- (5) Thrust vectoring by pivoting the engine about the thrust axis.

A. Demonstration System Test Criteria

The TCPS prototype demonstration system was designed and operated in a manner simulating a flight-type system as close as possible. Proven components were used wherever possible to produce a highly reliable and predictable test system. Component selection was based more on reliability than performance or size to minimize the possibility that component problems would jeopardize fulfillment of the system test objectives. Specially designed and fabricated components were limited to those elements well within current technology.

The test system consisted of a hydrazine monopropellant rocket engine, propellant tank, filter, valving, and propellant lines assembled with the necessary structure into a free-standing module similar to the flight system discussed later in Subsection V-D. Two components not in the flight system were included in the test system as a safety precaution: an accumulator was included to protect against any water hammer effect resulting from valve actuations, and a resistance heater was wrapped around the hydrazine

line to provide an artificially high hydrazine temperature for valve closure to prevent excessive, thermally induced expansion of the hydrazine trapped between valves. System performance was monitored by the onboard flight instrumentation set shown earlier in Fig. 6, and supplementary test instrumentation was restricted to those transducers that attach to the exterior of components where they cannot affect any of the system parameters under study.

The general, overall size and arrangement of components were compatible with the spacecraft configuration. The propulsion module space in the TOPS configuration in use at the time of test system design was 51 cm (20 in.) wide, 66 cm (26 in.) high, and 81 cm (32 in.) along the thrust axis. The system is installed in the spacecraft through one of the 66-cm (26-in.) by 81-cm (32-in.) side panels, and attached to the 51-cm (20-in.) by 66-cm (26-in.) end panel. The prelaunch fueling and installation procedures were not simulated, because of the special requirements of the test tank, and the vacuum chamber and thrust stand.

A constant vacuum was maintained in the test cell throughout the test program. Flight-like electrical control and sequencing of pyrovalves, solenoid valves, and thrust vector gimbal actuators were commanded from the control room. No special thermal control provisions were made in the vacuum chamber and flight-like thermal blankets were not provided for the demonstration system. Ambient temperatures met the test requirements and engine firings were spaced at least a day apart to allow adequate time for the test system to return to ambient temperatures and the engine catalytic bed to thoroughly outgas.

B. Demonstration System Design

The TCPS demonstration system was designed and assembled to meet the requirements listed in Table 24. Since there are few, if any, flight-qualified components for a 10- to 12-yr space mission, fully developed and proven components having a history of successful short term spacecraft application were selected where possible. Most of the components were obtained from the residual hardware of completed spacecraft programs, or loaned to JPL by interested manufacturers. A few items were purchased or manufactured by JPL.

Hydrazine flow passage materials selection was based on compatibility, availability, and cost. The most desirable material for long-term hydrazine compatibility is titanium. However, suitable flight hardware made of titanium was

Table 24. Demonstration system design requirements

No.	Item	Requirement
1	Propellant system	Pressurized blowdown
2	Propellant	Hydrazine (MIL-P-26536 C)
3	Pressurant	Nitrogen (MIL-P-27401 B)
4	Tank pressure range	2413 to 1207 kN/m ² (350 to 175 psia)
5	Tank temperature range	278 to 305 K (40 to 90°F)
6	Engine temperature range	278 to 289 K (40 to 60°F)
7	Engine ignition	Spontaneous catalyst (Shell 405)
8	Engine vacuum thrust range	111 to 67 N (25 to 15 lbf)
9	Chamber pressure range	1103 to 621 kN/m ² (160 to 90 psia)
10	Nozzle expansion ratio	40 to 1
11	Vacuum specific impulse	2255 N-s/kg (230 lbf-s/lbm)
12	Cumulative steady-state firing duration	1600 s
13	Propellant load	65.8 kg (145 lbm)
14	Number of engine firings	9 (see Table 1)
15	Thrust vector control	5° maximum angular axial deflection
16	Useful life	10 to 12 yr

limited almost exclusively to propellant tankage. Aluminum is the next most desirable material; however, available aluminum components were limited to the pyrovalve manifold and support structures. The most readily available component material was stainless steel: it was selected as the primary material of construction to maximize the use of welding and to minimize the number of mechanical joints of dissimilar metals.

Several general requirements related to ground testing in the vacuum test facility had to be met in addition to the system requirements. These involved operational safety practices such as remotely operated, closed-loop propellant loading and dumping, remote gas pressurization, and automatic overpressure relief and venting. These functions were accomplished through flexible umbilical lines that remained attached to the system throughout the test program. The demonstration system was oriented in the vacuum chamber cell with the engine pointed vertically downward. The propellant tank was then located above the engine, so gravity could be used to feed hydrazine to the engine in place of a propellant acquisition device.

The selection of a propellant tank for the demonstration system was a compromise of many factors. During the test

planning period, the four-planet mission was replaced with a pair of three-planet missions resulting in a lower ΔV and a reduced estimated total firing duration of 800 s. The continuing changes of the ΔV requirement estimate, coupled with test program resource limitations, precluded buying a special TOPS tank. Further, the relationship between propellant load or tank volume and total engine firing time had not yet been accurately established either experimentally or analytically for the 2:1 blowdown mode of operation. Thus, a survey of Ref. 40 and of residual tanks available at JPL led to the selection of a tank from the Gemini program, with the idea that a smaller second

tank could be selected much later in the program, when requirements were firmer, to adjust the initial ullage volume to the required 50%.

A schematic diagram of the demonstration system is shown in Fig. 30. Hydrazine is loaded into the system through the top right-hand service valve (VM1). The fill rate can be measured with the orifice flow meter, and by a weight check measurement made with the thrust stand load cell. Gas venting and pressurization are accomplished with the top left-hand service valve (VM2) and a stand pipe mounted in the center of the tank access port flange,

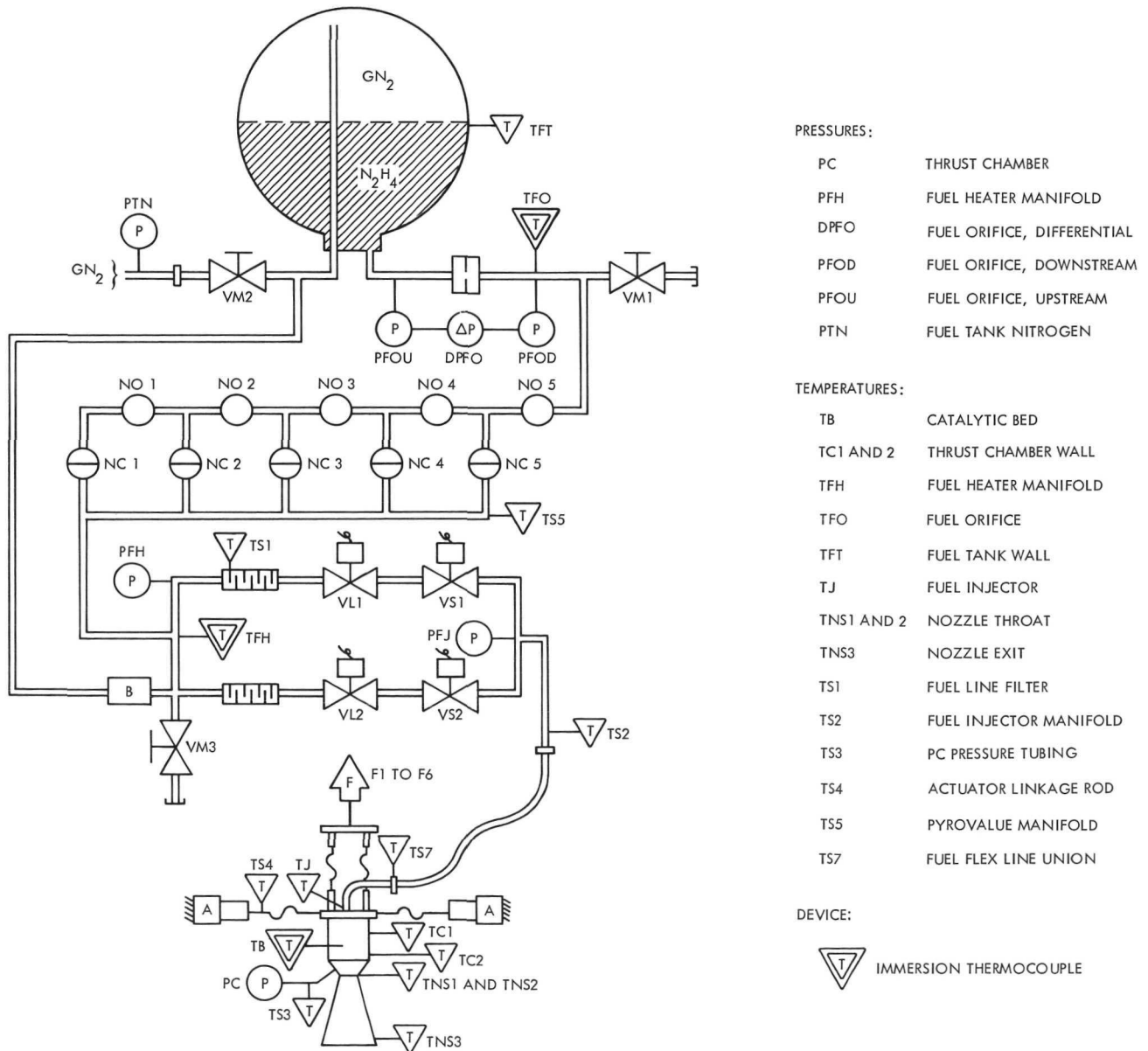


Fig. 30. TOPS-TCPS demonstration test system schematic diagram

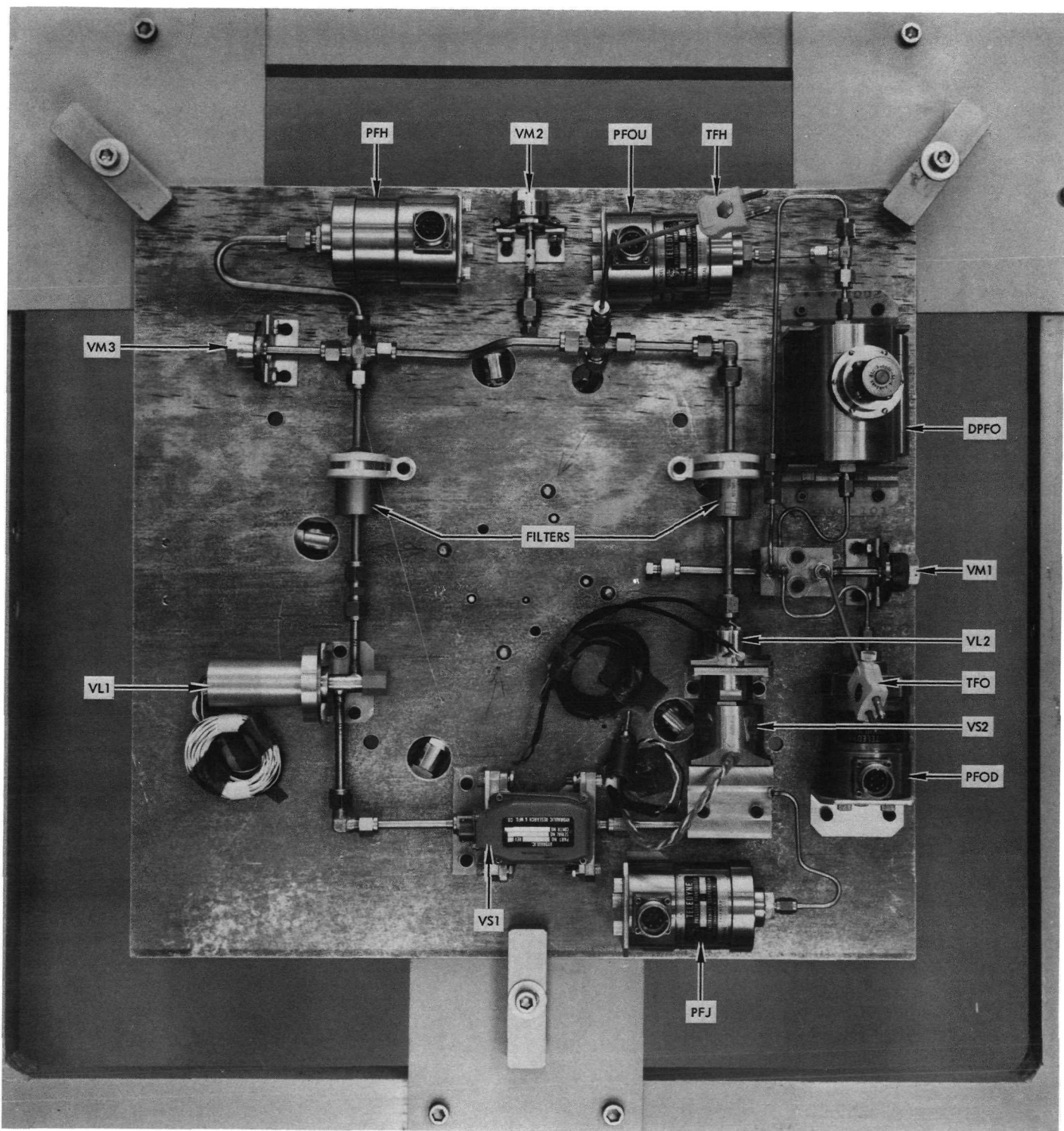


Fig. 31. Component arrangement on the tank side of the support plate

which extends above the hydrazine liquid surface. Hydrazine is discharged under pressure through the tank fill line, the orifice flowmeter, and into the normally open side of the pyrovalve manifold.

Hydrazine is introduced into the solenoid valve manifold by opening the first, normally closed pyrovalve (NC 1). A bellows accumulator (B), which is pressurized on one side by tank pressure, is designed to dampen the hydraulic shock of valve actuations on the system. Line filters remove particulate contamination, including particles from the pyrovalve shearing operation, from the hydrazine before it passes through the controlling series pair of solenoid valves (VL1 and VS1, or VL2 and VS2).

A third service valve (VM3) is located at the inlet to the solenoid valve manifold to bypass the untestable pyrovalves; this service valve provides for system pretest functional checkout. A flexible line takes the hydrazine from the solenoid valve manifold to the injector inlet of the gimbal-mounted engine.

All propellant lines are 0.64-cm- ($\frac{1}{4}$ -in.-) diam stainless steel tubing, with the exception of a teflon-lined, flexible injector inlet line, and the heavy walled aluminum tubing used in the pyrovalve manifold. To simplify assembly and service, all components were installed with mechanical tubing joints of either the standard AN-flared-type, or the two-piece swaged-ferrule-type.

A single 50-cm- (20.25-in.-) square by 1.27-cm- ($\frac{1}{2}$ -in.-) thick aluminum plate serves as the common mounting substructure for all components. The propellant tank, orifice flowmeter, service valves, bellows accumulator, filter, latching and normally closed solenoid valves, and the propellant system pressure transducers are located on the top surface of the plate. The arrangement of these components on the plate, with the propellant tank removed for clarity, is shown in Fig. 31. On the lower surface of the plate are mounted the pyrovalve manifold, thrust chamber and support assembly, gimbal actuators, and the chamber pressure transducer. This arrangement is shown in Fig. 32.

The component parts used in the TCPS prototype demonstration system are listed in Table 25. Specific components were selected for each function on the basis of their reliability, availability, cost and performance; their selection is not an endorsement for use on future outer planets missions. Each flight project selects hardware designs or existing hardware from the available candidates meeting its specific requirements. The TOPS propulsion hardware

is representative of present technology and design and development. A brief description and background of the major TCPS test components is given in the following subsections.

1. Rocket engine. The 118-N (26.5-lbf) thrust monopropellant hydrazine rocket engine used in the TOPS demonstration system was originally developed for the Titan IIIC Transtage reaction control system. The Transtage application requires mostly pulse-mode operation, although some longer steady-state firings are sometimes needed. Two Transtage qualification engines were transferred by the U. S. Air Force to NASA for the TOPS program. Both engines were initially used for the exploratory life testing described in Subsection III-A-7.

Later, one engine was rebuilt to "new" condition by the engine manufacturer under a JPL contract. This and a competing engine both successfully completed the TOPS engine life tests described in Subsections III-A-5 and -7. The Transtage engine was selected for the demonstration system primarily because of its advanced state of development and overall reliability, although its performance was slightly lower than that of the competing engine. This first Transtage engine was reserved for possible further testing to experimentally find its life limit, and the second engine was rebuilt to "new" condition for the demonstration system.

Both Transtage engines were slightly modified when they were rebuilt with the addition of a catalytic-bed immersion thermocouple. The thermocouple was included to monitor catalytic-bed temperature during engine life tests, and to determine its feasibility as a solenoid-valve leakage monitor in a separate set of calibrated leakage tests. The latter set of tests was never completed. The second engine was further modified at JPL to adapt it to the engine gimbal support mounting. The short injector feed tube, which slips directly into the control valve in the Transtage configuration, was welded to a transition tube that mechanically joined a 0.64-cm- (0.25-in.-) diam flexible tube for the TOPS gimbaled-engine application (Fig. 33). The injector hold-up volume was necessarily increased by these changes; however, this was not considered critical, because all firings were made in the steady-state mode. New engine start and shutdown transient characteristics were expected.

2. Engine gimbal assembly. The rocket engine gimbal assembly was designed and manufactured at JPL to give 5° of angular displacement in two axes. The engine mounting surface is a solid ring with two legs that extend

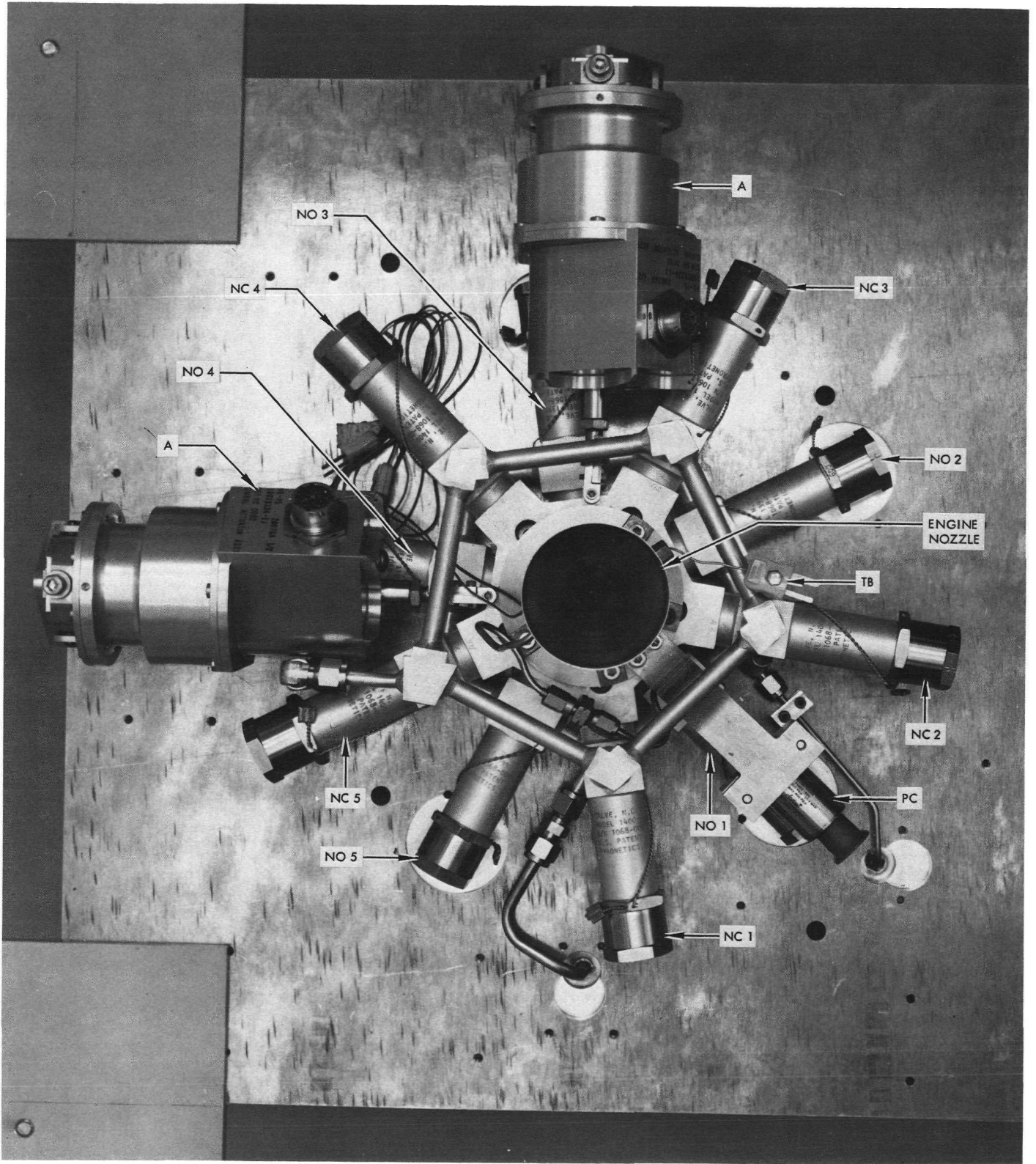


Fig. 32. Component arrangement of the engine side of the support plate

Table 25. Component parts for demonstration test system

No.	Component	Manufacturer	Program	Part No.	No. required	Mass, kg (lbm)
1	118 N (26.5 lbf) thrust rocket engine	Rocket Research	Titan IIIC Transtage	MR-3A-REA	1	0.85 (1.87)
2	Engine gimbal assembly	JPL	TOPS	10039971-1-J	1	0.47 (1.03)
3	Gimbal actuators	JPL	Mariner Mars 1971	10028334-1-J	2	2.49 (5.50)
4	Propellant tank	Rocketdyne	Gemini	103177	1	4.11 (9.07)
5	Orifice plate assembly ^a	JPL	TOPS	10039975-1-D	1	0.85 (1.88)
6	Pyrovalve manifold	JPL	TOPS	10039647-1-B	1	3.95 (8.70)
7	Pyrovalve squibs	JPL	Mariner Mars 1971	10028049-Rev. C	10	0.77 (1.70)
8	Fuel line filter	Vacco	Intelsat III	S1-81847-2	2	0.37 (0.82)
9	Bellows accumulator	JPL	TOPS	SK-10-15-71-384	1	0.54 (1.20)
10A	Latching solenoid valve	Marquardt	Prototype	T-8700	1	0.29 (0.63)
10B	Latching solenoid valve	Carleton Controls	Intelsat IV	2217001-2-1	1	0.34 (0.79)
11A	Engine solenoid valve	Marquardt	Apollo RCS	228511	1	0.42 (0.93)
11B	Engine solenoid valve	Hydraulics Research	Titan IIIC Transtage	48000360	1	1.02 (2.25)
12	Manual service valves	JPL	Mariner Mars 1971	10027723-1-B	3	0.92 (2.03)
13	Brackets and fasteners	JPL	TOPS	10039977 to 10039981	—	0.68 (1.50)
14	Base mounting plate	JPL	TOPS	10039972	1	7.24 (15.96)
15A	Pressure transducer	Taber	Ground test	226-500	4	6.01 (13.24)
15B	Pressure transducer (chamber pressure)	Statham	Ground test	PA822-200	1	0.13 (0.28)
15C	Pressure transducer	Statham	Ground test	PM385TC ± 50	1	2.95 (6.50)
15D	Accelerometer	Endevco	Ground test	2225	6	0.07 (0.17)
16	Tubing and fittings ^a	JPL	TOPS	—	—	0.67 (1.48)
17	Cables and connectors	JPL	TOPS	—	—	0.58 (1.28)
Total mass						35.75 (78.82)

^aIncludes immersion type K (chromel/alumel) thermocouples.

to two opposing pivots on the gimbal ring. The legs provide clearance for the injector feed tube adapter, and allow the engine to be mounted inside the center support structure of the pyrovalve manifold. The other two opposing pivots on the gimbal ring are attached to a U-shaped bracket mounted to the base plate. All four attachment points on the gimbal ring utilize the Bendix Free-Flex pivot, 5,000 series. The four mounting tabs on the injector of the rocket engine bolt to the gimbal support mounting ring. An assembly photograph of the engine and gimbal support is shown in Fig. 33. The two linkage rods for the gimbal actuators also attach to this mounting ring in slots 90° apart. The material used in the engine support assembly is Type 321 stainless steel, while the flexural pivots are made of Type 420 stainless steel.

3. Gimbal actuator. The gimbal actuators used to position the rocket engine for thrust vector control were developed for the Mariner Mars 1971 spacecraft propul-

sion system, and are scheduled for use on the Viking Orbiter spacecraft propulsion system. They are gearless, electromechanical, linear servomechanisms designed for long service life in the space environment with a capability of more than 50,000 h of continuous operation (Ref. 41).

The only required modification to the gimbal actuator for the TOPS application was the replacement of the spherical ball rod end with a specially designed spring pin flexure linkage rod shown attached to the actuator in Fig. 34. The strain gauge and thermocouple mounted on the linkage rod for performance analysis data, and the rear mounting bracket are also visible in the figure. This change was needed because of the limited space available for attachment of the linkage rod onto the engine support ring. Also, engine heat soakback could be damaging to the spherical ball joint if it were attached too close to the engine. Further, the spring pin flexure eliminates

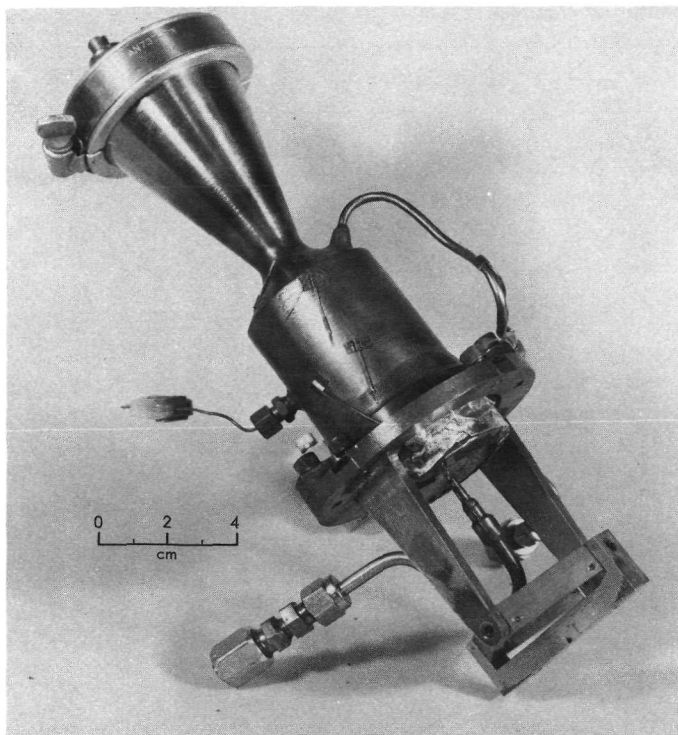


Fig. 33. Engine and gimbal support mount assembly

any chance of space welding or diffusion bonding that might occur between the closely fitted sliding metal parts in the spherical ball joint.

4. Hydrazine tank. A surplus Gemini titanium tank designed for use with a positive expulsion bladder was selected for the demonstration system. The Teflon bladder and titanium bladder support flange assembly were replaced with a new stainless steel flange assembly that provided a gas pressurization standpipe leading to the top of the tank. Also, the original laminated Teflon seal for the flange was replaced with a totally contained Teflon crush gasket that improved the leak-tight seal. The original gas inlet port, located in the tank neck, was modified for use as the liquid discharge port by removing the brazed titanium-to-stainless-steel tube joint and mechanically installing a stainless steel, double ferrule tube union onto the titanium tube stub. This new tank assembly was cryogenically proof-tested in liquid nitrogen to a maximum pressure of 5723 kN/m^2 (830 psia). As the result of this test, a new, maximum operating pressure of 2565 kN/m^2 (372 psia) was established by the fracture mechanics criteria for remote testing; for safety reasons, tank pressure was limited to 1641 kN/m^2 (238 psia) in the presence of personnel. Dimensions of the tank are 51-cm (20.08-in.) diam with a minimum wall thickness of 0.056 cm (0.022

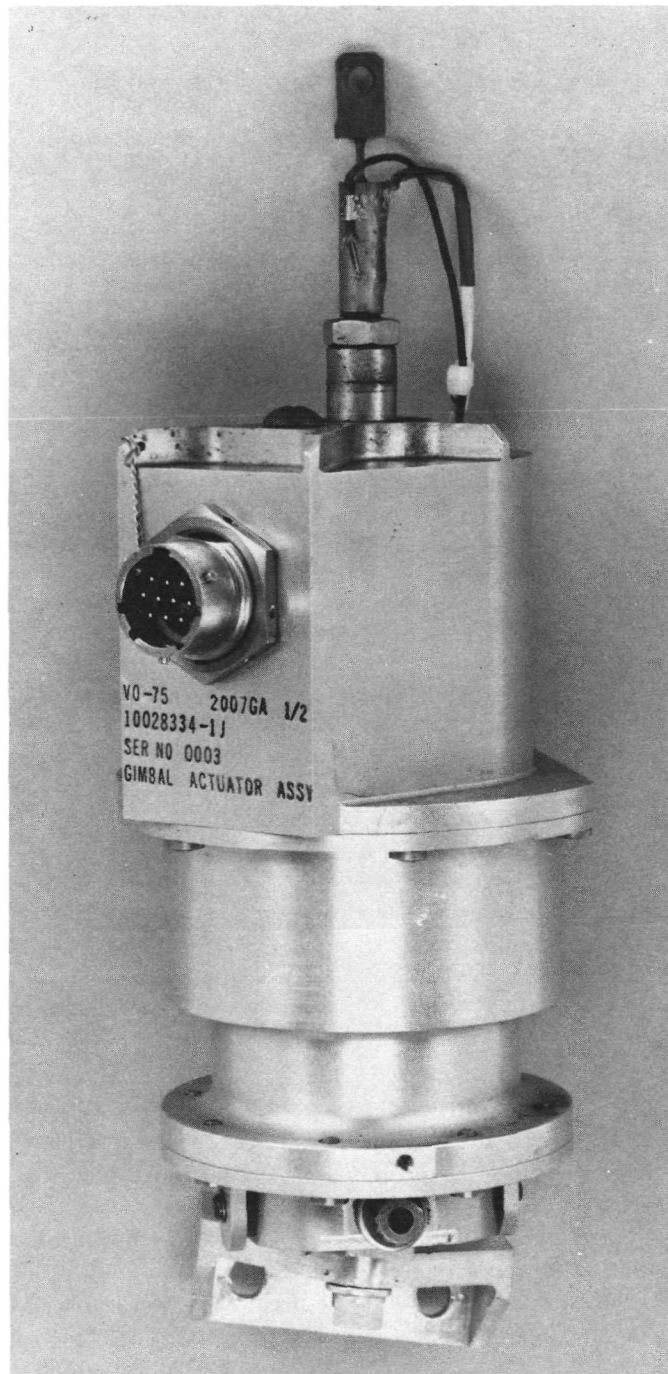


Fig. 34. Gimbal actuator with instrumented flexural engine attachment

in.). Internal volume of the new configuration is 0.07 m^3 (4,272 in.³).

5. Orifice plate assembly. A square-edged orifice plate assembly, designed according to the specifications presented in Ref. 42, was selected to measure propellant

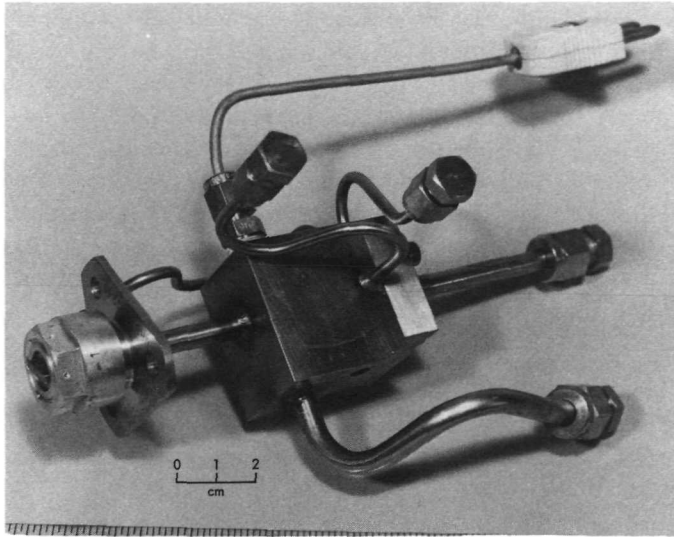


Fig. 35. Orifice plate flowmeter assembly

flowrate. The 0.025-cm- (0.097-in.-) diam orifice was sized to give 34.5- to 344.8-kN/m² (5- to 50-psid) pressure drop over the 0.0227- to 0.0680-kg/s (0.05- to 0.15-lbm/s) range of propellant flowrate. The upstream and downstream pressure taps, an immersion thermocouple and a service valve for propellant filling are shown installed on the orifice plate assembly block in Fig. 35. The orifice plate is installed at the flange joint of this assembly.

6. Pyrovalve manifold. The pyrovalve manifold was designed to provide a minimum package envelope that would distribute the bulk of the valve assembly symmetrically around the central axis of the propulsion module. The totally self-contained structure of valves, tubing, and support frame is rigidly bolted to the base plate without any means of shock or vibration isolation. Figure 36 shows the final assembly of the rocket engine in the center of the pyrovalve manifold with the attached gimbal actuators

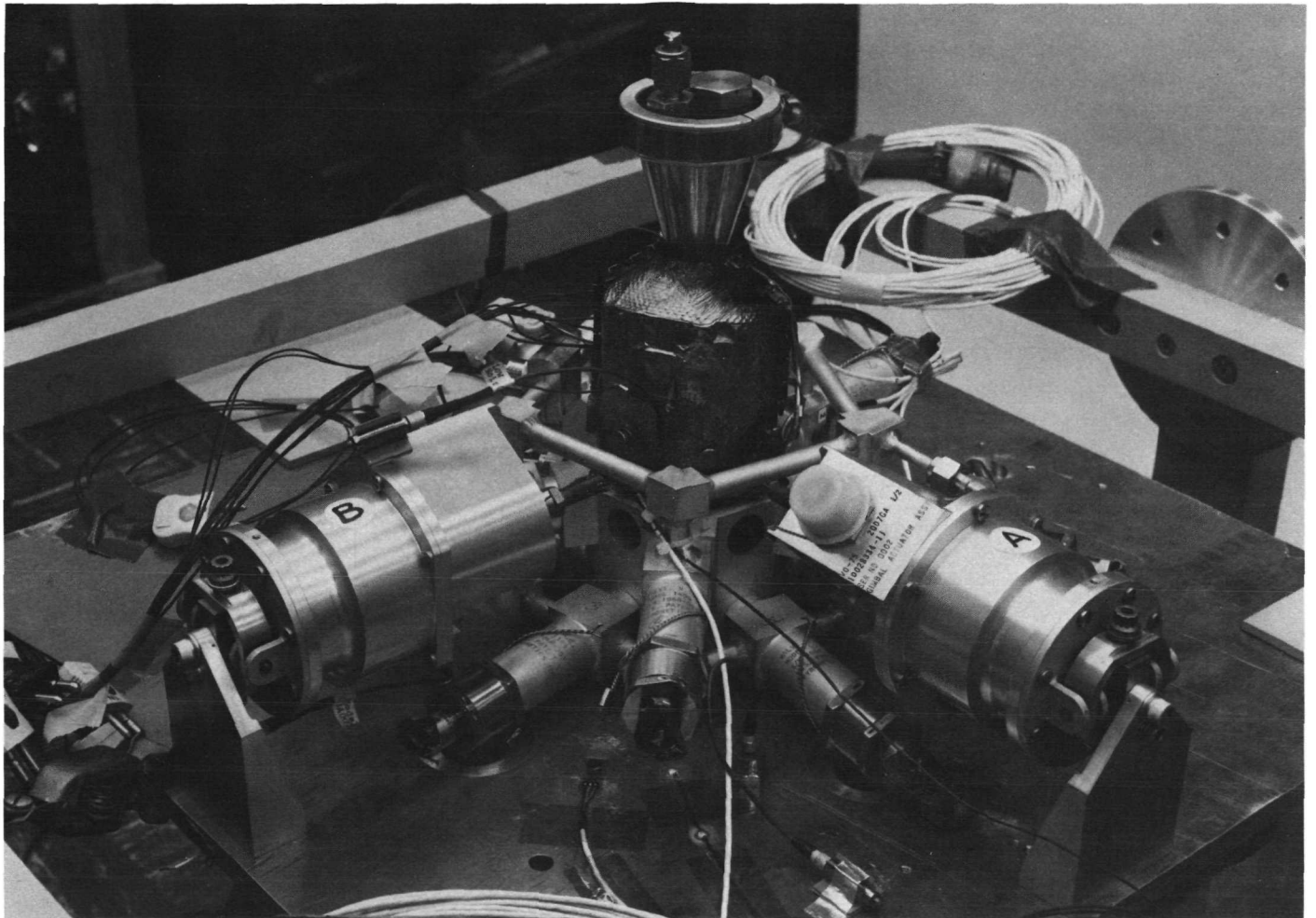


Fig. 36. Final assembly of engine, gimbal actuators, and pyrovalve manifold

positioned 90° apart. Actuator linkage rods reach through and under the pyrovalve discharge line to attach to the engine gimbal support. The radial orientation of the 10 pyrovalves allowed reasonable access for the installation of the squibs and firing cable connectors.

7. Pyrovalve squibs. The squibs used to operate the pyrovalves were developed by JPL for use on Mariner spacecraft. The latest version was used on Mariner Mars 1971 spacecraft (Refs. 26 and 27).

8. Fuel-line filter. An in-line fuel filter of the stacked-disk-type with a 5- μ m (-micron) nominal and a 12- μ m (-micron) absolute filter rating was installed in each branch of the solenoid valve manifold. Although originally designed for use in the gas pressurization system of the INTELSAT III spacecraft, these filters are also suitable for liquid hydrazine service.

9. Bellows accumulator. The bellows accumulator designed and fabricated at JPL served a dual role in the liquid propellant system. First, it acted as a shock dam-

pening chamber to help absorb the hydraulic hammer effects on the propellant components and lines caused primarily by actuating pyrovalves. Secondly, it provided volume compensation for the propellant locked up between the pyrovalves and solenoid valves during thermal cycling. The all-welded, stainless steel unit used a single hydroform convoluted bellows pressurized internally with gaseous nitrogen from the gas side of the propellant tank. A drawing of the cross section of the bellows accumulator is shown in Fig. 37.

10. Latching solenoid valves. Two different latching (bistable) solenoid valves are used in the propellant control system. They were discussed and illustrated earlier in Subsection III-B-2.

11. Normally closed solenoid valves. The two different, normally closed solenoid valves used for engine control

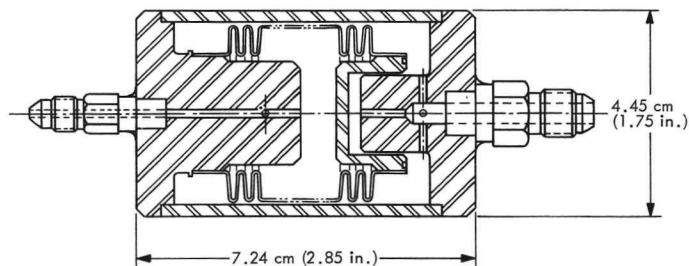


Fig. 37. Bellows accumulator cross-section drawing

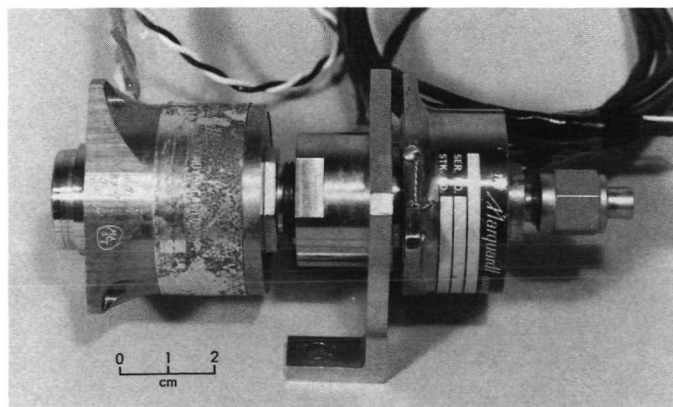


Fig. 38. Compact latching and normally closed solenoid valve assembly

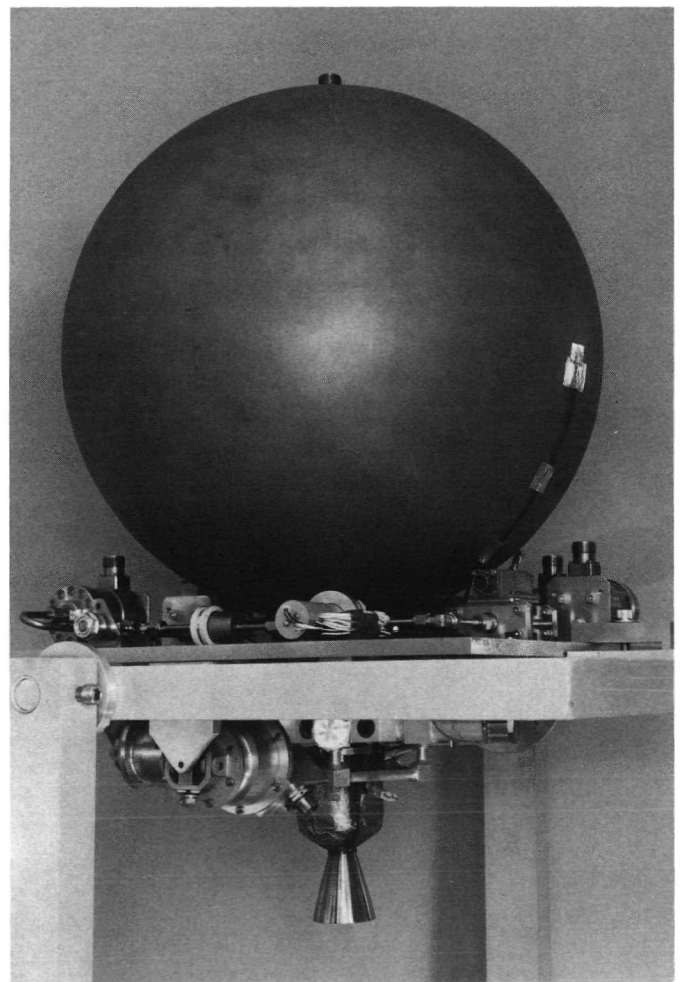


Fig. 39. Final assembly of demonstration system

are described and illustrated in Subsection III-B-2. A specially designed adapter was fabricated at JPL that compactly manifolds the Marquardt latching and normally closed solenoid valves together in series for one branch of the parallel valve system. This adapter houses the different seals required by each valve, and eliminates the need for connective tubing, thus minimizing the liquid volume between valves. This assembly is shown in Fig. 38.

12. Manual service valves. Three manual service valves were required for functional checkout, propellant filling, and gas pressurization of the demonstration system. The JPL Mariner service valve was available from the residual hardware of the Mariner Mars 1971 program. This valve separates into two halves—the flight half, shown in Fig. 35 attached to the propellant system, containing the valve seat and plunger, and the ground service half containing the valve stem and operator. The ground half is normally removed after servicing, and a lockable sealing cap is installed in its place on the flight side. During the demonstration test, the ground halves for the gas pressurization and propellant filling valves remained installed, so that these operations could be conducted remotely while the entire system remained under vacuum on the test stand.

13. Assembled demonstration system. A side-view photograph of the demonstration system mounted in a portable assembly and shipping stand during build-up is shown in Fig. 39. The overall compactness and minimum assembly length is well illustrated in this view.

C. Test Program

1. Test facilities. The TOPS-TCPS prototype demonstration system was tested at ETS. The vertical test stand at station D (DV) was utilized because this engine test cell could be held under continuous vacuum for extended periods of time (24 h/day), and it contained the six-component thrust stand needed to measure thrust vector control parameters. No elaborate thermal conditioning of the propellant system was required to obtain the desired low temperatures of 278 to 289 K (40 to 60°F) for the test series because of the low ambient temperatures during the test period—December through January.

The DV vacuum test cell is 2.44 m (8 ft) in diameter by 6.1 m (20 ft) long. The 28.3 m³ (1,000 ft³) volume was evacuated and held at a pressure of 0.667 kN/m² (5 torr) by a mechanical vacuum pump. During engine firings,

the HYPROX steam generator was used to drive the three-stage ejector pumping system shown in Fig. 40 to lower and hold the test cell pressure at 0.133 kN/m² (1 torr). The engine nozzle exit pressure was further reduced to 0.067 kN/m² (0.5 torr or 0.01 psia) by directing the engine exhaust gases into a series of two diffusers, one 30.5 cm (12 in.) in diameter, and the other 16 cm (6.3 in.) in diameter. The diffuser pipe entrance, located 0.7 cm (0.25 in.) below the nozzle exit plane, contained the total pressure probe through which exhaust gas samples were collected near the end of each test firing.

The six-component thrust stand was developed for the Mariner-Venus/Mercury 1973 thrust vector control assembly (TVCA) test program. A new support frame, shown in Fig. 41, was fabricated to accommodate the larger propellant tank of the TOPS-TCPS test configuration. The stand is a vertical, thrust-up- (exhaust-down-) type consisting of a metric or floating support frame that is tied to ground through six force transmitting load lines—namely, axial thrust, roll, fore and aft pitch, and fore and aft yaw. Each load line terminates in a force-measuring load cell mounted on the ground-end framework. Transverse forces are isolated from the load lines by means of a pair of flexures—one at the load cell end, and the other at the metric frame. Thus, the load cells see only axial forces along the load line. A schematic diagram of the six-component thrust stand and significant dimensions are shown in Figs. 42 and 43.

The stand was calibrated in tension and compression using dead weights. For the side force and roll calibrations, a flexure loader was used to apply dead weights in both tension and compression directly opposite the sensing load line. The pitch, yaw, and axial thrust dead weights were applied directly at the bottom of the thrust stand. These calibrations were made at the beginning and at the end of the test program. During the program, when the test cell was under continuous vacuum, only electrical system calibrations could be made. The pre- and posttest dead weight calibrations showed only negligible change. Figure 44 shows the six-component thrust stand installed inside the test cell with the demonstration system in place. The axial thrust load line can be seen suspending the test system assembly from the horizontal beam in the center of this photograph.

The instrumentation system for test stand DV is capable of visual display and recording both low frequency and high frequency test data. Test stand transducers are wired to the remote blockhouse through an underground

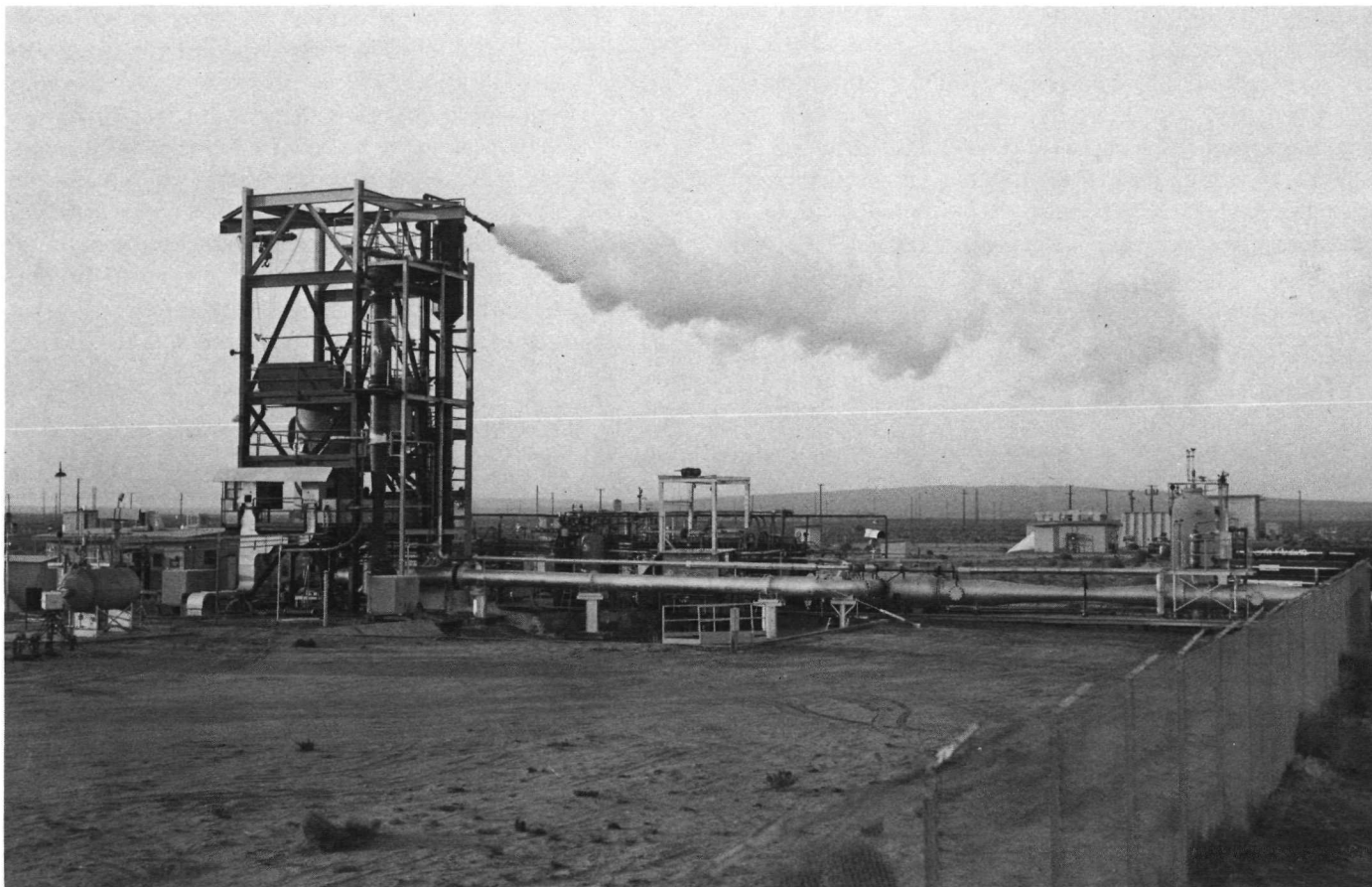


Fig. 40. DV test stand complex at JPL's Edwards Test Station

tunnel network. A test monitoring area within the block-house contains visual meters, including digital voltmeters, dial indicators, a 36-channel oscillograph, power supplies, and calibrating equipment. The low frequency recording area consists of a 10-Hz digital magnetic tape recorder, 1-Hz strip chart recorders, a master patching system, a signal conditioning system, and a quick-look digital printer. The high-frequency recorder area contains three 14-channel, 10-kHz FM analog tape recorders, an 18-channel, 2-kHz oscillograph and the associated signal conditioning equipment. Figure 45 shows recording system block diagrams for the various types of measurements made during these tests, including:

- (1) Pressures (also resistance bulb temperature).
- (2) Temperatures.
- (3) Strains (including thrust stand load cells).
- (4) Accelerations.
- (5) Voltages and currents.

A complete listing of all test instrumentation parameters is given in Table A-1 of the Appendix.

Test data were recorded in digital form on magnetic tape by the MicroSadic Data System. This system samples a maximum of 59 data channels 50 times/s, or a maximum of 78 channels 10 times/s using a time sharing technique. The nine demonstration system tests used all 78 data channels. Several seconds of transient data were recorded at both engine start and shutdown at the highest rate by deleting 19 facility and slow changing system parameters to fit the 59-channel limit. The lower rate was used for the rest of the test. Posttest thermal effects were monitored at 1 sample/s for the first 100 s after shutdown, and at 1 sample every 10 s for the next hour or more.

The raw data and various parameters calculated from it were printed and plotted by the JPL COMPROP program run on an Univac 1108 computer. The graphs and tables of data from the demonstration system tests are based on smoothed data obtained from a five-point aver-

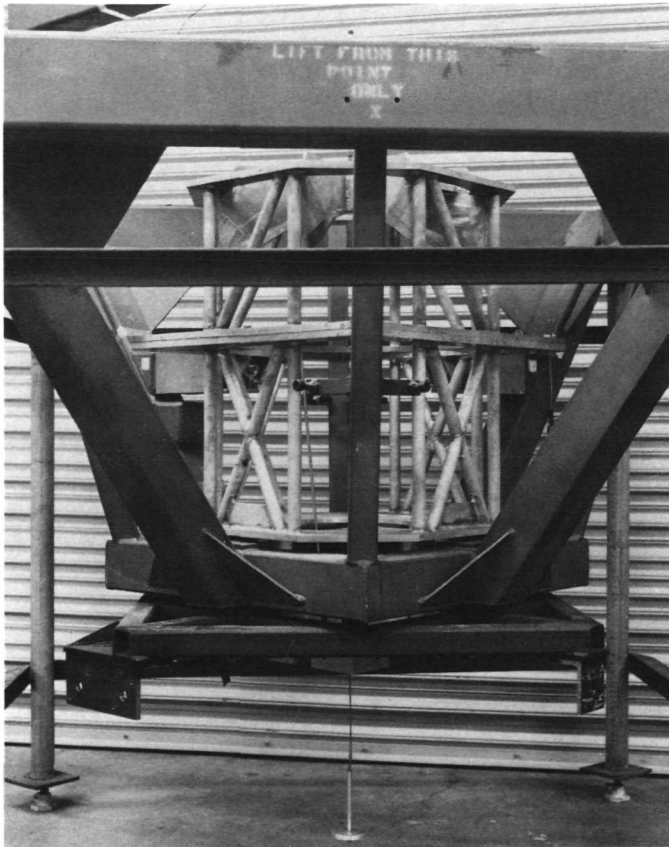


Fig. 41. Metric frame installed in six-component thrust stand

age of the raw data to eliminate as much of the noise from the transducers and data recording system as possible.

The hydrazine used in the demonstration system test program was obtained from U.S. Air Force stocks. A liquid sample was taken for analysis from the sampling port in the transfer line connecting the original shipping drum with the test system. The sampling port was downstream from a 5- μ m (-micron) nominal facility filter to assure the removal of most of any particulate contamination present. The sample was tested to see if it met the Military Specification for hydrazine, MIL-P-26536 C, although it was manufactured under the "A" revision of the Specification. Another sample was taken for analysis from the hydrazine remaining in the test system after completion of the test program a month later.

The results of the two assays are presented in Table 26. The hydrazine purity is well above the 98% minimum, and the water contamination is well below the 1.5% maximum limits of the specification. All other contamination was very low. There was very little change in the liquid

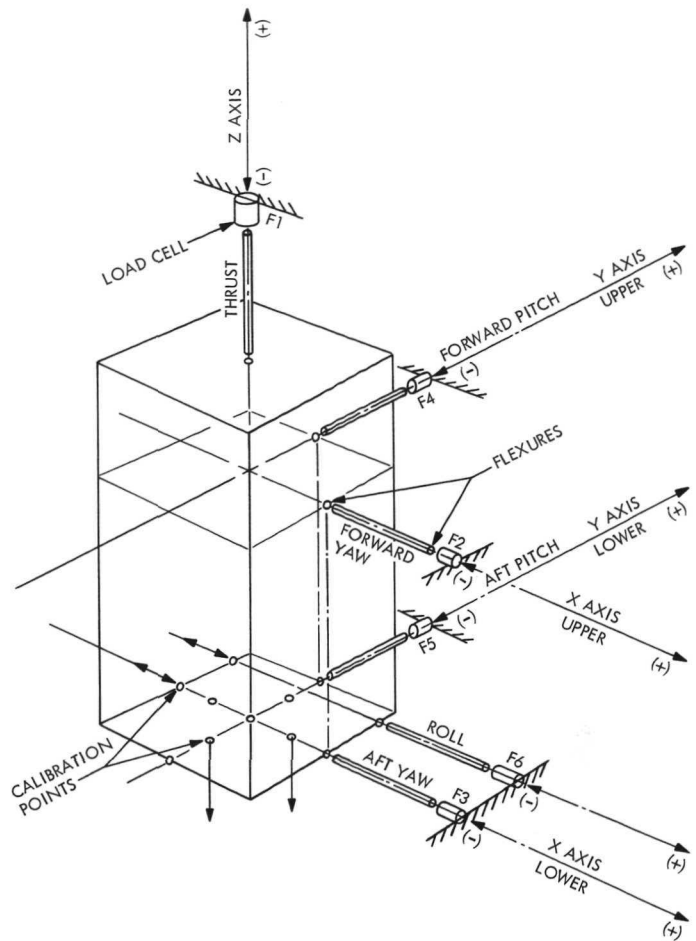


Fig. 42. Schematic diagram of the six-component thrust stand load lines

analysis over the test period: analysis of the ignited sulfated-ash showed the slight increase in metallic content expected from storage in the test system. In general, the metallic contamination is at least an order of magnitude lower than normally found. This hydrazine actually approaches the purity desired for purified hydrazine (Subsection III-F-1).

The level of contamination was unexpectedly low for hydrazine stored almost 12 years in a stainless steel drum. The variance of this experience with the results of formal compatibility tests discussed in Subsection III-F graphically demonstrates the difficulties involved in determining unqualified material compatibility ratings that are valid in most or all cases.

The gaseous nitrogen used as the pressurant for the hydrazine was derived from liquid nitrogen obtained from the Edwards Air Force Base supply. As such, it met

Table 26. Hydrazine assay—demonstration tests^a

Liquid sample analysis, % mass					
Sample taken	N ₂ H ₄	NH ₃	H ₂ O	Aniline	Nonvolatile residue ^b
Pretest	99.51	0.11	0.17	0.21	0.031
Posttest	99.55	0.11	0.08	0.26	0.032

Atomic absorption analysis of the sulfated-ash residue, ppm by mass					
Sample taken	Fe	Cr	Ni	Na	Al
Pretest	0.09	0.01	0.01	<0.01	—
Posttest	0.16	0.01	0.02	0.04	<0.04

^aThis hydrazine was drawn from Drum No. H-3256 of Batch No. 1033-64.
^bNonvolatile at 383 K (230°F).

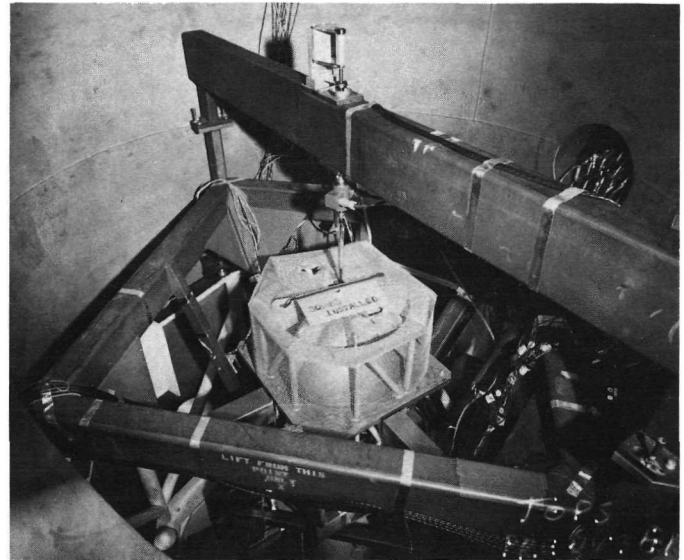


Fig. 44. Demonstration system installed in thrust stand in test cell

and lines measured 0.049 m³ (2986 in.³). When added to the ullage volume, 0.0056 m³ (339 in.³), in the hydrazine tank, the total gas volume was 0.0545 m³ (3325 in.³). Since the liquid hydrazine volume was 0.0645 m³ (3933 in.³), the liquid-to-gas volume ratio of the demonstration system was 1.18 to 1, which is very near the required 1:1 ratio (2:1 blow-down ratio of initial to final tank pressure).

2. Test description. The test program plan for the TOPS-TCPS demonstration system was designed to simulate the maneuver schedule presented in Table 23. Once installed into the test stand and pressurized with gaseous nitrogen, the demonstration system was to be held at continuous vacuum for as long as required to complete the series of nine pyro events and nine engine firings. The tenth pyro event was not performed to leave the propellant line open for further testing should the need for such tests arise during or after the nine scheduled firings.

The engine firings were planned for the morning hours when the test cell ambient temperature was in the desired range of 278 to 289 K (40 to 60°F). A minimum of 24 hours was allowed between test firings to provide ample time for vacuum purging the rocket engine catalytic bed, and to return the propellant system hardware to ambient temperature. On the three tests where the run duration exceeded 180 s, the thrust vector control gimbal actuators were operated by a taped calibration program developed by the Mariner Mars 1971 Project. Finally, an exhaust gas sample was collected and analyzed for each engine firing.

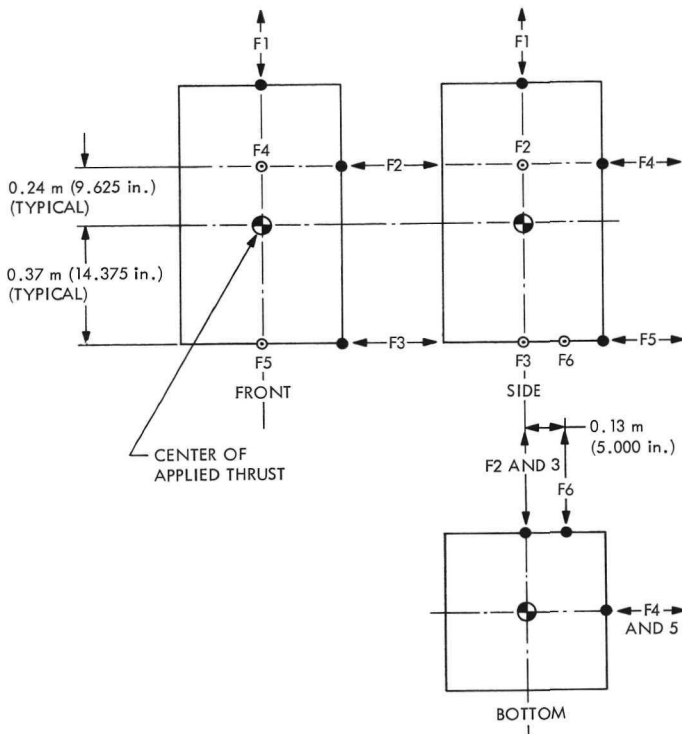
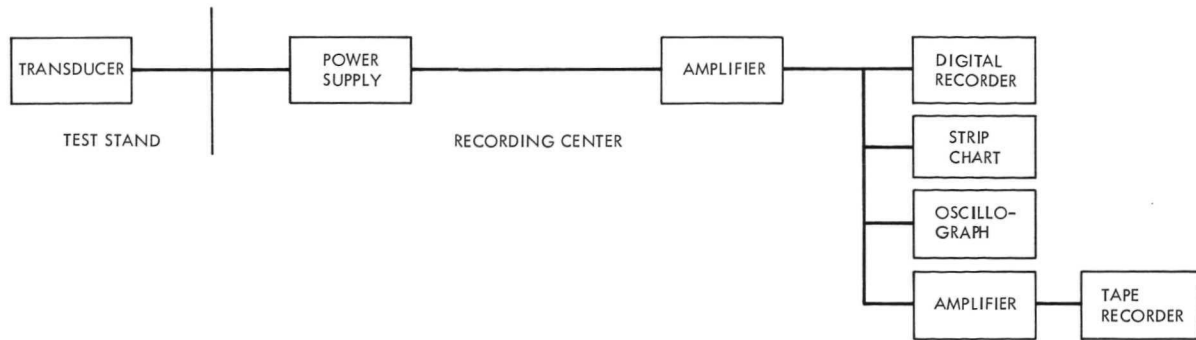


Fig. 43. Location of force application and measurement points on the metric frame

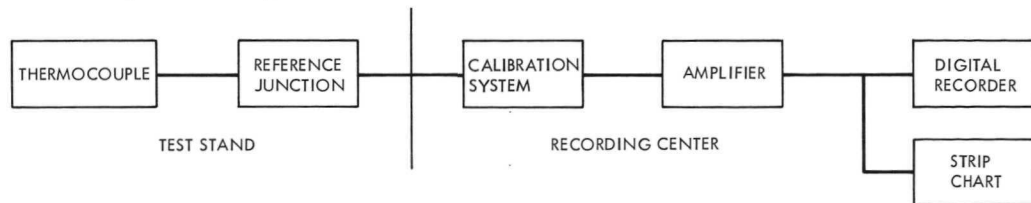
the Air Force Specification AF-PID-9135-10 for purity. The dew point was measured to be below 219 K (−65°F).

The supplemental ullage tank used to blow down the test system propellant tank was a Type 321 stainless steel sphere, 47.6 cm (18.75 in.) in diameter with a 0.953 cm (0.375 in.) minimum wall thickness. The volume of the gas system, including supplemental tank, filter, valves,

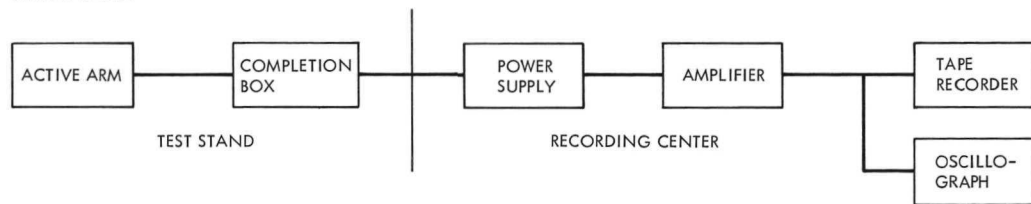
PRESSURE AND RESISTANCE BULB TEMPERATURE MEASUREMENTS:



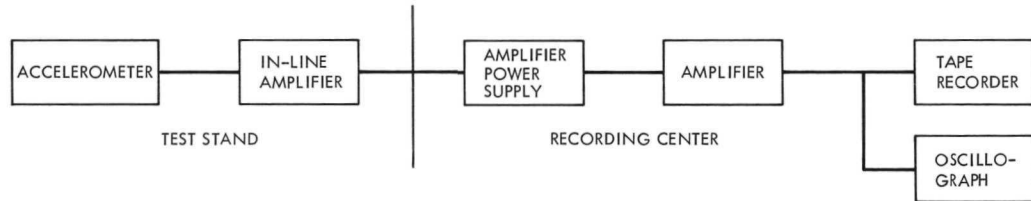
TEMPERATURE (THERMOCOUPLE):



STRAIN GAGE:



ACCELEROMETERS:



VOLTAGE AND CURRENT:

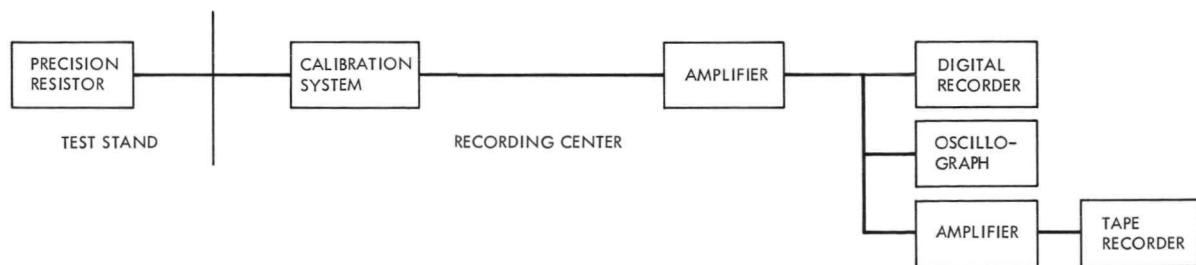


Fig. 45. Block diagrams of instrumentation systems used for demonstration tests

During the initial passivation, filling, and pressurization of the hydrazine system, a pinhole leak was opened in a weld joint of the bellows accumulator. This component was removed and replaced with a spare unit, and the fueling process was started again. A full load of 65.8 kg (145 lbm) of hydrazine was transferred into the test tank and slowly pressurized to 2517 kN/m² (365 psia) while a vacuum was drawn on the test cell to lower the pressure to 0.665 kN/m² (0.097 psia). The test system was allowed to stabilize for 48 hours to thoroughly saturate the hydrazine with gaseous nitrogen, and to thermally condition the propellant and hardware to about 283 K (50°F).

The first operation in the test sequence was the priming of the solenoid valve manifold. Trapped gases in the manifold were evacuated through the engine by opening the latching and engine valves in one branch of the feed system for 120 s. Then the first normally closed pyrovalve (NC1) was opened by energizing the squib firing circuit to introduce hydrazine into the solenoid valve manifold up to the seats of the two parallel latching valves. Verification of this operation was made by monitoring the solenoid valve manifold pressure trace (PFH, Fig. 30).

The engine start sequence began with opening the latching solenoid valve in the selected branch of the feed system, and confirming its position by referring either to the position indicating microswitches, or to a momentary drop in the manifold pressure trace. Thirty seconds later, the engine valve in the same branch was opened to start hydrazine flow to the engine; the test was terminated by closing the same valve. The latching solenoid valve was closed only after the hydrazine line temperature had stabilized, which usually required between 200 and 400 s.

A pyrovalve closing sequence began by establishing a descending temperature gradient in the solenoid valve manifold at a temperature above 310 K (100°F). This was accomplished by energizing strip heaters wrapped around the solenoid valve manifold. When the descending temperature gradient was verified, the normally open pyrovalve (NO1, Fig. 30) was activated to lock up the propellant system. The ambient temperature was not expected to exceed 310 K (100°F), so the pressure of the hydrazine trapped in the solenoid valve manifold would not exceed the lockup pressure. If, however, the temperature were to rise higher than 310 K (100°F), the volumetric expansion of hydrazine in the manifold was compensated automatically by adjustment within the bellows accumulator.

The first five tests were made using the Carlton latching, and the Hydraulic Research normally closed sole-

noid valve branch. The last four tests used the branch made up of the Marquardt latching and normally closed solenoid valves. The sequences just described apply to all tests except the first where priming was necessary.

3. Test system instrumentation. The demonstration system was thoroughly instrumented for measuring a total of 63 test parameters. A summary of the measured test parameters, their symbols, types, descriptions, units of measure, scale range, and accuracy are given in Table A-1 of the Appendix. The values of full scale accuracy were determined by applying the method of root sum square (rss) to all of the elements of the measurement system shown in Fig. 44, and carry a probability or confidence level of 95% (2 sigma). The physical location of most of the pressure and temperature transducers can be determined by a quick comparison of Figs. 30, 31 and 32.

Solenoid and pyrovalve current and voltage levels were recorded to verify operational response. The input signal voltage to the gimbal actuators and the output signal voltage from the actuator linear position potentiometers provided monitoring of the thrust vector control sequences. Six accelerometers and six strain gauges were mounted on the pyrovalve manifold, various support structures, and other selected component locations to record the response of the demonstration system to the shock loading caused by pyrovalve squib firings.

Detailed information on the test system calculated parameters is given in Table A-2, which is organized like Table A-1. The principal performance parameters listed there are vacuum thrust (F_{vac}), vacuum specific impulse (I_{vac}), characteristic exhaust velocity (c^*) and total delivered impulse (I_{tot}). In general, the rocket engine performance calculations were made according to the methods used in Ref. 43. The rss method was used to determine the full scale accuracy levels as before; however, the accuracies of some parameters vary with time, depending on the duration of the individual tests. For example, axial thrust (F_{avg}), which was measured directly, must be corrected for the change in mass of the suspended test system by the amount of propellant (M_{tot}) expended ($F_{corr} = F_{avg} - M_{tot}$). Although the percentage error in the total hydrazine expended during a test is approximately constant, the absolute value of the error in kilograms (pounds) increases with increased firing time. Since thrust is a slowly decreasing function of firing time, the ratio of total hydrazine (M_{tot}) error to the corrected thrust (F_{corr}) increases during a single test as a function of firing time. This particular case will be treated further in Subsection IV-D.

D. Test Results

The TCPS demonstration system successfully demonstrated the performance and multiple restart capability required by the TOPS mission duty cycle. A series of nine steady-state engine firings was made in sequence following a rerun of the first test. Nine pyrovalves were operated on command to alternately open and isolate the hydrazine feed system. Thrust vector control by engine deflection was demonstrated in three tests. Rocket engine performance was monitored by instrumentation installed on the demonstration system and confirmed by the direct measurement of the thrust and analysis of exhaust gas samples.

The test series was conducted over a period of 30 days. The minimum time interval between tests was 24 h and the maximum was 13 days. The test system was maintained under continuous vacuum over the entire test period. Ambient temperature within the test cell ranged between 278 to 294 K (37 to 70°F). All tests were started with the hydrazine and system hardware temperatures averaging around 281 K (47°F).

The first test in the series had to be repeated following replacement of the line between the solenoid valve manifold and the gimbal-mounted engine. The original coiled

hard-wall tubing proved to have too high a pressure loss and restricted the hydrazine flow rate. This tubing was replaced by a larger-diameter Teflon-lined flexible hose sheathed with braided wire. Although the change measurably increased the holdup volume of the propellant downstream of the engine valve, it did not affect the overall steady-state operation of the engine.

1. Steady-state performance. Steady-state performance is summarized in the graphs of Figs. 46 to 52 as a function of engine firing time. The total accumulated engine operating time for the nine tests was 1600 s—the shortest test being 15 s, and the longest, 749 s.

Propellant tank supply pressure at the start of test 1A was 2466.5 kN/m² (357.7 psia), and dropped steadily with each test firing to the final pressure level of 1195.5 kN/m² (174.7 psia), resulting in an initial to final pressure ratio of 2.06 to 1. The graph in Fig. 46 shows how tank pressure decayed with time. The discontinuity in the curve between the shutdown and start pressures of adjacent tests were caused by variations in the starting ambient temperatures, both in the hydrazine tank under vacuum inside the test cell, and in the supplementary ullage tank under ambient conditions outside the test cell.

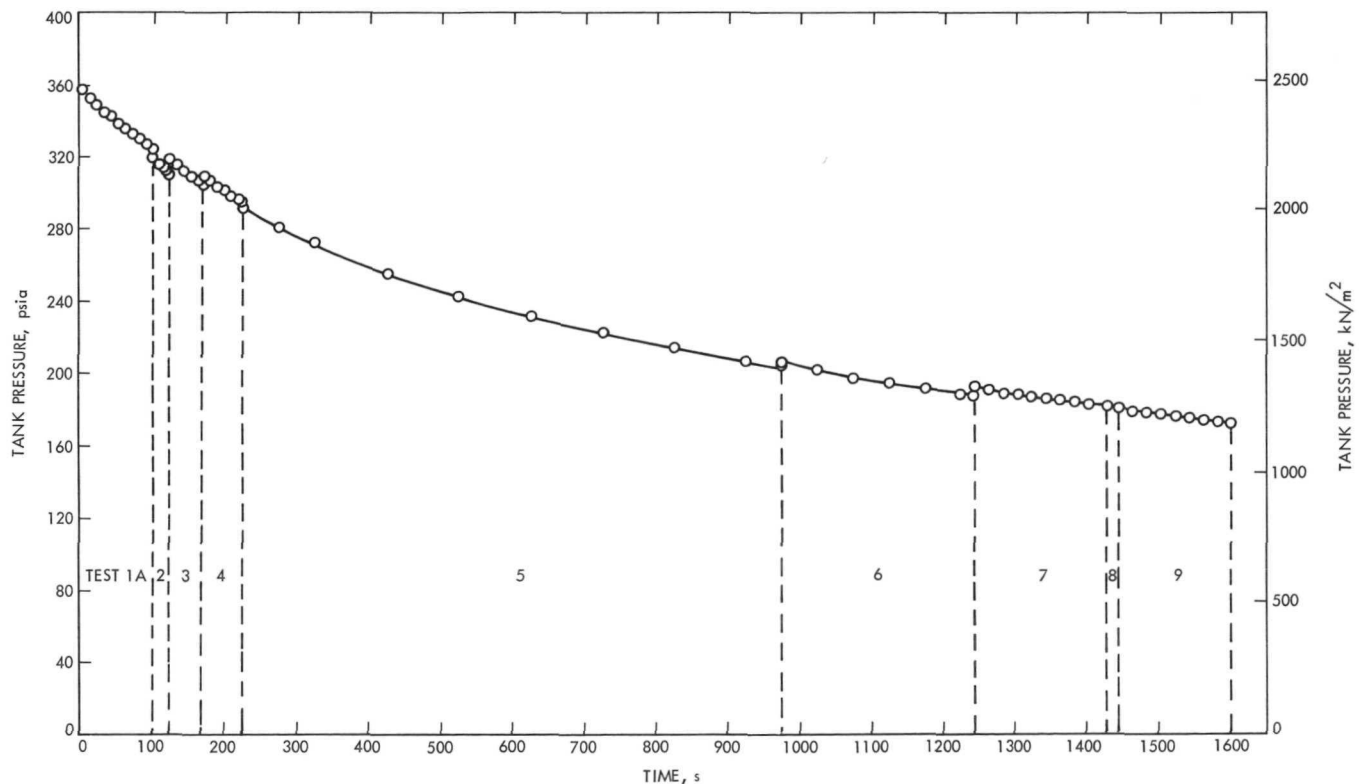


Fig. 46. Steady-state tank pressure versus time

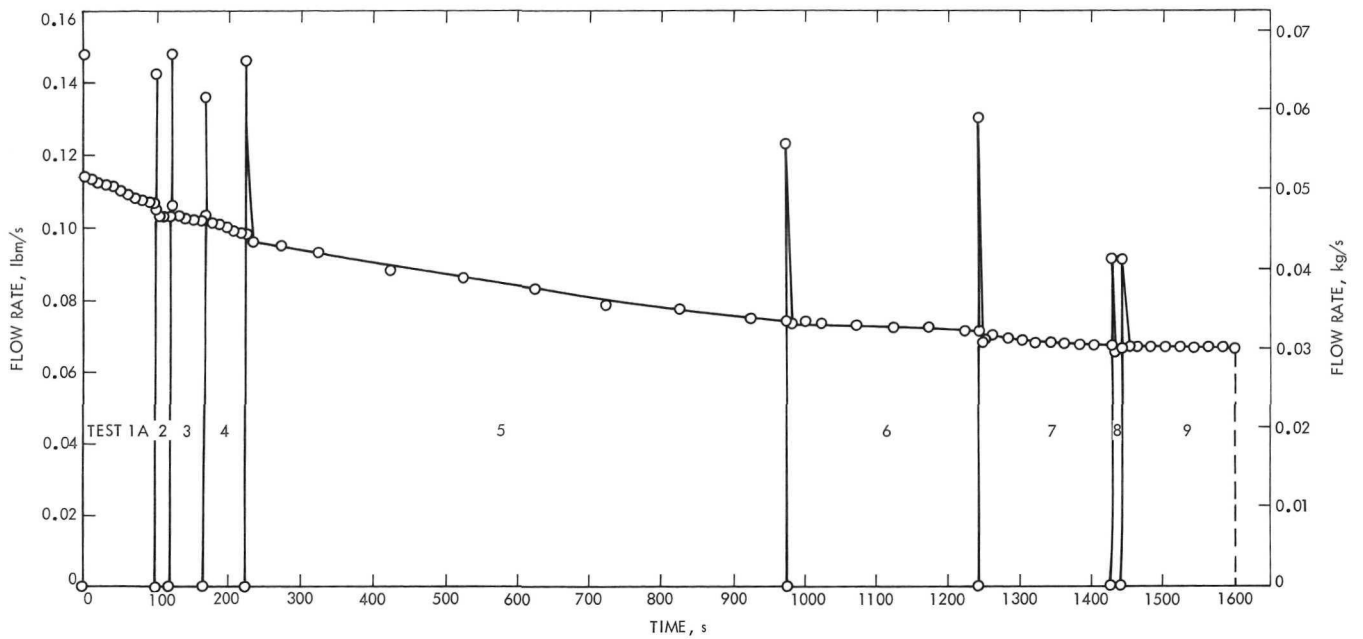


Fig. 47. Steady-state propellant flow rate versus time

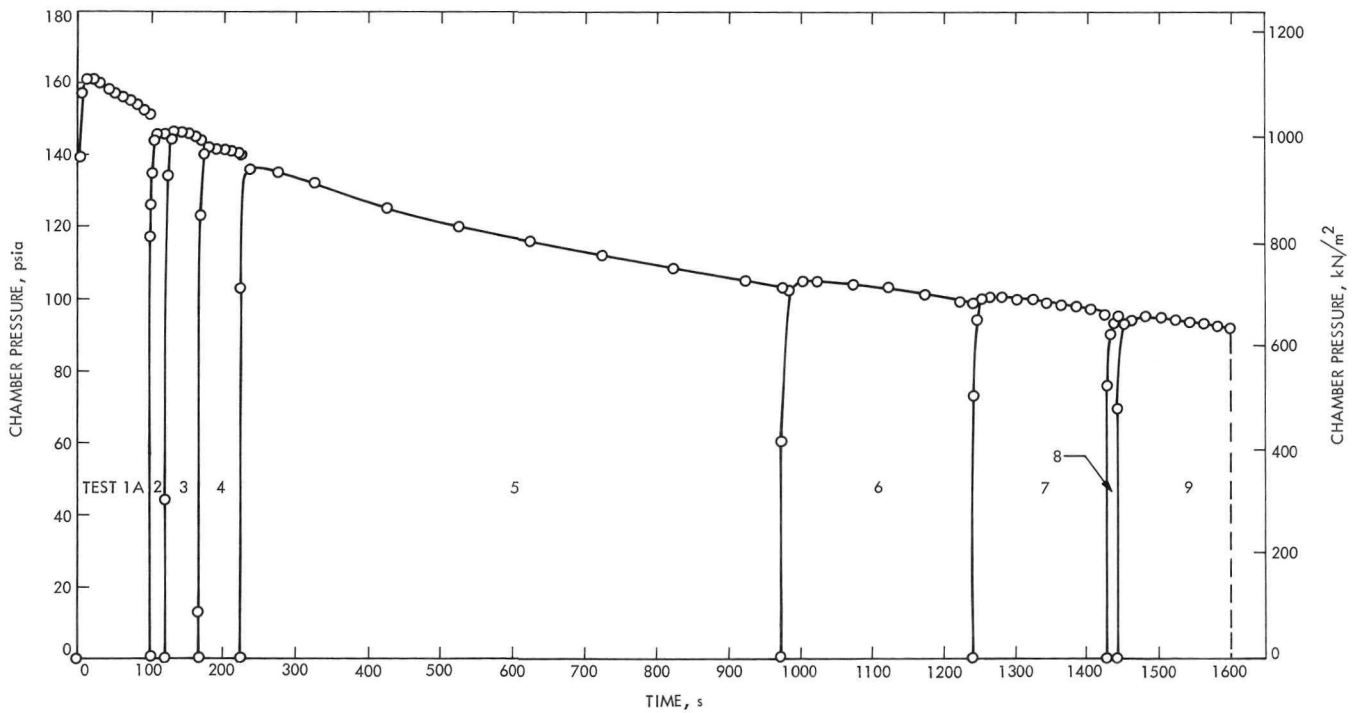


Fig. 48. Steady-state chamber pressure versus time

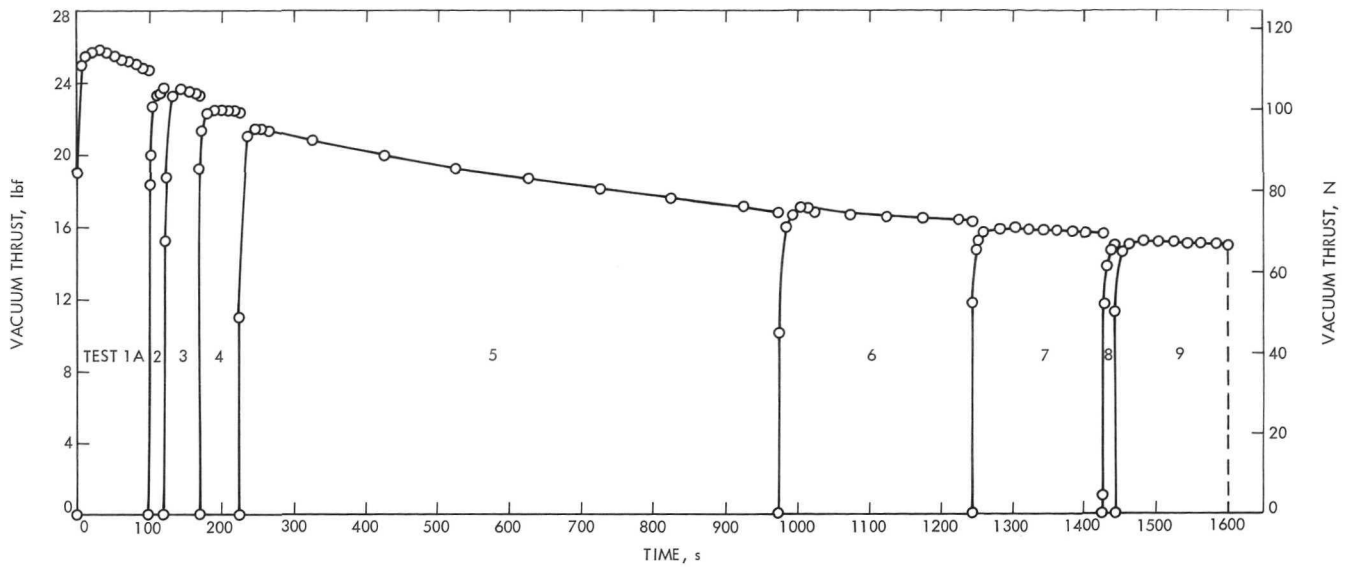


Fig. 49. Steady-state thrust versus time

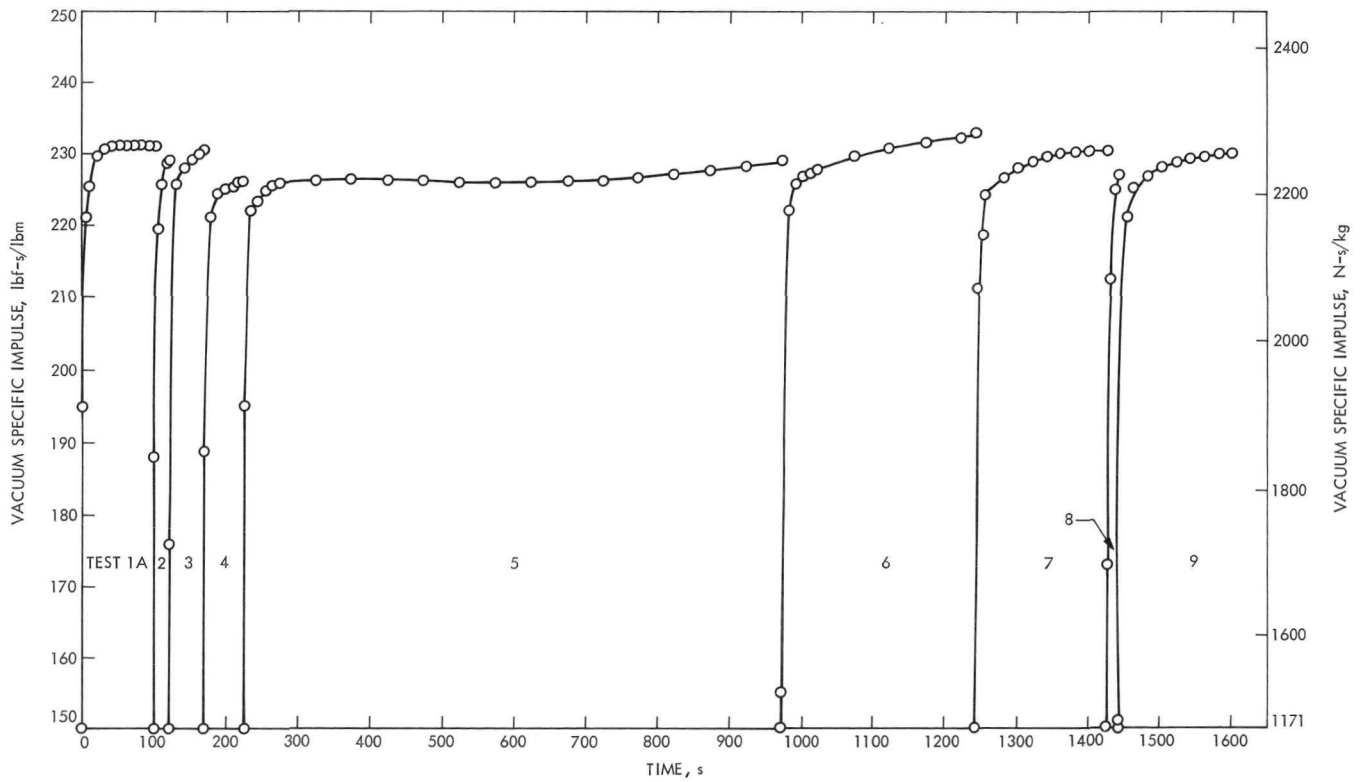


Fig. 50. Steady-state specific impulse versus time

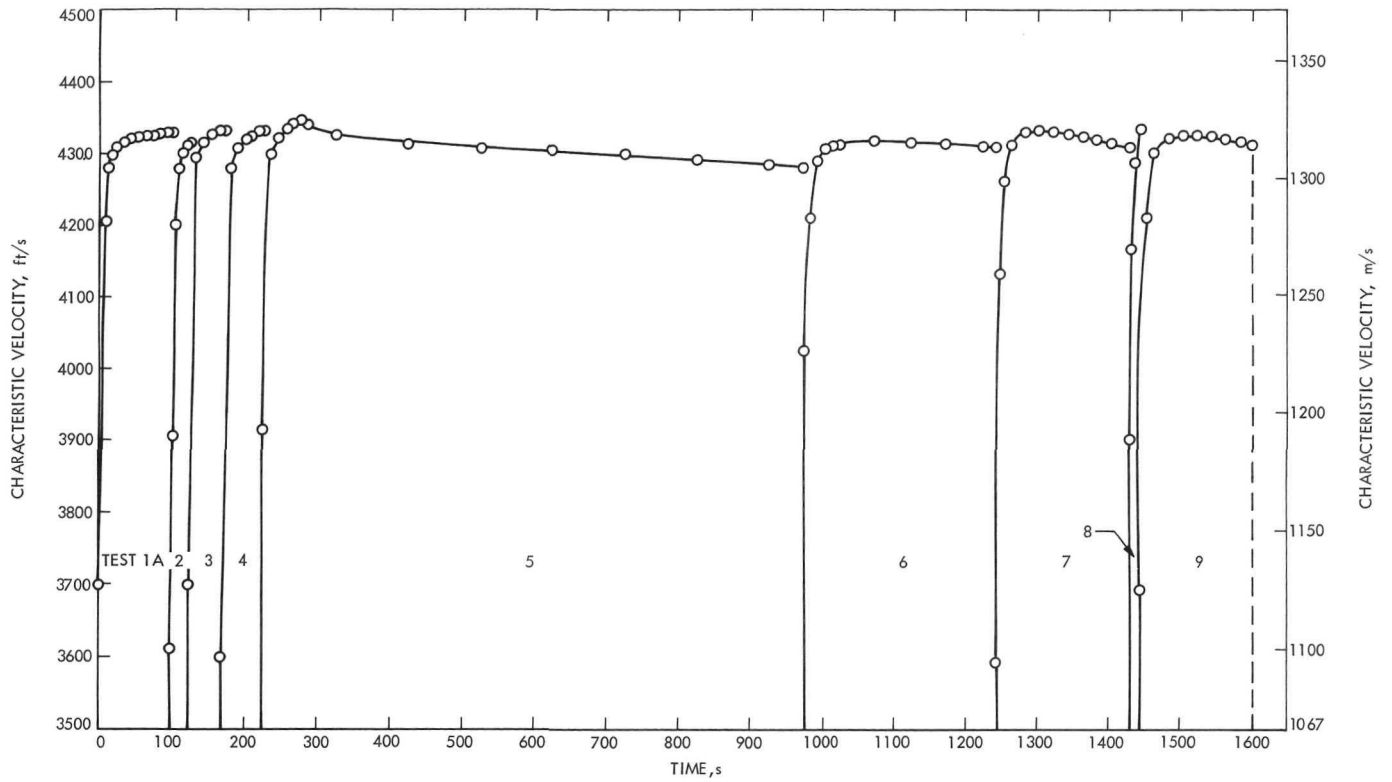


Fig. 51. Steady-state characteristic velocity versus time

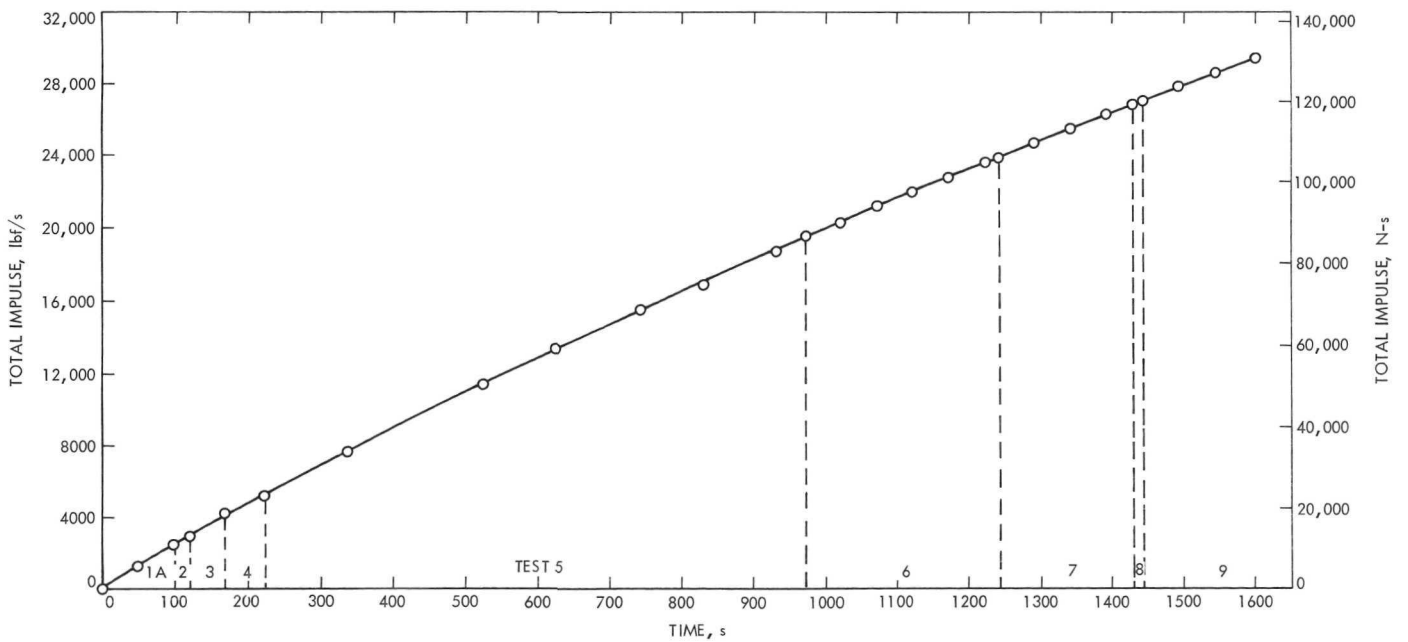


Fig. 52. Steady-state total impulse versus time

The variation of hydrazine propellant flow rate with time is shown in Fig. 47. An overshoot in flow rate at the start of each test was caused by surge-type filling of the flex line between the engine valve and injector and the slight lag in the rise of P_c due to catalytic-bed ignition delay. Normally about 0.43 s was required for propellant flow stabilization.

The steady-state flow rate ranged from a maximum of 0.05124 kg/s (0.145 lbm/s) down to 0.02948 kg/s (0.065 lbm/s). The sharp-edged orifice plate flowmeter combined with a bidirectional differential pressure transducer, proved to be a rugged, reliable, and accurate instrument. No apparent damage or loss of accuracy was inflicted by the hydraulic shocks induced by repeated pyro and solenoid valve operations. The instrumentation accuracy of propellant mass flow-rate calculations, given in Table 27, was ± 0.0003 kg/s (± 0.0006 lbm/s). The flow-rate accuracy values were used in determining the accuracy of other calculated parameters, as described in Subsection IV-C-3.

The time integral of instantaneous mass flow rate was used to determine the total mass of propellant expended during each test firing. At the end of each test, the change in mass of the test system was also determined from the axial load cell in the thrust measuring stand. A summary of the measured mass change versus the calculated integral of flow rate for each test is presented in Table 27. The percentage differences given in the table use the load cell mass measurement as a basis of comparison; a positive difference indicates integrated flow rate is less than the mass measurement, and a negative difference indicates the opposite. The range of difference varies from +0.94 to -3.85%. The total difference at the end of nine test firings was only -0.99%. The orifice flowmeter is recommended for flight use as a simple source

Table 27. Summary of mass change versus integrated propellant flow rate

Test No.	Mass change, kg	(lbm)	Integrated flowrate, kg	(lbm)	Percent of difference
1A	4.985	(10.99)	4.981	(10.98)	0.91
2	1.007	(2.22)	1.025	(2.26)	-1.79
3	2.150	(4.74)	2.164	(4.77)	-0.63
4	2.481	(5.47)	2.567	(5.66)	-3.85
5	28.486	(62.80)	28.563	(62.97)	-0.27
6	8.954	(19.74)	8.881	(19.58)	0.81
7	5.865	(12.93)	5.838	(12.87)	0.46
8	0.440	(0.97)	0.454	(1.00)	-3.09
9	4.813	(10.61)	4.767	(10.51)	0.94
Total	59.181	(130.47)	59.240	(130.60)	-0.99

for accurate performance data for the analysis of past events and the prediction of the characteristics of future events.

The drop in thrust chamber pressure with time or blow-down, shown in the graph of Fig. 48, was caused by the steady depletion of hydrazine. No loss of chamber pressure resulting from reduced catalytic-bed activity was discernible from the test data. The maximum chamber pressure reached during the first firing was 1111.9 kN/m² (161.3 psia), and it dropped to 623.5 kN/m² (93.5 psia) by the end of the last test. As was the case with the engine life test data (Subsection III-A-4), these P_c data were not corrected for the small difference between static and stagnation pressure existing at the engine pressure tap location. Maximum chamber pressure was reached 14 s into the first test. This corresponds closely to the time required to reach maximum catalytic-bed temperature. Chamber pressure stability and pressure rise time are covered later in Subsection IV-E-3.

The chamber pressure transducer was mounted on a bracket attached to the engine gimbal support, allowing it to move with the engine during thrust vector control tests. The pressure transmitting line was a 15.24 cm (6 in.) length of 0.3175-cm (1/8-in.) diam stainless steel tubing. The transducer was of the strain gauge type with thermal compensation up to 478 K (400°F); however, the temperature measured along the transmitting line exceeded 534 K (600°F) on long-duration tests. Zero shifts, due to temperature effects, as high as 29.2 kN/m² (4.2 psia) were seen at the end of the longer tests.

Steady-state vacuum thrust plotted versus time in Fig. 49 is the corrected value of the average actual thrust measured with a dual bridge load cell. The first correction was for the change in mass of the suspended test system, due to the expenditure of propellant. The second correction was for nozzle back pressure caused by the small but finite pressure within the test cell. Cell pressure ranged from 0.205 to 0.056 kN/m² (0.032 to 0.009 psia) during engine firings. Thrust data taken during thrust vector control (TVC) test periods was not corrected for the small loss to the side component; this deficit is most noticeable in test No. 5 where a 145-s TVC sequence was started 300 s into the test. Vacuum thrust showed a gradual decrease from 115.6 N (25.99 lbf) on the first test to 60.34 N (15.02 lbf) at the end of the ninth test. Time to peak thrust averaged around 23 s, which was a lag of some 9 s behind the corresponding peak chamber pressure.

Vacuum specific impulse was calculated from vacuum thrust and propellant mass flow rate. Figure 50 shows the variation of vacuum specific impulse with time for each test firing. The values appear to increase slowly during each test, which is contrary to normal experience on monopropellant engines. This can be explained by the cumulative errors in the vacuum thrust calculations pointed out previously. The curve dips slightly in the middle of test No. 5 because thrust was not corrected for the small losses incurred during the 145-s TVC test made at that time. The remaining TVC tests were much shorter and their thrust losses much less noticeable. On tests of 90 s or more, the vacuum specific impulse varies from 2207 N-s/kg (225 lbf-s/lbm) up to 2275 N-s/kg (232 lbf-s/lbm). Over the total 1600 s of engine firing time, a nominal value of 2226 N-s/kg (227 lbf-s/lbm) is a good average of the data. Since performance did not decrease with cumulative firing time, the pressure-blowdown system (at least a 2:1 blowdown system) performs just as well as a pressure-regulated system.

Characteristic velocity (c^*) was calculated from chamber pressure, nozzle-throat area corrected for temperature, and propellant mass flow rate. The graph of c^* versus time is presented in Fig. 51. In this graph, c^* reaches a maximum value shortly after engine start, and then appears to decrease slowly. In the previously discussed steady-state performance curves, chamber pressure and propellant mass flow rate both decrease with time, but chamber pressure decreases more rapidly. This is due, in part, to the negative thermally induced zero shift of the chamber pressure transducer caused by heat soakback through the pressure transmitting line. The maximum value of c^* recorded on test No. 5 was 1325 m/s (4347 ft/s), which then decreased slowly to 1302 m/s (4271 ft/s) at engine cutoff. A nominal value for all tests is about 1315 m/s (4315 ft/s), which is a reasonable value for a monopropellant hydrazine engine.

The total impulse was calculated by integrating vacuum thrust with engine firing time for each test. The steady-state total impulse versus time curve, presented in Fig. 52, is made up from the cumulative total of the impulse delivered in each test of the series. Total impulse delivered over 1600 s was 130,785 N-s (29,403 lbf-s). The curve is not quite linear, having a slight decreasing slope with time that is characteristic of a blowdown propulsion system.

The data just discussed is a general summary of the steady-state performance for the demonstration system.

A detailed summary is given in Tables A-3 to A-8 of the Appendix. This table includes a listing of important measured test parameters and calculated performance parameters taken for specified times from the digital data for each test. Each data slice represents slightly different operating conditions, since steady-state conditions are never truly reached for blowdown-mode engine operation. The engine temperature influence on performance is minimized by comparing data at the same time after engine ignition for all tests. The times of 10, 20, 40, 90, and 150 s were selected to maximize the number of tests lasting longer than the given time slice; thus, test No. 8 appears once, and tests 5, 6, 7, and 9 appear all five times. Thermal equilibrium for the rocket engine is established after about 100 s of steady-state operation.

2. Transient response and roughness. Transient response and chamber pressure roughness for the demonstration system were obtained from analyses of the oscillographs (O-graph) data traces. The definition and calculation of the transient response parameters are similar to those identified in Ref. 43. The only difference occurs in the definition of start time: Actual engine valve opening time is used as the start time rather than the time of voltage application. Actual valve opening is identified by the slight characteristic inflection that appears in the increasing valve current trace. The momentary current drop caused by the valve armature moving in the magnetic field of the solenoid coil accurately identifies the actual valve opening time. It is more meaningful than the time of initial valve voltage rise. The engine shut-off time, or valve closure, is identified in a similar manner from the decreasing valve current trace.

A tabular summary of the transient start, shutdown, and roughness characteristics for all test firings is given in Table 28. Typical O-graph traces of the hard start and shutdown that occurred on test No. 2 are shown in Figs. 53 and 54. The only smooth start and shutdown recorded in this test series occurred on test No. 6 for which the O-graph traces are shown in Figs. 55 and 56. A hard start is identified by a sharp pressure spike on the chamber pressure (P_c) trace, normally exceeding the nominal level by 100% or more. The injector manifold pressure (PFJ) also witnesses the hydraulic shock propagated back into the propellant feed system.

The transient response parameters, including ignition delay, pressure rise time, pressure decay time, and response (thrust) rise time are identified on the O-graph traces. Of these, the least well defined is response time.

Table 28. Rocket engine transient start, stop, and roughness characteristics

Test No.	Propellant temperature, K (°F)	Catalytic-bed temperature, K (°F)	Ignition delay, ms	Response time, ms	P_c rise time, ms	P_c decay time, ms	F spike N (lbf)	PFJ spike kN/m ² , (psia)	P_c spike kN/m ² , (psia)	P_c nominal kN/m ² , (psia)	ΔP_c maximum kN/m ² (psi)	ΔP_c frequency, Hz	$\frac{\Delta P_c}{P_c}$, %
1	281 (45)	290 (63)	167	NA	204	48	648 (94)	4240 (615)	2834 (411)	565 (82)	17.2 (2.5)	210	3.28
1A	293 (68)	299 (79)	134	142	163	41	765 (111)	2751 (399)	2220 (322)	1089 (158)	17.9 (2.6)	190	1.65
2	281 (45)	284 (52)	133	140	152	33	614 (89)	3192 (463)	1669 (242)	1014 (147)	22.1 (3.2)	205	2.17
3	284 (52)	292 (65)	177	191	238	30	>910 (>132)	4916 (713)	>2744 (>398)	1007 (146)	24.1 (3.5)	190	2.40
4	280 (44)	286 (54)	142	NA	165	37	NA	3344 (485)	2172 (315)	986 (143)	24.8 (3.6)	190	2.51
5	271 (38)	283 (50)	204	NA	261	53	NA	5213 (756)	>2903 (>421)	917 (133)	31.7 (4.6)	190	3.44
6	279 (43)	281 (45)	144	150	154	63	207 (30)	1262 (183)	448 (65)	710 (103)	42.1 (6.1)	185	5.92
7	280 (44)	283 (49)	183	194	230	54	786 (114)	2806 (407)	1565 (227)	683 (99)	20.7 (3.0)	185	3.30
8	282 (47)	284 (51)	183	189	219	54	676 (98)	2593 (376)	1682 (244)	648 (94)	22.1 (3.2)	185	2.93
9	281 (46)	285 (53)	184	193	224	54	648 (94)	2482 (360)	1669 (242)	648 (94)	22.1 (3.2)	180	2.95
			(Avg 165)		(Avg 201)	(Avg 48)							

A 25-Hz resonant frequency, requiring 2 to 3 s to damp out, persisted in the thrust measurement obscuring the true engine response. Ignition delay times for this engine configuration ranged from 133 to 204 ms. The longest delay time occurred at the lowest propellant temperature on test No. 5. One of the shorter ignition delays occurred at the highest propellant and engine temperature on test No. 1.A. It is interesting to note that the system configuration for test No. 1, which had the smaller holdup volume, did not produce the shortest ignition delay time.

Chamber pressure rise times ranged from 154 to 261 ms, and decay times from 33 to 63 ms. Chamber pressure spikes occurred on all but one test; several exceeded 2758 kN/m² (400 psia). The highest recorded injector manifold pressure spike was 5213 kN/m² (756 psia) which occurred on test No. 5.

Chamber pressure roughness was calculated from the maximum peak-to-peak pressure oscillations that occurred anywhere during the test and is reported as a percentage of the nominal chamber pressure. The values

range from 1.65 to 5.92%. The highest value of 5.92% was recorded during test No. 6, whereas during test No. 9, it was back down to 2.95%. It is apparent from the smooth engine operation that all the hard starts and steady-state firing time did not cause significant degradation of the catalytic bed or seriously reduce engine life expectancy.

The slope of the start transient of engine performance parameters decreases with decreasing mass (chemical energy) flow rate. The time required to reach specific values of six performance parameters is given for each of the nine tests in Table 29. Since the steady-state value of each parameter is nearly constant, and the shape of its transient curve is similar for all nine tests, the times in the table show that the transient rise rate decreases with decreasing flow rate and that predictability of the transient of computed parameters is poor. The use of these parameters in system modeling will be difficult. The unpredictability of the transient stems largely from the engine start spike; smoother starting engines are expected to be more predictable. The last three parameters presented in Table 29 will be defined and discussed in more detail in Subsection IV.D.7.

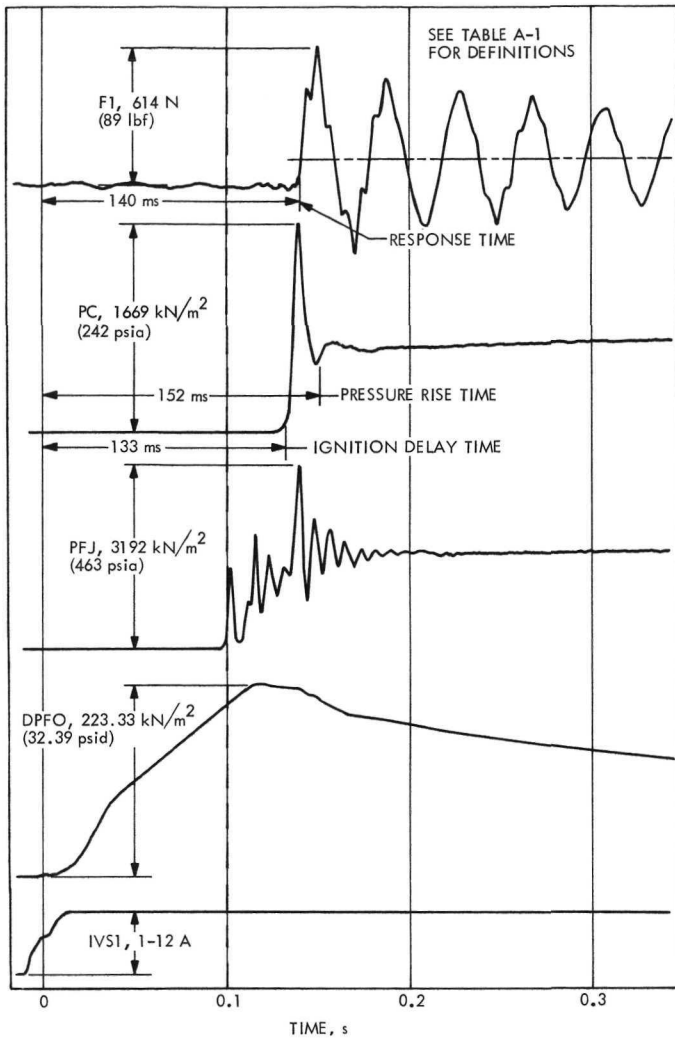


Fig. 53. Typical hard-start transient (test No. 2)

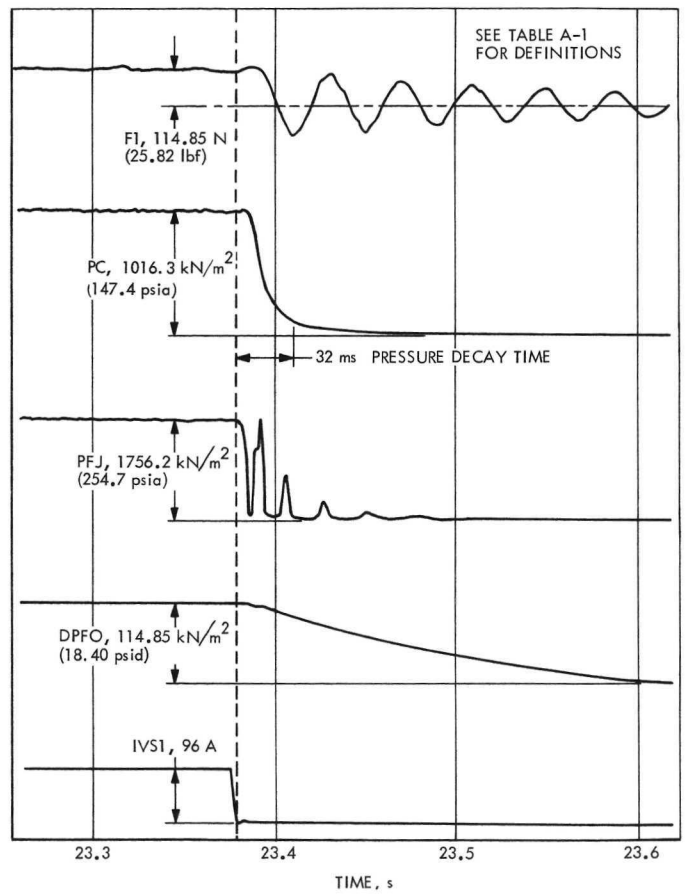


Fig. 54. Typical hard-stop transient (test No. 2)

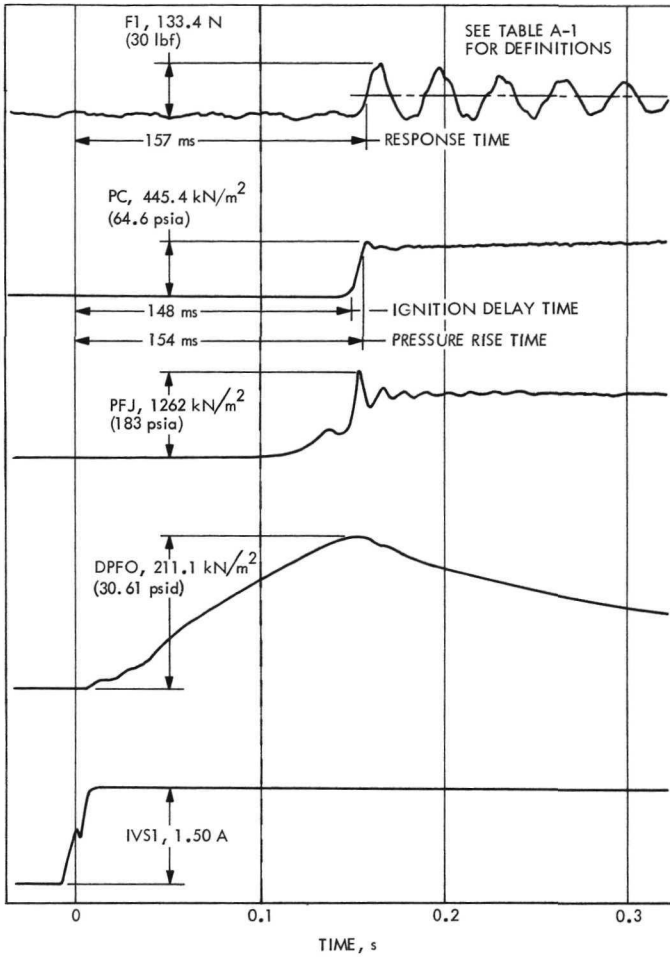


Fig. 55. Typical smooth-start transient (test No. 6)

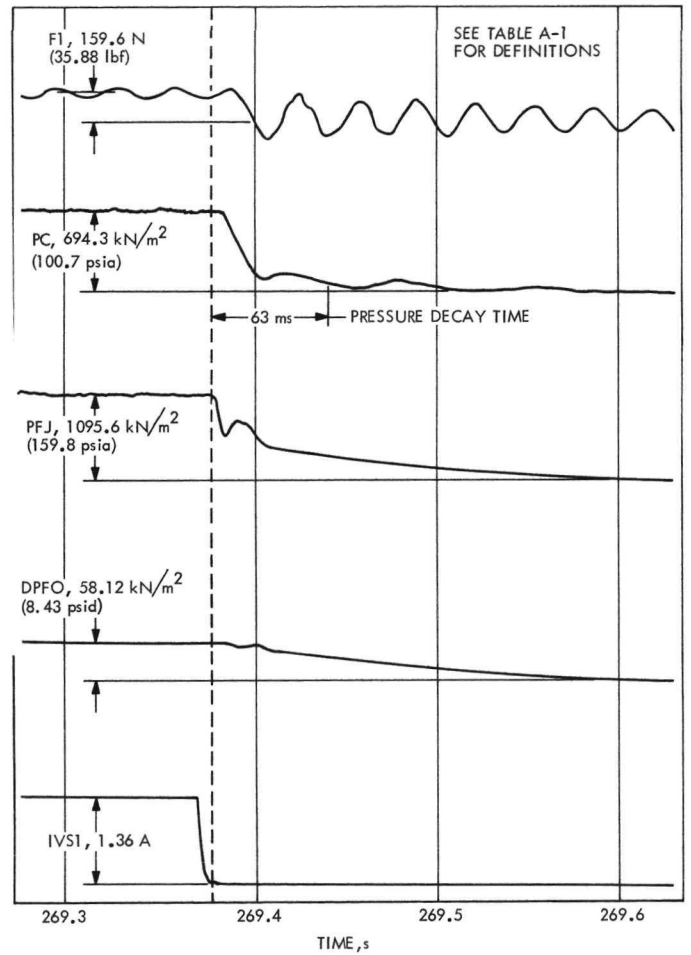


Fig. 56. Typical smooth-stop transient (test No. 6)

Table 29. Rocket engine performance transient characteristics

Time (in seconds) from valving signal to specified parameter value						
Test No.	Chamber wall temperature at TC2, 1089K (1500°F)	Vacuum specific impulse I_{vac} , 2157 N-s/kg (220 lbf-s/lbm)	Characteristic velocity c^* , 1310 m/s (4300 ft/s)	Liquid flow resistance R_l , $17.6 \times 10^{10} \frac{N-s^2}{kg-m^5}$ ($190 \frac{lbf-s^2}{lbm-in.^5}$)	Mass flow-rate constant K_m , 0.279N ^{1/2} -m (5.2 lbf ^{1/2} -in.)	Chamber pressure constant K_{pc} , 0.0001 m ² (0.155 in. ²)
1A	8.1	4.6	14.1	0.1	20.1	1.0
2	8.5	5.0	14.5	0.5	19.7	5.0
3	9.0	3.5	9.1	0.6	19.1	11.9
4	9.6	7.6	14.4	0.6	36.5	46.5
5	11.1	8.8	10.1	0.6	40.6	57.8
6	17.1	8.2	19.7	0.9	31.7	17.6
7	19.7	9.0	12.7	0.8	38.7	43.5
8	a	8.4	11.9	a	a	a
9	22.3	9.9	17.9	0.9	53.8	117.1

^aSpecified value not reached during test.

3. Temperature response. No serious temperature problems were uncovered in demonstration system tests. Engine and neighboring component temperatures reached expected levels during engine firings. High temperatures recorded on the injector inlet during postfiring thermal soakback may set a lower bound for the safe time between successive firings. A summary of the minimum-to-maximum temperature ranges recorded on the demonstration system throughout the test program are listed in Table 30 as a guide for system thermal control design. The location of the measurement points on the engine assembly and neighboring components are shown in the cutaway assembly drawing given in Fig. 57.

The maximum temperature recorded during the test was the catalytic bed-temperature (T_B) of 1180 K (1675°F) measured just before engine shutdown at the end of test No. 5. This catalytic-bed temperature is less than the 1256 K (1800°F) commonly reported for mono-propellant hydrazine engines because the engine immersion thermocouple is probably not located precisely at the hydrazine decomposition or flame front. This thermocouple failed 30 s after engine shutdown on test No. 5, indicating a shorted circuit or secondary junction. The failure was probably due to a breakdown of the tube sheath insulation caused by severe thermal cycling and mechanical forces exerted by catalytic pellets shifting in response to the same thermal cycling.

The thrust chamber wall temperature was measured with a thermocouple tack-welded to the outer chamber surface at the same axial location on the chamber as the bed probe. The engine Min-K insulation was fastened

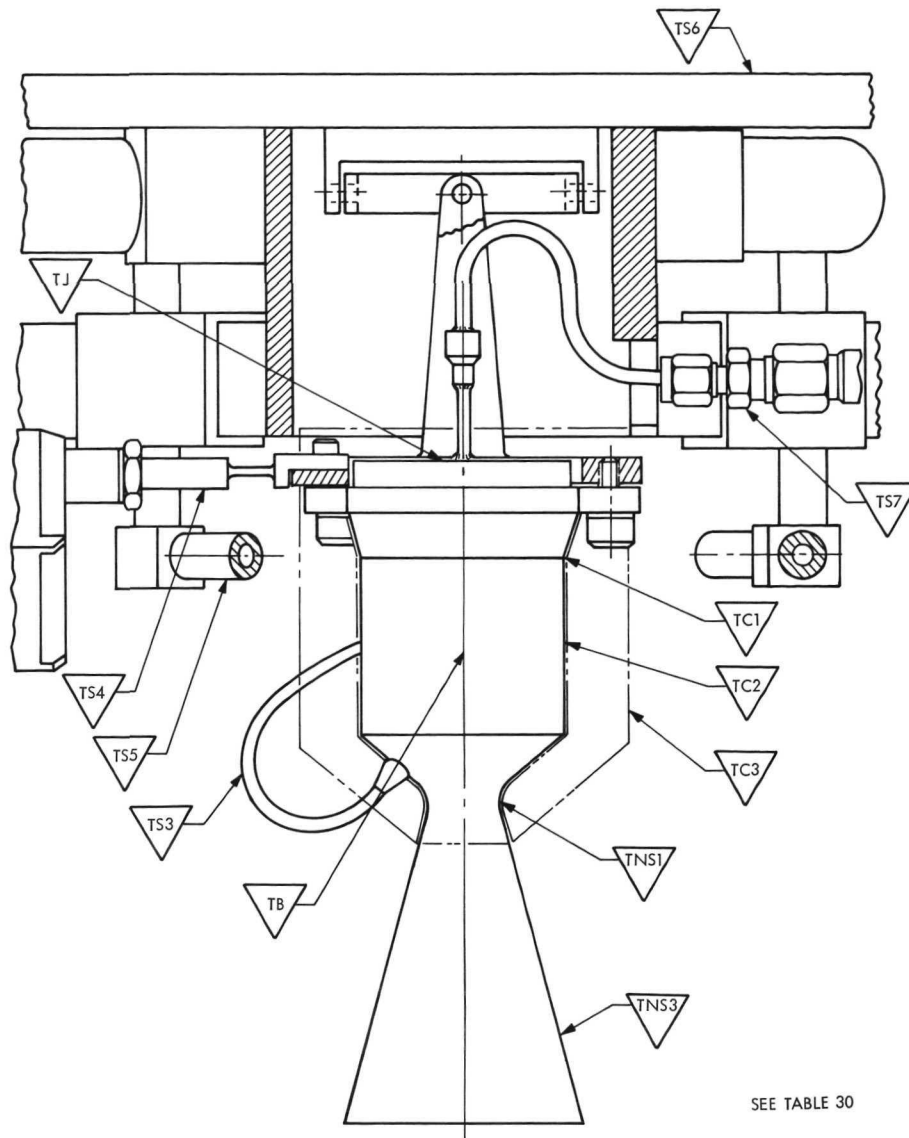
Table 30. Minimum to maximum temperature range for engine components and support structures

Symbol	Location	Temperature range, K (°F)	
Propellant system			
TN2	Nitrogen pressure tank	273-287	(31-56)
TFT	Fuel tank wall	277-290	(39-62)
TFO	Fuel orifice flowmeter	276-293	(37-68)
TFH	Fuel heater manifold	276-293	(37-68)
Engine assembly			
TJ	Engine injector head	281-882 ^a	(46-1117)
TB	Center catalyst bed	283-1186	(49-1675)
TC1	Upper thrust chamber wall	276-1170	(37-1646)
TC2	Middle thrust chamber wall	276-1166	(37-1639)
TC3	Insulation outer wall	282-419	(47-294)
TNS1	Nozzle throat surface	278-1087	(42-1497)
TNS3	Nozzle exit surface	282-886 ^b	(47-1135)
Components and structures			
TS1	Fuel line filter	277-292	(39-66)
TS2	Engine valve manifold	277-299	(39-78)
TS3	Chamber pressure tube	277->592	(39->606)
TS4	Actuator linkage rod	279-411 ^a	(42-280)
TS5	Pyrovalve manifold tube	278-299	(40-78)
TS6	Support base plate	276-294	(37-69)
TS7	Injector flextube union	276-298	(37-76)
TCL2	Vacuum test cell	274-412 ^a	(33-282)

^aThermal soakback temperature

^bThrust vectoring anomaly

over this thermocouple. The catalytic-bed temperature time profile, shown in Fig. 58, exceeds the chamber wall profile by 17 to 39 K (30 to 70°F). Only the wall temperature is plotted after test No. 5, because the bed thermocouple was unreliable after that. The peak value of thrust



SEE TABLE 30

Fig. 57. Engine components and structures thermocouple locations

chamber wall temperature dropped from 1173 to 1115 K (1652 to 1550°F) over the 1600 s of engine operation.

The rate of engine warmup decreases over the nine firings. The change in the transient rate is quantitatively illustrated in Table 29 by the increasing time needed for the thrust chamber wall to reach 1089 K (1500°F), going from 8.1 s (test No. 1A) to 22.3 s (test No. 9). The change in both the transient rate and the peak value of the engine-wall temperature is primarily a nonlinear function of mass flow rate, which is equivalent to the rate of total energy input.

Injector inlet temperature was measured with a thermocouple tack-welded to the outer surface, adjacent to

the injector inlet tubing, and under the Min-K insulation. The maximum temperature recorded by this thermocouple during an engine firing was 437 K (326°F) on test No. 5; however, 70 s after engine shutdown on this test, the temperature increased to 882 K (1117°F). This rapid temperature rise was due to the combined effects of thermal soakback from the thrust chamber, and the decomposition reaction of hydrazine venting from the holdup volume in the flexible injector feed tube. The hydrazine reaction was further identified by the numerous perks or low-level pulses present in the O-graph traces of decaying chamber pressure and injector manifold pressure. Since these perks were small, and not sharp (Fig. 56), the reaction is assumed to have taken place within the thrust chamber at the upper surface of the 25-30 mesh

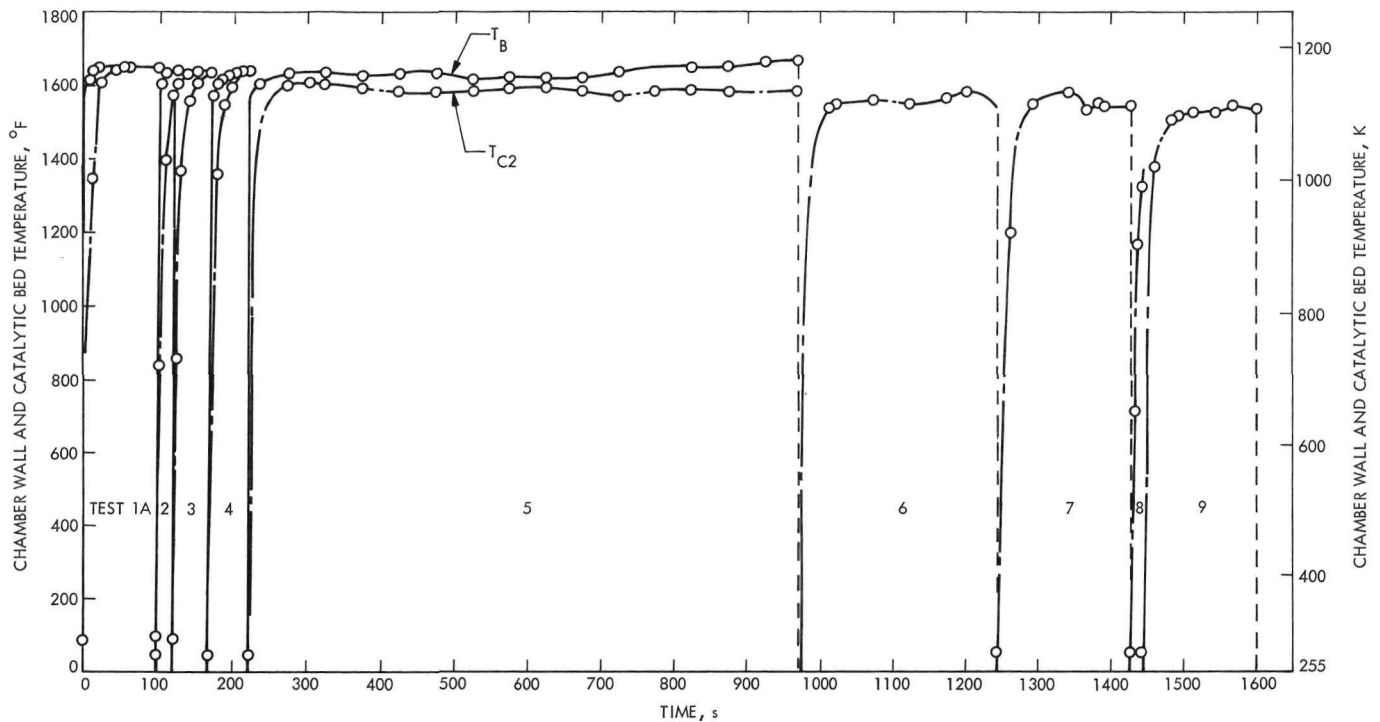


Fig. 58. Steady-state engine temperatures (T_B and T_{C2}) versus time

catalyst of the upper bed (Fig. 8). The venting process required 30 to 40 s to completely evaporate the trapped propellant which coincides roughly with the time of fastest posttest temperature rise. The graph of engine injector inlet temperature versus time (Fig. 59), shows the results of the shortest test (No. 8) of 15 s duration, and the longest test (No. 5) of 749 s duration.

The difference in peak temperature results from the difference in thermal energy acquired by the thrust chamber assembly during firing. Figure 60 shows maximum injector inlet posttest temperature as a function of engine firing duration. The peak temperature exceeded the auto-decomposition temperature for hydrazine—approximately 533 K (500°F)—in all cases. Thus, it would be unwise to attempt an engine restart until the injector cools, to avoid the possibility of starting a reaction in the injector instead of the upper catalytic bed. On test No. 8, it took 1585 s for the injector inlet to drop below 533 K, and on test No. 5, it required 2350 s. Any atmospheric test firing for this test system configuration should be followed with a posttest GN_2 purge of the injector manifold immediately after engine shutdown to avoid decomposition of hydrazine in the injector, since the atmospheric back pressure could possibly increase hydrazine residence time in the injector manifold to the point where destructive decomposition occurs in the manifold.

All test system components in the immediate vicinity of the engine, except one, experienced no overheating. The exception was the chamber pressure transducer which exhibited significant zero shifts due to thermal gradients through the transducer assembly. The temperature measured on the 0.32 cm ($\frac{1}{8}$ in.) transducer pressure tube at a point 12.7 cm (5 in.) from the engine and 17.8 cm (7 in.) from the transducer (TS3) exceeded the 592 K (606°F) scale setting 325 s into test No. 5; the temperature was less than 589 K (600°F) on all other tests, the longest of which lasted 269 s. Although the transducer temperature probably did not exceed the temperature compensation limit of 478 K (400°F), compensation was not completely effective because of the large temperature gradient that existed between the sensing diaphragm, strain gauge, and electronics. Some form of thermal isolation is thus necessary to protect the chamber pressure transducer from conductive heating, especially for firings exceeding 300 s.

The next warmest component was also attached to the engine. The gimbal actuator push rods bolted to the engine gimbal support ring experienced a maximum temperature (TS4) of 411 K (280°F). The outer surface of the engine insulating jacket (TC3) reached a similar high of 419 K (294°F), although this measurement is questionable because of some unexplained anomalous behavior during the test. The temperature of other components

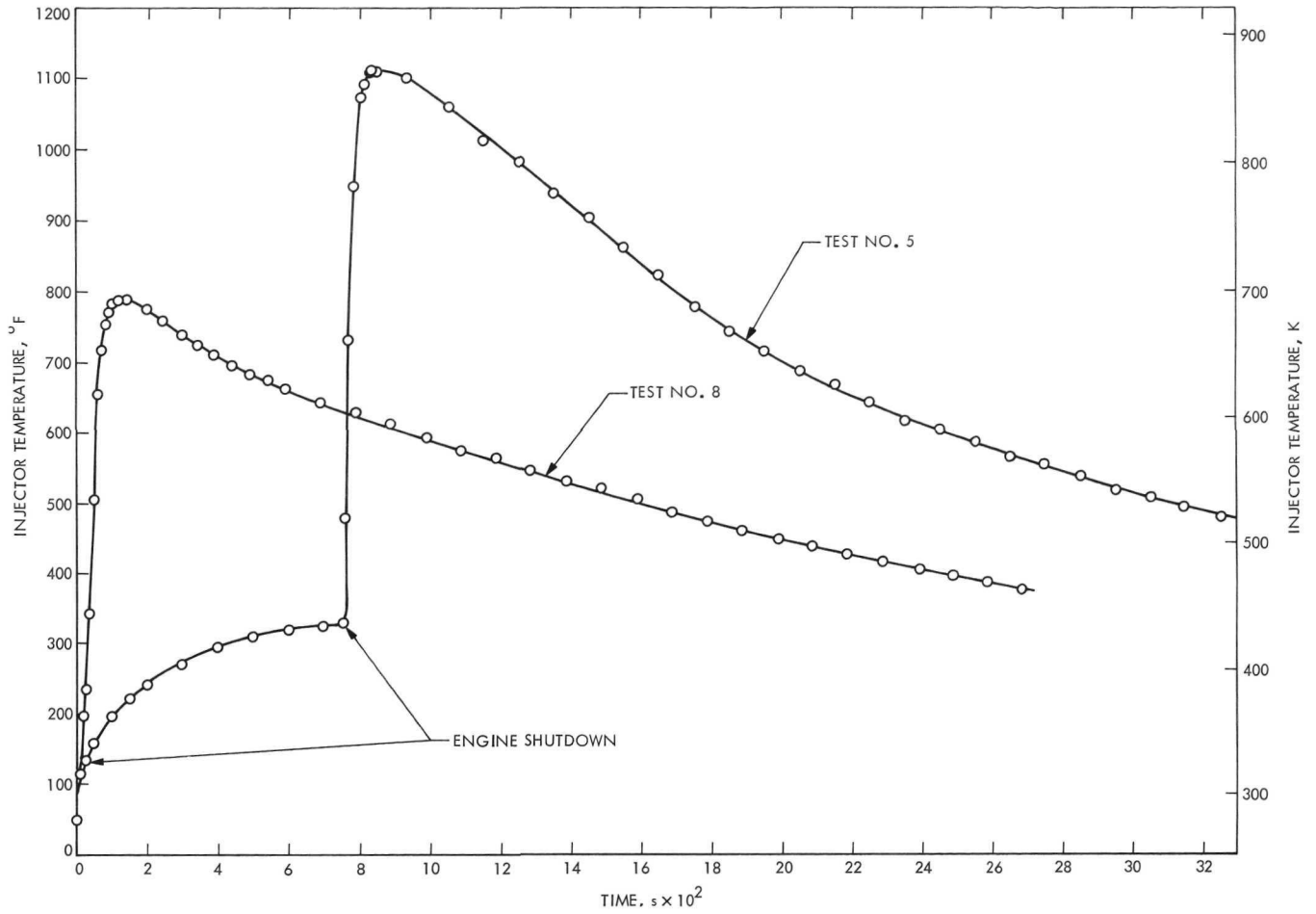


Fig. 59. Engine injector temperature versus time

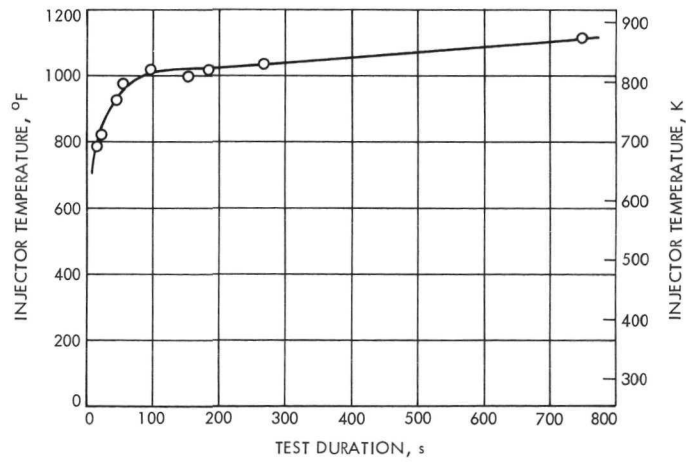


Fig. 60. Injector maximum posttest temperature versus test duration

close to, but not touching, the engine rose 17 K (30°F) at most from their initial values (Table 30).

The engine exhaust nozzle temperature (TNS3) was measured by a thermocouple tack welded to the outer surface of the expansion nozzle at an area ratio of approximately 35 (the nozzle exit area ratio was 39.31). The maximum temperature recorded at this location, 886 K (1135°F), occurred during thrust vector control testing when the bow shock wave from the gas sample probe hit the nozzle wall near the thermocouple location. The highest temperature recorded when the engine was centered (gimbal actuators in null position) was 793 K (967°F).

The demonstration system did not thermally simulate a flight system in all respects because no thermal insulation blanket was provided. The presence of such a blanket probably would not significantly change the temperature levels just discussed, and certainly not change the trends and relative relationships.

4. Exhaust gas analysis. The percentage of ammonia dissociation taking place within the catalytic bed of the engine—an indicator of engine performance efficiency—was determined from the chemical composition of the exhaust gas. It is assumed that the composition of this gas mixture remains frozen upon leaving the catalytic bed, and that no further change occurs during the collection and analysis process.

Exhaust gas samples were collected in an evacuated 5×10^{-4} m³ (31 in.³) stainless steel cylinder just prior to engine shutdown on each test firing. The sampling probe was attached to the diffuser inlet, and located along the

nozzle centerline with the tip of the probe extending just inside the plane of the nozzle exit. The probe was connected by a long tube to the collection system hardware located outside the vacuum test cell. The sampling system was operated remotely from the blockhouse. The probe line was vacuum-purged with a secondary vacuum source for 10 s to make certain that representative gas was in the line at the time the sample was collected. The sample was analyzed within 4 to 8 hours after the test.

The analysis procedure involved two steps. First, all gases, including hydrogen and nitrogen, were pumped off from the sample cylinder using a Toepler pump through a series of two liquid nitrogen cold traps held at 78 K (-319°F). The sample cylinder was heated during pumping to drive out all condensables, such as water, hydrazine, and ammonia. The gas not frozen in the cold traps were measured manometrically and analyzed with a mass spectrometer. The cold traps were then warmed to 243 K (-22°F) in an acetone bath and the condensable gas residue from the Toepler pumping system was drawn off and collected. This gas was also measured manometrically and analyzed with the mass spectrometer. Typically, the condensables assay more than 99% ammonia. Any liquid hydrazine present in the sample was caught in the first cold trap and was detected with a colorimetric technique using 2, 4, 6-trinitrobenzenesulfonic acid.

The results of the exhaust gas sample assays are summarized in Table 31. Only the main constituents are listed in the gas composition column; the argon, oxygen, methane, and water vapor detected normally added to less than 1% of the total, and are therefore not given in the table. The gas probe pressure given is representative of

Table 31. Exhaust gas sample assay

Test No.	Sample time, s	Gas probe pressure, kN/m ² (psia)	Sample volume ^a , 10 ⁻⁶ m ³	Composition ^b			H ₂ /NH ₃ mole fraction	NH ₃ dissociation, mole %
				N ₂ , %	H ₂ , %	NH ₃ , %		
1	70	20.27 (2.94)	97.71	31.9	51.8	15.9	3.26	68.5
1A	70	36.54 (5.30)	180.94	29.7	51.9	17.7	2.93	66.5
2	15	34.20 (4.96)	175.24	31.2	50.0	18.7	2.67	64.0
3	35	34.41 (4.99)	169.12	31.3	50.5	18.0	2.81	65.5
4	44	33.30 (4.83)	165.51	30.3	51.3	18.3	2.80	65.5
5	735	26.55 (3.85)	133.22	32.1	50.0	16.9	2.96	66.5
6	255	24.34 (3.53)	111.66	29.6	50.2	20.0	2.59	62.5
7	170	23.10 (3.35)	111.97	31.0	51.7	17.1	3.02	66.7
8	9	20.13 (2.92)	104.79	30.7	53.1	15.9	3.34	68.5
9 ^c	145	21.86 (3.17)	104.83	31.5	51.6	16.7	3.09	67.0

^aManometric measurements accurate to $\pm 0.25\%$.

^bMass spectrometric analysis accurate to $\pm 1.0\%$ in range of 10 to 100%.

^c11 μ g of unreacted hydrazine were detected on test No. 9 only.

the final pressure within the sample cylinder. Leakage is detected as air (oxygen) contamination of the sample; none was found in the ten samples analyzed. The mole percent of nitrogen present in the exhaust is slightly greater than the theoretical decomposition of hydrazine would predict. This was caused by nitrogen saturation of the hydrazine by the nitrogen pressurant in the hydrazine tank. Since this is a variable quantity, and not easily predicted, the mole percent of ammonia dissociation was determined from the mole fraction ratio of hydrogen to ammonia. No correction was made for the small amount of ammonia initially present in the liquid hydrazine (Table 26). Ammonia dissociation values for all tests range between 62.5 and 68.5% with no recognizable trend, either up or down. Because the samples were taken at different times in the engine heating cycle, and under varying engine operating conditions, the results are constant within acceptable limits of accuracy. The theoretical characteristic exhaust velocities associated with this range of ammonia dissociation are 1388 m/s (4290 ft/s) to 1295 m/s (4250 ft/s), which is comparable to the experimental results reported in Fig. 51 in Subsection IV-D-1.

5. Pyrotechnic valve shock loading. The shock loading imparted to the demonstration system in the metric frame structure by pyrovalve actuations was measured with accelerometers and strain gages. The pyrovalve motion occurs in the X-Y plane, parallel to the base mounting plate and perpendicular to the Z axis or engine centerline. The pyrovalve assembly has been generally called the pyrovalve manifold in previous sections of this report; the three parts of this assembly (valves, tubing manifold, and pentagon-shaped support structure to which the valves are bolted) will be treated separately in the following discussion. The locations of the six accelerometers and six strain gauges are identified in the photograph of the lower half of the test system (Fig. 61) and are summarized as follows:

Accelerometers

- A1, on the side of the pyrovalve support structure, axis parallel to the X-Y plane
- A2, on the lower end of the pyrovalve support structure, axis perpendicular to the X-Y plane.
- A3, on the pyrovalve manifold outlet tubing, axis parallel to the X-Y plane.
- A4, on the P_c transducer mounting bracket, axis perpendicular to the X-Y plane
- A5, on the lower side of the base mounting plate, axis perpendicular to the X-Y plane.

- A6, on the side of the gimbal actuator mounting bracket, axis parallel to the X-Y plane.

Strain Gauges

- E1, on the side of the pyrovalve support structure, aligned perpendicular to the X-Y plane.
- E2, on the body of pyrovalve NC 1, aligned parallel to the X-Y plane.
- E3, on the pyrovalve manifold outlet tubing, aligned parallel to the central axis of the tube in the X-Y plane.
- E4, on the side of the pyrovalve support structure, aligned parallel to the X-Y plane.
- E5, on the lower half of the base mounting plate, aligned parallel to the X-Y plane.
- E6, on the gimbal actuator linkage rod, aligned parallel to the X-Y plane.

Pyrovalve actuations produced no structural anomalies; there were no adverse effects noted in any of the mechanical, hydraulic, electrical, or instrumentation components or assemblies. The shock accelerations measured directly on the pyrovalve support structure were moderately severe. The maximum level recorded by A1 was $\pm 56 \text{ km/s}^2$ (5700 g). The maximum shock acceleration measured on the base mounting plate by A5 was $\pm 9.6 \text{ km/s}^2$ (980 g).

Shock data were recorded on an analog FM tape, which was later digitized for input to a JPL digital computer program that computes various representations of structural response to shock. The graphs in Fig. 62 are typical digitized shock acceleration versus time plots for accelerometers A1, A3, and A5 recorded during the actuation of pyrovalve NO 2 following engine firing No. 3. The peak acceleration at the shock source measured by A1 was $\pm 36.3 \text{ km/s}^2$ (3700 g). Shock pulse risetime to peak level was 0.5 ms with a total pulse duration of 3.0 ms. The rapid decay in shock amplitude is indicative of a rigid structure. A more elastic response was measured by A3, where the peak acceleration was reduced to $\pm 28.4 \text{ km/s}^2$ (2900 g); however, the response lasted longer, having a duration of 22 ms. The response to the same shock pulse recorded at A5, on the base plate, was further reduced to a peak acceleration of $\pm 5.5 \text{ km/s}^2$ (560 g), which fell below $\pm 0.98 \text{ km/s}^2$ (100 g) in 8 ms and $\pm 0.49 \text{ km/s}^2$ (50 g) at 22 ms. The response died out at 42 ms.

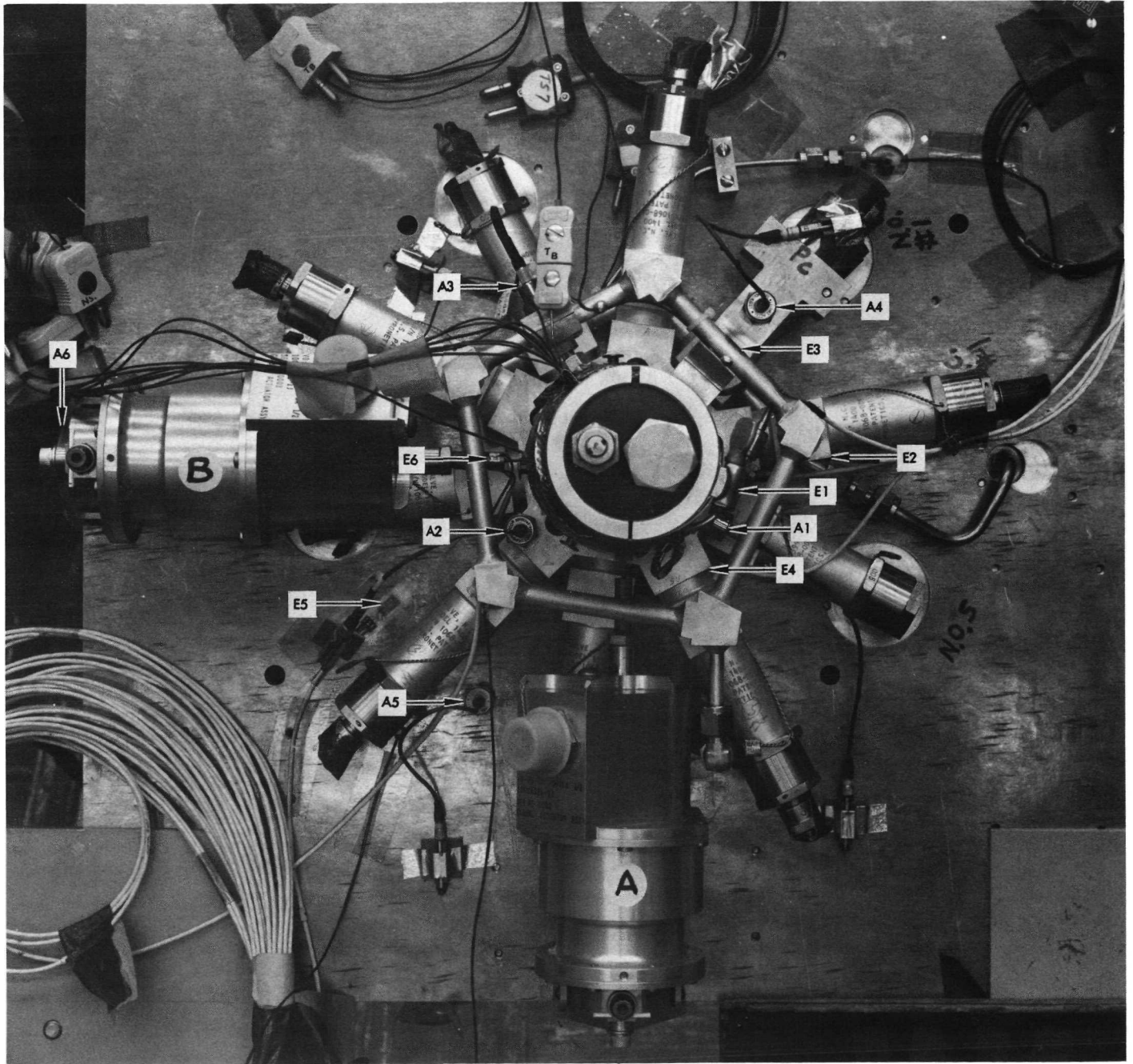


Fig. 61. Accelerometer and strain gauge locations

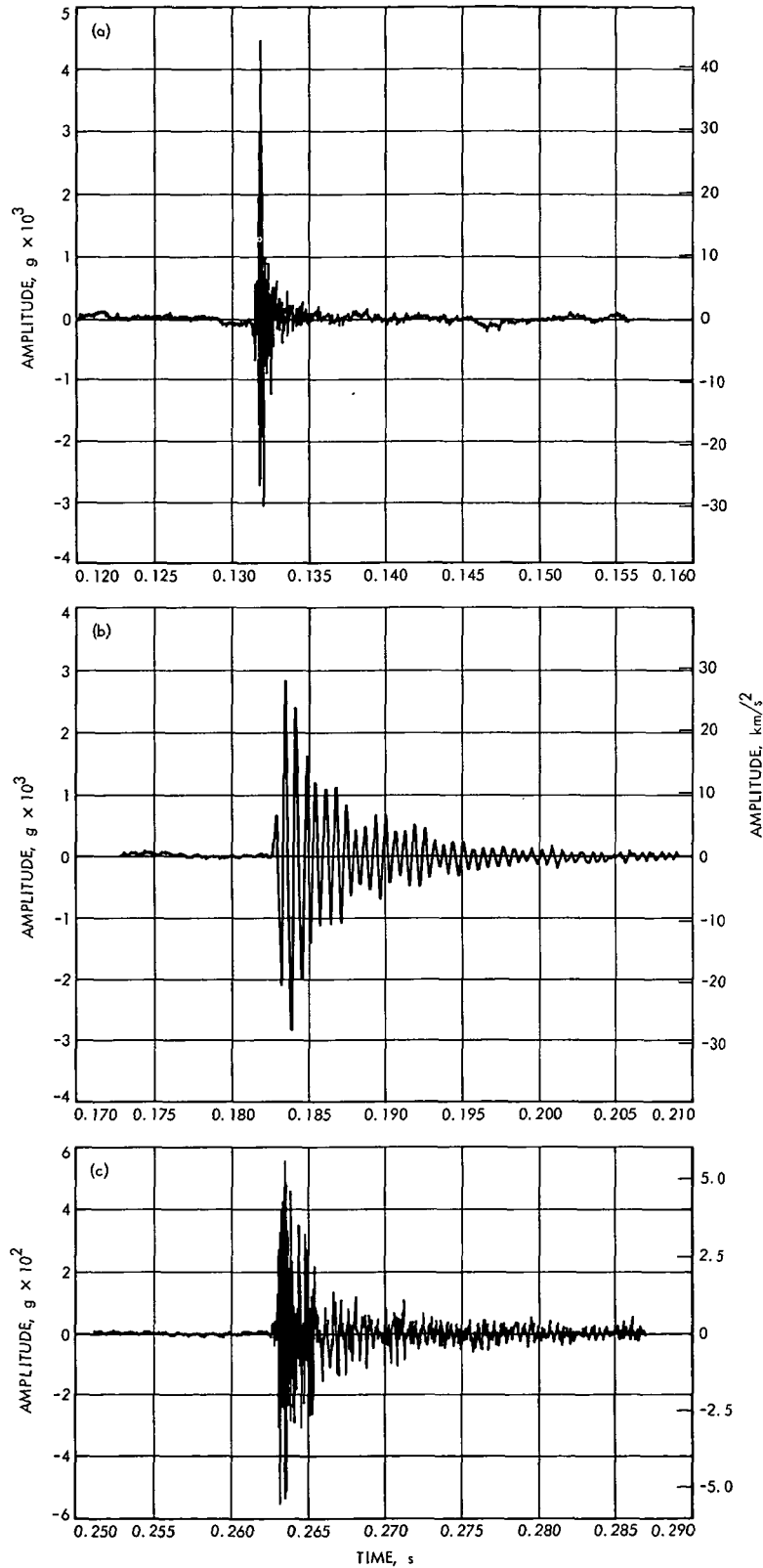


Fig. 62. Acceleration responses to pyrovalve actuation shock: (a) support structure, (b) manifold, (c) base mounting plate

The attenuation in peak acceleration as measured by A1 down to A5 is the result of shock transference through the hard attachment of the pyrovalve support structure to the base mounting plate. A greater degree of attenuation could be achieved through shock isolation mounting, such as the Lord mount assembly, which provides an elastic cushion to absorb most of the shock loading.

Shock-frequency spectrums for all accelerometer recordings were determined using a computer program that modeled the test assembly as a damped spring-loaded mass with a Q value of 20. This analysis was

limited to a frequency of 10,000 Hz by the data recording system. Composite plots were made of the peak shock response versus frequency for all pyrovalve actuations at each accelerometer location. Typical examples of these composite plots for A1, A3, and A5 are shown in Fig. 63(a), (b), and (c). Accelerometer A1 had an increasing response peak from around 0.98 km/s^2 (100 g) at 10 Hz up to 98.1 km/s^2 (10,000 g) at 10,000 Hz. A few random spikes occur between 100 and 1000 Hz. Similarly, A3 had an increasing response ranging from around 0.49 km/s^2 (50 g) at 10 Hz to 39.2 km/s^2 (4000 g) at 10,000 Hz. Two peak resonance points for A3 are 2.9

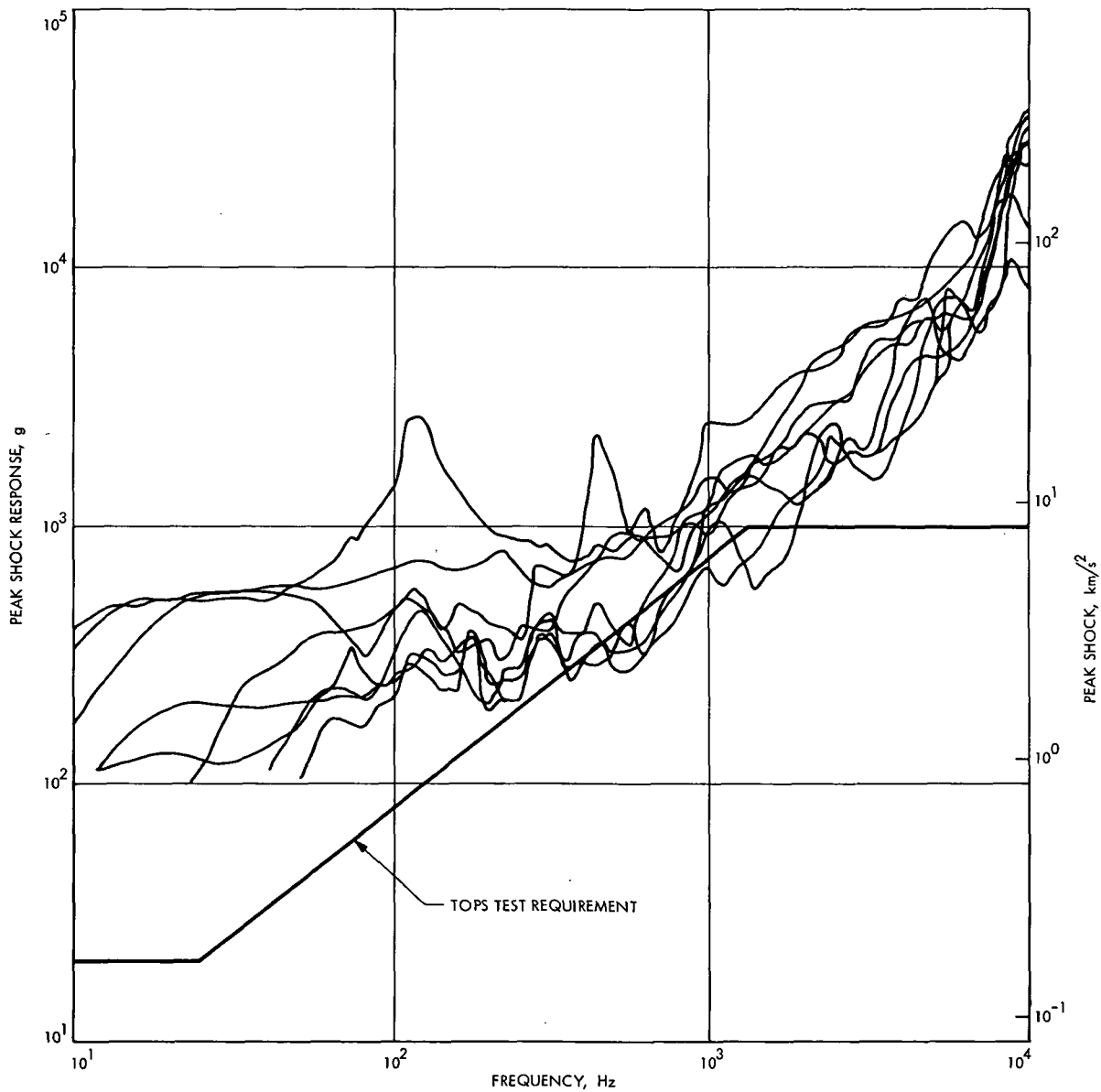


Fig. 63(a). Peak shock response versus frequency for accelerometer A1, test Nos. 1 to 8

km/s² (300 g) at 125 Hz and 196 km/s² (20,000 g) at 1500 Hz. The shock spectrum for A5 starts at 0.1 km/s² (10 g) at 10 Hz, increases to 2 km/s² (200 g) at 1000 Hz and continues to increase up to 58.8 km/s² (6000 g) at 10,000 Hz. A resonant peak of about 9.8 km/s² (1000 g) is located at 2000 Hz.

mounted on the pyrovalve manifold and support structure, which are designed to withstand high shock loads and are exempted from the assembly-level requirement. The peak accelerations recorded at A5 are mostly below the specified levels up to a frequency just above 1000 Hz where the requirement becomes constant, whereas the recorded accelerations continue to increase with higher frequencies. The addition of shock isolation mounting between the pyrovalve support structure and a more rigid base plate would readily eliminate the high-frequency peak accelerations and lower the low-frequency response sufficiently to meet the spacecraft design and test requirement. The other alternative is to change the requirement.

The experimental shock spectra just presented exceed the TOPS pyrotechnic shock test requirement (Ref. 11) which is shown as the heavy line on each plot. Both A1 and A3 responses exceed the requirement over the entire frequency range; however, these accelerometers are

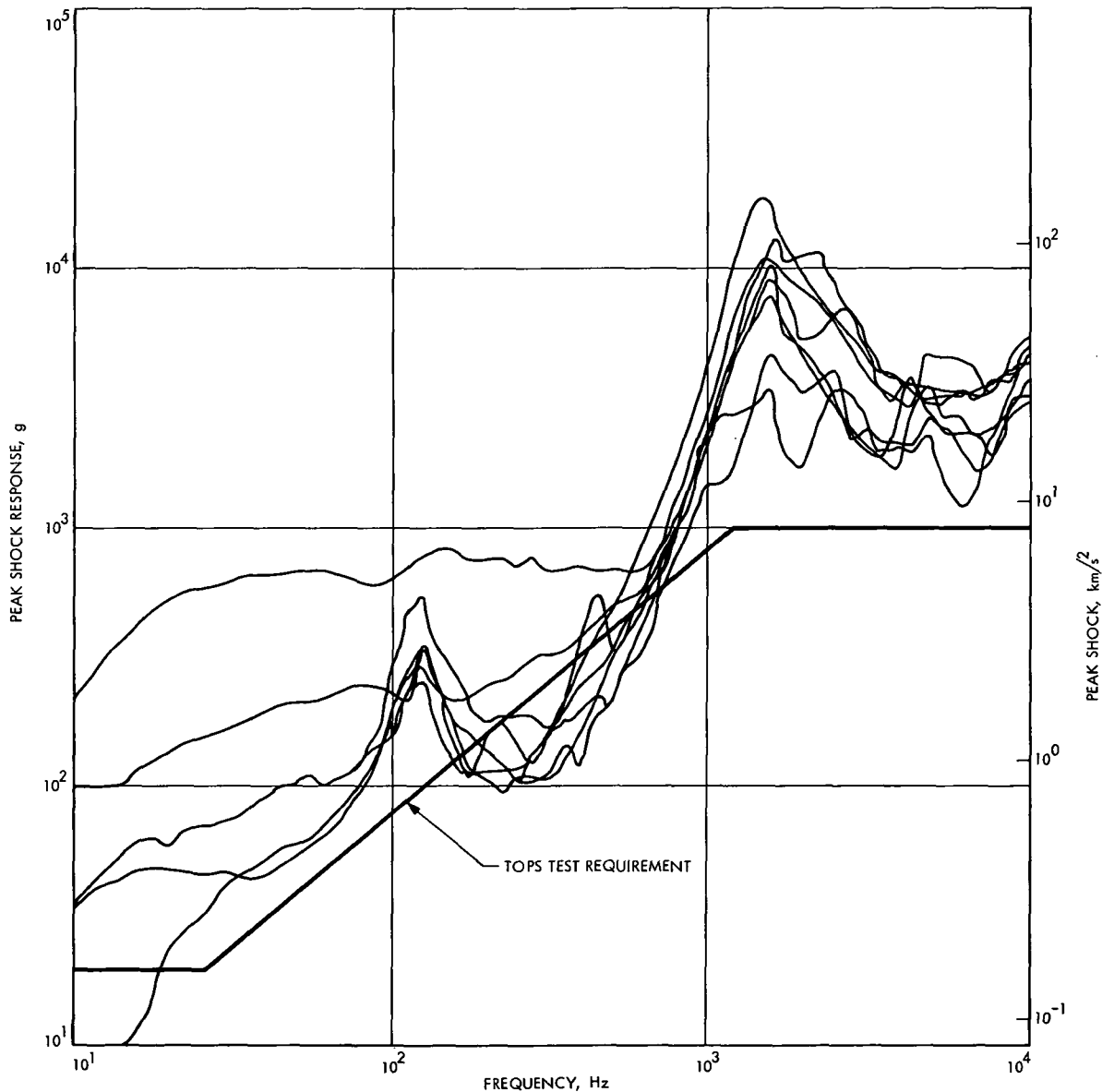


Fig. 63(b). Peak shock response versus frequency for accelerometer A3, test Nos. 1 to 8

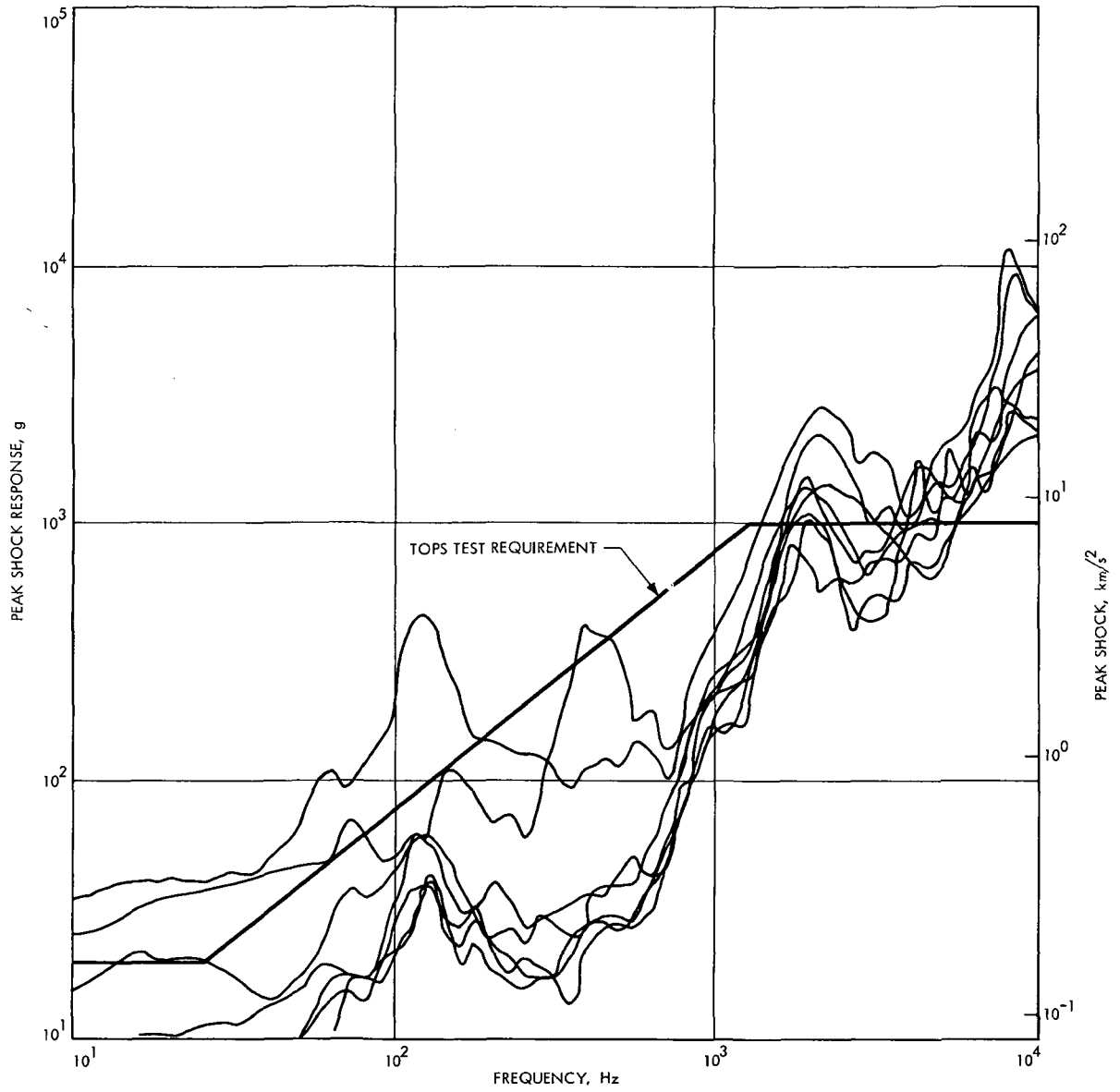


Fig. 63(c). Peak shock response versus frequency for accelerometer A5, test Nos. 1 to 8

A new higher requirement could be applied to the TCPS with the old requirement applying to the remainder of the spacecraft, or the requirement could be increased for all spacecraft subsystems. This conflict cannot be resolved until final spacecraft design and test requirements are developed.

The shock energy density spectra for all accelerometer recordings were determined from the standard Fourier Transform analysis. Plots of peak energy response versus frequency, and the integrated total energy value for the analyzed pulse time width were produced. Typical shock energy spectra are presented in Figs. 64(a), (b), and (c) for the A1, A3, and A5 response to the same pyrovalve event, NO 2, discussed earlier. The response of A1 peaked at 60 and 10,000 Hz. The total energy level was around $0.31 \text{ km}^2/\text{s}^3$ ($3200 \text{ g}^2\text{-s}$). A3 also showed two very well-defined energy peaks, a lesser one at 120 Hz and a much higher one at 1500 Hz. The total shock energy calculated for this location was $0.77 \text{ km}^2/\text{s}^3$ ($8046 \text{ g}^2\text{-s}$). The

energy at this location is quite high because of a major resonance. The strength of this resonance is probably increased over its natural value by the presence of the accelerometer mounting block added for the measurement. The energy density spectrum for A5 has prominent peaks at 120, 200, and 10,000 Hz and shows evidence of high-frequency resonance between 2000 and 10,000 Hz. The total shock energy was reduced to $0.016 \text{ km}^2/\text{s}^3$ ($170 \text{ g}^2\text{-s}$) at this location.

The results of accelerometer measurements at other test locations can be summarized as follows: A2 was very similar to A1 in response but at about one third the acceleration levels. A6 was also similar to A5 with comparable acceleration levels. Finally, the shock accelerations recorded by A4 were so low that they were barely discernible above the background noise levels of the high-range transducers used. A summary of peak accelerations and total energies of all accelerometer measurements is given in Table 32.

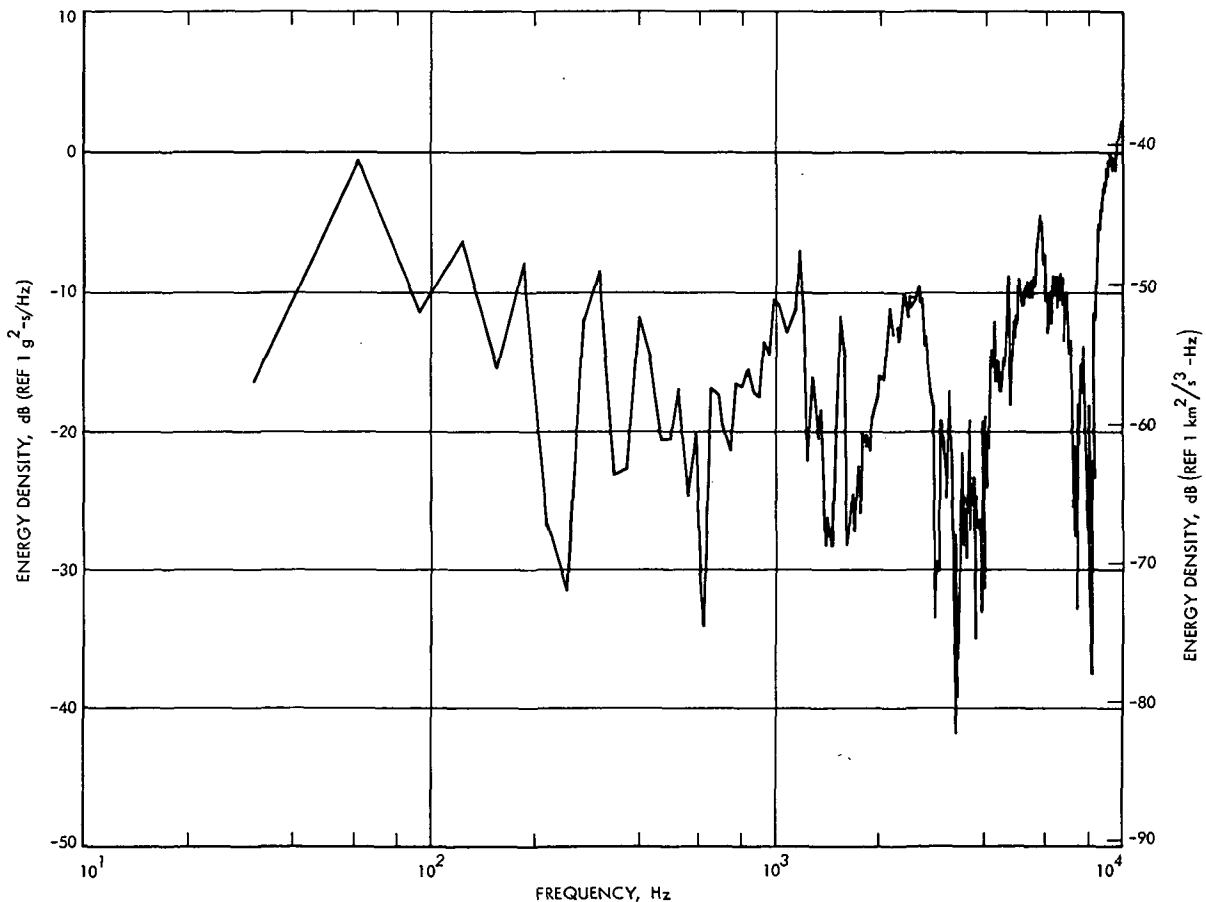


Fig. 64(a). Energy density spectrum for acceleration response of pyrovalve support structure

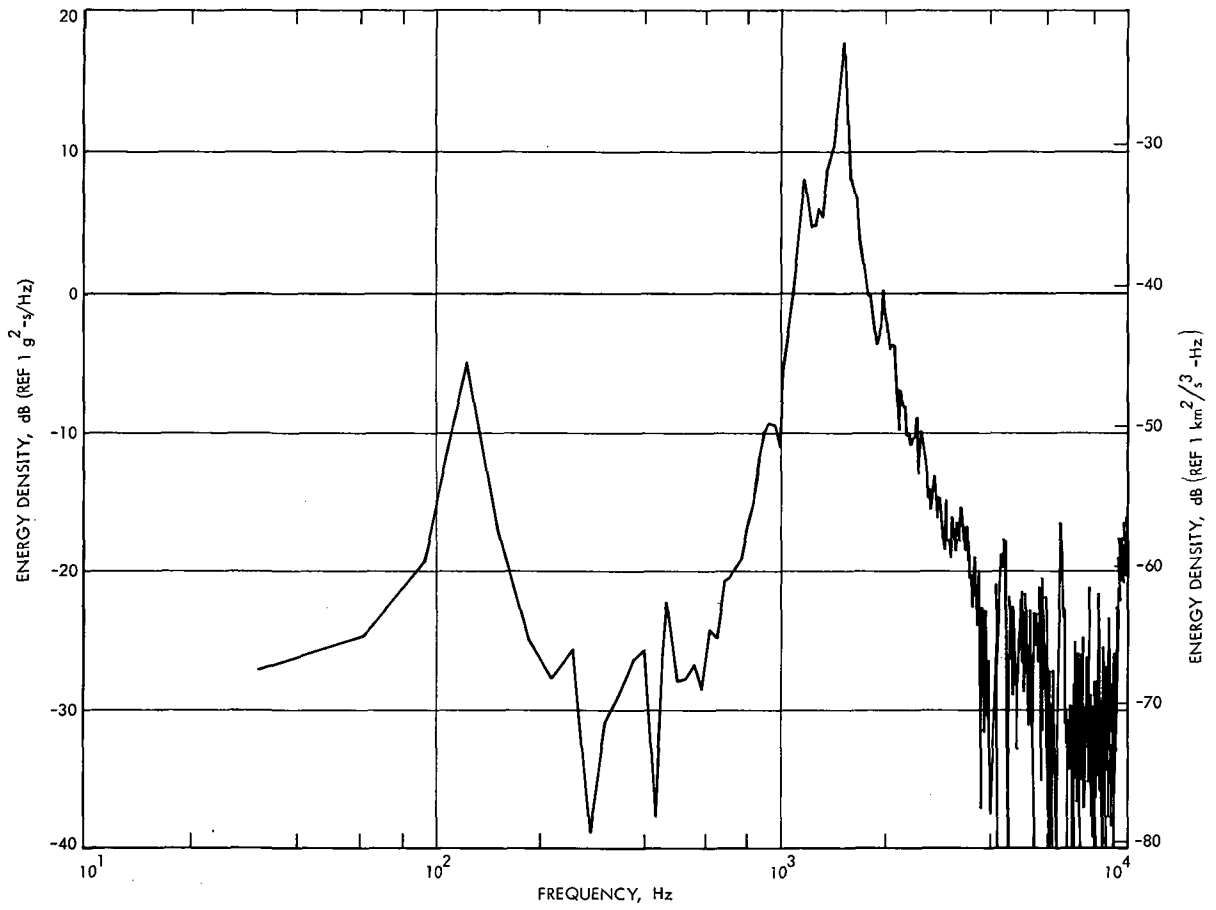


Fig. 64(b). Energy density spectrum for acceleration response of pyrovalve manifold

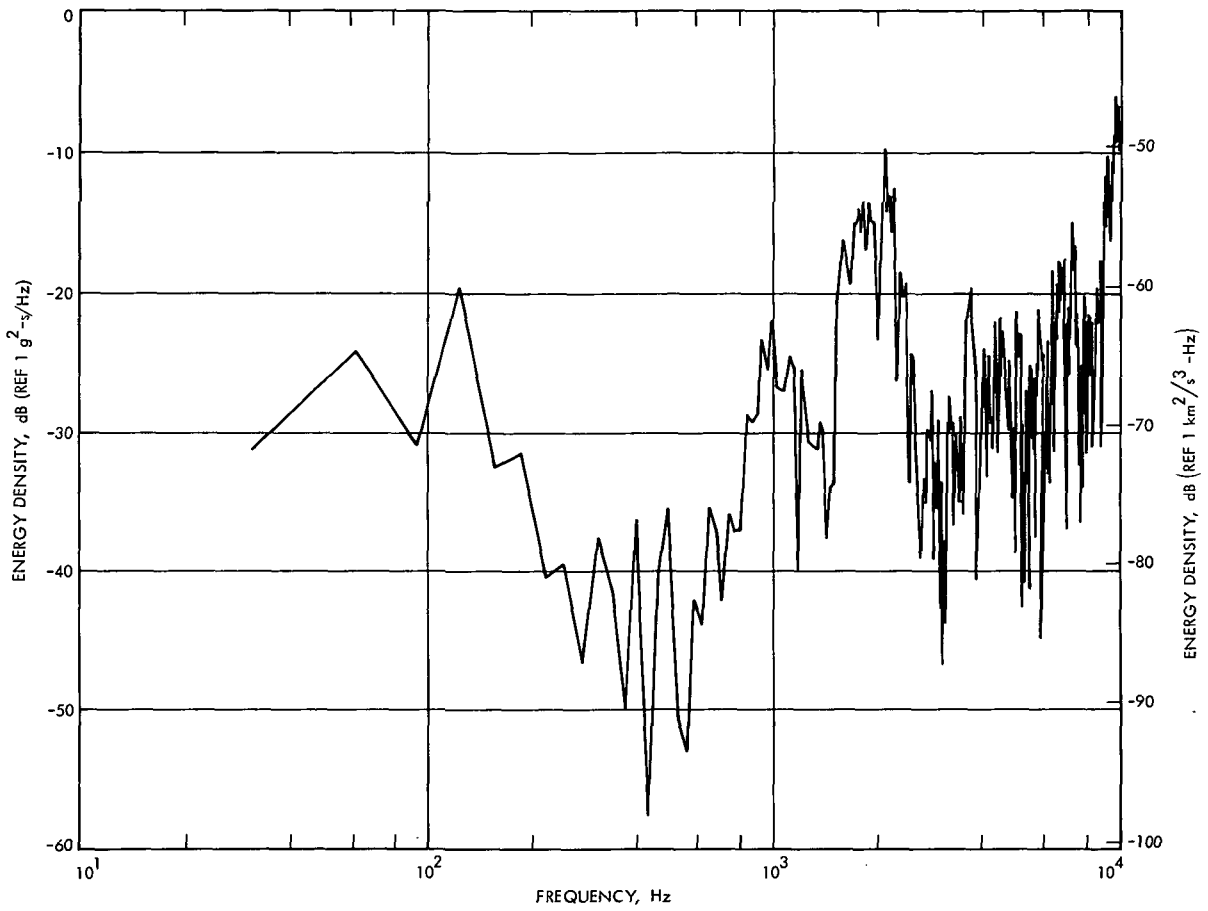


Fig. 64(c). Energy density spectrum for acceleration response of base mounting plate

Table 32. Summary of acceleration response to pyrovalve actuation shock

Accelerometers (locations given in text)	Pyrotechnic valve numbers									
	NC 1	NO 1	NC 2	NO 2	NC 3	NO 3	NC 4	NO 4	NC 5	NO 5
A1										
Peak acceleration, km/s ² (g)	±15.7 (1600)	±34.3 (3500)	NA	±36.3 (3700)	±37.3 (3800)	±34.3 (3500)	±49.0 (5000)	±55.9 (5700)	±53.9 (5500)	NU
Total energy, km ² /s ³ (g ² -s)	0.39 (4066)	0.42 (4351)	NA	0.31 (3198)	0.28 (2703)	0.27 (2834)	0.42 (4369)	0.47 (4904)	0.48 (4945)	NU
A2										
Peak acceleration, km/s ² (g)	±5.5 (560)	±11.3 (1150)	NA	±12.7 (1300)	±11.8 (1200)	±11.8 (1200)	±13.7 (1400)	±16.7 (1700)	±19.6 (2000)	NU
Total energy, km ² /s ³ (g ² -s)	0.032 (332)	0.043 (445)	NA	0.062 (640)	0.048 (494)	0.078 (810)	0.087 (904)	0.11 (1164)	0.037 (382)	NU
A3										
Peak acceleration, km/s ² (g)	±25.5 (2600)	±13.5 (1380)	NA	±28.4 (2900)	±19.6 (2000)	±15.5 (1580)	±22.1 (2250)	±11.2 (1140)	±11.3 (1150)	NU
Total energy, km ² /s ³ (g ² -s)	0.42 (4413)	0.22 (2264)	NA	0.77 (8046)	0.26 (2681)	0.15 (1575)	0.30 (3094)	0.069 (713)	0.066 (688)	NU
A4										
Peak acceleration, km/s ² (g)	NMR	NMR	NA	±0.2 (24)	±0.2 (20)	±0.2 (20)	±0.2 (17)	±0.2 (22)	±0.2 (18)	NU
Total energy, km ² /s ³ (g ² -s)	NMR	NMR	NA	9.6 × 10 ⁻⁵ (1)	NU					
A5										
Peak acceleration, km/s ² (g)	±4.5 (460)	±7.8 (800)	NA	±5.5 (560)	±6.7 (680)	±9.6 (980)	±4.5 (460)	±8.4 (860)	±2.4 (240)	NU
Total energy, km ² /s ³ (g ² -s)	0.016 (164)	0.029 (297)	NA	0.016 (170)	0.018 (186)	0.042 (432)	0.012 (126)	0.029 (304)	0.0087 (90)	NU
A6										
Peak acceleration, km/s ² (g)	±5.1 (520)	±5.4 (550)	NA	±4.0 (410)	±3.8 (390)	±5.2 (530)	±4.7 (480)	±4.9 (500)	±4.3 (440)	NU
Total energy, km ² /s ³ (g ² -s)	0.021 (217)	0.025 (256)	NA	0.0094 (98)	0.0086 (89)	0.014 (143)	0.012 (129)	0.011 (116)	0.0088 (91)	NU

NMR = no measurable results; NA = not available; NU = not used; NO = normally open; NC = normally closed

The strain gauge locations were selected primarily to provide backup information for the accelerometers and not because the structures were subject to high strains. Most strain gauges were mounted adjacent to accelerometers or at corresponding locations on identical parts. As a result, the measured strains were quite low, none exceeding $\pm 700 \mu\text{m}/\text{m}$ ($700 \mu\text{in.}/\text{in.}$). The pulse shapes were basically comparable to accelerometer responses.

Typical digitized shock strain responses for E4, E3, and E5 recorded during the pyrovalve NO 2 actuation on test No. 3 are shown in Figs. 65(a), (b), and (c). Strain gauge E4 was mounted close to accelerometer A1 and aligned along the same axis. At this point, close to the shock source, a maximum strain of $\pm 250 \mu\text{m}/\text{m}$ was recorded with a pulse duration around 10 ms. E3 was located on a pyrovalve manifold outlet tube section similar to the A3 accelerometer, but without the addition of a mounting block; it recorded a maximum strain of about $\pm 700 \mu\text{m}/\text{m}$ over a pulse duration of 15 ms. The response of E3 appears to be more damped than A3 due to a smaller mass involved in the instrumentation sensing device. E5, like A5, shows a lower shock loading level with a peak strain of $\pm 100 \mu\text{m}/\text{m}$, which quickly decays to below $\pm 30 \mu\text{m}/\text{m}$. The pulse duration continues out to 30 ms, the limit of this plot.

Strain energy density spectra and total strain energies were computed from all strain gauge recordings. Typical plots of strain energy versus frequency for E4, E3, and E5 from the actuation of pyrovalve NO 2 on test No. 3 are shown in Figs. 66(a), (b), and (c). The peak strain energy for E4 occurs at 1200 Hz and the total energy was $36 (\mu\text{m}/\text{m})^2\text{-s}$. For E3, the peak strain energy is at 1500 Hz and the total energy was $289 (\mu\text{m}/\text{m})^2\text{-s}$. There are three peaks of strain energy for E5, approximately located at 150, 350, and 1800 Hz. The total energy at E5 was only $10 (\mu\text{m}/\text{m})^2\text{-s}$. The decrease in energy shows the degree of attenuation of the shock with increasing distance from the source at E4. E3 shows a gain in total energy over E4 because of the more elastic response resulting in resonance in the tube structure. A summary of the peak strains and total strain energies calculated for all strain gauges are presented in Table 33.

The actuation of the pyrovalves produced two types of hydraulic shock or surges in the propellant delivery system. The first one occurred during the priming of the evacuated solenoid valve manifold when the first normally closed pyrovalve (NC 1) was opened and the hydrazine surged into the void spaces in the tubing, solenoid

valve bodies, pressure transducer cavities and, in this test configuration, the bellows accumulator. The $2494 \text{ kN}/\text{m}^2$ (357 psia) tank pressure provided a driving force which could have produced a high-intensity hydraulic shock (hydraulic hammer effect) were it not cushioned by elastic compression within the bellows accumulator. The maximum pressure surge measured by the PFH pressure transducer in the solenoid valve manifold was only $\pm 96.5 \text{ kN}/\text{m}^2$ ($\pm 14 \text{ psid}$) during this operation.

The second type of hydraulic shock occurs whenever a pyrovalve is activated to open or close the liquid-filled propellant line. The action of the valve ram cutting the tube causes a sudden change in line volume—a decrease with pyrovalve closing and an increase with pyrovalve opening. Both actions create a momentary high intensity pressure wave. The maximum hydraulic pressure shock measured on the downstream side of the pyrovalve by the PFH transducer was $\pm 358 \text{ kN}/\text{m}^2$ ($\pm 52 \text{ psid}$). A corresponding pressure surge measured on the upstream side of the pyrovalve manifold by the orifice flowmeter differential pressure transducer (DPFO) was only $\pm 13.8 \text{ kN}/\text{m}^2$ ($\pm 2 \text{ psid}$). On this side, the propellant system was cushioned by the tank volume.

Mechanical shocks transmitted to the six-axis thrust measuring system by the pyrovalve actuations were very mild. The highest surge force recorded by the axial (Z-axis) load cell was only $\pm 44.5 \text{ N}$ ($\pm 10 \text{ lbf}$).

6. Thrust vector control. Thrust vector control of the test system was demonstrated on three of the nine tests using a preprogrammed tape to input command signals to position the two gimbal actuators. The actuators were operated both singly and together using a series of four stepped input commands followed by a similar series of four continuously variable commands. A typical command signal program as used in test No. 5 is shown in Fig. 67. Beginning at 300 s after engine start, actuator B was signaled for both a positive and negative stepped command, followed by similar commands to actuator A, and then the same series of commands to both actuators simultaneously. The same sequence was repeated using the variable signal command. The complete program required 145 s as used in tests Nos. 5 and 6, but was shortened to 50 s on test No. 7 by using only the stepped portion of the command tape program.

Command signal voltage input ranged from 0 to $\pm 1.0 \text{ V}$. A positive voltage extended the actuator push rods and a negative voltage retracted them. Zero voltage

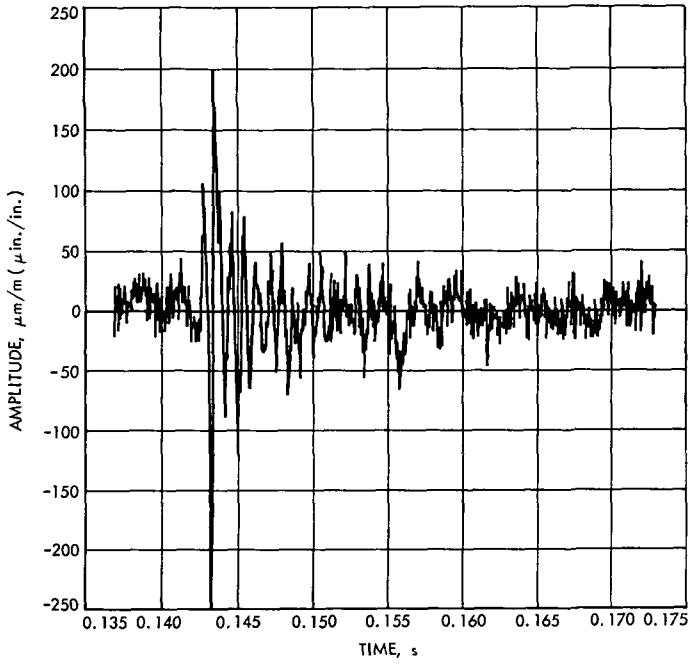


Fig. 65(a). Pyrovalve support structure strain response to actuation shock

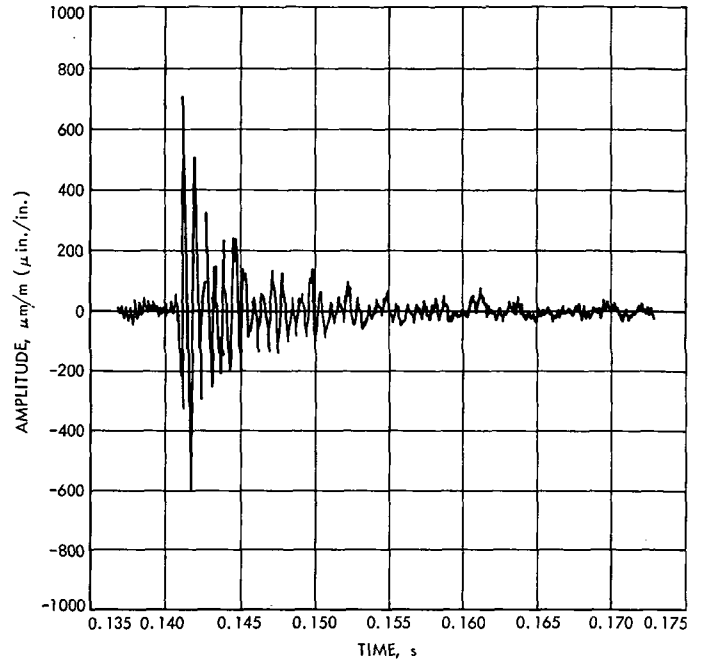


Fig. 65(b). Pyrovalve manifold strain to actuation shock

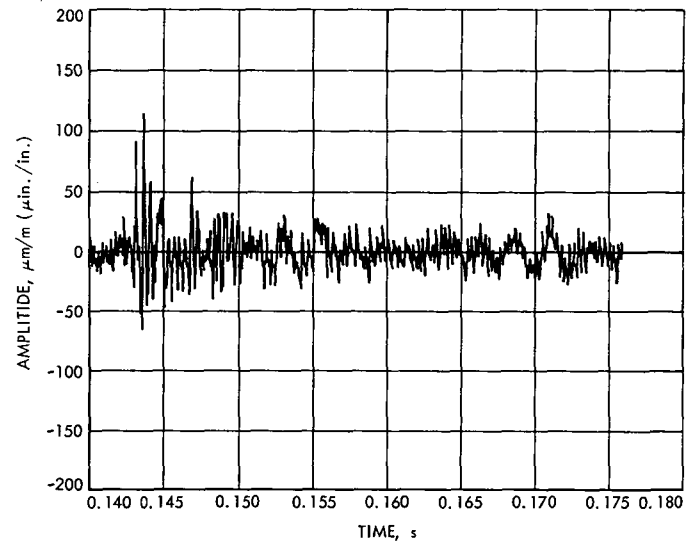


Fig. 65(c). Base mounting plate strain response to actuation shock

Table 33. Summary of strain response to pyrovalve actuation shock

Strain gauges (locations given in text)	Pyrovalve									
	NC 1	NO 1	NC 2	NO 2	NC 3	NO 3	NC 4	NO 4	NC 5	NO 5
	Peak strain, $\mu\text{m}/\text{m}$ (total energy, $(\mu\text{m}/\text{m})^2\text{-s}$)									
E1	± 180 (35)	± 520 (80)	NA NA	± 300 (44)	± 210 (32)	± 54 (10)	± 240 (25)	± 390 (59)	± 200 (23)	NU NU
E2	± 380 (106)	± 90 (13)	NA NA	± 100 (12)	± 30 (19)	± 40 (6)	± 56 (10)	± 84 (11)	± 95 (13)	NU NU
E3	± 480 (159)	± 370 (146)	NA NA	± 650 (289)	± 500 (135)	± 50 (11)	± 600 (149)	± 460 (122)	± 460 (108)	NU NU
E4	± 200 (36)	± 260 (35)	NA NA	± 220 (36)	± 80 (22)	± 270 (39)	± 220 (21)	± 150 (21)	± 300 (34)	NU NU
E5	± 60 (25)	± 100 (19)	NA NA	± 90 (10)	± 240 (63)	± 180 (21)	± 160 (15)	± 100 (12)	± 70 (7)	NU NU
E6	± 40 (20)	± 50 (13)	NA NA	± 70 (130)	± 110 (42)	± 46 (8)	± 48 (8)	± 60 (11)	± 45 (6)	NU NU

NMR = no measurable results; NA = not available; NU = not used; NO = normally open; NC = normally closed

to both actuators centered the engine on the axial or Z-axis perpendicular to the support plate. Actuator A controlled angular deflection along the yaw or X-axis and actuator B along the pitch or Y-axis. The retraction of an actuator push rod was designated as positive angular deflection and extension was negative angular deflection.

A summary of the results from the thrust vector control program performed on test No. 5 are presented in Table 34. The reference points are identified in the command signal versus time graph of Fig. 67. The location of the six-axis thrust measurement points are identified in the schematic of the thrust stand presented previously in Figs. 42 and 43 of Subsection IV-C-1. Only the maximum positive or negative values of angular deflection and thrust are listed in the table. Positive thrust in any axis was designated as compression on the load cell and conversely negative thrust was a tension load.

Reference points Nos. 1 and 14 were recorded with a zero command signal at the start and end of the thrust vector control program. The nonaxial thrust recorded at these times indicate that the center of thrust was not aligned with the center of mass for the test system. This was expected because no mass balancing was performed on the test system as installed in the thrust stand. The

nonaxial thrust measured on the upper and lower X and Y axes change in level and sign during thrust vector control tests as a function of the orientation of the thrust axis and the coupling moments established between the load lines and the center of mass of the test system. Roll forces were also recorded indicating a lack of symmetry about the thrust axis. Determination of the relationship between the center of mass and the center of thrust, which varied during testing as a function of hydrazine depletion, was not an objective of the test program.

The test objective of demonstrating a gimbaled thrust vector control assembly using flexural, instead of ball-swivel, joints to connect to the engine was met. Although limited to 5 deg deflection, increasing the inside radius of the pyrovalve support structure would easily allow a 10-deg deflection.

7. Performance prediction parameters. Three parameters having possible application to propulsion system modeling or impulse control were calculated from demonstration system test data. These parameters are theoretically constant over the steady-state portion of a rocket firing, and it is desirable to treat them as constants for the entire firing. Thus, the length and repeatability of the transient, and the constancy of the steady-state values of these parameters, define their utility as general constants.

Table 34. Summary of results from thrust vector control program for test No. 5

	Reference points (from Fig. 67)													
	1	2	3	4	5	6	7	8	9	10	11	12	13	14
	300	304	312	322	329	338	346	356	369	381	394	406	419	429
	Time, s													
	Angular deflection from Z-axis, deg													
A-actuator (X-axis)	0.01	0.03	0.00	-3.70	3.74	-3.67	4.02	0.06	0.02	-4.18	4.53	-2.81	2.97	0.01
B-actuator (Y-axis)	0.01	-3.85	3.91	0.02	0.01	-3.85	4.18	-4.38	4.44	0.16	.01	-2.84	2.99	0.01
	Thrust, N (lbf)													
F1, Z-axis, axial	86.11 (19.35)	85.66 (19.25)	85.17 (19.14)	84.68 (19.03)	85.40 (19.19)	83.35 (18.73)	84.24 (18.93)	83.62 (18.79)	83.70 (18.81)	83.53 (18.77)	83.17 (18.69)	83.13 (18.68)	82.64 (18.57)	81.92 (18.41)
F2, X-axis, upper	2.49 (0.56)	2.76 (0.62)	2.49 (0.56)	-0.40 (-0.09)	5.96 (1.34)	-0.18 (-0.04)	6.14 (1.38)	2.76 (0.62)	2.67 (0.60)	-0.67 (-0.15)	6.68 (1.50)	0.53 (0.12)	5.07 (1.14)	2.67 (0.60)
F3, X-axis, lower	-1.34 (-0.30)	-1.02 (-0.23)	-0.98 (-0.22)	-3.16 (-0.71)	1.78 (0.40)	-3.16 (-0.71)	2.14 (0.48)	-0.85 (-0.19)	-0.71 (-0.16)	-3.65 (-0.82)	2.54 (0.57)	-2.45 (-0.55)	1.16 (0.26)	-1.02 (-0.23)
F4, Y-axis, upper	0.62 (0.14)	-2.94 (-0.66)	4.58 (1.03)	0.80 (0.18)	0.72 (0.16)	-2.80 (-0.63)	4.54 (1.02)	-3.34 (-0.75)	5.16 (1.16)	0.80 (0.18)	0.67 (0.15)	-1.69 (-0.38)	3.47 (0.78)	0.58 (0.13)
F5, Y-axis, lower	-0.27 (-0.06)	-2.67 (-0.80)	3.16 (0.71)	-0.18 (-0.04)	-0.22 (-0.05)	-3.29 (-0.74)	3.56 (0.80)	-3.56 (-0.80)	3.78 (0.85)	-0.22 (-0.05)	-0.36 (-0.08)	-2.31 (-0.52)	2.09 (0.47)	-0.40 (-0.09)
F6, Z-axis, roll	0.53 (0.12)	0.31 (0.07)	2.31 (0.52)	-0.09 (-0.02)	0.68 (0.13)	-0.36 (-0.08)	0.71 (0.16)	1.25 (0.28)	0.04 (0.01)	-0.27 (-0.06)	0.67 (0.15)	-0.22 (-0.05)	0.36 (0.08)	0.13 (0.03)

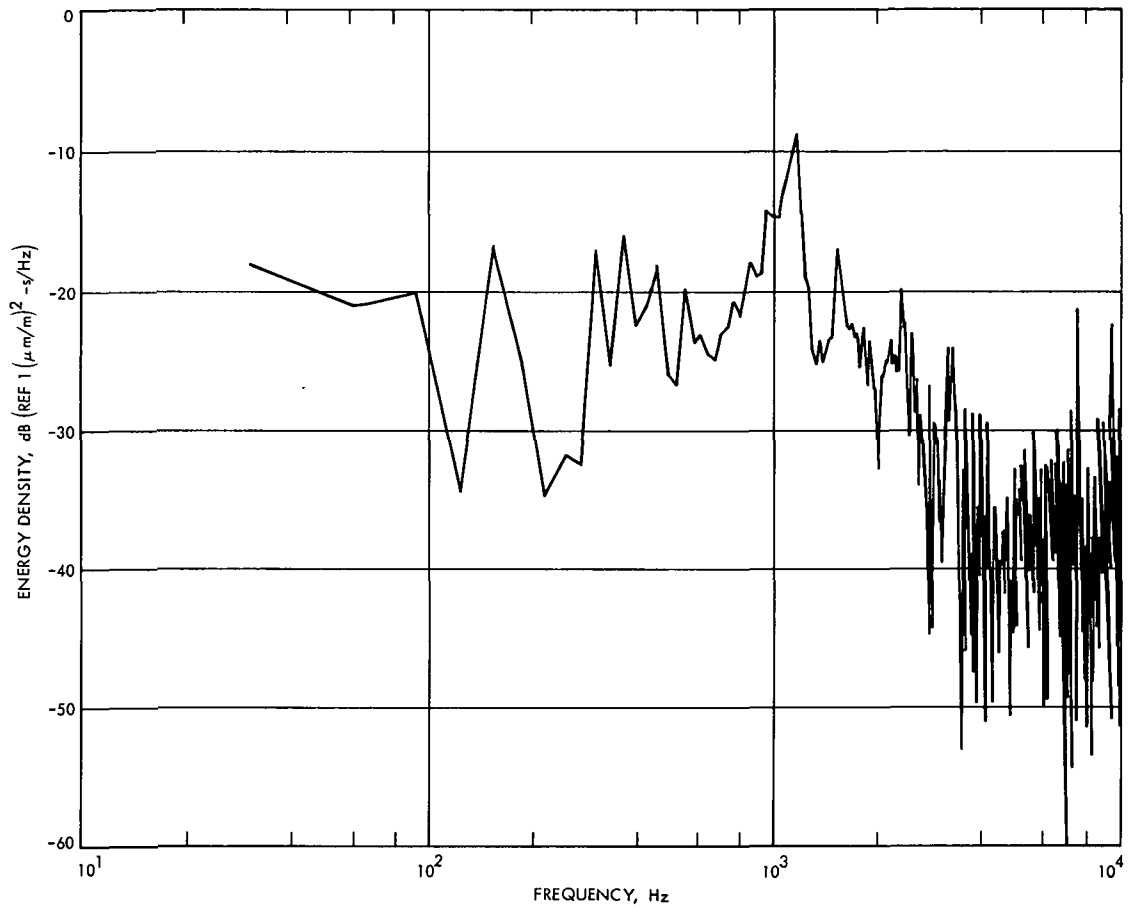


Fig. 66(a). Energy density spectrum for strain response of pyrovalve support structure

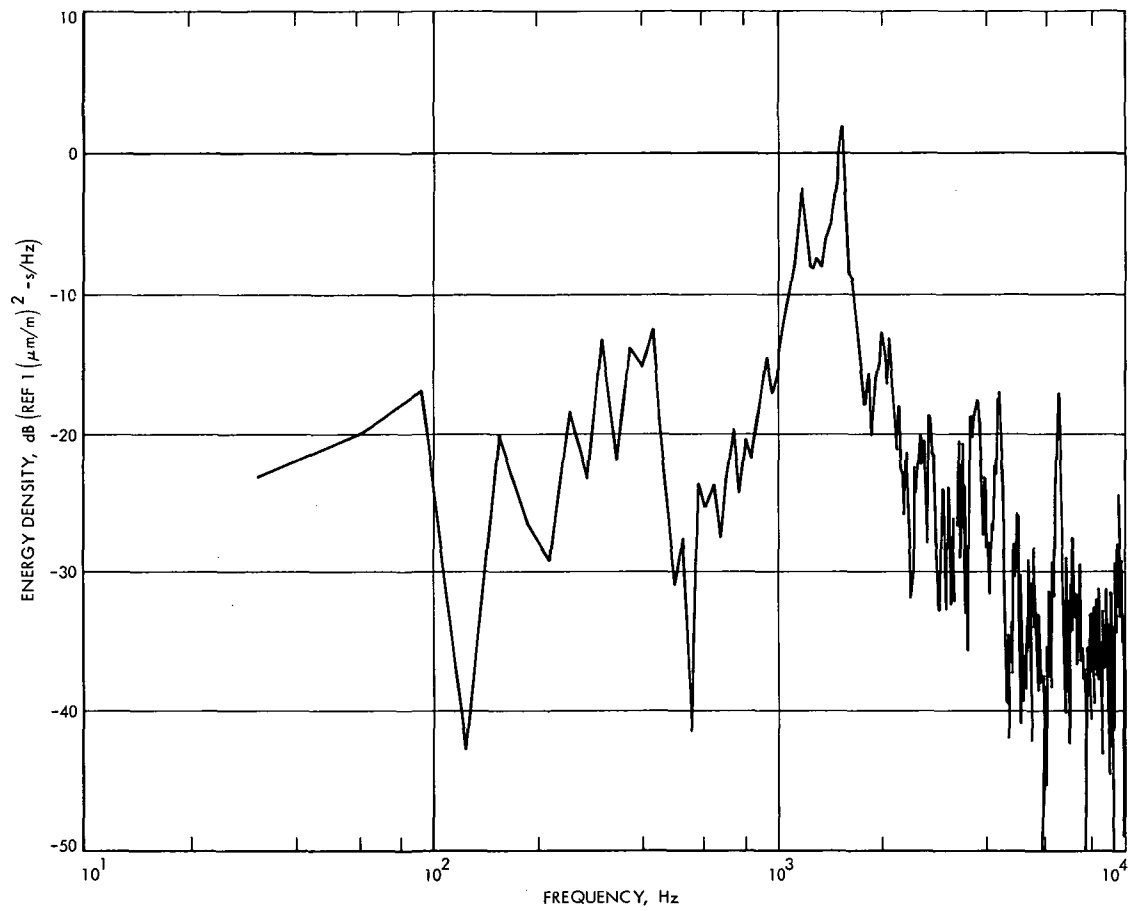


Fig. 66(b). Energy density spectrum for strain response of pyrovalve manifold

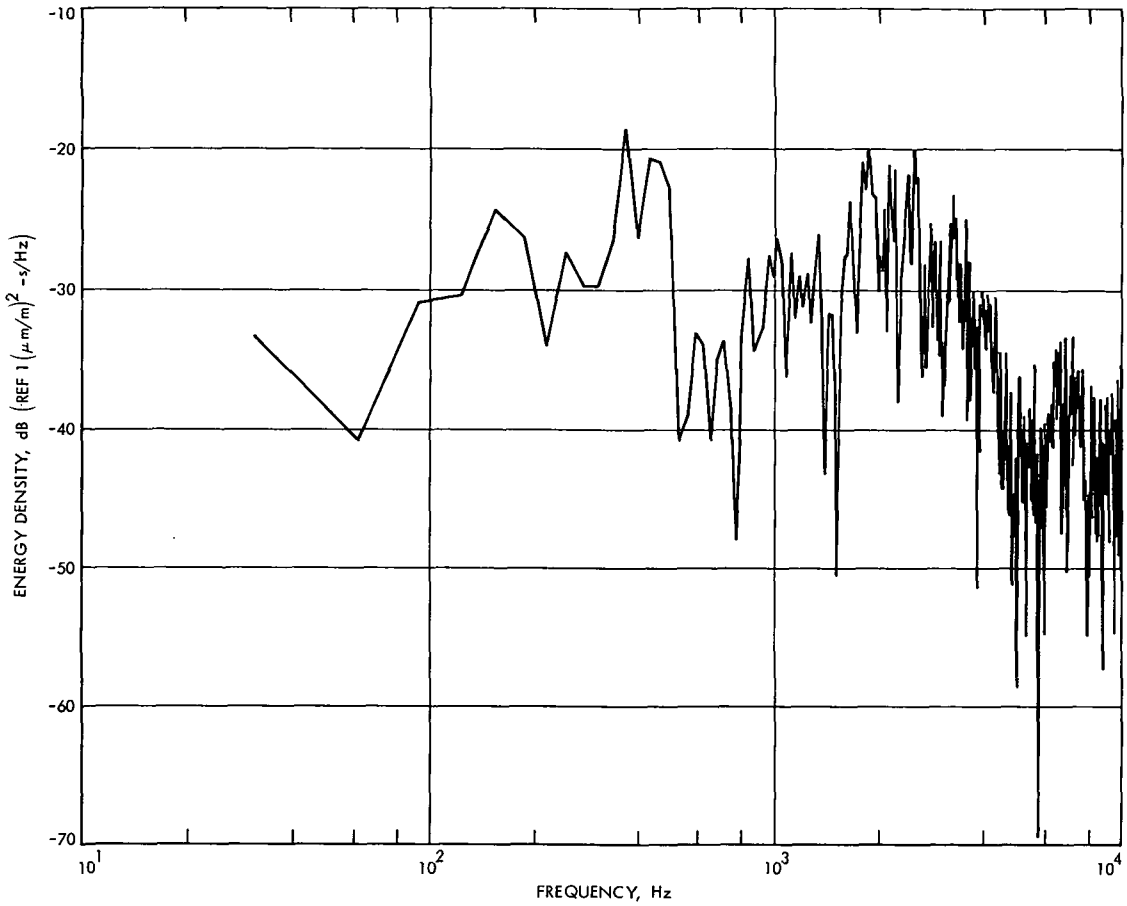


Fig. 66(c). Energy density spectrum for strain response of base mounting plate

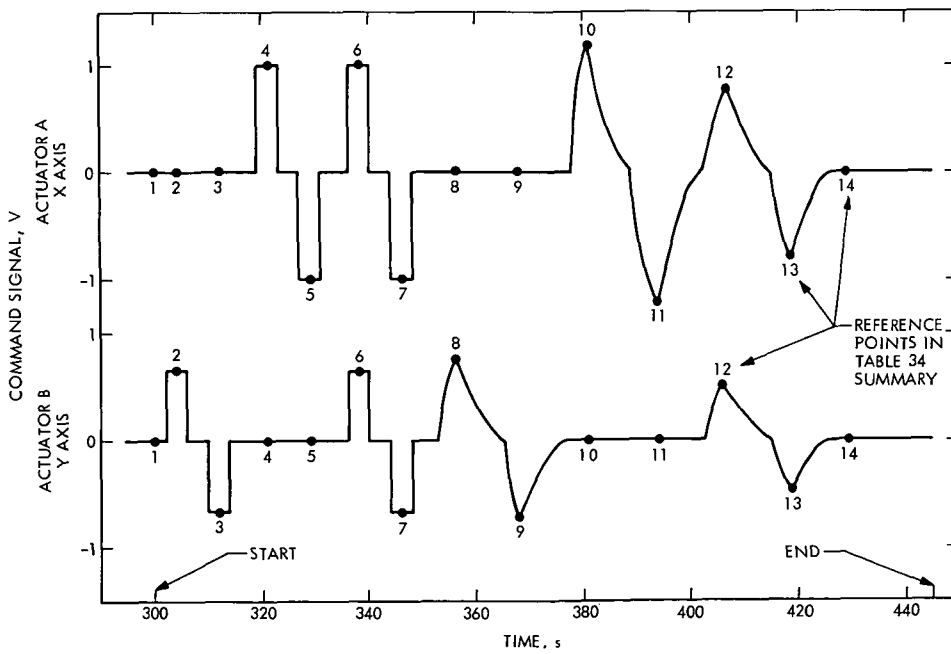


Fig. 67. Test No. 5 thrust vector control program command signal versus time

The parameters are the fluid resistance factor, R , the fuel mass flow rate constant, $K_{\dot{m}}$, and the thrust chamber pressure constant, K_{P_c} . The first parameter is used extensively in fluid flow modeling; for a given propellant tank pressure, it relates the pressure at a downstream point with the mass flow rate between the tank and that point. The use of this factor in a propulsion system model is illustrated in Ref. 44. The second and third parameters are constants in the proposed spacecraft impulse control mechanization that may be competitive with the often-used accelerometer. This application is described in more detail in Subsection V-E-2.

Consider the fluid resistance factor first. It is defined as

$$R = \frac{\rho \Delta P}{\dot{m}^2} \quad (1)$$

where ρ is the density, ΔP the pressure drop, and \dot{m} the mass flow rate of the fluid flowing between the points of interest. Since the density of a liquid is relatively constant, liquid resistance is primarily a function of ΔP and \dot{m}^2 ,

$$R_l = f\left(\frac{\Delta P}{\dot{m}^2}\right) \quad (2)$$

Since the density of a gas is a function of \dot{m} , gas resistance is primarily a function of ΔP and \dot{m} ,

$$R_g = f\left(\frac{\Delta P}{\dot{m}}\right) \quad (3)$$

Fluid resistance factors were calculated for both the liquid system, R_l , and the total system, R_t , using Eq. (1). The liquid system includes only the pressure loss from the tank to the engine solenoid valve manifold outlet ($\Delta P_t = PTN - PFJ$). Since the rocket engine was not equipped with an injector face pressure tap, the injector feed tube and injector passage pressure drops were not measured. The entire system pressure drop was treated as a liquid drop ($\Delta P_t = PTN - PC$), because the gas pressure drop through the catalytic bed could not be separately measured and was thought to be small. The factor R_t is thus a test of the significance of the bed pressure drop.

The calculated values of R_l and R_t for each test are plotted versus cumulative engine firing time in Fig. 68. The factor R_t is relatively constant with a nominal value of about 1.85×10^{11} N-s²/kg-m⁵ (200 lbf-s²/lbm-in.⁵) for both solenoid valve branches. Branch 1 was used for

tests Nos. 1 through 5, and Branch 2 was used for tests Nos. 6 through 9.⁹

The data for valve branch No. 1 varies $\pm 12\%$ from the nominal value. The variation for branch No. 2 is less. The range of hydrazine temperature was 276 to 293 K (37 to 68°F); the data scatter for R_t would probably be reduced if the results were normalized to a single reference temperature. The length of the transients for R_t increased from 0.1 to 0.9 s over the nine tests (Table 29). Thus, R_t can be considered constant over the full flow-rate range (Fig. 47) which is equivalent to a Reynolds No. range of 13,500 to 30,200 for the sharp edge orifice flowmeter.

The factor R_t increases from 5×10^{11} to 6.4×10^{11} N-s²/kg-m⁵ (520 to 690 lbf-s²/lbm-in.⁵) over the 1600 s of firing time (Fig. 68). The significance of the gas flow in the engine is illustrated by the spike transient and the changing magnitude of the R_t response. Thus, the gas effect cannot be neglected, and Eq. (3) must be used with Eq. (2) to accurately specify the total system flow resistance (Ref. 44 and Appendix A of Ref. 45).

Now consider the two prospective impulse control parameters. Steady-state impulse is directly proportional to either chamber pressure or mass flow rate, as explained in Subsection V-E-2. The utility of this concept depends on whether the constants of proportionality can be applied to the entire firing, both transient and steady state, with acceptable error. The mass flow-rate constant, $K_{\dot{m}}$, is defined as

$$K_{\dot{m}} = \frac{\int_0^t F_{vac} dt}{\int_0^t \sqrt{\Delta P} dt} \quad (4)$$

and the chamber pressure constant, K_{P_c} , is defined as

$$K_{P_c} = \frac{\int_0^t F_{vac} dt}{\int_0^t P_c dt} \quad (5)$$

where F_{vac} is vacuum thrust, ΔP is the orifice differential pressure, and P_c is thrust chamber pressure. If $K_{\dot{m}}$ and K_{P_c} are acceptably constant, then the numerically integrated output from either transducer can be used to signal engine shutdown on a specific value of total impulse.

⁹The results for test No. 9 are estimated because the PFJ measurement did not function properly during that test.

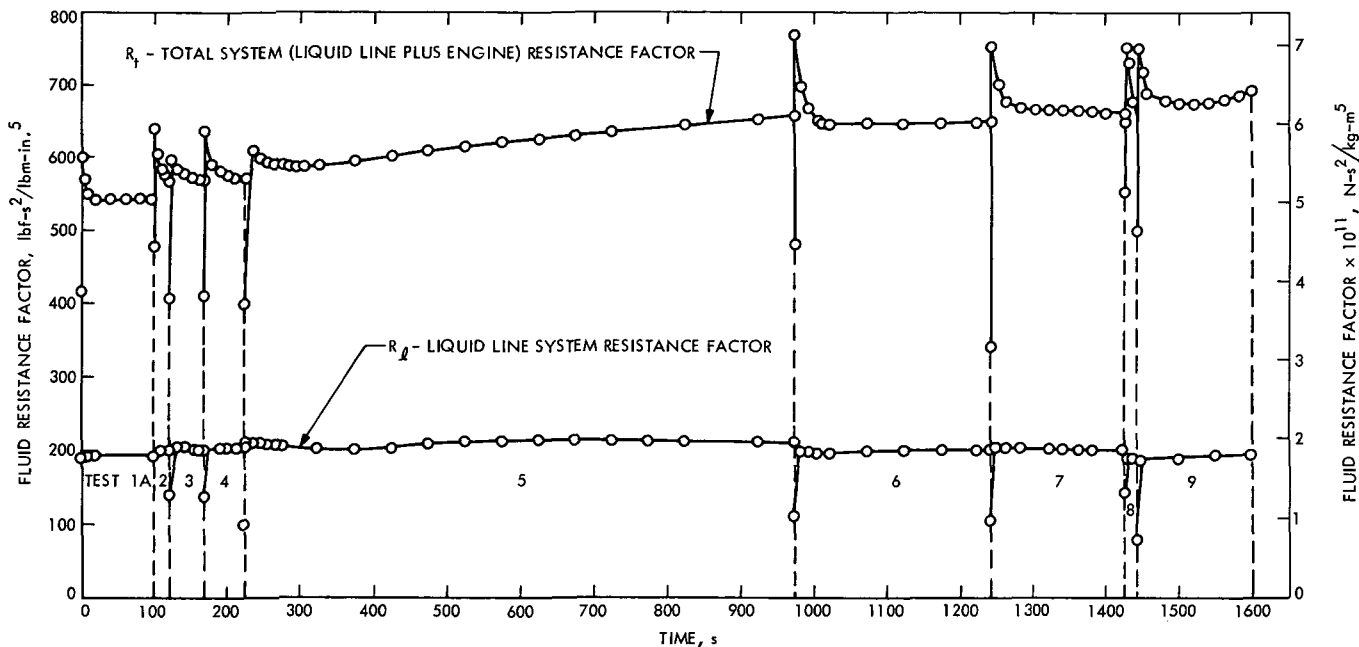


Fig. 68. Steady-state fluid resistance factor versus time

Values of K_m and K_{P_c} calculated from demonstration system test data are plotted against cumulative engine firing time in Figs. 69 and 70, respectively. The nominal steady-state value of K_m is about $0.29 \text{ N}^{1/2}\text{-m}$ ($5.4 \text{ lbf}^{1/2}\text{-in.}$) with a maximum deviation from the nominal for the nine firings of $\pm 4.6\%$. Data given in Table 29 indicate that the transient lasts at least 19 s and increases with run time (decreasing flow rate). The nominal value of K_{P_c} is about 0.0001 m^2 (0.158 in.^2) with a maximum deviation over the test program of $\pm 3.2\%$. The initial K_{P_c} transient is considerably shorter, with a minimum duration of 1 s; however, the transient appears to increase more with run time.

The data show that the K_m and K_{P_c} impulse control concept in this case is marginal at best. However, the results are undoubtedly influenced by the transient flow-rate surges, and chamber pressure and thrust spiking. Since these conditions are strongly engine-dependent and are known not to occur so severely in all engines, the impulse control concept proposed here cannot be judged unworkable, but is rather of restricted utility.

8. Posttest inspection. A thorough posttest inspection was made of the demonstration test system before it was removed from the vacuum test cell. There was no evidence of damage or malfunction of any component or structure. The final GN_2 tank pressure was 1186 kN/m^2 (172 psia). Liquid hydrazine propellant remaining in the

test system amounted to 6.251 kg (13.78 lbm). A sample of this hydrazine was collected and assayed for comparison with the initial loading: The results presented in Table 26 of Subsection IV-C-1 show very little change.

The axial load cell of the thrust stand and the thrust vector control system were recalibrated. No significant changes were observed from the pretest calibration. All pressure transducers were also recalibrated and showed no changes.

After vacuum deservicing, the test system was removed from the test cell for disassembly and inspection. There was no evidence of leakage or corrosion in any of the components. The two line filters were back-flushed with isopropyl alcohol and the particulate matter collected on $5\text{-}\mu\text{m}$ filter pads. Both filters had too many particles to estimate an accurate size/range count; however, sizes ran as high as $600 \times 1200 \mu\text{m}$ for nonmetallic, and $120 \times 600 \mu\text{m}$ for metallic particles. A spectrographic analysis made of the residue is presented in Table 35. Filter No. F-25166-2 was from valve branch No. 1, which contained the Carleton and Hydraulic Research solenoid valves. Filter No. F-25165-3 was from branch No. 2, which contained the Marquardt solenoid valves. The weight of each ash sample was only 0.0001 g, which indicates that a very small quantity of metallics were actually collected. The principal elements appear to be silicon, iron, aluminum,

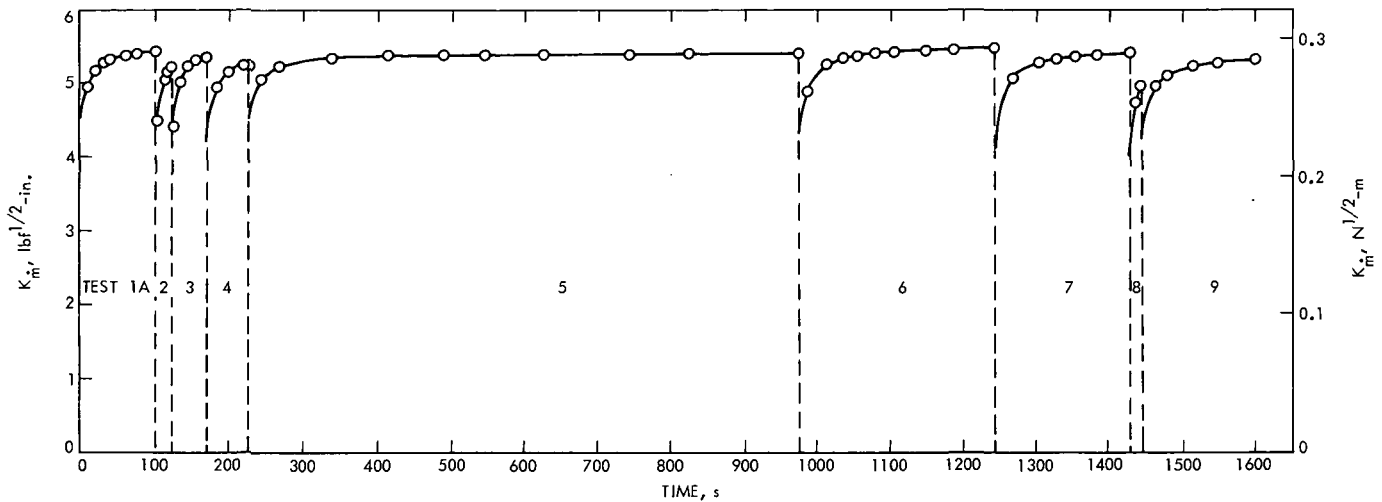


Fig. 69. Mass flow rate constant versus time

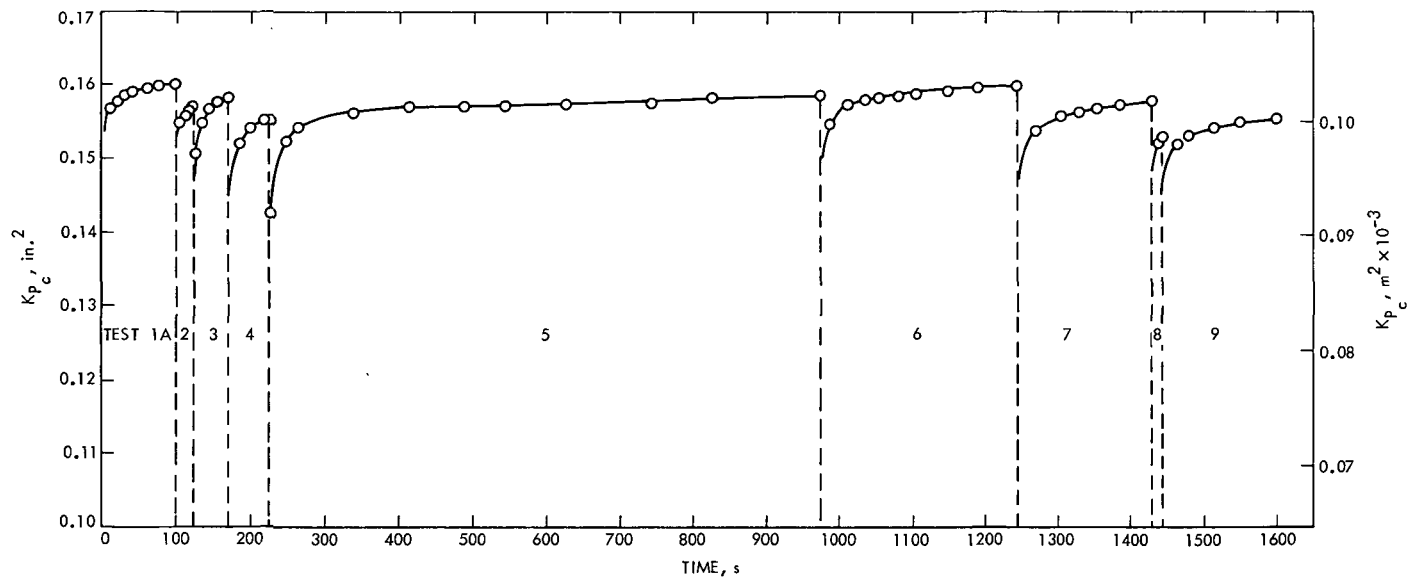


Fig. 70. Chamber pressure constant versus time

chromium, nickel, and calcium. Aluminum and iron probably came from the pyrovalve operations. Silicon was a contaminant introduced during the cryogenic proofing of the propellant tank and was never completely removed by repeated cleaning.

Bubble leakage tests on all solenoid valves indicated no leaks or valve seat deterioration. A close inspection of the pyrovalve manifold revealed no evidence of weld cracks or distortion of the manifold tubing and support structure. The engine was not disassembled for internal inspection and appears to be in useable condition for any further life testing.

E. Discussion of Demonstration Test Results

The objectives of the TCPS prototype demonstration system test program listed at the outset of Section IV were successfully accomplished. A brief summary of the test results as related to these test objectives and a few comments on possible improvements that should be included in a flight system design are given in the following sections.

1. Configuration verification. Reliable performance and multiple restart capability satisfying TOPS mission requirements were demonstrated by nine engine firings totaling 1600 s of operation with 9 pyrovalve actuations

Table 35. Spectrographic analysis of particulate residue from propellant line filters

Filter No.	F-25166-2	F-25166-3
Ash sample weight, g	0.0001	0.0001
Metallic elements, weight %		
Silicon	10.0	4.6
Iron	17.0	9.7
Aluminum	9.2	24.0
Manganese	2.0	0.88
Magnesium	3.1	1.7
Chromium	6.3	5.1
Nickel	4.1	5.5
Calcium	4.1	4.6
Copper	0.47	0.31
Silver	0.099	0.064
Titanium	2.1	1.5
Strontium	nil	trace
Other elements	nil	nil

for successive propellant system activation and isolation. All system components, particularly the engine assembly and the solenoid valves, were capable of extended operations without degradation. The simulation of a space-flight environment consisting of continuous vacuum and limited low temperatures did not reveal any system incompatibilities or malfunctions.

2. Steady-state performance. Steady-state rocket engine performance remained at a constant high level over the full 2:1 blowdown pressure range. Although vacuum thrust ranged from a high of 115.6 N (25.99 lbf) down to 60.34 N (15.02 lbf), the vacuum specific impulse remained about 2226 N-s/kg (227 lbf-s/lbm) and the characteristic velocity remained about 1315 m/s (4315 ft/s). Total delivered impulse for the 1600 s of operation was 130,785 N-s (29,403 lbf-s) which was derived from the expenditure of 59.18 kg (130.47 lbm) of hydrazine propellant. Theoretical performance values derived from the average ammonia dissociation level of 65.5% determined by analysis of exhaust gas samples agree within experimental accuracy with the measured performance values.

3. Transient performance. Transient engine performance characteristics during start and shutdown were influenced by the basic engine design, the large propellant holdup volume between the engine valves and the engine injector, and to an extent, by the cold temperatures of the hydrazine and catalytic bed. Ignition delay times averaged around 165 ms and PC rise times averaged 201 ms. These comparatively long response times were accompanied by high-pressure spikes in the injector line and catalytic bed. Although basically hard on the engine, the pressure spikes did not cause any damage or reduction in

useful life. Engine P_c roughness did not exceed 6% (the oscillation frequency was around 195 Hz). P_c decay times averaged 48 ms and were occasioned by numerous, low-level, pressure "perks" as the propellant in the holdup volume was expended through the hot engine.

The engine response time could be shortened by locating the engine valve manifold outlet closer to the engine inlet and reducing the internal size of the flexible line connecting the two points. However, this design change would not necessarily reduce the magnitude of engine start spiking, because this phenomenon is primarily associated with injector design configuration, physical and chemical condition of the catalytic bed, and propellant and catalytic bed temperature. In general, the engine performed as described in Ref. 9.

4. Thermal response. Thermal measurements made on the engine and support structure during the nine test firings revealed no serious heat-up problems and only one potential thermal soakback problem. Catalytic bed and thrust chamber wall temperatures both reached and exceeded 1089 K (1500°F) with rise times that increased from 8.1 to 22.3 s. The chamber pressure transducer was the only component that appeared to suffer temporary degradation from heating; a zero shift that recovered after cooldown apparently resulted from nonisothermal operation of the transducer, because the maximum temperature probably did not exceed the transducer's temperature compensation limit. A more effective thermal barrier should be incorporated into the pressure transmitting line.

The posttest soakback temperature of the engine injector manifold exceeded the vaporization and autodecomposition temperature of hydrazine and required as long as 2350 s to cooldown. The original Transtage engine and valve configuration was stressed for restarts in this condition. TOPS modifications for gimballed operation required the addition of a flexline which also increased the propellant holdup volume. The use of the flexible injector feed line permitted a reduction of the size and complexity of the gimbal engine support by allowing remote mounting of the redundant pair of engine solenoid valves. However, the flexline was not stressed for high-temperature restarts, so at least one or more hours is required between engine firings to allow for adequate cooling of the test system.

5. Shock response. The shock loading imparted to the test system structure by pyrovalve actuations was shown to be moderately severe. No component malfunctions

or structural damage was caused, although the measured peak shock acceleration spectra exceeded preliminary TOPS type-approval test levels. The engine gimbal assembly provided adequate shock isolation to protect the engine from excessive shock acceleration loading. Shock isolators should be installed between the pyrovalve manifold assembly and a stiffened base plate. This would reduce the severity of the low-frequency shock transferred through the mounting joint as well as eliminate most of the shock-induced high-frequency resonant vibrations.

6. Thrust vector control characteristics. Gimbal thrust vector control was demonstrated using programmed input signals to position a pair of gimbal actuators which deflected the rocket engine assembly about the Z-axis. The test configuration was limited to 5 deg maximum angular deflection in all directions by the design clearance inside of the pyrovalve manifold support. The maximum angular deflection could be increased by opening this clearance with enlargement of the pyrovalve support structure or by relocating the engine pivot point below that structure. The latter would necessitate an increase in overall length of the test assembly which, by design, has been kept to a minimum.

All thrust components were measured by the six-axis thrust stand. Nonsymmetrical pitch, yaw, and roll torque moments were observed in these measurements because the thrust axis was not aligned with the center of mass of the test assembly. This type of alignment was not practical because the center of mass shifted with the expenditure of on-board propellant.

7. Modeling and control parameter characteristics. Three propulsion system performance prediction parameters were developed from the experimental test data. The parameters are the fluid resistance factor, R , the fuel mass flow-rate constant, K_m , and the thrust chamber pressure constant, K_{p_c} . Fluid resistance factors were calculated for both the liquid portion of the propellant feed system, R_l , and the total system, R_t , which included the engine gas flow as well as the system liquid flow. R_l had a constant nominal value of 1.85×10^{11} N-s²/k-m⁵ (200 lbf-s²/lbm-in.⁵). R_t increased from 5×10^{11} to 6.4×10^{11} N-s²/k-m⁵ (520 to 690 lbf-s²/lbm-in.⁵) demonstrating that the effect of the gas flow was not negligible.

Both K_m and K_{p_c} are prospective impulse control parameters which could be used as backups for the on-board spacecraft accelerometers now used to signal engine shutdown during trajectory correction maneuvers. The nominal steady-state value computed for K_m was 0.29 N^{1/2}-m

(5.4 lbf^{1/2}-in.) and that for K_{p_c} was 1.0×10^{-4} m² (0.158 in.²). There was significant deviation from these nominal values from firing to firing, and the transient was long on the first firing and became longer with each succeeding firing. Their usefulness in actual application will have to be further evaluated. Any design changes that would reduce the levels of flow-rate surges, chamber pressure spiking, and thrust instability would undoubtedly improve the reliability of K_m and K_{p_c} as performance prediction parameters.

The changes recommended in the preceding sections are basically design or mechanization changes not requiring new technology. System performance should be smoother with them. The demonstration system design is not the only way to mechanize the TCPS configuration; however, the factors forcing the changes apply to other designs also. The preliminary flight design discussed in the next section is such a different design. It was completed before the demonstration system testing started, so it does not include the changes discussed here. Both the test experience reported in this section and the flight-type design experience reported in the next section will be factored into future design studies.

V. Definition of Flight TCPS

The design of a flight propulsion system depends on the mission, spacecraft requirements, and the available technology and component designs. The requirements were discussed in Section II, and the available technology was discussed in Section III. The melding of the requirements and technology together to produce a propulsion system for flyby missions of the late 1970s is described in this section. The TOPS AST Project, and particularly the TOPS design team, formed an excellent forum for this work. The final product was a preliminary design for the TOPS TCPS.

The TCPS was conceived as a spacecraft-independent module from the start of the TOPS project. This approach has been used on all Mariner spacecraft, and it was found suitable also for TOPS. The advantage of such a module is that it can be tested and prepared for launch separate from the remainder of the spacecraft. Thus the propulsion system can follow a separate schedule of activities while the spacecraft is electrically tested at length. Difficulties such as part malfunction or propellant leak with one do not affect the other. The disadvantage of the module is perhaps a slight duplication of structure between the module and spacecraft proper. This mass penalty is usually small for monopropellant hydrazine systems.

A. System Characteristics

A nominal set of system characteristics can be estimated from the results of the component evaluation and system demonstration programs. The values listed in Table 36 were selected to represent components in general, although components known to be adequate for the TOPS program were emphasized. The values will very likely change when actual flight projects later select components for their specific requirements.

Table 36. Estimate of nominal system characteristics

Parameter	Initial condition	Final condition
Propellant tank pressure	2760 kN/m ² (400 lbf/in. ²)	1400 kN/m ² (203 lbf/in. ²)
Propellant tank temperature	295 K (70°F)	295 K (70°F)
Orifice differential pressure	345 kN/m ² (50 lbf/in. ²)	121 kN/m ² (17.5 lbf/in. ²)
Thrust chamber pressure	1100 kN/m ² (160 lbf/in. ²)	640 kN/m ² (93 lbf/in. ²)
Thrust chamber temperature	1256–1158 K (1800–1625°F)	1256–1117 K (1800–1550°F)
Engine thrust (vac)	111 N (25 lbf)	67 N (15 lbf)
Specific impulse (vac)	2256 N-s/kg (230 lbf-s/lbm)	2256 N-s/kg (230 lbf-s/lbm)
Propellant flow rate	0.049 kg/s (0.11 lbm/s)	0.029 kg/s (0.065 lbm/s)

A change is particularly likely in the pressure budget because it is so dependent on engine chamber pressure, which varies broadly among current engines. The orifice differential pressure can be changed to make up for small differences; however, a tank pressure change is recommended for large differences. The specific impulse value is an average for the entire blowdown process which will vary somewhat from engine to engine. All other characteristics will not change unless engine thrust or the blowdown ratio is changed.

B. System Sizing

Propulsion system dimensions and mass follow directly from the requirements listed in Table 1, the system characteristics listed in Table 36, and the configuration shown in Fig. 6. The tank, tubing, all component passages in contact with hydrazine, and most component cases are assumed to be made of titanium. The major nontitanium elements are the engine, solenoid valve actuators, cabling, and perhaps the propulsion module structure.

Estimates of the masses of all propellant-independent components, i.e., all components except the hydrazine tank and associated propellant acquisition device, are based on the results of the evaluation program. The masses of the tank and acquisition device are treated as linear functions of hydrazine mass, and are calculated only for the TCPS hydrazine requirement. Then the tank and acquisition device are sized for combined TCPS and APS hydrazine requirement, and the mass difference is ascribed to the APS.

The mass of the TCPS is thus written as the sum of the fixed component masses and the propellant-dependent masses:

$$M_{TCPS} = M_{fixed} + C_1 \times M_{N_2H_4} \quad (6)$$

Equation (6) substituted into the standard Tsiolkovskii mass/ ΔV relationship

$$M_{N_2H_4} = (M_{payload} + M_{TCPS})(1 - \exp[-\Delta V/I_{sp}]) \quad (7)$$

uniquely determines the usable propellant mass without iteration:

$$M_{N_2H_4} = \frac{M_{payload} + M_{fixed}}{\left[\frac{1}{1 - \exp(-\Delta V/I_{sp})} \right] - C_1} \quad (8)$$

where $M_{payload}$ is the spacecraft mass less M_{TCPS} . The TOPS values for the parameters of Eq. (8) are

$$M_{payload} = 715.3 \text{ kg (1577 lbm)}$$

$$M_{fixed} = 11.5 \text{ kg (25.4 lbm)}$$

$$\Delta V = 205 \text{ m/s (673 ft/s)}$$

$$I_{sp} = 2256 \text{ N-s/kg (230 lbf-s/lbm)}$$

$$C_1 = 1.2084$$

(The factor C_1 is the sum of C_1 (tank) = 0.1327, C_1 (propellant acquisition) = 0.0133, C_1 (N_2) = 0.0324, C_1 (holdup N_2H_4) = 0.03, and C_1 (usable N_2H_4) = 1.0).

The final TCPS mass calculated from the preceding equations is itemized in Table 37. The hardware or dry mass is 21.8 kg (48.1 lbm) and the total, or wet mass, is 96.8 kg (213.3 lbm). The resulting mass fraction of 0.73 is higher than the values shown in Table 38 for monopropellant hydrazine systems used on past planetary spacecraft primarily because of the larger fuel load, although significant hardware improvements have also been made.

Table 37. Mass estimate for TOPS TCPS

Component	Quantity	System mass, kg (lbm)
Propellant tank (ID = 0.67 m)	1	9.3 (20.6) ^a
Propellant acquisition device	1	1. (2.1) ^a
Fill valves	2	0.3 (0.6)
Transducers (<i>P</i> , <i>T</i> , <i>F</i>)	10	0.9 (2.0)
Explosive valves (NO, NC)	10	1.8 (4.0)
Filter	3	0.5 (1.0)
Orifice assembly	1	0.1 (0.3)
Solenoid valves	4	1.3 (2.8)
Engine assembly ($F_{vac} = 111.2$ N)	1	0.8 (1.7)
Mounting hardware (for gimbal TVC system)	—	4.5 (10.0)
Cable harness	—	1.4 (3.0)
Hardware total		21.8 (48.1)
Propellant (N ₂ H ₄)	—	72.7 (160.) ^a
Pressurant (GN ₂)	—	2.3 (5.0) ^a
Subsystem total		96.8 (213.4)

^aAPS portion not included.

Table 38. Monopropellant hydrazine propulsion system mass fraction

Spacecraft	Mass fraction
Mariner IV (1964)	0.45
Mariner V (1967)	0.44
Mariners VI and VII (1969)	0.48
Mariner J (1973)	0.67
TOPS (1977)	0.73

C. Spacecraft Interfaces

The TCPS is a spacecraft-independent module in that it can be moved around, tested, and prepared for launch independent of the spacecraft. It is a plug-in unit with simple connections to the rest of the spacecraft. This independence does not include the ability to accomplish its flight function without the assistance of other spacecraft subsystems. The TCPS interacts directly with six other subsystems as described in the following subsections.

1. Attitude propulsion subsystem (APS). One of the major advantages of the TOPS APS is that it draws propellant from the TCPS tank and thus needs no tank of its own. Further, since the APS engines have short lever arms, it is advantageous to combine the TCPS and APS

together into a single propulsion module. Combining the TCPS and APS into a single module also combines significant portions of their design, fabrication, and test programs. The APS is described in detail in Ref. 4.

2. Pyrotechnic subsystem (PYRO). The driver circuits for the TCPS solenoid valves and the firing circuits for the TCPS pyrovalves are part of the pyrotechnic subsystem. The TCPS-PYRO interface for the solenoid valves consists of several connectors located at the boundary between the propulsion and electronics bays of the spacecraft. PYRO provides a separate driver circuit for each of the two parallel valve branches in the TCPS. The pyrovalve interface is the valve/squib joint.

The TCPS has no direct interface with the power subsystem; the power required by TCPS components is switched by PYRO on the command of the control computer subsystem (CCS) which controls the entire maneuver sequence. The three distinct power profiles required to actuate TCPS valves are listed in Table 39. These valves are operated one at a time to minimize the peak power demand during the maneuver period; the NC solenoid valve must be actuated at a specific time, but the two types of isolation valves can be opened and closed during low-power periods occurring hours or days before or after the maneuver. The line voltage from PYRO to TCPS valves is controlled to 28 Vdc \pm 5%. PYRO provides the appropriate circuitry to suppress the back EMF surge generated on closing one of the solenoid valves.

Table 39. Power supplied by PYRO to TCPS

Component	Maximum power, W	Demand duration	Comments
Explosive valve	75	100 ms	Not time-critical event
Latching solenoid valve	10	100 ms	May be time-critical event
NC solenoid valve	10	Engine firing period	Time-critical event

3. Attitude-control subsystem (A/C). The TCPS-A/C interface is a mechanical one involving the mounting of two gimbal actuators that provide thrust vector control (see Subsection II.C). Both the rear mounting bracket and the engine attachment for the gimbal actuators are part of the TCPS. The maximum gimbal angle was identified as being at least 5 deg; a final value was never set. The calibration of the completed engine assembly is a joint task supported by A/C personnel. The electronic sys-

tem that senses upsetting torques due to thrust vector misalignment and drives the actuators to a position where the torques are nulled out is a major part of the A/C.

The A/C subsystem also contains the accelerometer system that terminates rocket engine firing via a signal to the CCS and thereon to PYRO. The accelerometer is backed up with a maximum value of firing time telemetered from Earth to the CCS.

4. Measurement processor subsystem (MPS). The measurement processor subsystem monitors TCPS transducers and encodes the data for transmission to Earth. TCPS maneuver telemetry is summarized in Table 40. A ten-bit data word is used for most measurements to limit the

Table 40. TCPS telemetry during maneuvers

No.	Measurement	Range	Bits per data word
1	Thrust chamber pressure	0 to 1720 kN/m ² (0 to 250 psia)	10
2	Thrust chamber temperature	227 to 1367 K (-50 to 2000°F)	10
3	Catalytic bed temperature	227 to 1367 K (-50 to 2000°F)	10
4	Orifice flow pressure differential	0 to 1720 kN/m ² (0 to 250 psia)	10
5	Orifice downstream pressure	0 to 3450 kN/m ² (0 to 500 psia)	10
6	Orifice flow temperature	255 to 325 K (0 to 125°F)	7
7	Propellant tank pressure No. 1	0 to 3450 kN/m ² (0 to 500 psia)	10
8	Propellant tank pressure No. 2	0 to 3450 kN/m ² (0 to 500 psia)	10
9	Propellant tank temperature	255 to 325 K (0 to 125°F)	7
10	Thrust level	0 to 133 N (0 to 30 lbf)	10
11	Propulsion subsystem status channel ^a	—	7

^aStatus channel definition:

Bit	
1	Latching solenoid valve No. 1 open or closed
2	Latching solenoid valve No. 2 open or closed
3	} Spare bits
4	
5	
6	
7	

analog-to-digital conversion error to 0.1%. The sampling rate for each measurement could be changed at any time. Details of telemetry measurement operation were not finalized by the TOPS Project.

Three maneuver sampling rates were requested for TCPS measurements: a start transient mode, a steady-state mode, and a stop transient mode. Key measurements would be sampled 100 times per second during transients and ten times per second during steady state. These high sampling rates are well within the MPS total capability of 10,000 samples per second. Cruise sampling of key measurements would be one per hour and secondary measurements would be reduced to one per day or deleted altogether.

The MPS provides the power needed to energize TCPS transducers. The required power is itemized in Table 41. The power values given are those of a strain gauge thrust transducer, microswitch position indicators, strain gauge pressure transducers, and resistance temperature transducers.

Table 41. Power required for TCPS measurements

Transducer	Maximum power, W
Thrust (1 unit @ 0.25 W each)	0.250
Latching valve position indicator (2 units @ 15 mW each)	0.030
Pressure (5 units @ 0.25 W each)	1.25
Temperature (4 units @ 0.5 mW each)	0.002

Some information on the electrical performance of TCPS solenoid valves can be gleaned from PYRO measurements of driver circuit current and voltage. Thrust vector control operations are characterized by A/C measurements of gimbal position. This information completes the data picture needed for detailed performance analysis.

5. Structure subsystem (STRU). The TCPS module interface with the structure subsystem is a mounting or attachment arrangement subject to specified alignment accuracies. The TCPS rocket engine thrust vector must be aligned to within 0.74 deg of the spacecraft center of gravity (CG) measured experimentally during final launch preparations. The actual CG must be in a box 0.16 m (6.3 in.) (X) by 0.06 m (2.4 in.) (Y) by 0.16 m (6.3 in.) (Z) centered on the nominal CG location, so the maximum (3σ) alignment offset adjustment required is about 8 deg. The propulsion module is cantilevered from

the propulsion bay structure, so all TCPS and APS alignment is fixed at the mounting points.

6. Temperature control subsystem (T/C). The propulsion bay is a truss structure without solid sides. A temperature control blanket covers the bay to maintain internal temperatures between 289 and 305 K (60 to 90°F). The TCPS engine nozzle penetrates the bay and the thermal blanket, and thus represents the location of greatest thermal energy loss from the bay. The nozzle will be fitted with a flexible collar to keep the edges of the pass-through hole covered for all gimbal actuator positions.

Heat dissipated from the electric equipment located in the propulsion bay and from the electronics compartment should be sufficient to maintain the required temperature. However, either electrical or radioisotope heaters are attached to the engine and perhaps the hydrazine tank in case electric power consumption in or near the propulsion bay is reduced for some reason. The absolute lower limit for bay temperature is 275 K (35°F) where hydrazine freezes, although the engine should not be operated below 277 K (40°F).

D. Preliminary Propulsion Module Design

The TCPS configuration, component technology and design evaluation, and system interface definitions discussed previously are the basic elements of system design. The design is the culmination of the technology evaluation program in the sense that it is only here that component interaction—size, shape, and arrangement—can be studied. The work described in this section is very preliminary because TOPS spacecraft design on the whole did not enter the detailed design phase.

The general location of the propulsion bay in relation to other spacecraft assemblies is shown in Fig. 71 (see also Fig. 1). The electronics bay is on one side and the RTGs are cantilevered from the other. The remaining two sides have a clear view to space. Part of the radio subsystem and some electric equipment are housed at the antenna end of the bay. The cross section of the propulsion bay is not rectangular because the hydrazine tank is larger than the smaller dimension. This configuration is used to avoid changing the structure design every time tank size changes in response to a ΔV change and it is lighter. Although this arrangement presents no structural problems because that side is open and the thermal blanket is easily formed to fit, it does require that the propulsion module be loaded from the side rather than the end of the bay. Therefore the dimension of the module along the thrust axis should be minimized.

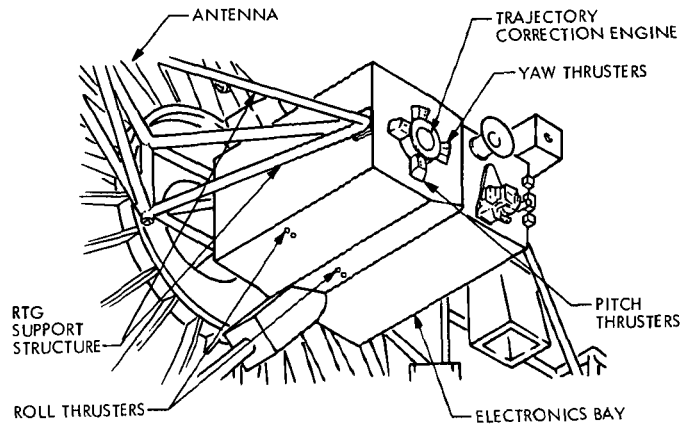


Fig. 71. TOPS propulsion bay and neighboring assemblies

An artist's rendering (to scale) of the preliminary propulsion module design is shown in Fig. 72 with cabling omitted. The tank diameter of 0.5 m (20 in.) corresponds to an earlier lower ΔV requirement. The outer dimensions of the module shown in the figure are 1 m (38.5 in.) by 0.6 m (24.8 in.) by 0.5 m (20 in.). The final TOPS tank (ID of 0.7 m (26.3 in.)) is slightly too large for the current propulsion bay structure; the outer dimensions of the final module are at least 1.1 m (44.8 in.) by 0.7 m (26.3 in.) square.

Propulsion components were assumed to be advanced lightweight designs fabricated from titanium. Estimates of component dimensions were based on the results from the component evaluation program. Components not evaluated, such as the ΔP transducer in the foreground of Fig. 72 and the gimbal actuators in the background, were dimensioned from current designs; hopefully smaller, lighter designs exist or will exist by the mid 1970's.

APS roll thrusters located in the plane of the CG perpendicular to the roll axis are shown in Fig. 72. The pitch and yaw thrusters are located around the TCPS engine nozzle on the other side of the large plate. An attractive alternate configuration has all of the APS thrusters on the plate. The thrusters are located such that they have the proper moment arm and the thruster nozzles protrude just outside the thermal blanket. (See also the APS-oriented view of the propulsion module given in Ref. 4.)

As indicated earlier, the design shown in Fig. 72 is just one of many possible arrangements that will satisfy all the requirements. The general design of the TCPS prototype demonstration system represents another major class with the tank mounted directly to the main plate structure. Both appear acceptable, although the latter might

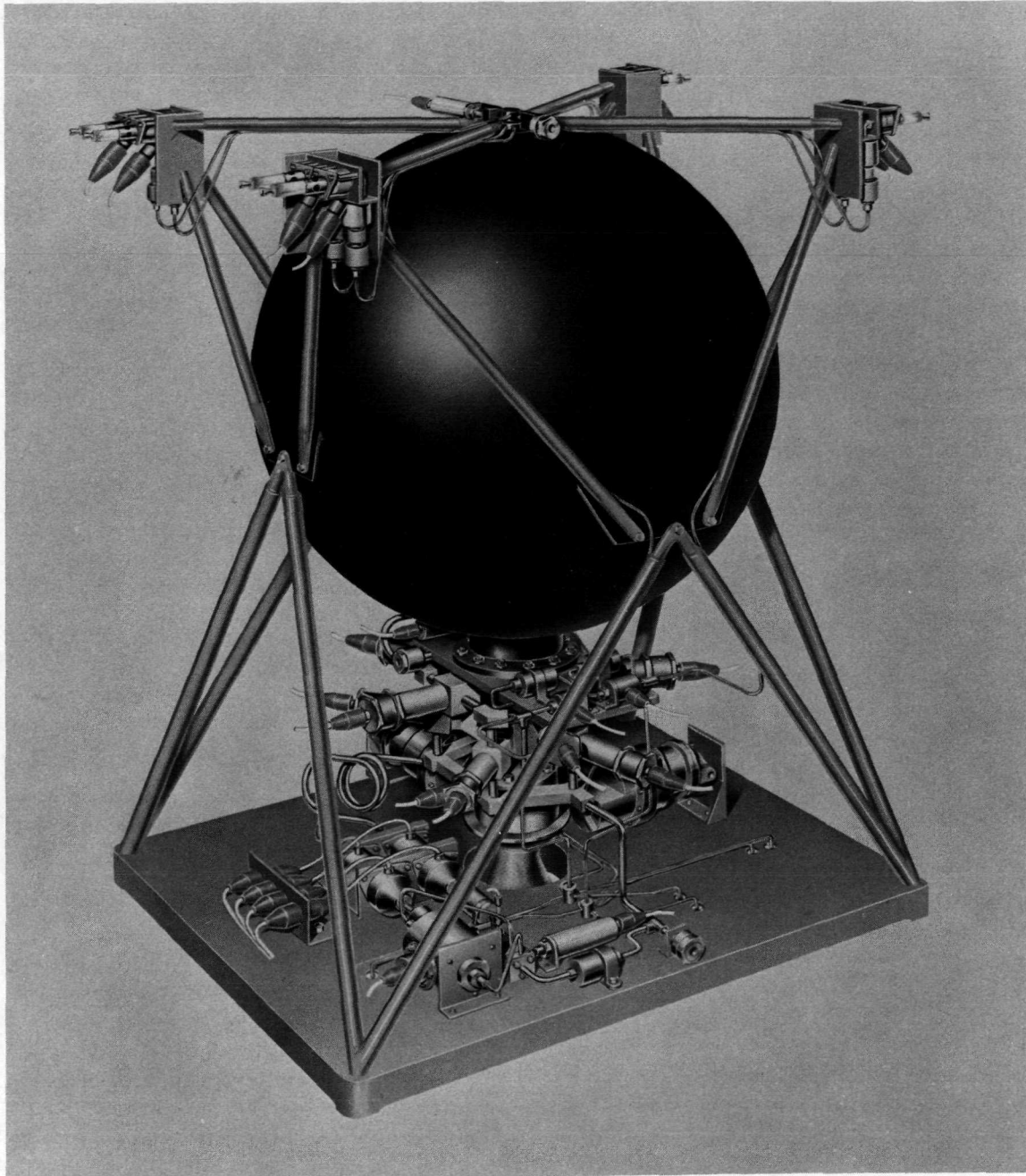


Fig. 72. Preliminary TOPS propulsion module design emphasizing TCPS components

be more difficult from a thermal control standpoint. Overall, pyrovalve manifolding and gimbal articulation are the major design challenges.

E. TCPS Operation and Control

Nine trajectory correction maneuvers are planned for the three-planet missions. The first maneuver is made at the outset of the mission to correct for the planetary

quarantine launch bias and injection errors. Then two preencounter and one postencounter maneuvers are made at each planet except the last where a postencounter maneuver is unnecessary. These maneuvers are scheduled during the 40 days before and after passage of the planet where trajectory determination is easiest.

There are several reasons for scheduling two pre-encounter maneuvers instead of one. First, the spacecraft

trajectory must be adjusted for planet ephemeris prediction inaccuracies, especially on the first passage of each planet. Second, the time of passage must be adjusted for optimum viewing of the various moons whose orbits come near the selected spacecraft trajectory. Third, the spacecraft must pass through a very small circle in space near each planet to be accurately deflected to the next planet. An error of 1 km in this target area typically maps to a miss of 1000 km at the next planet. The postencounter maneuver is used to correct for accumulated preencounter errors and establish the best possible trajectory for the next encounter.

1. Maneuver sequence. Preparations for a given maneuver start several days before the actual rocket firing with the final orbit determination. Then the ΔV required to move the spacecraft from its current flight path to one leading to the target point is calculated. Finally the required roll and yaw turns and the maneuver firing time estimate are calculated.

The actual maneuver sequence lasts two to three hours. The principal events for a typical maneuver are listed in Table 42. Specific times have been assumed for the variable events: the roll and yaw turns are assumed to last 600 and 1200 s, respectively (corresponding to 60 and 120 deg), and the engine firing is assumed to last 600 s. The spacecraft would thus be on inertial reference (gyros)

Table 42. Typical maneuver sequence of events

Time	Event
- days	Open NC explosive valve (first pre-planet maneuver only)
0	Initiate trajectory correction maneuver: turn on gyros and PYRO
+ 40 min	Switch to inertial reference system.
+ 45 min	Start turns: roll, then yaw (turns take 0 to 1800 s each; $T_R = 600$ s and $T_Y = 1200$ s assumed here.)
+ 81 min	Turn on autopilot and accelerometer
+ 84 min	Open latching solenoid valve
+ 86 min	Start rocket engine
+ 96 min	Stop rocket engine (firings take 5 to 750 s each; $T_B = 600$ s assumed here)
+ 97 min	Turn off autopilot and accelerometer
+ 99 min	Start turns: inverse yaw, then inverse roll
+ 134 min	Return to celestial reference. Turn off gyros
+ hours	Close latching solenoid valve
+ days	Close NO explosive valve (last post-planet maneuver only)

for 134 min, provided a special celestial reference acquisition sequence is not required after the inverse turns are performed.

Many spacecraft subsystems play a role in a maneuver. They and their roles are:

- (1) The A/C subsystem switches from celestial to inertial references for three-axis control, provides the accelerometer that generates the engine cutoff signal, and provides the autopilot and gimbal actuators that control the thrust vector during engine firing.
- (2) The attitude propulsion subsystem executes the commanded roll and yaw turns to the proper maneuver alignment, and provides roll control during engine firing (the gimbal actuators control only pitch and yaw).
- (3) The pyrotechnic subsystem switches power to the TCPS valves at the command of the CCS.
- (4) The control computer subsystem orchestrates the maneuver sequence by commanding and controlling all events. The computer stores a ground-calculated engine firing time that protects the spacecraft from accelerometer failure.
- (5) The radio subsystem must switch from the fixed high-gain antenna to the steerable medium gain and change the data rate.
- (6) The measurement processor subsystem switches from encounter data formats to the maneuver formats and to maneuver sampling rates.

The TCPS provides the necessary impulse to change spacecraft velocity to the desired value. The system is prepared for the maneuver sequence by opening the pyro isolation valve before the first preencounter maneuver. The remaining latching solenoid isolation valve is opened two minutes before the maneuver. If the latching valve is the back-pressure-relieving type, then it can be closed shortly after the maneuver, thus effectively guarding against a failed-open failure of the normally closed solenoid control valve. The sequence given in Table 42 assumes that the latching valve is not the back-pressure-relieving type, so it must be closed after the peak soak-back temperature has passed to avoid overpressurization of the hydrazine trapped between it and the NC solenoid valve.

2. Engine cutoff control. The engine firing duration is controlled by the output of the integrating accelerom-

eter. The accelerometer is backed up by a fixed value of firing time calculated by mission control. The time value is the predicted firing time plus a small safety margin to keep the timer from prematurely stopping the firing when the TCPS is slightly underperforming.

An alternate concept for the backup function is to use an on-board computed time. This concept can be used for the prime control function if the accuracy requirement for an individual maneuver could be relaxed somewhat. The engine cutoff time can be determined on-board the spacecraft as the time when a given total impulse is reached through numerical integration of either

$$I_{tot} = \int_0^{t_f} F_{vac} dt \quad (9)$$

or

$$I_{tot} = \int_0^{t_f} C_f A_t P_c dt = K_{P_c} \int_0^{t_f} P_c dt \quad (10)$$

or

$$I_{tot} = \int_0^{t_f} I_{sp} K \rho \sqrt{\Delta P} dt = K_m \int_0^{t_f} \sqrt{\Delta P} dt \quad (11)$$

where the variables I_{tot} = total impulse, F_{vac} = vacuum thrust, t = time, t_f = firing time, C_f = thrust coefficient, A_t = nozzle throat area, P_c = chamber pressure, I_{sp} = specific impulse, K = orifice constant, ρ = hydrazine density, and ΔP = orifice differential pressure. In addition, a high degree of redundancy can be achieved by using all three equations in a majority vote arrangement.

The high TOPS sampling rates for the primary propulsion measurements of F_{vac} , P_c , and ΔP minimize computational error. The significant error sources are thus the transducer error, which is typically about 0.25% of full scale, the error in using the steady-state values of K_{P_c} and K_m for the constants in Eqs. (10) and (11) which averages 5% for the Transtage engine, and a small analog-to-digital conversion error of about 0.1%. The error in the constant results largely from the long transient of the Transtage engine; the use of a faster responding engine and the selection of the constant value from calibration curves will greatly reduce this part of the error. The total error is always higher than the accelerometer system total error value of 0.25%; however, in some cases it may be close enough to make using the proposed alternative preferable to using the accelerometer. A high measurement sampling rate may not be required to use this concept, although it is probably the easiest way.

A simple on-board analog integration of the transducer voltage which is digitized by a saturable core oscillator appears practical.¹⁰ The counts from the oscillator are totaled in a register like accelerometer counts, resulting in engine cutoff when a predetermined (ground-commanded) total count is reached. This method applies to Eqs. (4) and (5) because transducer voltage is linearly proportional to the parameter; however, arithmetic logic is needed in addition to the integrator to integrate the square root function of Eq. (6).

The analog integration technique is subject to analog-to-digital (A to D) conversion errors as well as the transducer and proportionality constant errors. The A-to-D conversion error can be reduced to less than 0.1% by tailoring the circuit design to give more than 1000 counts for very short firings.

3. Fault detection and correction. Most of the propulsion components have partial and total failure modes, and most of these are very improbable. Some, such as decreasing flow rate through the filter or decreasing engine performance, can be lived with through operational changes. Others, such as the loss of signal from a transducer, do not impact basic system capability.

The solenoid valves are the greatest concern, as a look at the system configuration (Fig. 5) shows. This is particularly true during each 80-day encounter period when these valves control the system. The primary detection of valve leakage into the engine would come from a telemetry doppler shift and increased engine catalytic-bed temperature. Such a leak would alter the trajectory, but not perturb spacecraft attitude stability as long as the thrust vector is aligned through the CG. The pyrovalves could be used for maneuver control in the improbable event of a major leak through the series solenoid valves.

All propellant system joints are welded to preclude any other source of leakage. Leakage that does not pass through the engine would be noticed first from a telemetry doppler shift, and much later by system pressure changes. Nothing could then be done to save the propulsion subsystem, although the spacecraft would likely survive.

The only fault detection and correction capability given to the control computer subsystem involves closure of the active latching solenoid valve if the NC solenoid valve did

¹⁰Personal communication with Walter S. Wuest, Jet Propulsion Laboratory, Pasadena, Calif., April 26, 1972.

not close completely. This protection must be spacecraft-controlled because of the very long round-trip communication times involved. The failure of a valve to open to start the maneuver or small leaks would be analyzed and remedied by mission control. The development of sufficiently explicit decision rules to govern spacecraft control over irrevocable events, such as firing pyrovalves, appears unlikely.

VI. Summary and Recommendations

The evaluation program described in previous sections demonstrated that current monopropellant hydrazine system *technology* meets the TCPS requirements of TOPS-type missions. Both performance and interface requirements were evaluated in this program which culminated with the successful prototype system demonstration test. The valve configuration operation and rocket engine life were demonstrated in the nine firings totaling 1600 s. Information on TCPS/spacecraft interfaces was gathered.

Component *design* changes—based on existing advanced technology—are necessary for optimum system design. The TOPS program made significant progress in changing component materials from stainless steel to titanium which is more compatible with hydrazine. Titanium designs probably represent the smallest, lightest designs presently feasible. Further changes are needed to minimize:

- (1) Power consumption
- (2) External magnetic field
- (3) Mass
- (4) Size
- (5) Hydrazine contact with less compatible materials

Specific values of these parameters that were found feasible in the TOPS evaluation program, and which meet or exceed TOPS requirements, are given for each component in the sections of this report dealing with that component and the flight-weight system.

New designs are required for:

- (1) Normally closed and latching solenoid valves

- (2) Propellant acquisition device
- (3) Pyrovalve
- (4) Transducers
- (5) Filter

The solenoid valves need the greatest change and will present the greatest challenge. Although a maximum leakage level was not established for the TOPS program, it is obvious that current values must be improved and testing methods developed to conclusively demonstrate long-term life at the improved leakage levels. Development versions of the remaining components have been made of titanium, so the primary remaining task is to qualify appropriately sized versions for specific outer planets mission requirements.

The TOPS hydrazine/material compatibility program did not conclusively define a set of completely acceptable materials. The selection of titanium is widely accepted, although it is still provisional, awaiting final long-term data. Nuclear radiation did not significantly affect hydrazine decomposition or corrosivity. The prime radiation problem centers on polymeric materials used as seats and insulation in solenoid valves.

The performance of the TOPS TCPS can be improved by substituting the hydrazine/hydrazine nitrate blend for the neat hydrazine. Providing that titanium is compatible with the blend, and that all titanium system can be built, the only component affected is the rocket engine. The higher decomposition temperature of the blend severely degrades catalytic beds made of Shell-405. Thus, either a new catalyst must be found or a thermal decomposition engine using electrical or radioisotope heater ignition must be adopted. The recent progress with electrothermal hydrazine engines indicates that such an engine is the key to use of the higher performing blend.

Another performance improvement, in the form of a mass savings, may be gained by substituting on-board firing time computation for engine cutoff rather than an accelerometer. The majority vote system based on thrust, chamber pressure, and mass flow rate proposed for TOPS appears to have the block and functional reliability of redundant accelerometers while weighing less. This concept should be investigated further.

References

1. *Astronautics and Aeronautics*, Vol. 8, No. 9, September 1970.
2. *Final Report, Thermoelectric Outer Planets Spacecraft (TOPS) Study Project, Vols. I and II*, Document 701-141, Jet Propulsion Laboratory, Pasadena, Calif., (JPL internal document), to be published.
3. *Thermoelectric Outer Planet Spacecraft Advanced System Technology, Function Description*, Delta Microfilm Co., Culver City, Calif., Sept. 20, 1971.
4. Moynihan, P. I., *Attitude Propulsion Technology for TOPS*, Technical Report 32-1560, Jet Propulsion Laboratory, Pasadena, Calif., Nov. 1, 1972.
5. *Functional Requirement, Thermoelectric Outer Planet Spacecraft, Trajectory Correction Propulsion Subsystem*, TOPS-4-2010A, Jet Propulsion Laboratory, Pasadena, Calif., Sept. 16, 1971 (JPL internal document).
6. Lee, D. H., *Development of the Midcourse Trajectory-Correction Propulsion System for the Ranger Spacecraft*, Technical Report 32-335, Jet Propulsion Laboratory, Pasadena, Calif., Mar. 1963.
7. *Mariner Mars 1964 Project Report: Mission and Spacecraft Development. Volume 1. From Project Inception Through Midcourse Maneuver*, Technical Report 32-740, Jet Propulsion Laboratory, Pasadena, Calif., Mar. 1, 1965.
8. *Mariner Venus '67 Final Project Report*, Technical Report 32-1203, Jet Propulsion Laboratory, Pasadena, Calif., June 15, 1968.
9. Morrissey, D. C., et al., "Development of the Titan III Transtage ACS Hydrazine Monopropellant Rocket Engine Modules," AIAA Paper No. 69-422, presented at AIAA 5th Propulsion Joint Specialist Conference, U.S. Air Force Academy, Colo., June 9-13, 1969.
10. Katter, L. B., *Development of Long Life Catalyst Beds for Monopropellant Hydrazine Reactors*, Final Report, Contract NAS 7-583, Rocket Research Corp., Redmond, Wash., for the Jet Propulsion Laboratory, Pasadena, Calif., Jan. 1969.
11. *Functional Requirement, Thermoelectric Outer Planet Spacecraft Environmental Design Characteristics and Restraints*, TOPS-3-300A, Jet Propulsion Laboratory, Pasadena, Calif., Sept. 17, 1971 (JPL internal document).
12. Steele, D., et al., *Titan IIIC Transtage Hydrazine Attitude Control System Users' Manual*, Report No. MCR-69-543, Martin Marietta Corp., Denver, Colo., Nov. 1969.
13. Lieberman, M., and Taylor, W., *Development of a Low Cost Catalyst for Hydrazine*, AFRPL-TR-70-7, Air Force Rocket Propulsion Laboratory, Edwards, Calif., Jan. 1970 (Confidential).
14. Smith, W., *Development of Design and Scaling Criteria for Monopropellant Hydrazine Reactors Employing Shell-405 Spontaneous Catalyst, Final Report Under NAS 7-372, RRC-66R-76, Vol. II*, Rocket Research Corp., Seattle, Wash., Jan. 18, 1967.
15. Kesten, A., *Study of Hydrazine Reactor Vacuum Start Characteristics*, First Annual Progress Report under NAS 7-696, United Aircraft Research Labs, East Hartford, Conn., Dec. 1969.

References (contd)

16. Greer, H., "Vacuum Startup of Reactors for Catalytic Decomposition of Hydrazine," *J. Space. Rock.*, Vol. 7, No. 5, May 1970.
17. *Steady State Operating Characteristics of the MR-3A 26.5 Pound Thrust Rocket Engine Assembly*, Report 70-R-239, Rocket Research Corp., Redmond, Wash., Dec. 31, 1970.
18. Lee, D. H., *Performance Calculations for Monopropellant Hydrazine and Monopropellant Hydrazine-Hydrazine Nitrate Mixtures*, Technical Report 32-348, Jet Propulsion Laboratory, Pasadena, Calif., Dec. 3, 1962.
19. Rockenfeller, J. D., "Low Temperature Monopropellants," paper presented at the Hydrazine Monopropellant Technology Symposium, John Hopkins University, Silver Spring, Md., Nov. 28-30, 1967. Chemical Propulsion Information Agency, CPIA Publication No. 160, (Confidential).
20. Rockenfeller, J. D., *Development of Improved Stable Monopropellants*, AFRPL-TR-70-108, Air Force Rocket Propulsion Laboratory, Edwards, Calif., Sept. 1970 (distribution limited).
21. Martinkovic, P. J., *Monopropellant Exhaust Contamination Investigation*, Technical Report AFRPL-TR-69-72, Air Force Rocket Propulsion Laboratory, Edwards, Calif., Apr. 1969.
22. Simon, W., "Nozzle Exhaust Plume Backscatter Experiment Using the JPL Molsink Facility." *JPL Quarterly Technical Report*, Vol. 1, No. 4, Jan. 1972.
23. Simon, W., *Plume Backscatter Measurements Using Quartz Crystal Microbalances in JPL Molsink (Molecular Sink)*, Technical Memorandum 33-540, Jet Propulsion Laboratory, Pasadena, Calif., May 15, 1972.
24. "Valve Assembly, Propellant Flow Control, Solenoid-Actuated, Detail Specification for," Specification No. CS506221B, Jet Propulsion Laboratory, Pasadena, Calif., Jan. 18, 1972 (JPL internal document).
25. *Valve Assembly, Propellant Shutoff, Solenoid-Actuated, Bi-Stable, Detail Specification for*, Specification No. CS506226A, Jet Propulsion Laboratory, Pasadena, Calif., Jan. 7, 1972 (JPL internal document).
26. *Squib, Dual Bridge, 1W/1A, Mariner Mars 1971 Spacecraft Flight Equipment, Detail Specification for*, JPL Specification No. ES504522, Rev. A, Jet Propulsion Laboratory, Pasadena, Calif., Apr. 10, 1970 (JPL internal document).
27. *Squib, Dual Bridge, 1W/1A, 7/8-14 Thread*, JPL Drawing 10028049, Rev. C, Jet Propulsion Laboratory, Pasadena, Calif., Dec. 15, 1969 (JPL internal document).
28. Avalos, E., *Evaluation Test Program, Valve, Explosive-Actuated, Normally-Open Model 1399*, Final Report QC&R 6-045, Pyronetics, Inc., Santa Fe Springs, Calif., Oct. 5, 1971.
29. Avalos, E., *Evaluation Test Program, Valve, Explosive-Actuated Normally-Closed Model 1400*, Final Report QC&R 6-046, Pyronetics, Inc., Santa Fe Springs, Calif., Oct. 5, 1971.

References (contd)

30. Avalos, E., *Valve, Normally Open, Titanium Model 1425*, Final Report QC&R 6-050, Pyronetics, Inc., Santa Fe Springs, Calif., March 2, 1972.
31. Avalos, E., *Valve, Normally Closed, Titanium, Model 1426*, Final Report QC&R 6-051, Pyronetics, Inc., Santa Fe Springs, Calif., Mar. 2, 1972.
32. *Investigation of Space Storable Propellant Acquisition Devices, Volume I—Evaluation*, Final Report for Contract NAS7-754, MCR-70-171, Martin Marietta Corp., Denver, Colo., Dec. 1970.
33. *Investigation of Space Storable Propellant Acquisition Devices, Volume II—Design and Analysis, Final Report for Contract NAS7-754*, MCR-70-171, Martin Marietta Corp., Denver, Colo., Dec. 1970.
34. Weiner, R. S., "Material Compatibility," in *Supporting Research and Advanced Development*, Space Programs Summary 37-22, Vol. IV, pp. 133–134. Jet Propulsion Laboratory, Pasadena, Calif., Aug. 31, 1963.
35. *Specimen/Capsule Preparation Used on the JPL Material Compatibility Program, Final Report*, PSI Report No. 525902-1, Pressure Systems, Inc., Los Angeles, Calif., Apr. 1971.
36. *Chemical and Metallurgical Analyses of 6Al-4V Titanium Test Specimens Exposed to Hydrazine (N₂H₄) Liquid Propellant*, Report No. 951581-11, Stanford Research Institute, Menlo Park, Calif., Apr. 15, 1971.
37. *NASA Pre-Alert: Test Specimen, Metallic, 6Al-4V Titanium, Immersed in Hydrazine, and Glass-Encapsulated*, Alert No. E4-70-03A, National Aeronautics and Space Administration, Washington, D.C., Aug. 16, 1971.
38. Kircher, J. F., and Vaughan, D. A., *Radiation Effects on Liquid Propellants, Final Report*, CR 109767, Part 2, under Contract NAS 7-722, Battelle Memorial Institute, Columbus, Ohio, Jan. 22, 1971.
39. Kircher, J. F., Best, R. E., and Rollins, J. E., *Radiation Effects on Liquid Propellants, Final Report*, CR 109767, under Contract NAS 7-722, Battelle Memorial Institute, Columbus, Ohio, Feb. 2, 1970.
40. *Aerospace Tanks: Characteristics of Existing Propellant Tanks and Pressure Vessels for Spacecraft Applications*, Final Report for NASA Contract NAS7-388, IIT Research Institute, Chicago, Ill., Jan. 1969.
41. Perkins, G. S., "The Mariner Mars 1971 Gimbal Actuator," paper presented at the 5th Aerospace Mechanisms Symposium, June 15-16, 1970. Appears in NASA SP 282, National Aeronautics and Space Administration, Washington, D.C., June 1970.
42. *ASME Power Test Codes*, Supplement on Instruments and Apparatus, Part 5, Chapt. 4, PTC 19.5; 4-1959, American Society of Mechanical Engineers, New York, Feb. 1959.
43. *Facility Operation Procedure Manual, Data Reduction, Transtage ACS Monopropellant Hydrazine REA/REM Data*, Specification RRC-FP-0010, Rev. A, Rocket Research Corp., Redmond, Wash., Sept. 9, 1968.

References (contd)

44. Kelley, J. H., *Mariner IV Midcourse Propulsion System Impulse and Accuracy Prediction*, Technical Report 32-1194, Jet Propulsion Laboratory, Pasadena, Calif., Sept. 1967.
45. Schatz, W. J., et al., *Development, Qualification and Performance of the Propulsion Subsystem for the Mariner Mars 1969 Spacecraft*, Technical Report 605-245, Jet Propulsion Laboratory, Pasadena, Calif. (JPL internal document), to be published.

Appendix

Summary of Demonstration System Test Instrumentation and Digital Data

All measurements made on the demonstration system are defined in detail in Table A-1. Corresponding data for calculated parameters are given in Table A-2. A detailed summary of the most important test data is given in Tables A-3 to A-8. The data are presented for the same times in each test firing to eliminate time effects as much as possible, especially those associated with engine tem-

perature. This effort could not be entirely successful, however, because system pressures decreased or blew down throughout the test series. The data given in Tables A-3 to A-8 are five-point averages of the raw digital data centered on the actual data sample closest to the desired times of 10, 20, 40, 90, and 150 s. The test results are discussed in detail in Subsection IV-D.

Table A-1. Summary of test system measured parameters

Computer symbol	Parameter description	Full-scale range		Accuracy	
		Pressures, kN/m ² (lbf/in. ² abs)			
PTN	Fuel tank nitrogen	0-3448	(0-500)	± 11	(1.6)
PFOU	Fuel orifice upstream	0-3448	(0-500)	± 11	(1.6)
PFOD	Fuel orifice downstream	0-3448	(0-500)	± 11	(1.6)
DPFO	Differential pressure, fuel orifice	0-345	(0-50)	± 11	(0.16)
PFH	Fuel heater manifold	0-3448	(0-500)	± 11	(1.6)
PFJ	Fuel injector manifold	0-3448	(0-500)	± 11	(1.6)
PC	Thrust chamber	0-1379	(0-200)	± 4.3	(0.62)
PG	Exhaust gas sampler	0-138	(0-20)	± 0.14	(0.02)
PCL2	Vacuum test cell	0-3.5	(0-0.5)	± 0.013	(0.002)
Temperatures, K (°F)					
TN2	Nitrogen pressurant	0-339	(0-150)	± 4	(2)
TFT	Fuel tank wall	0-339	(0-150)	± 4	(2)
TFO	Fuel orifice	0-339	(0-150)	± 4	(2)
TFH	Fuel heater manifold	0-339	(0-150)	± 4	(2)
TJ	Fuel injector head	0-811	(0-1000)	± 10	(12)
TJX	Fuel injector head	0-811	(0-1000)	± 10	(12)
TC1	Thrust chamber wall	0-1367	(0-2000)	± 16	(19)
TC2	Thrust chamber wall	0-1367	(0-2000)	± 16	(19)
TC3	Thrust chamber insulation	0-533	(0-500)	± 6	(7)
TB	Catalytic bed	0-1367	(0-2000)	± 16	(19)
TNS1	Nozzle throat	0-1367	(0-2000)	± 16	(19)
TNS2	Nozzle throat	0-1367	(0-2000)	± 16	(19)
TNS3	Nozzle exit	0-811	(0-1000)	± 10	(12)
TS1	Fuel line filter	0-339	(0-150)	± 4	(2)
TS2	Fuel injector manifold	0-533	(0-500)	± 6	(7)
TS3	PC pressure tubing	0-811	(0-1000)	± 10	(12)
TS4	Actuator linkage rod	0-533	(0-500)	± 6	(7)
TS5	Pyrovalve manifold	0-339	(0-150)	± 4	(2)
TS6	Support base plate	0-339	(0-150)	± 4	(2)
TS7	Fuel flex line union	0-533	(0-500)	± 6	(7)
TCL2	Vacuum test cell	0-339	(0-150)	± 4	(2)
Forces, N (lbf)					
F1A	Z-Axis, axial load	0-222.5	(0-50)	± 0.53	(0.12)
F1B	Z-Axis, axial load	0-222.5	(0-50)	± 0.53	(0.12)
F2	X-Axis, upper side load	0-8.9	(0-2)	± 0.18	(0.04)
F3	X-Axis, lower-side load	0-8.9	(0-2)	± 0.18	(0.04)
F4	Y-Axis, upper side load	0-8.9	(0-2)	± 0.18	(0.04)
F5	Y-Axis, lower side load	0-8.9	(0-2)	± 0.18	(0.04)
F6	Roll about Z-axis	0-8.9	(0-2)	± 0.18	(0.04)

Table A-1 (contd)

Computer symbol	Parameter description	Full-scale range		Accuracy	
Current, A					
IVS	Engine solenoid valve	0-2		±	0.02
IVLO	Latching valve open	0-2		±	0.02
IVLC	Latching valve closed	0-2		±	0.02
INC	Pyrovalve NC	0-20		±	0.2
INO	Pyrovalve NO	0-20		±	0.2
Voltage, V					
VVS	Engine solenoid valve	0-30		±	0.3
VVLO	Latching valve open	0-30		±	0.3
VVLC	Latching valve closed	0-30		±	0.3
VNC	Pyrovalve NC	0-50		±	0.5
VNO	Pyrovalve NO	0-50		±	0.5
VAA	Actuator A, X-axis	0 ± 2		±	0.01
VAB	Actuator B, Y-axis	0 ± 2		±	0.01
Angular deflection, deg					
XAA	Position, actuator A, X-axis	0 ± 5		±	0.02
XAB	Position, actuator B, Y-axis	0 ± 5		±	0.02
Acceleration, 10 ⁸ m/s ² (10 ³ g)					
A1	Accelerometer, pyrovalves, lateral	0-98.1	(0-10)	±	4.9 (0.5)
A2	Accelerometer, pyrovalves, axial	0-10.6	(0-2)	±	1.0 (0.1)
A3	Accelerometer, pyrovalves manifold	0-98.1	(0-10)	±	4.9 (0.5)
A4	Accelerometer, PC mounting bracket	0-9.8	(0-1)	±	0.5 (0.05)
A5	Accelerometer, base plate, axial	0-19.6	(0-2)	±	1.0 (0.1)
A6	Accelerometer, actuator support	0-9.8	(0-1)	±	0.5 (0.05)
Strain, μm/m					
E1	Strain gauge, pyrovalves, axial	0-3000		±	60
E2	Strain gauge, pyrovalve body NC 1	0-3000		±	60
E3	Strain gauge, pyrovalves manifold	0-3000		±	60
E4	Strain gauge, pyrovalves, lateral	0-3000		±	60
E5	Strain gauge, base plate, lateral	0-1500		±	30
E6	Strain gauge, actuator linkage rod	0-1500		±	30
Nozzle dimensions, cm (in.)					
DT Cold	Diameter, nozzle throat cold	0.8735	(0.3439)	±	0.00127 (0.0005)
DE Cold	Diameter, nozzle exit cold	5.631	(2.217)	±	0.00254 (0.001)

Table A-2. Summary of test system calculated parameters

Symbol	Parameter description	Units	Full-scale range	Accuracy
A_T (hot)	Area, nozzle throat, hot	m ² (in. ²)	0.5994 to 0.6097 × 10 ⁻⁴ (0.0929 to 0.0945)	±0.0006 × 10 ⁻⁴ (±0.0001)
A_E (hot)	Area, nozzle exit, hot	m ² (in. ²)	24.90 to 25.10 × 10 ⁻⁴ (3.86 to 3.89)	±0.019 × 10 ⁻⁴ (±0.003)
ρ_F	Density, hydrazine fuel	kg/m ³ (lbm/in. ³)	968.8 to 1023.3 (0.03650 to 0.03697)	±6 (±0.00002)
\dot{m}	Mass, fuel flowrate	kg/s (lbm/s)	0 to 0.068 (0 to 0.15)	±0.0002 to ±0.0003 (±0.0004 to ±0.0006)
M_{tot}	Mass, total fuel used	kg (lbm)	0 to 28-58 (0 to 63)	±0.002 to ±0.187 (±0.005 to ±0.412)
F_1 (avg)	Thrust, axial average	N (lbf)	0 to 444.8 (0 to 100)	±0.31 to ±0.53 (±0.07 to ±0.12)

Table A-2 (contd)

Symbol	Parameter description	Units	Full-scale range	Accuracy
F_{corr}	Thrust, axial corrected	N (lbf)	0 to 444.8 (0 to 100)	± 0.36 to ± 2.05 (± 0.08 to ± 0.46)
F_{vac}	Thrust, axial vacuum	N (lbf)	0 to 444.8 (0 to 100)	± 0.36 to ± 2.31 (± 0.08 to ± 0.52)
c^*	Characteristic velocity	m/s (ft/s)	0 to 1326 (0 to 4350)	± 9 to ± 19 (± 31 to ± 63)
C_F	Thrust coefficient	—	0 to 1.72	± 0.015 to ± 0.055
I_{vac}	Specific impulse, vacuum	N-s/kg (lbf-s/lbm)	0 to 2452 (0 to 250)	± 15 to ± 70 (± 1.5 to ± 7.1)
I_{tot}	Total impulse, delivered	N-s (lbf-s)	0 to 63,606 (0 to 14,300)	± 0.36 to ± 2.31 (± 0.087 to ± 0.52)

Table A-3. Summary of steady-state test data at time 0 s

No.	Parameter		Test No.									
	Computer symbol	Units	1A	2	3	4	5	6	7	8	9	
1	PTN	kN/m ² (psia)	2477.5 (359.3)	2210.4 (320.6)	2203.2 (319.5)	2134.6 (309.6)	2014.0 (292.1)	1425.8 (206.8)	1332.5 (193.2)	1252.8 (181.7)	1249.6 (181.2)	
2	TFT	K (°F)	289.7 (61.8)	282.2 (49.3)	284.1 (51.6)	281.2 (46.4)	279.9 (44.1)	279.5 (43.4)	280.5 (45.2)	280.7 (45.6)	281.7 (47.3)	
3	DPFO	kN/m ² (psid)	0 (0)	—————→								0 (0)
4	TFO	K (°F)	293.5 (68.6)	280.7 (45.6)	284.6 (52.5)	279.8 (44.0)	276.5 (38.1)	279.6 (43.5)	280.0 (44.3)	282.4 (48.6)	281.2 (46.4)	
5	PFOD	kN/m ² (psia)	2477.4 (359.2)	2210.3 (320.4)	2203.1 (319.4)	2134.4 (309.4)	2013.8 (292.0)	1425.6 (206.4)	1332.4 (193.1)	1252.7 (181.7)	1249.4 (181.2)	
6	PFH	kN/m ² (psia)	2477.4 (359.2)	2210.3 (320.4)	2203.1 (319.4)	2134.5 (309.5)	2013.9 (292.0)	1425.4 (206.3)	1332.3 (193.0)	1252.6 (181.7)	1249.5 (181.2)	
7	PHJ	kN/m ² (psia)	0 (0)	—————→								0 (0)
8	TJ	K (°F)	332.6 ^a (138.9)	284.2 (51.8)	289.2 (60.9)	286.3 (55.7)	282.6 (49.0)	283.6 (50.7)	281.8 (47.5)	297.5 (75.8)	296.1 (73.3)	
9	TC2	K (°F)	316.7 ^a (110.4)	283.6 (50.6)	287.9 (58.4)	277.2 (39.3)	276.0 (37.0)	280.9 (45.9)	282.7 (49.2)	284.3 (52.0)	283.7 (50.9)	
10	TB	K (°F)	325.9 ^a (126.9)	287.4 (57.6)	291.5 (65.0)	288.7 (65.0)	286.8 (56.6)	287.0 (56.8)	286.8 (56.5)	287.0 (60.0)	283.4 (50.3)	
11	TNS1	K (°F)	316.8 ^a (110.6)	285.5 (54.1)	290.0 (63.9)	288.7 (60.1)	285.9 (54.9)	284.6 (52.6)	289.5 (61.4)	291.6 (65.2)	287.3 (57.4)	
12	AT HOT	10 ⁻⁴ m ² (in. ²)	0.05995 (0.09291)	—————→								0.05995 (0.09291)
13	TNS3	K (°F)	300.1 ^a (80.4)	283.0 (49.7)	289.3 (61.1)	284.3 (52.0)	285.5 (54.3)	284.3 (52.0)	284.3 (52.0)	286.8 (56.6)	280.5 (45.2)	
14	AE HOT	10 ⁻⁴ m ² (in. ²)	24.9 (3.860)	—————→								24.9 (3.860)
15	PCL2	kN/m ² (psia)	0.327 (0.047)	0.376 (0.055)	0.441 (0.064)	0.376 (0.054)	0.342 (0.050)	0.292 (0.042)	0.386 (0.056)	0.369 (0.054)	0.973 (0.141)	

^aAbnormally high initial engine temperatures occurred on test No. 1A because the gas purged from the line between the pyro and solenoid valves just prior to the test contained hydrazine vapor which reacted in the engine. The vapor remained in the system because the lines were cleared of liquid hydrazine but not hydrazine vapor before the injector feed tube was changed after test No. 1.

Table A-4. Summary of steady-state test data at time 10 s

No.	Parameter		Test No.								
	Computer symbol	Units	1A	2	3	4	5	6	7	8	9
1	PTN	kN/m ² (psia)	2441.5 (354.1)	2179.5 (316.1)	2178.8 (316.0)	2118.1 (307.2)	1997.5 (289.7)	1418.3 (205.7)	1321.1 (191.6)	1194.9 (173.3)	1246.6 (180.8)
2	TFT	K (°F)	289.8 (62.0)	283.2 (50.0)	284.3 (52.0)	280.9 (46)	279.3 (43)	279.8 (44)	280.4 (45)	280.9 (46)	282.0 (48)
3	DPFO	kN/m ² (psid)	153.55 (22.27)	127.07 (18.43)	126.04 (18.28)	120.94 (17.54)	108.87 (15.79)	63.23 (9.170)	57.13 (8.286)	51.09 (7.410)	51.59 (7.482)
4	TFO	K (°F)	289.8 (62.0)	281.5 (47)	283.7 (51)	279.8 (44)	277.6 (40)	279.3 (43)	279.8 (44)	282.0 (48)	282.6 (49)
5	PFOD	kN/m ² (psia)	2267.1 (328.8)	2067.8 (299.9)	2065.0 (299.5)	1998.9 (289.9)	1893.4 (274.6)	1352.1 (196.1)	1273.5 (184.7)	1199.0 (173.9)	1201.1 (174.2)
6	PFH	kN/m ² (psia)	2245.7 (325.7)	2032.6 (294.8)	2029.9 (294.4)	1952.0 (283.1)	1866.5 (270.7)	1333.5 (193.4)	1265.9 (183.6)	1188.7 (172.4)	1198.4 (173.8)
7	PFJ ^a	kN/m ² (psia)	1979.6 (287.1)	1776.2 (257.6)	1773.4 (257.2)	1737.5 (252.0)	1636.2 (237.3)	1218.3 (176.7)	1137.7 (165.0)	1081.8 (156.9)	1090.8 (158.2)
8	TJ	K (°F)	381.5 (227)	322.1 (120)	307.1 (93.0)	308.4 (95.4)	300.3 (80.9)	298.4 (77.5)	296.6 (74.2)	307.1 (93.1)	312.6 (103)
9	TC2	K (°F)	1109.3 (1537)	1108.2 (1535)	1101.5 (1523)	1089.8 (1502)	1074.8 (1475)	1034.8 (1403)	1025.4 (1388)	1020.4 (1377)	1003.2 (1346)
10	TB	K (°F)	1169.8 (1646)	1163.7 (1635)	1160.4 (1629)	1152.1 (1614)	1147.1 (1605)	b	b	b	b
11	TNSI	K (°F)	753.2 (896)	757.1 (903)	759.3 (907)	741.5 (875)	730.4 (855)	664.3 (736)	663.2 (734)	650.4 (711)	614.3 (646)
12	AT HOT	10 ⁻⁴ m ² (in. ²)	0.6034 (0.09352)	0.6029 (0.09344)	0.6029 (0.09345)	0.6027 (0.09341)	0.6025 (0.09338)	0.6016 (0.09324)	0.6016 (0.09324)	0.6014 (0.09321)	0.6010 (0.09315)
13	TNS3	K (°F)	429.3 (313)	405.4 (270)	413.2 (284)	402.1 (264)	404.3 (268)	362.6 (193)	362.1 (192)	357.6 (184)	344.3 (160)
14	AE HOT	10 ⁻⁴ m ² (in. ²)	24.90 (3.860)								
15	PCL2	kN/m ² (psia)	0.103 (0.015)	0.193 (0.028)	0.248 (0.036)	0.131 (0.019)	0.110 (0.016)	0.096 (0.014)	0.200 (0.029)	0.131 (0.019)	0.503 (0.073)
16	PC	kN/m ² (psia)	1111.89 (161.26)	1015.63 (147.30)	1015.29 (147.25)	992.05 (143.88)	945.37 (137.11)	715.91 (103.83)	685.09 (99.36)	646.75 (93.80)	646.82 (93.81)
17	M DOT	kg/s (lbm/s)	0.05138 (0.11324)	0.04668 (0.10348)	0.04668 (0.10292)	0.04581 (0.10100)	0.04349 (0.09588)	0.03335 (0.07352)	0.03170 (0.06988)	0.02975 (0.06558)	0.03012 (0.06640)
18	F VAC	N (lbf)	113.60 (25.54)	103.86 (23.39)	103.86 (23.35)	99.50 (22.37)	94.25 (21.19)	72.95 (16.40)	68.28 (15.35)	65.74 (14.78)	65.16 (14.65)
19	C STAR	m/s (ft/s)	1305.8 (4284)	1311.2 (4281)	1311.2 (4302)	1305.5 (4283)	1309.4 (4296)	1291.1 (4236)	1300.6 (4267)	1307.6 (4290)	1291.4 (4237)
20	I VAC	N-s/kg (lbf-s/lbm)	2210.3 (225.4)	2225.0 (226.1)	2225.0 (226.9)	2172.0 (221.5)	2165.2 (220.8)	2187.7 (223.1)	2154.4 (219.7)	2269.1 (231.4)	2163.2 (220.6)
21	CF	-	1.693	1.697	1.697	1.664	1.654	1.695	1.657	1.691	1.676
22	I TOT	N-s (lbf-s)	1063.1 (239.0)	955.6 (215.2)	955.6 (214.8)	851.9 (191.5)	858.5 (193.0)	648.6 (145.8)	622.2 (139.9)	595.7 (133.9)	593.9 (133.5)

^aThe PFJ value for test No. 9 is estimated because of measurement problems on that test.

^bTemperature transducer malfunctioned.

Table A-4 (contd)

Parameter			Test No.								
No.	Computer symbol	Units	1A	2	3	4	5	6	7	8	9
23	RL	$\frac{N \cdot s^2}{kg \cdot m^5}$	0.1768	0.1875	0.1891	0.1847	0.1945	0.1833	0.1872	0.1293	0.2059
		$\left(\frac{lbf \cdot s^2}{lbfm \cdot in.^5}\right)$	(190.6)	(202.2)	(203.9)	(199.1)	(209.7)	(197.6)	(201.8)	(139.4)	(222.0)
24	RT	$\frac{N \cdot s^2}{kg \cdot m^5}$	0.5072	0.5405	0.5432	0.5483	0.5683	0.6444	0.6490	0.6302	0.6741
		$\left(\frac{lbf \cdot s^2}{lbfm \cdot in.^5}\right)$	(546.8)	(582.7)	(585.7)	(591.2)	(612.7)	(694.8)	(699.7)	(679.5)	(726.8)
25	K M DOT	$N^{1/2} \cdot m$ ($lbf^{1/2} \cdot in.$)	0.2665 (4.974)	0.2666 (4.977)	0.2660 (4.965)	0.2568 (4.793)	0.2494 (4.655)	0.2510 (4.685)	0.2477 (4.624)	0.2538 (4.738)	0.2451 (4.576)
26	KPC	$10^{-3} m^2$ ($in.^2$)	0.1013 (0.1570)	0.1004 (0.1557)	0.0996 (0.1544)	0.0975 (0.1511)	0.0962 (0.1491)	0.0993 (0.1539)	0.0981 (0.1521)	0.0981 (0.1520)	0.0973 (0.1508)

Table A-5. Summary of steady-state test data at time 20 s

Parameter			Test No.								
No.	Computer symbol	Units	1A	2	3	4	5	6	7	8 ^a	9
1	PTN	kN/m^2 (psia)	2416.7 (350.5)	2158.8 (313.1)	2160.2 (313.1)	2099.5 (304.5)	1978.9 (287.0)	1413.5 (205.0)	1319.0 (191.3)		1242.5 (180.2)
2	TFT	K (°F)	289.8 (62)	283.2 (50)	284.3 (52)	280.9 (46)	279.8 (44)	279.3 (43)	280.4 (45)		282.1 (48)
3	DPFO	kN/m^2 (psid)	152.79 (22.16)	126.87 (18.40)	125.83 (18.25)	120.80 (17.52)	109.38 (15.86)	64.40 (9.34)	57.92 (8.40)		52.54 (7.62)
4	TFO	K (°F)	289.8 (62)	281.5 (47)	283.7 (51)	279.8 (44)	277.6 (40)	279.8 (44)	279.8 (44)		282.6 (49)
5	PFOD	kN/m^2 (psia)	2242.2 (325.2)	2047.8 (297.0)	2040.9 (296.0)	1979.6 (287.1)	1876.1 (272.1)	1345.2 (195.1)	1268.0 (183.9)		1196.3 (173.5)
6	PFH	kN/m^2 (psia)	2216.0 (321.4)	2014.7 (292.2)	2003.7 (290.6)	1927.8 (279.6)	1850.6 (268.4)	1332.8 (193.3)	1260.4 (182.8)		1192.1 (172.9)
7	PFJ ^b	kN/m^2 (psia)	1947.8 (282.5)	1758.9 (255.1)	1752.7 (254.2)	1716.9 (249.0)	1621.7 (235.2)	1211.4 (175.7)	1130.8 (164.0)		1079.1 (156.5)
8	TJ	K (°F)	451.5 (353)	385.9 (235)	343.2 (158)	335.4 (144)	328.2 (131)	321.5 (119)	314.8 (107)		322.6 (121)
9	TC2	K (°F)	1140.9 (1594)	1136.5 (1586)	1138.2 (1589)	1133.7 (1581)	1122.1 (1560)	1095.9 (1513)	1090.9 (1504)		1080.9 (1486)
10	TB	K (°F)	1173.2 (1652)	1168.2 (1643)	1163.2 (1634)	1157.6 (1624)	1150.9 (1612)	c	c		c
11	TNSI	K (°F)	980.4 (1305)	969.8 (1286)	968.2 (1283)	960.9 (1270)	952.1 (1254)	902.6 (1165)	900.9 (1162)		877.1 (1119)
12	AT HOT	$10^{-4} m^2$ ($in.^2$)	0.6073 (0.09412)	0.6070 (0.09408)	0.6070 (0.09407)	0.6068 (0.09405)	0.6066 (0.09402)	0.6055 (0.09385)	0.6055 (0.09385)		0.6051 (0.09379)
13	TNS3	K (°F)	560.9 (550)	540.4 (513)	542.6 (517)	534.3 (502)	534.3 (502)	505.8 (451)	477.1 (399)		455.4 (360)

^aTest No. 8 lasted only 15 s.

^bThe PFJ value for test No. 9 is estimated because of measurement problems on that test.

^cTemperature transducer malfunctioned.

Table A-5 (contd)

Parameter			Test No.								
No.	Computer symbol	Units	1A	2	3	4	5	6	7	8 ^a	9
14	AE HOT	10 ⁻⁴ m ² (in. ²)	24.97 (3.870)	24.97 (3.870)	24.97 (3.870)	24.94 (3.866)	24.94 (3.866)	24.92 (3.863)	24.90 (3.860)		24.90 (3.860)
15	PCL2	kN/m ² (psia)	0.0827 (0.012)	0.1793 (0.026)	0.2275 (0.033)	0.1103 (0.016)	0.0896 (0.013)	0.0758 (0.011)	0.1862 (0.027)		0.3241 (0.047)
16	PC	kN/m ² (psia)	1107.8 (160.67)	1015.9 (147.34)	1011.2 (146.65)	992.2 (143.9)	947.0 (137.34)	726.6 (105.38)	694.0 (100.65)		658.8 (95.55)
17	M DOT	kg/s (lbm/s)	0.05126 (0.11300)	0.04687 (0.10334)	0.04665 (0.10284)	0.04577 (0.10090)	0.04360 (0.09612)	0.03363 (0.07414)	0.03189 (0.07030)		0.03038 (0.06698)
18	F VAC	N (lbf)	115.56 (25.98)	105.33 (23.68)	104.97 (23.60)	100.66 (22.63)	95.85 (21.55)	74.82 (16.82)	70.41 (15.83)		67.08 (15.08)
19	C STAR	m/sec (ft/s)	1312.2 (4305)	1315.5 (4316)	1315.8 (4317)	1315.2 (4315)	1317.3 (4322)	1308.2 (4292)	1317.3 (4322)		1311.6 (4303)
20	I VAC	N-s/kg (lbf-s/lbm)	2254.4 (229.9)	2246.6 (229.1)	2250.5 (229.5)	2199.5 (224.3)	2198.5 (224.2)	2224.0 (226.8)	2208.3 (225.2)		2206.4 (225.0)
21	CF	—	1.718	1.708	1.710	1.672	1.669	1.700	1.676		1.676
22	I TOT	N-s (lbf-s)	2199.1 (494.4)	1996.5 (448.9)	1993.3 (448.1)	1790.6 (402.6)	1809.9 (406.9)	1377.0 (309.6)	1316.7 (296.0)		1252.6 (281.6)
23	RL	$\frac{N-s^2}{kg-m^5}$ $\left(\frac{lbf-s^2}{lbm-in.^5}\right)$	0.1805 (194.6)	0.1859 (200.4)	0.1897 (204.5)	0.1863 (200.9)	0.1927 (207.8)	0.1817 (195.9)	0.1892 (204.0)		0.2059 (222.0)
24	RT	$\frac{N-s^2}{kg-m^5}$ $\left(\frac{lbf-s^2}{lbm-in.^5}\right)$	0.5038 (543.2)	0.5298 (571.2)	0.5363 (578.2)	0.5395 (581.7)	0.5554 (598.8)	0.6202 (668.7)	0.6279 (677.0)		0.6419 (692.1)
25	K M DOT	N ^{1/2} -m (lbf ^{1/2} -in.)	0.2785 (5.198)	0.2790 (5.208)	0.2791 (5.210)	0.2712 (5.062)	0.2688 (5.017)	0.2855 (5.330)	0.2674 (4.992)		0.2640 (4.928)
26	KPC	10 ⁻³ m ² (in. ²)	0.1018 (0.1578)	0.1014 (0.1572)	0.1010 (0.1565)	0.0988 (0.1531)	0.0981 (0.1520)	0.0989 (0.1533)	0.0989 (0.1533)		0.0979 (0.1518)

Table A-6. Summary of steady-state test data at time 40 s

Parameter			Test No.								
No.	Computer symbol	Units	1A	2 ^a	3	4	5	6	7	8 ^a	9
1	PTN	kN/m ² (psia)	2366.4 (343.2)		2101.6 (304.8)	2064.4 (299.4)	1945.1 (282.1)	1399.7 (203.0)	1308.0 (189.7)		1232.1 (178.7)
2	TFT	K (°F)	289.8 (62)		283.7 (51)	280.9 (46)	279.3 (43)	279.8 (44)	280.4 (45)		281.5 (47)
3	DPFO	kN/m ² (psid)	149.35 (21.66)		123.42 (17.90)	118.87 (17.24)	107.58 (15.60)	64.81 (9.40)	58.06 (8.42)		52.88 (7.67)
4	TFO	K (°F)	289.8 (62)		283.7 (51)	279.8 (44)	277.6 (40)	279.8 (44)	279.8 (44)		282.6 (49)

^aTest Nos. 2 and 8 already terminated.

Table A-6 (contd)

No.	Parameter		Test No.								
	Computer symbol	Units	1A	2 ^a	3	4	5	6	7	8 ^a	9
5	PFOD	kN/m ² (psia)	2196.1 (318.5)		1510.7 (219.1)	1946.5 (282.3)	1849.2 (268.2)	1337.6 (194.0)	1256.3 (182.2)		1188.0 (172.3)
6	PFH	kN/m ² (psia)	2168.5 (314.5)		1977.5 (286.8)	1895.4 (274.9)	1818.2 (263.7)	1325.9 (192.3)	1249.4 (181.2)		1183.2 (171.6)
7	PFJ ^b	kN/m ² (psia)	1912.0 (277.3)		1727.2 (250.5)	1683.1 (244.1)	1598.3 (231.8)	1199.0 (173.9)	1120.4 (162.5)		1063.9 (154.3)
8	TJ	K (°F)	548.2 (527)		370.9 (208)	356.5 (182)	338.7 (150)	330.9 (136)	323.2 (122)		326.5 (128)
9	TC2	K (°F)	1155.4 (1620)		1152.1 (1614)	1147.1 (1605)	1139.3 (1591)	1117.1 (1551)	1113.7 (1545)		1110.4 (1539)
10	TB	K (°F)	1173.7 (1653)		1164.8 (1637)	1172.1 (1650)	1162.6 (1633)	c	c		c
11	TNSI	K (°F)	1061.5 (1451)		1053.7 (1437)	1053.2 (1436)	1049.3 (1429)	1024.3 (1384)	1019.8 (1376)		1011.5 (1361)
12	AT HOT	10 ⁻⁴ m ² (in. ²)	0.6092 (0.09442)		0.6090 (0.09439)	0.6089 (0.09438)	0.6089 (0.09437)	0.6082 (0.09427)	0.6082 (0.09427)		0.6079 (0.09423)
13	TNS3	K (°F)	709.8 (818)		694.8 (791)	688.7 (780)	686.5 (776)	364.8 (197)	632.1 (678)		619.8 (656)
14	AE HOT	10 ⁻⁴ m ² (in. ²)	25.03 (3.880)		25.03 (3.880)	25.03 (3.880)	25.02 (3.878)	24.90 (3.860)	24.97 (3.870)		24.97 (3.870)
15	PCL2	kN/m ² (psia)	0.0690 (0.010)		0.2206 (0.032)	0.0965 (0.014)	0.0827 (0.012)	0.0690 (0.010)	0.1793 (0.026)		0.2137 (0.031)
16	PC	kN/m ² (psia)	1095.5 (158.88)		1001.9 (145.31)	983.6 (142.66)	939.4 (136.25)	730.2 (105.90)	693.7 (100.60)		661.0 (95.87)
17	M DOT	kg/s (lbm/s)	0.05069 (0.11176)		0.04620 (0.10186)	0.04540 (0.10010)	0.04332 (0.09550)	0.03376 (0.07442)	0.03192 (0.07038)		0.03049 (0.06722)
18	F VAC	N (lbf)	114.27 (25.69)		103.86 (23.35)	100.35 (22.56)	95.76 (21.53)	78.82 (17.27)	71.26 (16.02)		68.28 (15.35)
19	C STAR	m/s (ft/s)	1316.7 (4320)		1320.7 (4333)	1318.9 (4327)	1322.8 (4340)	1316.1 (4318)	1321.0 (4334)		1317.3 (4322)
20	I VAC	N-s/kg (lbf-s/lbm)	2254.4 (229.9)		2248.5 (229.3)	2209.2 (225.3)	2215.2 (225.9)	2276.0 (232.1)	2230.9 (227.5)		2237.7 (228.2)
21	CF	—	1.713		1.703	1.675	1.674	1.730	1.689		1.699
22	I TOT	N-s (lbf-s)	4476.9 (1006.5)		4062.0 (913.2)	3678.1 (826.9)	3732.4 (839.1)	2876.6 (646.7)	2729.2 (613.6)		2597.8 (584.0)
23	RL	$\frac{N-s^2}{kg-m^5}$ $\left(\frac{lbf-s^2}{lbm-in.^5}\right)$	0.1790 (193.0)		0.1848 (199.2)	0.1881 (202.8)	0.1902 (205.1)	0.1785 (192.4)	0.1874 (202.1)		0.1795 (195.0)
24	RT	$\frac{N-s^2}{kg-m^5}$ $\left(\frac{lbf-s^2}{lbm-in.^5}\right)$	0.5004 (539.5)		0.5307 (572.2)	0.5341 (575.3)	0.5493 (592.2)	0.5984 (645.2)	0.6146 (662.6)		0.6269 (675.9)

^aTest Nos. 2 and 8 already terminated.

^bThe PFJ value for test No. 9 is estimated because of measurement problems on that test.

^cTemperature transducer malfunctioned.

Table A-6 (contd)

Parameter			Test No.								
No.	Computer symbol	Units	1A	2 ^a	3	4	5	6	7	8 ^a	9
25	K M DOT	N ^{1/2} -s (lbf ^{1/2} -in.)	0.2858 (5.336)		0.2860 (5.339)	0.2747 (5.218)	0.2788 (5.205)	0.2823 (5.270)	0.2790 (5.208)		0.2753 (5.140)
26	KPC	10 ⁻³ m ² (in. ²)	0.1026 (0.1590)		0.1019 (0.1579)	0.0999 (0.1548)	0.0994 (0.1541)	0.1016 (0.1575)	0.0999 (0.1548)		0.0988 (0.1532)

^aTest Nos. 2 and 8 already terminated.

Table A-7. Summary of steady-state test data at time 90 s

Parameter			Test No. ^a								
No.	Computer symbol	Units	1A	2	3	4	5	6	7	8	9
1	PTN	kN/m ² (psia)	2252.6 (326.7)				1881.6 (272.9)	1374.2 (199.3)	1286.6 (186.6)		1214.2 (176.1)
2	TFT	K (°F)	289.8 (62)				279.8 (44)	279.3 (43)	280.4 (45)		281.5 (47)
3	DPFO	kN/m ² (psid)	139.49 (20.23)				103.56 (15.02)	63.36 (9.19)	56.54 (8.20)		51.46 (7.464)
4	TFO	K (°F)	289.8 (62)				278.2 (41)	279.8 (44)	279.8 (44)		282.6 (49)
5	PFOD	kN/m ² (psia)	2103.7 (305.1)				1794.1 (260.2)	1307.3 (189.6)	1236.3 (179.3)		1168.7 (169.5)
6	PFH	kN/m ² (psia)	2074.7 (300.9)				1767.9 (256.4)	1291.4 (187.3)	1228.0 (178.1)		1165.3 (169.0)
7	PFJ ^b	kN/m ² (psia)	1829.9 (265.4)				1549.3 (224.7)	1173.5 (170.2)	1103.9 (160.1)		1056.3 (153.2)
8	TJ	K (°F)	664.8 (737)				365.9 (199)	344.8 (161)	337.1 (147)		335.1 (143.4)
9	TC2	K (°F)	1158.7 (1626)				1147.1 (1605)	1121.5 (1559)	1135.9 (1585)		1112.1 (1542)
10	TB	K (°F)	1173.7 (1653)				1169.3 (1645)	c	c		c
11	TNSI	K (°F)	1087.1 (1497)				1074.8 (1475)	1053.7 (1437)	1053.2 (1436)		1059.8 (1448)
12	AT HOT	10 ⁻⁴ m ² (in. ²)	0.6098 (0.09452)				0.6097 (0.09447)	0.6090 (0.09439)	0.6090 (0.09438)		0.6091 (0.09440)
13	TNS3	K (°F)	792.1 (966)				773.7 (933)	756.7 (907)	739.8 (872)		735.4 (864)
14	AE HOT	10 ⁻⁴ m ² (in. ²)	25.10 (3.890)				25.03 (3.880)	25.03 (3.880)	25.03 (3.880)		25.03 (3.880)
15	PCL2	kN/m ² (psia)	0.0690 (0.010)				0.0758 (0.011)	0.0690 (0.010)	0.1793 (0.026)		0.1310 (0.019)
16	PC	kN/m ² (psia)	1059.3 (153.64)				918.3 (133.18)	720.7 (104.52)	682.9 (99.05)		650.1 (94.29)

^aTest Nos. 2, 3, 4, and 8 had terminated.

^bThe PFJ value for test No. 9 is estimated because of measurement problems on that test.

^cTemperature transducer malfunctioned.

Table A-7 (contd)

Parameter			Test No. ^a								
No.	Computer symbol	Units	1A	2	3	4	5	6	7	8	9
17	M DOT	kg/s (lbm/s)	0.04896 (0.10794)				0.04240 (0.09348)	0.03335 (0.07352)	0.03151 (0.06946)		0.03009 (0.06634)
18	F VAC	N (lbf)	111.11 (24.98)				93.90 (21.11)	74.46 (16.74)	70.14 (15.77)		67.48 (15.17)
19	C STAR	m/s (ft/s)	1318.9 (4327)				1319.4 (4329)	1315.2 (4315)	1319.7 (4329.8)		1316.3 (4318.7)
20	I VAC	N-s/kg (lbf-s/lbm)	2269.1 (231.4)				2214.2 (225.8)	2230.9 (227.5)	2226.0 (227.0)		2242.6 (228.7)
21	CF	—	1.720				1.678	1.697	1.687		1.704
22	I TOT	N-s (lbf/s)	10058.7 (2261.4)				8497.8 (1910.5)	6601.8 (1484.2)	6268.1 (1409.2)		5971.5 (1342.5)
23	RL	$\frac{N-s^2}{kg-m^5}$ $\left(\frac{lbf-s^2}{lbm-in.^5}\right)$	0.1782 (192.1)				0.1887 (203.5)	0.1833 (197.6)	0.1878 (202.5)		0.1688 (182.0)
24	RT	$\frac{N-s^2}{kg-m^5}$ $\left(\frac{lbf-s^2}{lbm-in.^5}\right)$	0.5029 (542.2)				0.5469 (589.7)	0.5981 (644.8)	0.6200 (668.5)		0.6353 (685.0)
25	K M DOT	N ^{1/2} -m (lbf ^{1/2} -in.)	0.2903 (5.420)				0.2854 (5.327)	0.2889 (5.393)	0.2868 (5.353)		0.2826 (5.276)
26	KPC	10 ⁻³ m ² (in. ²)	0.1032 (0.1600)				0.1006 (0.1559)	0.1022 (0.1584)	0.1010 (0.1565)		0.0997 (0.1546)

Table A-8. Summary of steady-state test data at time 150 s

Parameter			Test No. ^a								
No.	Computer symbol	Units	1A	2	3	4	5	6	7	8	9
1	PTN	kN/m ² (psia)					1812.7 (262.9)	1345.2 (195.1)	1260.4 (182.8)		1194.2 (173.2)
2	TFT	K (°F)					279.8 (44)	278.7 (42)	279.8 (44)		280.9 (46)
3	DPFO	kN/m ² (psid)					98.18 (14.24)	61.0 (8.85)	55.6 (8.064)		50.1 (7.260)
4	TFO	K (°F)					278.6 (41.82)	279.5 (43.48)	279.9 (44.18)		282.8 (49.26)
5	PFOD	kN/m ² (psia)					1730.6 (251.0)	1273.5 (184.7)	1217.6 (176.6)		1148.7 (166.6)
6	PFH	kN/m ² (psia)					1705.8 (247.4)	1269.4 (184.1)	1211.4 (175.7)		1144.6 (166.0)
7	PFJ ^b	kN/m ² (psia)					1501.7 (217.8)	1151.5 (167.0)	1085.3 (157.4)		1037.0 (150.4)

^aTest Nos. 1A, 2, 3, 4, and 8 already terminated.

^bThe PFJ value for test No. 9 is estimated because of measurement problems on that test.

Table A-8 (contd)

No.	Parameter		Test No. ^a								
	Computer symbol	Units	1A	2	3	4	5	6	7	8	9
8	TJ	K (°F)					382.6 (229)	351.5 (173)	339.3 (151)		338.7 (150)
9	TC2	K (°F)					1141.5 (1595)	1120.4 (1557)	1117.1 (1551)		1117.1 (1551)
10	TB	K (°F)					1160.9 (1630)	c	c		c
11	TNSI	K (°F)					1074.8 (1475)	1064.8 (1457)	1055.9 (1441)		1062.1 (1452)
12	AT HOT	10 ⁻⁴ m ² (in. ²)					0.6096 (0.09448)	0.6093 (0.09443)	0.6091 (0.09440)		0.6092 (0.09441)
13	TNS3	K (°F)					779.8 (944)	765.7 (919)	751.5 (893)		748.7 (888)
14	AE HOT	10 ⁻⁴ m ² (in. ²)					25.06 (3.884)	25.04 (3.882)	25.03 (3.880)		25.03 (3.880)
15	PCL2	kN/m ² (psia)					0.0758 (0.011)	0.0680 (0.010)	0.1793 (0.026)		0.1172 (0.017)
16	PC	kN/m ² (psia)					892.0 (129.37)	708.2 (102.71)	676.0 (98.04)		640.5 (92.89)
17	M DOT	kg/s (lbm/s)					0.04128 (0.091)	0.03266 (0.072)	0.03130 (0.069)		0.02948 (0.065)
18	F VAC	N (lbf)					92.03 (20.69)	74.28 (16.70)	71.03 (15.97)		67.08 (15.08)
19	C STAR	m/s (ft/s)					1316.7 (4320)	1317.3 (4322)	1318.6 (4326)		1314.9 (4314)
20	I VAC	N-s/kg (lbf-s/lbm)					2227.9 (227.2)	2267.1 (231.2)	2273.0 (231.8)		2261.3 (230.6)
21	CF	—					1.692	1.722	1.725		1.719
22	I TOT	N-s (lbf-s)					14073.6 (3164.0)	11014.3 (2476.2)	10489.0 (2358.1)		9971.8 (2241.9)
23	RL	$\frac{N \cdot s^2}{kg \cdot m^5}$ $\left(\frac{lbf \cdot s^2}{lbm \cdot in.^5}\right)$					0.1856 (200.1)	0.1843 (198.7)	0.1827 (197.0)		0.1725 (186.0)
24	RT	$\frac{N \cdot s^2}{kg \cdot m^5}$ $\left(\frac{lbf \cdot s^2}{lbm \cdot in.^5}\right)$					0.5521 (595.3)	0.6058 (653.2)	0.6102 (657.9)		0.6379 (687.9)
25	K M DOT	N ^{1/2} -m (lbf ^{1/2} -in.)					0.2872 (5.361)	0.2914 (5.440)	0.2898 (5.409)		0.2853 (5.326)
26	KPC	10 ⁻³ m ² (in. ²)					0.1010 (0.1566)	0.1025 (0.1589)	0.1016 (0.1575)		0.1002 (0.1553)

^aTemperature transducer malfunctioned.